École Doctorale
d'Informatique,
Télécommunications
et Électronique de Paris

Thèse

présentée pour obtenir le grade de Docteur
de l'École Nationale Supérieure des Télécommunications

Spécialité : **Électronique et Communications**

Nicolas GRESSET

Nouvelles techniques de codage spatio-temporel avec des modulations codées à bits entrelacés

Soutenue le 13 décembre 2004 devant le jury composé de

Hikmet Sari	Président
Raymond Knopp	Rapporteurs
Hans-Andrea Loeliger	
Geneviève Baudoin	Examinateurs
Jean-Claude Belfiore	
Gilles Zémor	
Joseph Boutros	Directeurs de thèse
Loïc Brunel	

Thesis abstract

This thesis report describes new designs for transmitters and receivers of bit-interleaved coded modulations over multiple antenna channels. The objective is to achieve near Shannon capacity performance over ergodic channels and near outage probability performance over block fading channels. Iterative joint detection and decoding are applied in the aim of achieving near maximum likelihood performance. Design criteria are derived for each block optimization from the error performance expressions under the ideal interleaving assumption. First, we describe the binary mapping optimization for ergodic channels by introducing the new concept of multidimensional mapping that provides large amount of coding gain. We achieve near capacity performance either with turbo-codes or with multi-dimensional mappings associated with a simple code. Then, we present the bit-interleaved coded modulation with linear precoding as a Space-Time code for multiple antenna block fading channels. We show that the channel interleaver is the fundamental part of the bit-interleaved coded modulation calling the shots about the achieved diversity. We describe the linear precoding optimality condition and a class of quasi-optimal linear precoders. The minimal linear precoder size providing full diversity is deduced from a modified Singleton bound applied to the global Euclidean code. We show that full diversity and quasi-optimal coding gains are observed for a given error correcting code. Finally, we achieve near outage capacity performance thanks to turbo-codes. Next, iterative joint detection and decoding techniques are considered, we describe a near optimum soft-input soft-output list sphere decoder which allows the computation of a posteriori probabilities for very high spectral efficiency transmitter schemes with reduced complexity.

Contents

List of Figures

List of Tables

List of notations

Mathematical tools notations

$.^t$	Transpose operand.
$.^*$	Transpose conjugate operand.
$\lfloor . \rfloor$	Floor function.
$\lceil . \rceil$	Ceil function.
$[.]$	Nearest integer function.
$\|.\|$	Module.
$\|\|.\|\|$	Euclidean norm.
$\|\|.\|\|_{\mathcal{F}}$	Frobenius norm, i.e. the square root of the sum of all the matrix coefficients squared norms.
det	Matrix determinant.
diag	Diagonal matrix.
vol	Fundamental volume of the lattice.
$n!$	Factorial of n, $n! = n.(n-1)\ldots 3.2.1$.
$\binom{n}{k}$	Binomial coefficient, *"n choose k"*.
$\Gamma(.)$	Complete gamma function, $\Gamma(x) = \int_0^\infty t^{x-1}e^{-t}dt$.
$\mathbb{Z}$	Set of integers.
$\mathbb{R}$	Set of reals.
$\mathbb{C}$	Set of complex numbers.

List of Variables

Error correcting code notations

$\mathcal{C}$	Error correcting Code.
$\mathcal{C}_E$	Euclidean code, contains all the noiseless transmitted codewords.
$R_{\mathcal{C}}$	Code Rate.
$K_{\mathcal{C}}$	Number of inputs of the convolutional code.
$l_{\mathcal{C}}$	Constraint length of the convolutional code.
$L_{\mathcal{C}}$	Number of branches of the convolutional code.
$N_{\mathcal{C}}$	Number of outputs of the convolutional code.
$(g_1, \ldots, g_{N_{\mathcal{C}}})_8$	Octal generator polynomials of the convolutional code.

Interleaver Notations

Π	Name of the channel interleaver.

Mapping and modulation notations

m	Spectral efficiency of the digital modulation, $m = \log_2(M)$.
M	Number of points in the digital modulation constellation, $M = 2^m$.
Ω	N_t dimensional constellation, also denotes the binary mapping associated to the constellation.
$\Omega(c_\ell)$	Set of constellation points with their ℓ-th labeling bit equal to c_ℓ.

Linear precoder notations

s	Spreading factor, i.e. the number of time periods grouped by the matrix S.
N_t	Number of inputs and outputs of S. $N_t = sn_t$.
S	The $N_t \times N_t$ linear precoder matrix.
n_s	Number of indepedent channel realizations seen by the matrix S.

Channel notations

H	Channel matrix, can be represented in the extended version for linear precoding.
n_r	Number of receive antennas.
n_t	Number of transmit antennas.
N_r	Number of outputs of the precoded channel matrix SH.
N_t	Number of inputs of the precoded channel matrix SH.
x	Transmitted noiseless vector, $x = zH$.
y	Received vector, $y = zH + \eta$.
z	Symbol vector to be transmitted.
η	Noise vector.

Lattices notations

G	Gram matrix of the lattice, $G = M_\Lambda M_\Lambda^t$.
M_Λ	Lattice generator matrix.
Λ	The equivalent channel lattice.

List of Acronyms

BPSK	Binary Phase Shift Keying.
BSK	Binary Shift Keying.
HIHO	Hard-Input Hard-Ouput.
LDPC	Low Density Parity Check Codes.
MIMO	Multiple-Input Multiple-Output, multiple antenna.
ML	Maximum likelihood.
MMSE	Minimum Mean Square Error.
OFDM	Orthogonal Frequency Division Multiplex.
QAM	Quadrature Amplitude Modulation.
SD	Sphere Decoder.
SD-SE	Sphere Decoder, Schnorr-Euchner strategy.
SIHO	Soft-Input Hard-Output.
SISO	Soft-Input Soft-Output.
ST	Space-Time.

Introduction and Thesis Outline

Digital communications in its electric form appeared in 1840 with the telegraphic transmission code invented by Samuel Morse. Emile Baudot improved the data rate of telegraphic lines in 1874 with his Baudot code (i.e., high data rate for text over electric wires). In 1880, Alexander G. Bell and Thomas Edison developped the theory of telephony (i.e., voice over electric wires). In 1924, Harry Nyquist proposed a simple theory for reducing the distortion in telegraph transmission. John Baird implemented a television system with a rate of 5 frames per second and a resolution of 30-lines per frame. Digital communications became a topic of great interest for both the mathematical and the engineering communities since the introduction of a mathematical model for information theory by Claude E. Shannon in 1948 at Bell Laboratories. He also introduced the fundamental concept of information and capacity: "what is the best transmission data rate over a given channel?". Once this theoretical limit is determined, one can expect to give an answer to the question: "How to design a practical transmitter that approaches this limit?". This question haunts the mind of thousands of researchers since that time. Undoubtedly, telecommunications are linked to the overall technical progress in the last century. They acquired a more and more important place in the daily life since the mobile phone became democratized in the mid 1990's.

The today objectives of mobile phone technologies are: improving the reliability of data or voice transmissions (Quality of Service), improving the data rate, i.e., the services, minimizing the hardware cost thanks to powerful software processing, and allowing a maximal number of users. All these objectives are related in part or entirely to the physical layer, and in particular to digital communications technologies. Finally, all these objectives are jointly achieved when finding a solution to transmit the data with a maximum data rate and a minimum error rate.

The first objective is to enhance the data rate on multi-path fading channels. The two convincing solutions introduced in the last decades were OFDM and multiple antennas in transmission. In order to enhance the bad performance observed on fading channels, we usually exploit some diversity provided by a channel ergodicity, and multiple transmit or receive antennas. Practically, multiple antennas are already chosen for UMTS, the third generation of mobile phones. For the fourth generation, a combination of multiple antennas and OFDM is considered as a good candidate.

In the (not so) far future, the most important wireless communications objective will be to provide high data rate wireless Internet connections. As an example, HiperLAN Type 1 is a wireless local area network standard designed to provide a 1Mb/s to 20Mb/s communication between portable devices. HiperLAN Type 2 or IEEE 802.11 standards are intended to provide 6Mb/s to 54Mb/s data rates. Actually, the objective is not to rival wired communications which already provide data rates around 1Gb/s for LANs, but to provide a comfortable connection with the great advantage of mobility. This will not be feasible without the use of multiple antennas.

This thesis report describes the design of transmitters and receivers for single user multiple antenna channels. We do not consider OFDM modulations or multi-user communications. However the ideas and principles described in this thesis report are applicable to OFDM with few changes. The direct practical issue of this thesis would be broadcasting, but the results are also transposable to multi-user techniques.

The outline of the thesis is:

- In Chapter 1, we introduce the multiple antenna channel and its mathematical model. We then introduce the essential material for an information theorical analysis of multiple antenna channels. The fundamental limits of an ergodic channel is Shannon capacity, we can also derive a discrete-input mutual information which is a more limiting quantity. For block fading channels, we recall that Shannon capacity is null, we derive the outage probability with Gaussian and discrete input. Next we recall the recently introduced diversity-multiplexing tradeoff which enables to see how optimal a given system is for multiple antenna channels and high data rates. Finally, we define the Singleton bound on the diversity when the transmitter rate is constant.
- In Chapter 2, we describe the system model and notations of a bit-interleaved coded modulation applied to multiple antenna channels. The receiver is supposed to be iterative in order to achieve quasi-optimal performance at feasible complexity and focus on the essential limitations imposed by the channel. After the presentation of the optimality conditions, we derive performance estimations for ergodic and block fading multiple antenna channels. These performance evaluations are based on the exact computation of the pairwise error probability. Next, classical upper bounding techniques such as union bound or tangential sphere bounds are used to estimate the optimal achievable frame error rate and bit error rate.
- In Chapter 3, we focus on the transmitter optimization. We decompose the BICM onto different blocks and optimize them independently before considering the global optimization. First, the labeling optimization is considered, we show how to achieve high potential gains, in particular for ergodic channels. Next, we consider linear precoding and introduce the conditions of optimality for ergodic, quasi-static and block fading channels. We describe a new construction of linear precoders that provide quasi-optimal coding gains for a given target diversity. We then consider the Singleton bound on the diversity order to determine the minimal precoder size that guarantees full diversity. Finally, we optimize interleavers in order to approach the perfect interleaving conditions.
- In Chapter 4, we study the receivers for bit-interleaved coded modulations and describe in detail the maximum likelihood lattice sphere decoder algorithm. We then introduce a new soft-input soft-output detector based on the a posteriori probability detection over a spherical list (soft-input soft-output sphere decoder). A classical soft-input soft-output minimum mean square equalizer is then described and some complexity reductions are considered. We then compare the complexity of such receivers and show near-capacity performance.

Finally, conclusions and future work perspectives are given. We report some complementary material in the appendices.

Chapter 1

Generalities about multiple antenna channels

Introduction

Multiple antenna channels became a widespread solution for near future wireless telecommunication systems. The receive antennas naturally enhance the performance providing multiple independent observations of the transmitted signal. Depending on the separation between the transmit antennas, the receiver observes correlated or independent observations of the transmitted signal. If the transmit antennas are not spatially de-correlated, the phased array antennas can produce single and multiple beams that allow spatial selectivity. This technique is particularly useful in downlink, where the base station can locate the receiver and transmit in a pinpointed direction with a lower amount of power. Moreover, the processing complexity is mainly at the transmitter end, which enhances the mobile phones autonomy. Beamforming techniques will not be discussed in this thesis report, which focuses on multiple antenna diversity techniques. When the transmit antennas are separated by a distance greater than half the wavelength, the observations at the receiver are supposed to be independent. In this case, the transmit antennas are basically used to either

1. transmit the same symbol over all the transmit antennas in a way to enhance the performance
2. or transmit different symbols over the transmit antennas in a way to enhance the data rate

These spatial diversity techniques are relevant in the uplink, when the transmitter has a limited complexity and the receiver should recover the information of multiple interfering transmitters. Moreover, this could be used to provide diversity for downlink reception at the handset, especially if it is stationary and does not observe temporal diversity. If the handset is moving fast, good performance is naturally provided by the temporal diversity. If a target error rate is fixed, the data rate can be adapted thanks to a channel feedback from the receiver. The tuning possibilities are enhanced thanks to the multiple transmit antennas and excellent data rates can be achieved in the case of *good* links.

In this first Chapter, we will present the channel mathematical model and its validity in Section 1.1. Then, we will present the state of the art of digital communication systems for

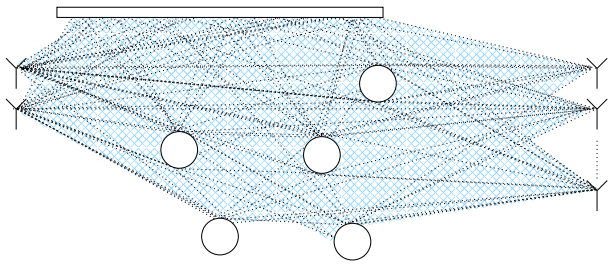

Figure 1.1: Rich scattering environment. Multiple antennas system.

multiple antenna channels in Section 1.2. In Section 1.3, we will expose the fundamental limits of multiple antenna channels, i.e., the Shannon capacity limit, the mutual information with discrete input, the outage error probability for block fading channels and the diversity-multiplexing tradeoff. We will also consider the coded modulations and the Singleton bound on the diversity order, depending on the code rate.

1.1 Multiple antenna channel model

In this section, we will present the multiple antenna channel model and its validity. Let us consider a rich scattering environment and a channel with multiple transmit and receive antennas. Wireless communications experience multi-path propagation because the signal is reflected from nearby surfaces on its way to a receiver. An example of some propagation paths are drawn in Fig. 1.1. Multi-path propagation causes dispersions in delay, frequency and spatial domains, and each antenna receives an infinity of different versions of the transmitted signals, each having a different attenuation, phase and propagation delay.

The main channel parameters are the coherence time and bandwidth. If the signal bandwidth is larger than the channel coherence bandwidth, a *frequency selectivity* is experienced. In this case, the multipath spread of the channel is longer than the signal time period and inter-symbol interference (ISI) is experienced after the channel digitalization. Some techniques such as Orthogonal Frequency Division Multiplex (OFDM) are used to spread the signal in the frequency domain and absorb the ISI. Without ISI, all the transmitted energy is collected with a matched filter into a single coefficient called *fading*. The paths summation provides a random variable, supposed to be complex Gaussian thanks to the central limit theorem.

The antennas are supposed to be sufficiently separated to observe very different path configurations, which lead to independent random variables. Finally, the system model is the following: each equivalent path between each transmit and receive antenna experiences a complex Gaussian attenuation of zero mean and unit variance ($\mathcal{N}_{\mathbb{C}}(0,1)$), as shown on Fig. 1.2.

When the channel coherence time is small enough, the channel is said to be ergodic, i.e., the random variables from one time period to another are independent. This situation for example occurs when a handset is moving fast or when an interleaver is used. If the coherence time is longer than a frame transmission length, the channel does not vary and is said to be quasi-static. However, we assume that the channel realizations are independent from frame to frame. Finally, we consider the case of block fading channels where n_c independent channel realizations occur during a frame. An example of block fading channel is given by the frequency hoping over a

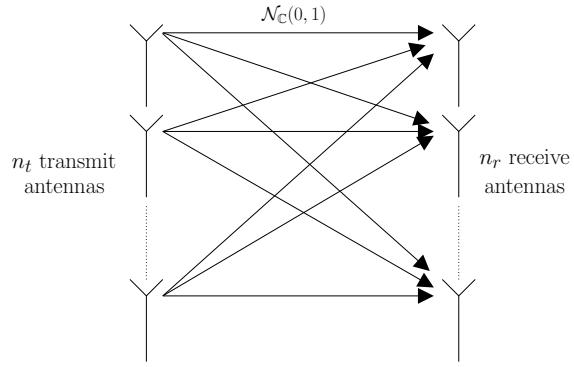

Figure 1.2: Non-frequency-selective MIMO channel Model.

quasi-static channel, where the different frequencies are separated by more than the coherence bandwidth.

As a remark, the block fading channel model for a frame transmitted over L time periods includes the quasi-static channel $n_c = 1$ and the ergodic channel $n_c = L$.

1.2 State of the art in digital communications for multiple antenna channels

Channel coding techniques for MIMO channels, commonly known as space-time coding can be classified into four major categories: multi-dimensional trellis coded modulations, space-time block coding, multilevel coding and bit-interleaved coded modulations. Each technique will be briefly presented in the following.

1.2.1 Trellis coded modulations

A multi-dimensional trellis coded modulation (TCM) [93][85] is a bandwidth efficient technique that combines an error-correcting code and a modulation scheme. It includes Ungerboeck-like coded modulations and the simple case of a classical convolutional code where each trellis transition is associated with one channel use. Trellis-based space-time codes provide diversity and some coding gain at additional encoding/decoding complexity. They usually perform better than space-time block codes, but their optimization is much more complex. There is no way to search for good codes that maximize the rank of certain codeword matrices, only few good codes are known. We notice that an inner full rank code can be added to improve the BER performance via interleaving gain.

1.2.2 Space-time block codes

The space-time block codes (STBC) consist of the transmission of $R_{\mathcal{C}}.n_t.s$ symbols over s time periods and n_t transmit antennas. The code rate is equal to $R_{\mathcal{C}}$. Usually, the transmission scheme is represented by an $n_t \times s$ matrix whose coefficients are linear combinations of the

symbols to be transmitted. The latency of space-time block coding is minimal compared to other techniques. The first space-time code was proposed by Alamouti [3] in 1998. It is designed for $n_t = 2$ transmit antennas and an arbitrary number of receive antennas n_r and it provides full transmit diversity, i.e., the diversity order is $n_t.n_r$. Some generalization to higher number of transmit antennas have been proposed, such as orthogonal and quasi-orthogonal designs (OD and QOD) [86][53]. Initially, people thought that the rate had to be reduced in order to achieve full transmit diversity but, recently, full-rate full-diversity space-time codes have been proposed for more transmit antennas [7][28][29][30][31][34][70].

Many people are working on this topic that is having a fast and important progress. However, the space-time block codes used alone do not provide sufficient coding gains. There are few studies on the joint design of STBCs and error correcting codes, as proposed in Chapter 3.

1.2.3 Multilevel coding

Since the original work by Imai and Hirakawa [51][99], it has been demonstrated that multilevel coding (MLC) can be applied to all types of channels, i.e., scalar and vector channels. In MIMO channels, different levels for coding are defined on QAM symbols fed at the channel input or directly on the binary labels of those symbols.

1.2.4 Bit-interleaved coded modulation

Combining the original ideas by Zehavi [103][22], Berrou & Glavieux [9], a bit-interleaved coded modulation is built by cascading a convolutional code, a pseudo-random interleaver, a QAM symbol mapper and the MIMO channel.

The main application of BICM to multiple antenna channels was the Bell Laboratories layered space-time (BLAST). It was initially motivated by the capability of canceling the interference of transmit antennas thanks to a greater number of receive antennas. Basically, independent data streams are transmitted over different transmit antennas. At the receiver, an ordered successive interference cancellation is processed from the strongest to the weakest data stream. The main drawback of this initial version of BLAST was the error propagation.

Of course, the concatenated nature of such a transmission scheme allows iterative joint detection and decoding: The receiver starts by an APP detection of the multiple antenna channel followed by a SISO decoding of the convolutional code. The latter procedure is iterated a finite number of times, where the convolutional code extrinsic probabilities are fed back as *a priori* information to the APP detector [15][82]. We will describe in detail the BICM structure and optimize it in the aim of achieving good performance on MIMO channels.

1.3 Information theory for multiple antenna channels

Let us now consider some information theory tools for multiple antenna channels. The fundamental limits presented below are derived from Shannon theory [79] and extended to multiple-input multiple-output channels [87].

1.3.1 Information theory tools: a reminder

We will introduce the main information tools necessary for computing the fundamental limits of MIMO channels [27][5]:

- Let Z and Y be two independent random variables. Their probability densities are $p(z)$ and $p(y)$, respectively. The entropy $\mathsf{H}(Z)$ is defined by

$$\mathsf{H}(Z) = E\left[-\log_2\left(p(z)\right)\right] = \int_z -\log_2\left(p(z)\right)p(z)dz \tag{1.1}$$

  where $E[.]$ denotes the mathematical expectation. The entropy $\mathsf{H}(Z)$ measures the necessary binary information to describe the variable Z. The highest the entropy, the more the randomness of the variable.

- The joint entropy $\mathsf{H}(Z,Y)$ of the two variables Z and Y is defined by

$$\mathsf{H}(Z,Y) = E\left[-\log_2\left(p(z,y)\right)\right] = \int_{z,y} -\log_2\left(p(z,y)\right)p(z,y)dzdy \tag{1.2}$$

  where $p(z,y)$ is the joint probability density of z and y. It measures the necessary binary information to jointly describe the variables Z and Y.

- The conditional entropy $\mathsf{H}(Y|Z)$ is defined by

$$\mathsf{H}(Y|Z) = E\left[\mathsf{H}(Y|Z=z)\right] = E\left[-\log_2\left(p(y|z)\right)\right] = \int_{z,y} -\log_2\left(p(y|z)\right)p(y|z)dzdy \tag{1.3}$$

  It measures the necessary binary information to describe the variables Y having a knowledge on Z.

- The mutual information $\mathcal{I}(Z;Y)$ between Z and Y is defined by

$$\mathcal{I}(Z;Y) = \mathsf{H}(Z) + \mathsf{H}(Y) - \mathsf{H}(Y,Z) = \mathsf{H}(Y) - \mathsf{H}(Y|Z) = \mathsf{H}(Z) - \mathsf{H}(Z|Y) \tag{1.4}$$

  It conversely measures the average supplementary quantity of information offered by Y on Z.

- The capacity C of a discrete memoryless channel with input Z and output Y is the maximal value of $I(Z;Y)$ over all possible probability densities $p(z)$:

$$C = \max_{p(z)}\left(I(Z;Y)\right) \tag{1.5}$$

  This induces that the capacity is obtained by optimizing the probability density function at the channel input.

- The capacity is linked to the system spectral efficiency by the Shannon's channel coding theorem. It is summed up in the following statement: for a given channel, there exists a code that allows error-free transmission across the channel at a rate R, provided $R \leq C$, where C is the channel capacity. Equivalently, if the system rate is fixed, the capacity gives a limit on the signal-to-noise ratio below which error-free transmission is not possible. Since the capacity is a fundamental non-achievable limit, it will be used as a reference to measure the quality of a given transmission system. This is why it is important to compute the Shannon's capacity limit of a given system before the transmitter design

step. For example, the capacity of an additive white Gaussian noise channel for a target rate R is $C = \log_2\left(1 + R\frac{E_b}{N_0}\right)$ bits/complex dimension and is obtained for Gaussian inputs. The signal-to-noise ratio limit is obtained by $\frac{E_b}{N_0} = \frac{2^C-1}{C}$. Using an infinitely good code with quasi-null rate, we obtain the limit $\lim_{C\to 0}\frac{2^C-1}{C} = \ln 2 = -1.6dB$.

Let us now describe the capacity limit for multiple antenna channels.

1.3.2 Capacity of ergodic MIMO channels

Let us first consider the case of ergodic MIMO channels with n_t-dimensional input z and n_r-dimensional output y. The input-output relation is supposed to be:

$$y = zH + \eta \tag{1.6}$$

where η is an n_r-dimensional Gaussian noise vector with covariance matrix $2N_0 I_{n_r}$. Such channel capacity has been expressed in parallel in [87] and [37]. The capacity is achieved for Gaussian input (more precisely for circularly symmetric complex Gaussian input, see [87]), it can be computed by the expectation of the conditional $C_{|H}$ over all possible H, where

$$C = E_H\left[C_{|H}\right] = E_H\left[\log_2\left(\det\left(I_{n_r} + \frac{P}{n_t}H^*H\right)\right)\right] \text{ bits/complex dimension} \tag{1.7}$$

and $P = \frac{E[ZZ^*]}{E[\eta\eta^*]} = \frac{n_t.E_s}{n_r.2N_0}$. Moreover, the capacity can be traced as a function of the bit error rate, which is equal to $\frac{CE_b}{N_0} = \frac{E_s}{2N_0}$. It can be demonstrated that $n_t \times n_r$ MIMO channels capacity in bit/complex dimension is equal to $n_r \times n_t$ MIMO channels capacity.

On Fig. 1.3, MIMO channels capacity are represented for n_t and n_r varying from 1 to 4. We can observe that for a given total number of transmit antennas $n_t + n_r$, the optimum repartition in the sense of capacity is obtained when $n_t = n_r$. We also observe that the slope of the asymptote is linked to $\min(n_t, n_r)$ and that the vertical sliding is linked to $\max(n_t, n_r)$. This is explained as $\min(n_t, n_r)$ fixes the number of equivalent sub-channels and $\max(n_t, n_r)$ the diversity order on each sub-channel. If $\max(n_t, n_r)/\min(n_t, n_r)$ grows to infinity, the capacity tends to $\min(n_t, n_r)C_{awgn}$, where C_{awgn} is the capacity of the additive white Gaussian noise channel.

The Shannon's capacity is given by Gaussian inputs that are impractical. For a given input law $p(z)$ associated with an input Z, the mutual information $\mathcal{I}(Z;Y)$ represents another fundamental limit on the rate or signal-to-noise ratio. This limit is more restrictive than the Shannon's Limit and enables to evaluate the modulation and preprocessing quality. Moreover, we can evaluate the quality of the error correcting code and detection process measuring the gap between the mutual information and the real performance.

Assume that $Z \in \Omega$, a discrete alphabet of $M^{n_t} = 2^{mn_t}$ vectors (e.g a $M - QAM$). We can express the Entropies:

$$\mathsf{H}(Y) = -\int_y p(y)log_2(p(y))dy = -\int_y \sum_z p(y/z)p(z)\log_2\left(\sum_{z'} p(y/z')p(z')\right)dy \tag{1.8}$$

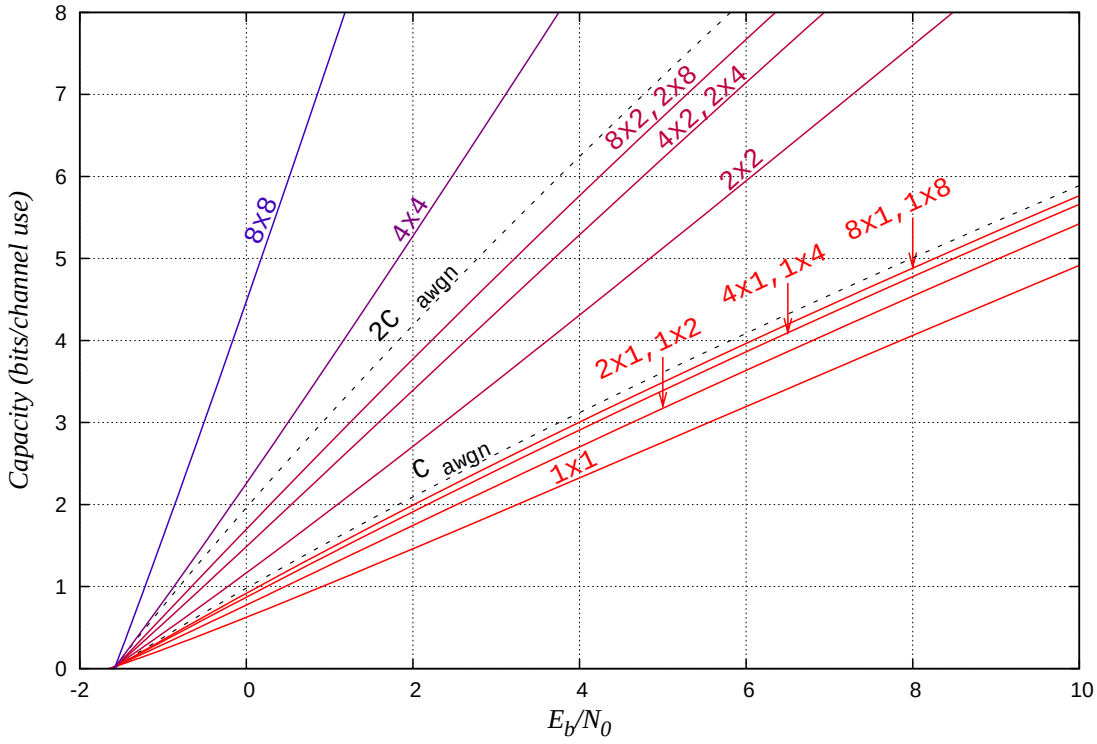

Figure 1.3: Shannon's capacity for MIMO channels

$$\mathsf{H}(Y/Z) = -\sum_{z} p(z) \int_{y} p(y/z) \log_2(p(y/z)) dy \tag{1.9}$$

The mutual information is given by

$$\mathcal{I}(Z;Y) = \mathsf{H}(Y) - \mathsf{H}(Y|Z) = mn_t - \frac{1}{M^{n_t}} \sum_{x} \int_{y} p(y/x) \log_2 \left(\frac{\sum_{x'} p(y/x')}{p(y/x)} \right) dy \tag{1.10}$$

The integral over y reduces to an integral over H and η. This mutual information does not exist in a closed form expression, we can use a Monte-Carlo simulation to evaluate it (see Appendix D for some simplifications of the mutual information computation).

We can observe that the mutual information saturates to the spectral efficiency mn_t. For low signal-to-noise ratios, the mutual information has the behavior of the Gaussian input capacity. If n_r tends to infinity, the mutual information tends to the AWGN case.

In Fig. 1.4 we notice that the mutual information of a $1 \times n_r$ MIMO channel with QPSK input saturates to 2 bits per channel use. In Fig. 1.5 we notice that the mutual information of a $1 \times n_r$ MIMO channel with 16QAM input saturates to 4 bits per channel use. In Fig. 1.6 the mutual information of a $2 \times n_r$ MIMO channel with QPSK input saturates to 4 bits per channel use. This shows us that from an information theory point of view, if the spectral efficiency is fixed to mn_t, the best performance is obtained by minimizing m and maximizing n_t.

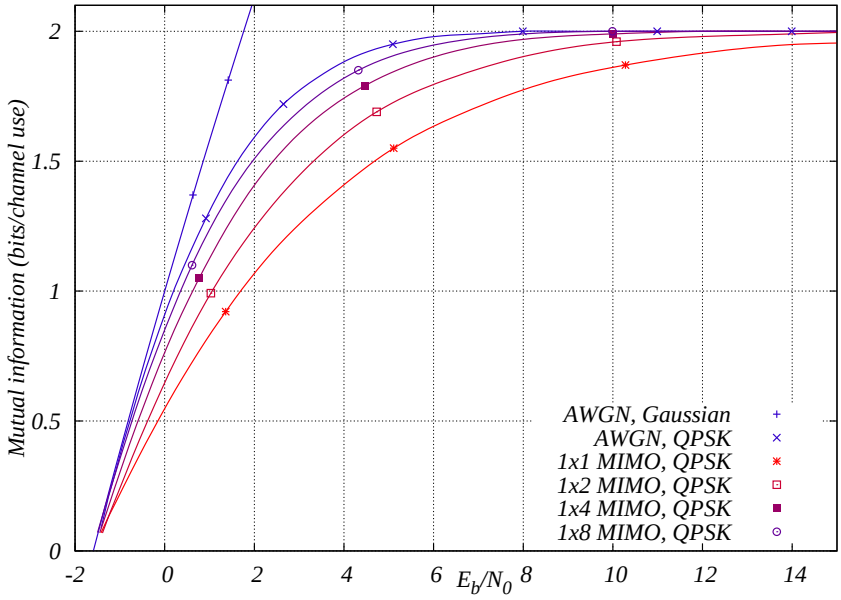

Figure 1.4: Mutual Information for QPSK input.

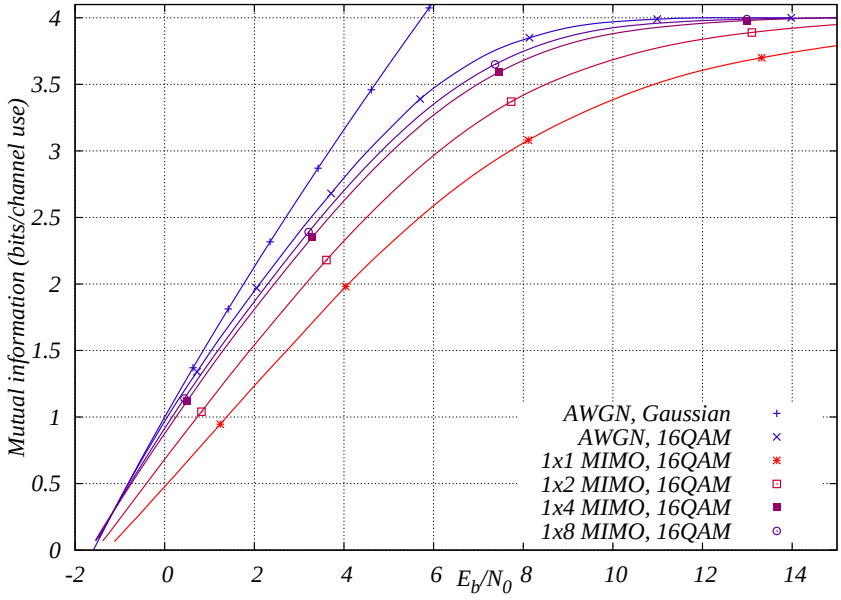

Figure 1.5: Mutual Information for 16-QAM input.

1.3.3 Outage probability for block-fading MIMO channels

The conditional capacity C_H is a random variable with probability density $p_{C_H}(x)$. Over ergodic channels, the capacity is the mean of C_H because an infinite length codeword sees an infinite number of channel states. However, when the channel is quasi-static, one codeword only sees one channel realization. For a given channel matrix H, we deduce an instantaneous capacity C_H. Consider a fixed transmission rate R. If $R < C_H$, there exists at least one code that provides error-free transmission. However, if $R > C_H$ every code would lead to a packet loss. Based on this observation, we can deduce that the capacity of quasi-static channels is null. Indeed, for

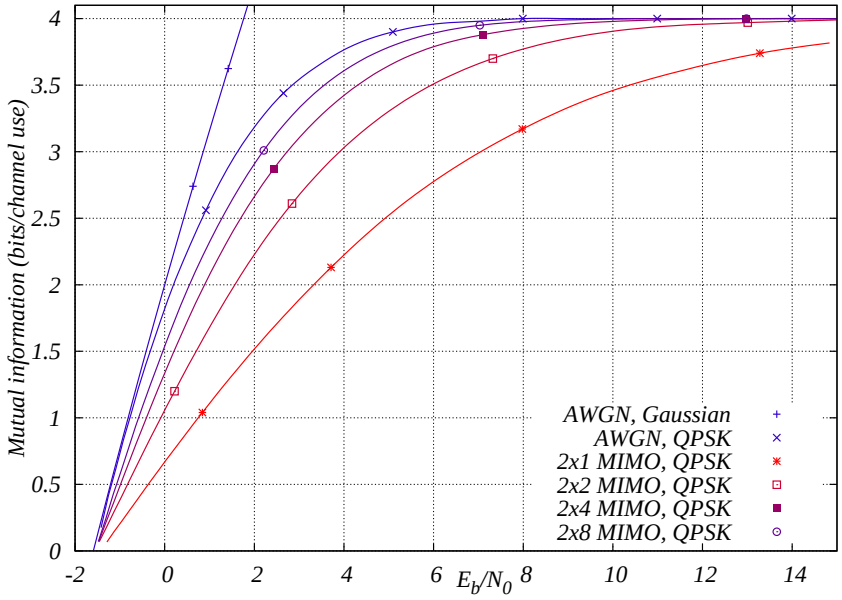

Figure 1.6: Mutual Information for QPSK input.

a fixed non-null R, there always exists a *bad* channel realization such that $R > C_H$. We can consider the probability P_{out} that such *outage* situation occurs, i.e.,

$$P_{out} = P(C_H < R) = \int_0^R p_{C_H}(x)dx \tag{1.11}$$

This outage probability gives a limit on the frame error rate only achievable with an infinitely good code and Gaussian input. We can obviously derive the outage probability with discrete input from the mutual information $\mathcal{I}_H(Z;Y)$

$$P_{out,\Omega} = P(\mathcal{I}_H(Z \in \Omega; Y) < R) \tag{1.12}$$

When the channel is block fading with parameter n_c, we can multiplex the data without changing the performance. We consider an equivalent quasi-static channel with block diagonal matrix

$$H_b = \text{diag}\,(H_1, \ldots, H_{n_c}) \tag{1.13}$$

where all blocks are $n_t \times n_r$ matrices corresponding to the n_c different channel realizations. Moreover, observing that H_b corresponds to n_c channel uses, we have

$$P_{out,n_c} = P\left(\frac{1}{n_c}\log_2 \det\left(I_{n_r n_c} + \frac{P}{n_t}H_b^* H_b\right) < R\right) \tag{1.14}$$

$$= P\left(\frac{1}{n_c}\sum_{i=1}^{n_c}\log_2 \det\left(I_{n_r} + \frac{P}{n_t}H_i^* H_i\right) < R\right) \tag{1.15}$$

The outage probability of a block fading MIMO channel is equal to the probability that the averaged instantaneous capacity (over the n_c realizations) is lower than the fixed rate R. Clearly,

the more the number of different realizations n_c, the lower the outage probability. This induces

$$P\left(\lim_{n_c\to+\infty}\frac{1}{n_c}\sum_{i=1}^{n_c}\log_2\det\left(I_{n_r}+\frac{P}{n_t}H_i^*H_i\right)<R\right)=P\left(C<R\right)=\mathbb{I}_H\left(C^{-1}(R)-x\right) \quad (1.16)$$

where $C^{-1}(R)$ is the minimal signal-to-noise for the existence of error-free rate R transmission and $\mathbb{I}_H$ is the Heaviside step function. Fig. 1.7 shows the outage probability for a single antenna block fading channel with n_c blocks for a rate equal to 1 and Gaussian input. The capacity limit for $R = 1$ bit per channel use is 0.96 dB.

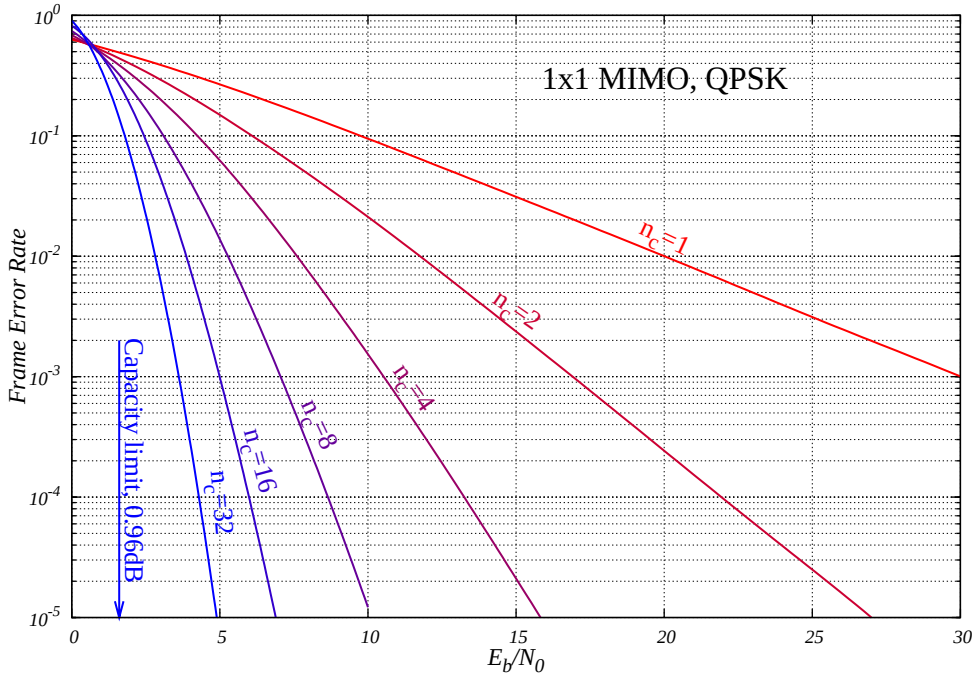

Figure 1.7: Outage probability, $R = 1$ bit per channel use, 1×1 MIMO channel.

1.3.4 Diversity-multiplexing tradeoff

We will present another fundamental limit called diversity-multiplexing tradeoff, presented in [104]. We can observe from subsection 1.3.2 that asymptotic behavior of the capacity of an ergodic MIMO channel is

$$C \underset{N_0\to 0}{\sim} \min(n_t, n_r)\log_2\left(\mathrm{SNR}\right)+\mathcal{O}(1) \quad (1.17)$$

where $\mathrm{SNR}=\frac{E_s}{2N_0}$. The single antenna system behaves like $\log_2(\mathrm{SNR})$, whereas the capacity of a MIMO channel grows linearly with $\log_2(\mathrm{SNR})$, the linear factor $\min(n_t, n_r)$ is called the multiplexing gain.

Consider a family of codes $\mathcal{C}$. Assume that for each signal-to-noise ratio value $\mathrm{SNR} = E_s/2N_0$, a code $\mathcal{C}(\mathrm{SNR}) \in \mathcal{C}$ with rate $R_{\mathcal{C}}(\mathrm{SNR})$ and error rate $P_e(\mathcal{C}(\mathrm{SNR}))$ is chosen. The

multiplexing gain r of such a family of codes is defined by

$$r \triangleq \lim_{SNR\to\infty} \frac{R_{\mathcal{C}}(\mathrm{SNR})}{\log_2 \mathrm{SNR}} \tag{1.18}$$

Notice that $r/\min(n_t, n_r) \sim R_{\mathcal{C}}(\mathrm{SNR})/C(\mathrm{SNR})$ indicates how far the system is operating from the Shannon limit. The diversity gain is obtained by the asymptotic error exponent

$$d \triangleq \lim_{SNR\to\infty} -\frac{\log_2 \left(P_e(\mathcal{C}(\mathrm{SNR}))\right)}{\log_2 \mathrm{SNR}} \tag{1.19}$$

The multiplexing-diversity tradeoff (r, d) gives the information about the optimality of a family of codes for very high data rates. However, it does not give any information on the coding gain. For example, if we choose a code with a constant rate that achieves the full-diversity order $n_t n_r$, the multiplexing-diversity tradeoff is $(0, n_t n_r)$. If a family of codes has maximal multiplexing gain, the data rates and the number of possible codewords respectively evolves linearly and exponentially with the capacity, and the achievable diversity disminishes. This induces that the best multiplexing-diversity point for full-multiplexing is $(n_t, 0)$.

There exists an optimal multiplexing-diversity tradeoff for any value of r, denoted $d^*(r)$:

$$d^*(r) = (n_t - r)(n_r - r), \quad 0 \le r \le \min(n_t, n_r) \tag{1.20}$$

The optimal multiplexing-diversity tradeoff shows that the diversity and multiplexing gains evolve inversely from each other. The extrema values are the full diversity gain $d^*(0) = n_t n_r$ and the full multiplexing gain $r^* = \min(n_t, n_r)$ for $d = 0$.

For block-fading channels with n_c blocks,the optimal tradeoff $d^*(r)$ is

$$d^*(r) = n_c(n_t - r)(n_r - r), \quad 0 \le r \le \min(n_t, n_r) \tag{1.21}$$

Fig. 1.8 illustrates the optimal diversity multiplexing tradeoff for a $4 \times n_r$ quasi-static MIMO channel. Again, we see how the receive antenna increases the fundamental limit, which induces a simplification of the transmission scheme optimization. If n_r tends to infinity, we approach the ideal case when both maximal diversity and multiplexing gain are achieved. Next, in Fig. 1.9, we observe the gain obtained with an increasing number of channel states n_c. Fig. 1.11 illustrates the optimal multiplexing-diversity tradeoff for system configurations having a maximal diversity order $n_c n_t n_r = 16$. We observe that advantaging the spatial diversity gives a better optimal multiplexing-diversity tradeoff.

1.3.5 Singleton bound for block fading channels

In most digital communication systems, a binary error correcting code is used to protect the information bits. This is the case for BICM, which is the system we will focus on in this thesis report.

In [54][55][68], the authors consider bounds on the diversity for the transmission of a binary code on block fading channels. Let us consider a binary code $\mathcal{C}$ of rate $R_{\mathcal{C}}$ and length $L_{\mathcal{C}}$ coded bits. The block fading channel is supposed to have $n_{\mathcal{C}}$ independent blocks. The diversity is upper-bounded by $n_{\mathcal{C}}$ and the minimal Hamming distance of the binary code which is denoted

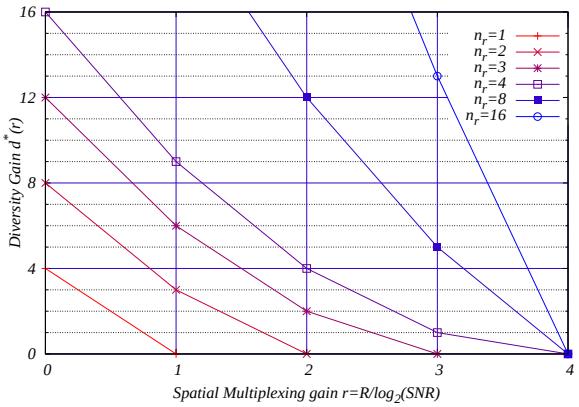

Figure 1.8: Optimal rate-diversity tradeoff for $n_t = 4$ quasi-static MIMO channels.

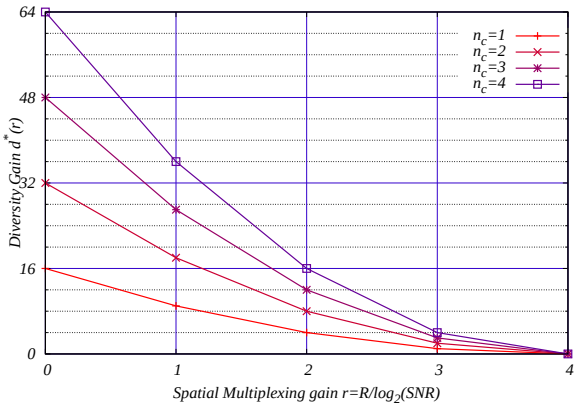

Figure 1.9: Optimal rate-diversity tradeoff for 4×4 block fading MIMO channels.

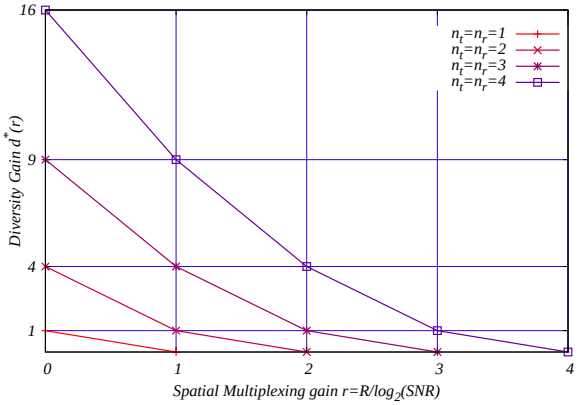

Figure 1.10: Optimal rate-diversity tradeoff for $n_t = n_r$ and n_c=1.

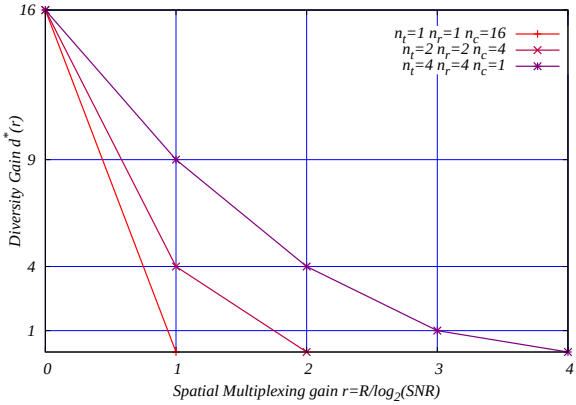

Figure 1.11: Optimal rate-diversity tradeoff for maximum diversity order 16.

d_{Hmin}. We will consider the Euclidean code $\mathcal{C}_E$ that corresponds to the transmission of all the codewords over the block fading channel. All the symbols transmitted on the same block are grouped into a hyper-symbol. The code $\mathcal{C}_E$ has a length $n_{\mathcal{C}}$ and an alphabet size $2^{L_{\mathcal{C}} R_{\mathcal{C}}/n_C}$. The minimal Hamming distance between two coderwords gives the diversity d upper bounded by the Singleton bound of the code $\mathcal{C}_E$ [54][55][68]:

$$d \leq 1 + \lfloor n_c \left(1 - R_{\mathcal{C}}\right) \rfloor \tag{1.22}$$

Fig. 1.12 draws the singleton bound values for a single antenna channel and an increasing number of blocks n_c. The full diversity is achieved if and only if $R_{\mathcal{C}} \geq 1/n_c$. In the following, we will consider the Singleton bound assuming that a detector perfectly converts an $n_t \times n_r$ MIMO block fading channel with n_c blocks into a $1 \times n_r$ block fading channel with $n_t n_c$ blocks. The Singleton bound will give the maximum achievable diversity for a given code rate $R_{\mathcal{C}}$.

As a remark, it was shown in [45] that the discrete input outage capacity is also constrained by the Singleton bound.

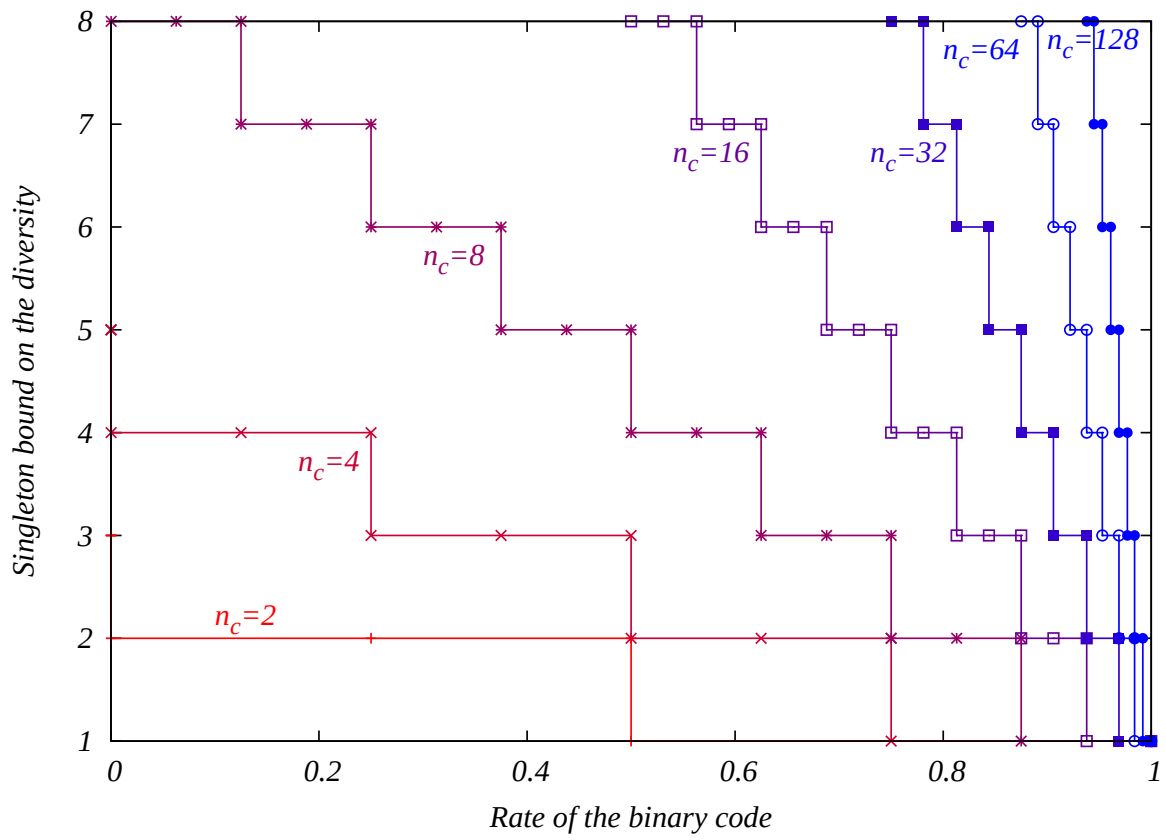

Figure 1.12: Singleton bound on the diversity order as a function of the rate of the error correcting code and the number of blocks of a block-fading channel.

Conclusions

We have presented the multiple antenna block fading channel model. We saw that the channel capacity (or outage probability) gives the fundamental SNR limit for high performance. Furthermore, we described the optimal multiplexing diversity tradeoff which gives an information on the quality of a transmission scheme for very high data rates. The two fundamental limits are enhanced by increasing the number of receive antennas. Moreover, we deduced that the spatial transmit diversity is preferable to time diversity in terms of information theory.

Chapter 2

BICM model and performance

Introduction

On AWGN channels, it is shown that the Shannon channel capacity is achieved for gaussian inputs. If the frame length is sufficiently high, the squared Euclidean square norm of the transmitted signal is quasi-deterministic since it has a high order chi-square distribution, and the phase is uniform. This sphere-hardening phenomenon tells us that a good coded modulation should place the codewords close to the surface of a sphere. The ideal Shannon code is located on this Shannon's sphere. In a BICM, thanks to the interleaver, the codewords have a squared Euclidean square norm with very low variance, which implies that they lie close to the surface of the Shannon's sphere. The coded modulation may be seen as a quantizer of this sphere and built in order to find the most uniform repartition of the codewords. This leads to larger Voronoi regions and minimizes the error rate.

At the output of a MIMO fading channels, the Shannon's sphere becomes an ellipsoid. Before transmission over the channel, the BICM aims at finding a good distribution of the points on the surface of the sphere since it is known to be capacity achieving. Designing a good space time code is equivalent to ensure large and uniform Voronoi regions at the surface of the ellipsoid, whatever the channel realization We show that the ideal BICM configuration achieves such a condition and how to design a practical system that approaches this condition.

Moreover, we have to focus on the construction of a low complexity decoder associated to such a code. The growing importance of iterative and probabilistic processing of information in communication systems during the last decade allows for exceptional performance on different types of data transmission channels. Graph codes for binary channels have been extensively analyzed [11][52][59][60][64][76][77] and bit-interleaved coded modulations (BICM) for non-binary channels became a widely known standard technique for coded modulations with and without frequency selective channels [103][22][15][57]. Under realistic conditions and without any mild theoretical constraint, the nature of such concatenated systems does not allow for the derivation of closed-form expressions for the error rate versus the number of decoding iterations.

This chapter first describes the bit-interleaved coded modulation (BICM) transmitter scheme applied to multiple antenna channels. Then the BICM iterative receiver will be described and the "a posteriori probability" (APP) exhaustive detector detailed. A new exact computation

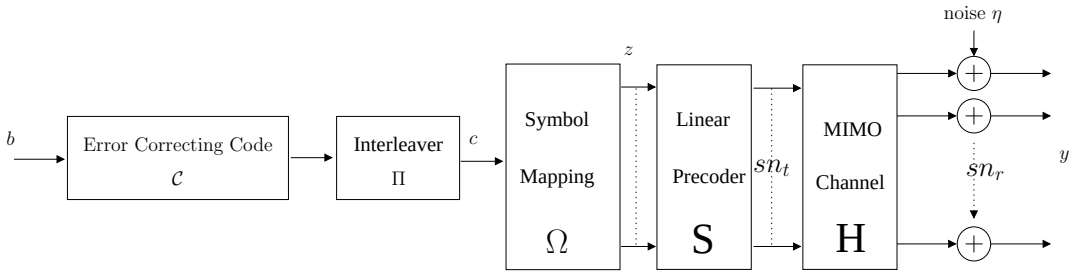

Figure 2.1: Bit-interleaved coded modulation transmitter and multiple antenna channel model.

of the codeword pairwise error probability will then be introduced in the perfect interleaving context. A union bound can then be computed to estimate the asymptotic performance when the channel is ergodic and the interleaving ideal.

Moreover, in the case of ergodic channels, an analogy between BICM with iterative joint detection and decoding performance and the maximum likelihood decoding performance is developed. This analogy is available when the channel interleaving is ideal and when the signal to noise ratio is sufficiently high to achieve a perfect convergence of the iterative processing.

2.1 Bit-Interleaved Coded Modulation with iterative decoding

2.1.1 Structure of the Bit-Interleaved Coded Modulation transmitter

The transmitter scheme is given by the following fundamental block concatenation: A binary error-correcting code $\mathcal{C}$ (e.g., a convolutional code) followed by a deterministic interleaver Π, a symbol mapper (e.g., for a QAM modulation), a full-rate space-time spreader S (i.e., a linear precoder) and a serial-to-parallel converter. Fig. 2.1 illustrates the BICM transmitter structure. We will now describe the notations and the role of each fundamental block.

a) The error correcting code:

The transmission of digital data with the minimum error rate is the objective of any telecommunication system. In many of those systems, the data rate is forfeited to binary protection by the way of an error correcting code. Let $R_{\mathcal{C}}$ denote the coding rate of the error correcting code $\mathcal{C}$ and b the information word at the encoder input. The encoder applies the bijection between the input information word b and the codeword $c \in \mathcal{C}$. The length of c is $1/R_{\mathcal{C}}$ times higher than the length of b. We can choose the error correcting code among a wide variety containing the following non-exhaustive list:

- Linear block codes: cyclic or non-cyclic linear block codes (BCH, Reed-Solomon). They have been developed in the 60-70's and used for high rate systems.
- Trellis codes: non-recursive non-systematic convolutional (NRNSC) codes, recursive systematic convolutional (RSC) codes. Traditionally, convolutional codes are considered for BICM. Indeed, they have the double advantage of having simple and low complexity encoders, maximum likelihood (ML) and soft-input soft-output (SISO) decoders. Indeed,

the code can be represented by a trellis, and the Viterbi algorithm [95][38] with Hamming distance (defined on the Galois field $GF(2^n)$) can be applied for maximum likelihood decoding. The trellis structure can also be exploited for SISO decoding via the forward-backward algorithm [4]. A convolutional code by default has an infinite length. However, finite linear block codes can easily be extracted selecting a finite window of the trellis. A coding gain enhancement is obtained by forcing the first and last states to 0, but this introduces a slight code rate reduction. The code is defined by its octal polynomial $(g_1, \ldots, g_{N_\mathcal{C}})_8$. It takes $K_\mathcal{C}$ bits and returns $N_\mathcal{C}$ bits by trellis transition. The constraint length of the code is denoted $l_\mathcal{C}$, and the codeword length is $L_\mathcal{C} N_\mathcal{C}$ coded bits. The code rate is $R_\mathcal{C} = [K_\mathcal{C} - (l_\mathcal{C} - 1)/L_\mathcal{C}]/N_\mathcal{C}$, but we consider $L_\mathcal{C} \gg l_\mathcal{C}$ which leads to $R_\mathcal{C} \simeq K_\mathcal{C}/N_\mathcal{C}$. As a remark, NRNSC codes have a slight coding advantage when compared to RSC codes with the same coding rate.

- Concatenated codes: concatenated codes have been discovered in the 60's [42][39]. We generally distinguish the turbo-codes from low density parity check (LDPC) codes. The turbo-codes are based on the serial or parallel concatenation of two convolutional codes, the revolutionary papers [9][10][8] gave birth to the iterative decoding techniques of concatenated codes. The LDPCs [42][66][67] are based on multiple simple parity equations grouped into sparse matrices. A factor graph can be constructed for the iterative decoding, based on message passing between the multiple parity check nodes [59].

b) The channel interleaver:

The interleaver Π scrambles the $L_\mathcal{C} N_\mathcal{C}$ coded bits. This is the main component of the BICM. It is crucial when performing iterative joint detection and decoding because it enhances the independence between extrinsic and a priori probabilities both in the soft-input soft-output detector and decoder. It is also very important for ML decoding (if such a decoding is tractable) because it limits the interference in the same time period between two erroneous bits of an error event. The interleaver Π can be a pseudo-random (PR interleaver) or a semi-deterministic interleaver with some deterministic constraints as described in Section 3.4.

c) The symbol mapper:

The interleaved coded bits are demultiplexed into blocks of m bits fed to the mapper that converts them into a constellation symbol. The bijection between the bit vectors and constellation symbols is called mapping or labeling. The number of points in the constellation is equal to $M = 2^m$. At each channel use, the mapper reads $m \times n_t$ coded bits and generates n_t modulation symbols. To make the reading easier, the n_t-dimensional constellation Ω will equally make reference to the set of symbols or their binary labelings. The mapping is not unique and can be very influent on the system's performance. The Gray mapping is one of the most famous, as it minimizes the number of different bits between two neighbors in the constellation, which minimizes the bit error rate of an uncoded system. We will see in this thesis report that in many cases, we can achieve better performance by using other mapping techniques, and even demonstrate that the Gray mapping is the worst for BICM with ideal interleaving. All along this thesis report, we will consider QAM (Quadrature Amplitude Modulations) as they achieve a good compromise between spectral efficiency (in bits/s/Hz or bits/dim) and performance. Moreover, they give a lattice constellation structure to the system and the access to the lattice theory toolbox, both

for the transmitter and receiver optimizations. If a M-QAM is used on each transmit antenna, the transmitted symbol energy per transmit antenna is equal to:

$$E_s = 2.\frac{M-1}{3} \tag{2.1}$$

d) The linear precoder:

The linear precoder S spreads the QAM symbols over s time periods. It converts the $n_t \times n_r$ vector channel into an $N_t \times N_r$ vector channel, where $N_t = n_t s$ and $N_r = n_r s$. The $N_t \times N_r$ matrix S multiplies a vector of N_t QAM symbols $z_k = (z_{k,1}, z_{k,2}, \ldots, z_{k,N_t})$ at the mapper output, generating N_t symbols to be transmitted during s time periods. Vector z_k is the k^{th} vector to be precoded. The role of S is to spread the transmitted symbols over a higher number of channel states, for example to exploit a time or space diversity. We suppose that S is normalized, so it does not act as an amplifier. This is satisfied if the square Frobenius norm $\|.\|_{\mathcal{F}}$ of S is equal to N_t:

$$\|S\|_{\mathcal{F}}^2 = \sum_{i=1}^{N_t}\sum_{j=1}^{N_t} S_{i,j}^2 = N_t \tag{2.2}$$

e) Channel input-output relation:

Without space-time spreading ($s = 1$ and S is the identity matrix), the channel path connecting antenna i to antenna j has a complex Gaussian distributed gain h_{ij}, where $H = [h_{ij}]$, $E[h_{ij}] = 0$, $E[|h_{ij}|^2] = 1$, $i = 1 \ldots n_t$ and $j = 1 \ldots n_r$. Here, the symbol $E[.]$ denotes mathematical expectation. The MIMO channel coefficients h_{ij} are supposed to be statistically independent. The correlated MIMO channels will be left for further studies. Denote $\mathcal{H}$ the set of channel realizations seen during the transmission of a codeword.

We assume a block fading channel with n_c distinct channel realizations during a code word. We denote n_s the number of distinct channel realizations during a precoded symbol. To simplify notations, we assume that n_s divides n_c. We will call "channel state" the $1 \times n_r$ SIMO channel associated to one of the n_t transmit antennas of one of the n_c channel realizations. The channel experienced by precoded symbol k is represented by a $N_t \times N_r$ block-diagonal matrix H_k with s blocks of size $n_t \times n_r$. We assume that each of the n_s channel realizations is repeated s/n_s times. Matrix H_k is organized as follows:

$$H_k = \text{diag}\left(H_k^{[1][1]}, \ldots, H_k^{[1][s/n_s]}, H_k^{[2][1]}, \ldots, H_k^{[2][s/n_s]}, \ldots, H_k^{[n_s][1]} \ldots, H_k^{[n_s][s/n_s]}\right) \tag{2.3}$$

where $H_k^{[t][i]}$ denotes the $n_t \times n_r$ complex matrix representing the i-th block of the t-th channel realization experienced by the precoded symbol k. Elements of $H_k^{[t][i]}$ are independent complex Gaussian variables with zero mean and unit variance. Let $\mathcal{H}$ denote the set of channel realizations observed during the transmission of a codeword. Thanks to the extended channel matrix, we write the channel input-output relation as:

$$y_k = x_k + \eta_k = z_k S H_k + \eta_k \tag{2.4}$$

where $y_k \in \mathbb{C}^{N_r}$ and each receive antenna is perturbed by an additive white complex Gaussian

noise $\eta_{k,j}$, $j = 1 \dots N_r$, with zero mean and variance $2N_0$. Thanks to linear precoding, the $n_t \times n_r$ MIMO n_c-block fading channel is converted into an $N_t \times N_r$ MIMO N_c-block fading channel where $N_c = n_c/n_s$. If $n_s = n_c$, we say that full time spreading is performed. If $n_s = 1$, the precoder experiences a quasi-static $n_t \times n_r$ MIMO channel. In the following, if a single precoded symbol is considered, the index k will be omitted and "precoding time period" will refer to a transmission over SH, i.e., over s time periods.

The global spectral efficiency is $R_{\mathcal{C}} \times m \times n_t$ bits per channel use. We consider a binary signal-to-noise ratio (E_b/N_0) at the receiver, where E_b is the band-pass information bit energy at the receiver, E_c is the band-pass coded bit energy at the receiver and $N_0/2$ the noise band-pass spectral density. In the case of M-QAM, we have

$$\frac{E_b}{N_0} = \frac{E_c}{N_0 R_{\mathcal{C}}} = \frac{E_s n_r}{2N_0 R_{\mathcal{C}} m} = \frac{n_r \left(2^m - 1\right)}{3N_0 R_{\mathcal{C}} m} \tag{2.5}$$

Usually, we consider the logarithmic signal-to-noise ratio $SNR = 10 \log_{10} \left(\frac{E_b}{N_0}\right)$ in decibels (dB).

f) The global Euclidean code $\mathcal{C}_E$:

The concatenation of the binary error correcting code $\mathcal{C}$, the interleaver Π, the mapper Ω, the linear precoder S and the channel describes a global Euclidean code. If we suppose that the error correcting code has a length $L_{\mathcal{C}} N_{\mathcal{C}}$ and a rate $R_{\mathcal{C}} = K_{\mathcal{C}}/N_{\mathcal{C}}$, the global Euclidean code $\mathcal{C}_E$ converts $L_{\mathcal{C}} K_{\mathcal{C}}$ information bits into a complex $L_{\mathcal{C}} N_{\mathcal{C}}/m$-dimensional point.

2.1.2 Structure of the iterative receiver

An ideal BICM receiver would directly perform a maximum-likelihood decoding on the set $\mathcal{C}_E$ of transmitted codewords. However, it requires an exhaustive search among the $2^{K_C L_C}$ codewords, which is intractable. All existing receivers use the concatenated structure of the BICM to split the reception into several steps. In this thesis report, we assume perfect synchronization and channel estimation. Thus, the receiver, as depicted on Fig. 2.2, is divided in two main elements: a soft-input soft-output (SISO) APP QAM detector, which acts as a soft-output equalizer for both the space-time spreader and the MIMO channel, converting the received point y into information on the coded bits in the estimated coded sequence $\hat{c}$, and a SISO decoder for $\mathcal{C}$, improving the information on coded bits and estimating the information bit sequence $\hat{b}$. The differences between all possible receivers depend essentially on the hardness or softness of the exchanged information. The detector has always a soft input y.

a) The decoder

Decoding of an error correcting code has always been a topic of interest for a wide population of researchers. Obviously, the decoder existence depends on the code nature. We can describe the state of the art of the most useful decoders for some families of error correcting codes:

- Algebraic decoders: for algebraic codes (RS, BCH), there exist many HIHO algebraic decoders, the most efficient being proposed in [83]. SIHO decoding of algebraic codes have been addressed in [56], but SISO decoding is still an open problem.

- Decoders for trellis codes: HIHO and SIHO , e.g., Viterbi algorithm (VA) [95][38]. SISO, e.g., Soft Output Viterbi algorithm (SOVA) [46], forward-backward (FB) [4]. The forward-backward algorithm computes the exact a posteriori probability (APP) using the trellis structure of the code. A trellis is a particular case of a graph, the forward-backward is a particular case of graph decoding.
- Iterative decoders: if the constituent codes of a concatenated scheme have SISO decoders (e.g., turbo-codes [9][10]), an iterative decoding can be performed exchanging extrinsic probabilities between the SISO decoders. However, a code can directly be constructed as a graph structure [59], and decoded by message passing on the graph.

b) The APP detector

There exists many kinds of SIHO or SISO detectors for multiple antenna channels. Hard output detectors find estimate $\hat{z} \in \Omega$ for each transmit antenna and time period, the symbols are then converted into bits thanks to a de-mapper, de-interleaved and given to the input of a hard input decoder. We can list the most current hard output detectors:

- Sub-optimal hard output decoders: an estimation of the transmitted symbols $\hat{z}$ can be obtained by linear equalizers followed by a hard decision (e.g., Zero-Forcing (ZF), Minimum Mean Square Error (MMSE)) or non-linear equalizers (e.g., Decision Feedback Equalizer (DFE)). They do not provide near optimum performance on MIMO channels, even at high signal-to-noise ratios. Indeed, such equalizer decision regions are an homothecy of the equivalent lattice fundamental parallelotope (volume defined by the basis vectors). The Voronoi region is a homothecy of the fundamental parallelotope only if the lattice basis is orthogonal, which is not the case for MIMO channels.
- Maximum likelihood hard output decoders: the maximum likelihood point z_{ML} can be found using exhaustive decoders or non-exhaustive algorithms such as sphere decoders (this algorithm is fully described in Section 4.2).

However, the separated detection and decoding process is sub-optimal in terms of global maximum likelihood criterion. Suppose that the detector finds the maximum likelihood points from the transmitted points, which is equivalent to finding all the maximum likelihood n_t-dimensional transmitted points for each time period. Moreover, suppose that the decoder finds the maximum likelihood codeword from the coded bits vector given by the detector. Even with these two conditions, the receiver does not achieve the global maximum likelihood performance. Indeed, the global code $\mathcal{C}_E$ contains $2^{K_c L_c}$ codewords whereas the hard output detector finds the maximum likelihood vector in a set of $2^{N_c L_c}$ vectors, considering non-existing points which misleads the decoder. As already said, the ideal but intractable receiver should directly decode $\mathcal{C}_E$. Another solution is to perform iterative joint detection and decoding thanks to iterative processing.

The receiver has two main elements as described in Fig. 2.2: An APP QAM-detector that acts as a soft output equalizer for both the space-time spreader and the MIMO channel, and a SISO decoder for $\mathcal{C}$. An iterative joint detection and decoding process is based on the exchange of soft values between the SISO QAM-detector and the SISO convolutional decoder. The SISO detector computes the extrinsic probabilities $\xi(c_\ell)$ thanks to the conditional likelihoods $p(y_k/z_k)$ and the *a priori* probabilities $\pi(c_\ell)$ fed back from the SISO decoder. At the first iteration, no information is available at the detector input, so it equally considers all the constellation

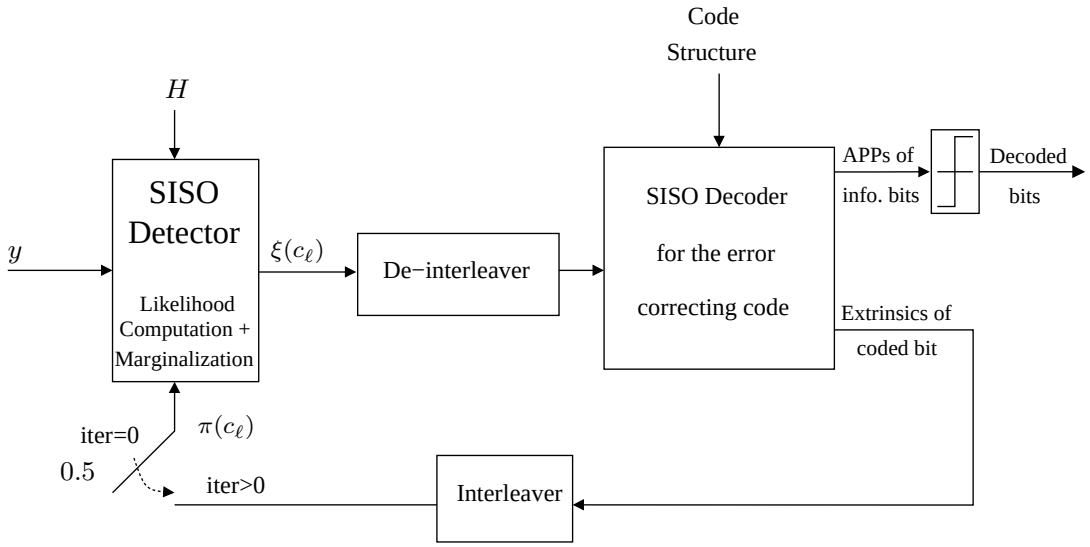

Figure 2.2: Iterative APP detection and decoding receiver.

points and gives probabilities on the coded bits to the SISO decoder. Through the iterations, the a priori probability of the constellation points computed from the probabilities given by the SISO decoder becomes more or less reliable. If an ideal convergence is achieved, near maximum likelihood performance is achieved. This technique requires a SISO detector that converts the received vector y_k of each time period into extrinsic probabilities on the coded bits $\xi(c_\ell)$ thanks to a priori probabilities on the coded bits $\pi(c_\ell)$. We can list some SISO detectors for MIMO channels:

- exhaustive APP detectors, list APP detectors (see Section 4.3).
- SISO MMSE (see Section 4.4)
- Serial Interference Cancellation, Parallel Interference Cancellation detectors (from multiuser detection theory).

We will now describe the optimal APP detector based on a marginalization over an exhaustive list. When the spectral efficiency is too high, such a detector becomes intractable. The complexity reduction of such a case is treated in Section 4.3. However, we need to describe the optimal detector for the performance computation and system performance optimizations.

The detector independently computes the soft outputs on each time period, the following APP probability expression is available for any coded bit c_ℓ of any time period. The received point during the considered time period is y_k. The APP probability of a coded bit c_ℓ is defined by the probability to detect the bit conditioned on the observation of y_k:

$$APP(c_\ell) = p(c_\ell/y_k) = \frac{p(y_k/c_\ell)p(c_\ell)}{p(y_k)} \tag{2.6}$$

In the above expression, we see that $APP(c_\ell)$ can be expressed as a function of different quantities.

- At each new detection step, the probabilities given by the output of the SISO decoder are independent from the received point y_k. They are called a priori probabilities on the coded bits c_ℓ: $\pi(c_\ell) = p(c_\ell)$.

- The probability $p(y_k)$ depends on the transmitted coded bits, the a priori probability and the AWGN, and is not computable. Fortunately, we will see that this is not a necessary quantity for the iterative processing.
- The conditionned observation $p(y_k/c_\ell)$ can be decomposed into more explicit probabilities. We use a marginalization over the set of labelings having the ℓ-th bit equal to c_ℓ, $c = \{c_1, \ldots, c_\ell, \ldots, c_{mN_t}\} \in \Omega(c_\ell)$, where c corresponds to a transmitted vector $z_k = \{z_{k,1}, \ldots, z_{k,N_t}\}$ and filtered vector $x_k = z_k H_k = \{x_{k,1}, \ldots, x_{k,N_r}\}$

$$p(y_k/c_\ell) = \sum_{c \in \Omega(c_\ell)} p(y_k, c/c_\ell) = \sum_{c \in \Omega(c_\ell)} p(y_k/c, c_\ell) p(c) \tag{2.7}$$

The condition over c, c_ℓ is equivalent to a condition over all the modulation symbols vectors $z_k \in \Omega(c_\ell)$. Using the independence of the receive antennas and the AWGN distribution, we can write that

$$p(y_k/c, c_\ell) = p(y_k/x_k) = \prod_{i=1}^{N_r} p(y_i/x_i) = \frac{1}{\sqrt{2\pi N_0}} e^{-\|y_k - z_k S H_k\|^2 / 2N_0} \tag{2.8}$$

The coded bits transmitted during the same time period are supposed to be independent, we have $\forall c \in \Omega(c_\ell), p(c) = \prod_{i \neq \ell} \pi(c_i)$ which leads to

$$p(y_k/c_\ell) = \sum_{x_k \in \Omega(c_\ell)} p(y_k/x_k) \prod_{i \neq \ell} \pi(c_i) \tag{2.9}$$

Let us now consider the information exchange between the SISO decoder and SISO detector. The two blocks compute the APP probabilities combining the information they gather independently (received point and modulation for the detector, trellis for the decoder) and information from the other block. The decoder gives a priori probabilities to the detector, this amount of information should not be given back to the decoder in order to keep the random variable independence. The detector computes $APP(c_\ell) = \pi(c_\ell)\xi(c_\ell)$, with $\xi(c_\ell)$ and $\pi(c_\ell)$ two independent variables, $\xi(c_\ell)$ is called extrinsic probability, given to the decoder soft input. Moreover, we have $APP(c_\ell) \propto \pi(c_\ell) p(y/c_\ell)$, and since $\xi(c_\ell)$ should be a probability, we can use the normalization:

$$\xi(c_\ell) = \frac{p(y_k/c_\ell = 1)}{p(y_k/c_\ell = 0) + p(y_k/c_\ell = 1)} \tag{2.10}$$

Finally, the SISO APP detector computes the extrinsic information, which corresponds to the extrinsic probability that the ℓ-th coded bit equals 1, as given in the following normalized marginalization:

$$\xi(c_\ell) = \frac{\sum_{z' \in \Omega(c_\ell = 1)} \left[\left(e^{-\frac{\|y_k - z' S H_k\|^2}{2N_0}} \right) \prod_{r \neq \ell} \pi(c_r) \right]}{\sum_{z \in \Omega} \left[\left(e^{-\frac{\|y_k - z S H_k\|^2}{2N_0}} \right) \prod_{r \neq \ell} \pi(c_r) \right]} \tag{2.11}$$

where Ω is the Cartesian product $(M\text{-QAM})^{N_t}$, i.e., the set of all vectors z generated by the QAM mapper, $|\Omega| = 2^{mN_t}$. The subset $\Omega(c_\ell = 1)$, for $\ell = 0, 1, \ldots, mN_t - 1$, is restricted to the vectors z in which the ℓ-th coded bit is equal to 1. The detector independently computes the

soft outputs for each precoding time period. At the first iteration, no a priori information is available at the detector input. Through the iterations, the a priori probability on constellation points computed from the probabilities fed back by the SISO decoder becomes more and more accurate. Ideal convergence is achieved when a priori probabilities provided by the decoder are perfect, i.e., equal to 0 or 1.

2.2 Ideally interleaved BICM exact pairwise error probabilities

This section describes a very accurate computation of bit error rates and frame error rates of BICM maximum likelihood performance over MIMO channel with ideal interleaving. This new technique is based on the original computation of the exact pairwise error probability between two codewords.

The digital communication systems become more and more complex to provide better performance. This technical progress increases the difficulty of theoretical analysis. The graph iterative decoding introduced in the 1960's by R.G.Gallager was extended to many kinds of iterative processing using the concatenated structure. As examples, we can cite turbo-decoding of concatenated codes, turbo-synchronization, turbo-equalization, joint turbo-detection and decoding of BICM.

If the signal-to-noise ratio is sufficiently high, the iterative processing converges to near maximum likelihood performance, which is particularly interesting when no maximum likelihood decoding can be processed. However, theoretical analysis for iterative processing is very difficult or in many cases impossible.

In this thesis report, we mainly consider iterative joint detection and decoding of BICM over multiple antenna channels. Heavy work has been made to estimate the frame error rate or bit error rate of this system, in particular using Gaussian approximations, but the exact pairwise error probability has not been presented yet.

Under the ideal interleaving condition, and when the MIMO channel is ergodic, we are able to derive a closed form expression of the Log Likelihood Ratio density probabilities at the output of the detector and a closed form expression of the pairwise error probability at the output of the decoder. It is then very simple to use the well known techniques to estimate the bit error rate or frame error rate of a coded modulation when the pairwise error probability is perfectly known. This subject has been fully discussed for coded modulations over AWGN channels, where the pairwise error probability is straightforward. As an example, we can cite the union bound of the transfer function of a convolutional code, or the more accurate tangential sphere bound. We will then extend these results to the block fading MIMO channels with linear precoding.

2.2.1 Ideal interleaving condition

The evaluation of the bit error rate (BER) or frame error rate (FER) of a coded modulation is usually based on the derivation of an upper bound on the actual performance obtained by a balanced summation of pairwise error probabilities. Each pairwise error probability involves the Euclidean distance between two codewords with a Hamming distance w.

For example with convolutional codes, consider a nearest neighbor in the trellis. It is defined by a block of $l_{\mathcal{C}}N_{\mathcal{C}}$ coded bits, d_{Hmin} of which are erroneous ($l_{\mathcal{C}}$ is the code constraint length). The channel provides a good protection if these coded bits see a maximum number of independent channel states.

Considering a general $n_t \times n_r$ MIMO block fading channel with n_c blocks, we collect a minimum diversity equal to n_r at the detector output, and, since the decoder cannot degrade performance, the reception diversity n_r is always obtained at the decoder output. The challenge is to collect the transmission diversity given by the n_t transmit antennas and the n_c channel realizations.

In order to achieve full diversity, the erroneous bits of an error event should be equally distributed over all channel states. Moreover, the interference of these bits in the precoding time periods should be limited to first enhance the diversity and then the coding gain. Let us consider an error event with w erroneous bits. Assume that the maximum diversity order is d_{max}. If $w \geq d_{max}$, we achieve full diversity if at least d_{max} bits among w see the d_{max} independent channel states. In a precoding time period k in which at least an erroneous bit is transmitted, the transmitted and competing points are called $x_k = z_k SH_k$ and $x'_k = z'_k SH_k$. When performing ML decoding or APP detection, we are interested in the equivalent Binary Shift Keying (BSK) modulation defined by the two points x_k and x'_k. The vector $(z_k - z'_k)SH_k$ has sn_r independent circular symmetric Gaussian components. Thus, whatever the number of erroneous bits on a precoding time period, the obtained diversity is limited to sn_r. Having several erroneous bits per precoding time period is useless. On the contrary, if the erroneous bits are located on different precoding time periods and experience different fading random variables, a higher diversity is achieved. This is what we call the non-interference property. Furthermore, we will see in section 3.3 that an equi-distribution of erroneous bits on channel states is required to achieve a maximum coding gain. We call it the equi-distribution property. The ideal interleaver is defined as follows:

Proposition 1 *For any pair of codewords with w different bits at positions $i_1, \ldots, i_k, \ldots, i_w$, an ideal interleaver allocates the bits to transmitted symbols as follows:*

- *Non-interference property: $\forall i_k, i_{k'}$, bits at positions i_k and $i_{k'}$ are transmitted on different precoding time periods,*
- *Equi-distribution property: the bits at positions $i_1, \ldots, i_k, \ldots, i_w$ are as equiprobably distributed over all channel states as allowed by w.*

In practice, such an interleaver does not always exist. We will see in the following that the Singleton bound gives an existence condition of the ideal interleaver. In section 3.4, we present optimized interleavers that approach the ideal condition.

2.2.2 Exact pairwise error probability for ergodic channels

A tight upper bound on the pairwise error probability of error-free decoding for a MIMO-BICM has been given in [50]. It is based on an integral expression that can be evaluated by the Gauss-Chebyshev quadrature [22]. Here, we establish a closed form expression for the exact pairwise error probability on ergodic MIMO channels under maximum likelihood decoding of the BICM and ideal channel interleaving. The mapping design criterion is directly derived from

this pairwise error probability expression as shown later in section 3.1. Furthermore, tight union bounds on both frame and bit error rates (FER and BER) will be presented and used to validate the asymptotic signal to noise ratio gain for optimized mappings.

Transmitted symbols are not precoded: $s = 1$, $S = I_{n_t}$ the $n_t \times n_t$ identity matrix. Thus, (2.3) reduces to $H_k = H_k^{[1][1]}$. Consider two codewords $X(c) \in \mathcal{C}_E$ and $X(c') \in \mathcal{C}_E$ with a Hamming distance $w = d_H(c, c')$ between the convolutional codewords c and c'. If we assume ideal channel interleaving, then the w difference positions are spread in space and time over w distinct transmission periods. Clearly, the conditional pairwise error probability $P_{\mathcal{H},w}(X(c) \rightarrow X(c'))$ only depends on those w positions. Hence, we will reduce the notation of $X(c)$ and $X(c')$ to the w time periods. We introduce $X = \{x_1, \ldots, x_w\}$ and $X' = \{x'_1, \ldots, x'_w\}$, where the components x_k and x'_k are points belonging to the set ΩH_k.

Our aim in this section is to compute $P_w(c \rightarrow c') = E_{\mathcal{H}}[P_{\mathcal{H},w}(c \rightarrow c')]$. The conditional pairwise error probability $P_{\mathcal{H},w}(c \rightarrow c')$ is expressed as

$$P_{\mathcal{H},w}\left(c \rightarrow c'\right) = P_{\mathcal{H},w}\left(X \rightarrow X'\right) = P\left(e^{-\sum_{k=1}^{w}\|y_k - x_k\|^2/2N_0} < e^{-\sum_{k=1}^{w}\|y_k - x'_k\|^2/2N_0}\right) \tag{2.12}$$

For a given set of channel realizations $\mathcal{H}$, a correct decision is taken by the ML decoder when the log-likelihood ratio LLR is positive:

$$\left\{\begin{array}{lcl} \mathrm{LLR} & = & \log\left(\frac{e^{-\sum_{k=1}^{w}\|y_k - x_k\|^2/2N_0}}{e^{-\sum_{k=1}^{w}\|y_k - x'_k\|^2/2N_0}}\right) = \frac{\sum_{k=1}^{w}\|y_k - x'_k\|^2 - \|y_k - x_k\|^2}{2N_0} = \sum_{k=1}^{w}\mathrm{LLR}_k \\ P_{w,\mathcal{H}}(c \rightarrow c') & = & P(\mathrm{LLR} < 0) = P\left(\sum_{k=1}^{w}\mathrm{LLR}_k < 0\right) \end{array}\right. \tag{2.13}$$

Thus,

$$P_w\left(c \rightarrow c'\right) = E_{\mathcal{H}}[P(\mathrm{LLR} < 0)] = E_{\mathcal{H}}\left[\int_{-\infty}^{0} p_{\mathrm{LLR}}(x)dx\right] = \int_{-\infty}^{0} p_{\overline{\mathrm{LLR}}}(x)dx \tag{2.14}$$

where $p_{\mathrm{LLR}}(x)$ is the probability density function of LLR and $p_{\overline{\mathrm{LLR}}}(x) = E_{\mathcal{H}}[p_{\mathrm{LLR}}(x)]$ is the probability density function of $\overline{\mathrm{LLR}} = E_{\mathcal{H}}[\mathrm{LLR}]$. We will first express the characteristic function $\psi_{\overline{\mathrm{LLR}}}(j\nu)$ of $\overline{\mathrm{LLR}}$. Since the w random variables LLR_k are independent and the channel is ergodic, using $\mathrm{LLR} = \sum_{k=1}^{w}\mathrm{LLR}_k$, we have

$$\psi_{\overline{\mathrm{LLR}}}(j\nu) = E_{\mathcal{H}}\left[\prod_k \psi_{\mathrm{LLR}_k}(j\nu)\right] = \prod_k \psi_{\overline{\mathrm{LLR}_k}}(j\nu) \tag{2.15}$$

where $\psi_{\overline{\mathrm{LLR}_k}}(j\nu) = E_{H_k}[\psi_{\mathrm{LLR}_k}(j\nu)]$ and $\psi_{\mathrm{LLR}_k}(j\nu)$ is the characteristic function of $p_{\mathrm{LLR}_k}(x)$.

Two points are involved in the expression of the partial log-likelihood ratio LLR_k: $x_k = z_k H_k$ and $x'_k = \bar{z}_k^{\ell_k} H_k$, where H_k denotes an instance of the channel matrix set $\mathcal{H}$ at time period k. As ideal interleaving is assumed, the point $z'_k = \bar{z}_k^{\ell_k}$ is obtained by flipping the bit at position ℓ_k in the binary labeling of z_k ($1 \leq \ell_k \leq mn_t$). The squared Euclidean distance between z_k and $\bar{z}^{\ell_k}$ is denoted $d_k^2 = \left\|z_k - \bar{z}_k^{\ell_k}\right\|^2$. The distance spectrum $\{d_k\}$ depends on the modulation type, its size and its binary labeling. For a given 2^m-QAM modulation, non-equivalent labelings lead to non-identical bit error rate performance.

a) Characteristic function of $\overline{\mathrm{LLR}_k}$

First, we compute the characteristic function of LLR_k for a binary modulation (BSK) defined by two points $\{z_k,\ \bar{z}_k^{\ell_k}\}$ transmitted over a MIMO channel. The expression of LLR_k is:

$$\mathrm{LLR}_k = \frac{1}{2N_0}\left(\left\|y_k - \bar{z}_k^{\ell_k} H_k\right\|^2 - \|y_k - z_k H_k\|^2\right) = \frac{1}{2N_0}\left(R_k + 2\Re\left((z_k - \bar{z}_k^{\ell_k}) H_k \eta_k^*\right)\right) \quad (2.16)$$

where * is the transpose conjugate and R_k is the square norm of the vector $(z_k - \bar{z}_k^{\ell_k})H_k$. If a classical mono-dimensional mapping is used independently on each transmit antenna, the difference vector $z_k - \bar{z}_k^{\ell_k}$ has only one non-null component in the position given by $\lfloor \ell_k/m \rfloor$. However, in order to stay in the general case which will be useful in the following, we do not take any assumption on vector $z_k - \bar{z}_k^{\ell_k}$. It can be shown that $\Re((z_k - \bar{z}_k^{\ell_k})/N_0.H_k\eta_k^*)$ is a Gaussian noise with zero mean and variance R_k/N_0. Moreover, since $(z_k - \bar{z}_k^{\ell_k})/d_k.H_k$ includes n_r independent identically distributed complex Gaussian random variables with zero mean and unit variance, then R_k/d_k^2 has a Chi-square distribution of order $2n_r$.

$$p_{R_k/d_k^2}(\alpha) = \frac{\alpha^{(n_r-1)} e^{-\alpha}}{(n_r-1)!} \quad (2.17)$$

First, notice that the random variable LLR_k is Gaussian distributed.

$$\mathrm{LLR}_k \sim \mathcal{N}\left(\frac{R_k}{2N_0}, \frac{R_k}{N_0}\right) \quad (2.18)$$

The characteristic function of LLR_k is

$$\psi_{\mathrm{LLR}_k}(j\nu) = E\left[e^{j\nu \mathrm{LLR}_k}\right] = \exp\left(\frac{\nu}{2}\frac{R_k}{N_0}(j-\nu)\right) \quad (2.19)$$

The mathematical expectation $E_{R_k}[.]$ over R_k is equivalent to the expectation over H_k. Thus,

$$\begin{cases} \psi_{\overline{\mathrm{LLR}_k}}(j\nu) &= E_{R_k}\left[\psi_{\mathrm{LLR}_k}(j\nu)\right] \\ &= \left(1 - \frac{d_k^2}{2N_0}\nu(j-\nu)\right)^{-n_r} \\ &= \left(\frac{d_k^2}{2N_0}(\nu - ja(d_k))(\nu - jb(d_k))\right)^{-n_r} \end{cases} \quad (2.20)$$

where

$$\begin{cases} a(d_k) &= \frac{1}{2}\left(1 + \left(\sqrt{1 + \frac{8N_0}{d_k^2}}\right)\right) \\ b(d_k) &= \frac{1}{2}\left(1 - \left(\sqrt{1 + \frac{8N_0}{d_k^2}}\right)\right) \end{cases} \quad (2.21)$$

b) Characteristic function of $\overline{\mathrm{LLR}}$

Let D denote the set of all Euclidean distances obtained by flipping one bit in the constellation Ω. Taking n_d as the number of different distances occuring in the sequence $(d_1, d_2, \ldots, d_w)$, we define the set $\Delta = \{\delta_1, \ldots, \delta_{n_d}\} \subset D$ from the sequence $(d_1, d_2, \ldots, d_w) \in \Delta^w \subset D^w$, i.e., the Euclidean distance d_k takes its values from the set Δ.

It is clear that $n_d = |\Delta| \leq |D|$. Let the integer λ_k denote the frequency of δ_k in the sequence

$(d_1, d_2, \ldots, d_w)$, $\sum_{k=1}^{n_d} \lambda_k = w$ and $\Lambda = \{\lambda_1, \ldots, \lambda_{n_d}\}$.
Using (2.15), (2.20) and (2.21), the averaged characteristic function becomes

$$\begin{aligned}
\psi_{\overline{\mathrm{LLR}}}(j\nu) &= \prod_{k=1}^{w} \left(\frac{-d_k^2}{2N_0} (j\nu + a(d_k))(j\nu + b(d_k)) \right)^{-n_r} && (2.22)\\
&= \left(\prod_{k=1}^{w} \left(\frac{-d_k^2}{2N_0} \right)^{-n_r} \right) \left(\prod_{k=1}^{n_d} \left([j\nu + a(\delta_k)][j\nu + b(\delta_k)] \right)^{-n_r \lambda_k} \right) && (2.23)\\
&= \left(\prod_{k=1}^{w} \left(\frac{-d_k^2}{2N_0} \right)^{-n_r} \right) \left(\prod_{k=-n_d, k\neq 0}^{n_d} [j\nu + \beta_k]^{-n_r \lambda_{|k|}} \right) && (2.24)
\end{aligned}$$

where the poles in the above product are defined by $\beta_{k>0} = a(\delta_k)$, $\beta_{k<0} = b(\delta_{-k})$.

c) The $\overline{\mathrm{LLR}}$ partial fraction expansion

To allow derivation of $p_{\overline{\mathrm{LLR}}}(x)$, we now compute the partial fractions expansion of $\psi_{\overline{\mathrm{LLR}}}(j\nu)$. A mathematical reminder about partial fraction expansion is described in Appendix C. The characteristic function $\psi_{\overline{\mathrm{LLR}}}(j\nu)$ can be written as:

$$\psi_{\overline{\mathrm{LLR}}}(j\nu) = \prod_{k=1}^{w} \left(\frac{-d_k^2}{2N_0} \right)^{-n_r} \sum_{k=-n_d, k\neq 0}^{n_d} \sum_{i=1}^{n_r \lambda_{|k|}} \frac{\alpha_{k,i}}{(j\nu + \beta_k)^i} \tag{2.25}$$

where the coefficients $\alpha_{k,i}$ are given by an identification of the coefficients of the two series expansions in ϵ:

$$\sum_{i=0}^{n_r\lambda_\ell - 1} \alpha_{\ell, n_r\lambda_\ell - i} \epsilon^i + \mathcal{O}(\epsilon^{n_r\lambda_\ell}) = \prod_{n=-n_d, n\neq \ell, n\neq 0}^{n_d} \sum_{i=0}^{n_r\lambda_\ell - 1} \frac{(-1)^i \binom{n_r\lambda_{|n|} + i - 1}{i}}{(\beta_n - \beta_\ell)^{n_r\lambda_{|n|} + i}} \epsilon^i + \mathcal{O}(\epsilon^{n_r\lambda_\ell}) \tag{2.26}$$

where $\binom{n}{k} = \frac{n!}{k!(n-k)!}$. From the simple properties $a(\delta_k) - 1/2 = 1/2 - b(\delta_k)$ and $\psi_{\overline{\mathrm{LLR}}}(j\nu - 1/2) = \psi_{\overline{\mathrm{LLR}}}(-1/2 - j\nu)$, we have $\alpha_{-k,i} = (-1)^i \alpha_{k,i}$. Hence, coefficients $\alpha_{k,i}$ are only evaluated for $k > 0$. Expression (2.25) becomes

$$\psi_{\overline{\mathrm{LLR}}}(j\nu) = \prod_{k=1}^{w} \left(\frac{-d_k^2}{2N_0} \right)^{-n_r} \sum_{k=1}^{n_d} \sum_{i=1}^{n_r\lambda_k} \frac{\alpha_{k,i}}{(j\nu + a(\delta_k))^i} + \frac{(-1)^i \alpha_{k,i}}{(j\nu + b(\delta_k))^i} \tag{2.27}$$

d) Conditional pairwise error probability closed form expression

Finally, we get the probability density function of $\overline{\mathrm{LLR}} = \sum_{k=1}^{w} \overline{\mathrm{LLR}}_k$ by the Fourier transform

$$\begin{aligned}
p_{\overline{\mathrm{LLR}}}(x) &= \frac{1}{2\pi} \int_{-\infty}^{+\infty} \psi_{\overline{\mathrm{LLR}}}(j\nu) e^{-j\nu x} d\nu && (2.28)\\
&= \frac{1}{2\pi} \prod_{k=1}^{w} \left(-\frac{2N_0}{d_k^2} \right)^{n_r} \sum_{k=1}^{n_d} \sum_{i=1}^{n_r\lambda_k} \alpha_{k,i} \left[I_i(x, a(\delta_k)) + (-1)^i I_i(x, b(\delta_k)) \right] && (2.29)
\end{aligned}$$

and the function $I_i(x, a(\delta_k))$ is defined by

$$I_i(x, a(\delta_k)) = \frac{(-x)^{i-1}}{(i-1)!} 2\pi \ \mathrm{sgn}(a(\delta_k)) e^{a(\delta_k)x} \mathbb{H}(-\mathrm{sgn}(a(\delta_k))x) \tag{2.30}$$

Indeed, we have

$$I_n(x, a(\delta_k)) = \frac{-x}{n-1} I_{n-1}(x, a(\delta_k)) = \frac{(-x)^{n-1}}{(n-1)!} I_1(x, a(\delta_k)) \tag{2.31}$$

and

$$I_1(x, a(\delta_k)) \quad = \quad \int_{-\infty}^{+\infty} \frac{e^{-j\nu x}}{j\nu + a(\delta_k)} d\nu = 2\pi sgn(a(\delta_k)) e^{a(\delta_k)x} \mathbb{H}(-sgn(a(\delta_k))x)$$

where $\mathrm{sgn}(x)$ is the sign function, and $\mathbb{H}$ is the Heaviside step function.

Using $\int_{-\infty}^{0} I_i(x, b(\delta_k))dx = 0$ and

$$\int_{-\infty}^{0} I_i(x, a(\delta_k))dx = 2\pi \int_{-\infty}^{0} \frac{(-x)^{i-1}}{(i-1)!} e^{a(\delta_k)x} dx = 2\pi \frac{1}{a(\delta_k)^i} \tag{2.32}$$

the conditional pairwise error probability is $P_w(c \to c') = \int_{-\infty}^{0} p_{\overline{\mathrm{LLR}}}(x)dx$ which yields the closed form expression

$$P_w(c \to c') = P_w(\Delta, \Lambda) = \prod_{k=1}^{w} \left(-\frac{2N_0}{d_k^2} \right)^{n_r} \sum_{k=1}^{n_d} \sum_{i=1}^{n_r \lambda_k} \frac{\alpha_{k,i}}{a(\delta_k)^i} \tag{2.33}$$

e) Asymptotic expression of the pairwise error probability

We can compute the asymptotic expression when the noise level is low. Indeed, the coding gain and diversity are measured for high signal-to-noise ratios (SNRs), where the performance have a linear asymptote on logarithmic scales.

$$P_w(\Delta, \Lambda) \underset{N_0 \to 0}{\sim} \binom{2n_r w - 1}{n_r w} \prod_{k=1}^{w} \left(\frac{2N_0}{d_k^2} \right)^{n_r} = \binom{2n_r w - 1}{n_r w} \left(\frac{2N_0}{\mathcal{G}_{ergo}(\Delta, \Lambda)} \right)^{w n_r} \tag{2.34}$$

The diversity associated with the considered pairs of Hamming weight w is the exponent of N_0, equal to wn_r. We define the coding gain or coding advantage as the coefficient dividing N_0, i.e.,

$$\mathcal{G}_{ergo}(\Delta, \Lambda) = \left(\prod_{k=1}^{w} d_k^2 \right)^{1/w} \tag{2.35}$$

All sequences $(d_1, \ldots, d_w)$ corresponding to the same pair (Δ, Λ) yield the same pairwise error probability. By averaging over all possible pairs (c, c') or equivalently over all sets of distances D^w, we obtain $P_w = E_{D^w}[P_w(\Delta, \Lambda)]$, the conditional probability that an error event of Hamming weight w occurs. From this pairwise error probability, it is easy to estimate the FER or BER of the BICM with ideal interleaving thanks to a classical union bound on the weight enumeration function of the error correcting code. Moreover, we derive a design criterion of the BICM from

the coding gain $\mathcal{G}_{ergo}(\Delta, \Lambda)$ expression. In the following, the objective is to derive this coding gain for block fading channels and linear precoding in order to derive the ML design criterion of the space-time (ST) BICM.

2.2.3 Exact pairwise error probability for Block Fading MIMO channels

In section 2.2.2 we computed the exact pairwise error probability of an ideally interleaved BICM over ergodic MIMO channels. We will now express the same pairwise error probability for block fading MIMO channels. We assume that proposition 1 is satisfied. Assume that the number of independent channel realizations in a frame is n_c. We use the previously introduced notation $X = \{x_1, \ldots, x_w\}$ and $X' = \{x'_1, \ldots, x'_w\}$ to denote the non-equal w components of the transmitted codewords c and c' (we consider $d_H(c, c') = w$). The involved channel matrices are not independent as for an ergodic channel. The conditions of independence are the following

- If two LLR random variables depend on two different channel realizations, they are independent.
- If two LLR random variables depend on the same channel realization but on different transmit antennas, the random variables are independent.

The maximum number of independent LLR variables is $n_c n_t$, which defines the transmit diversity order. We will call "channel state" the $1 \times n_r$ SIMO channel associated to one of the n_t transmit antennas of one of the n_c channel realizations. We choose the error correcting code so that $w \geq n_t n_c$.

We now group the w random variables LLR into $\min(n_t n_c, w) = n_t n_c$ independent blocks. Let $\mathrm{LLR}_{k,l,i}$ be the i-th log-likelihood ratio corresponding to the BSK transmission on the l-th antenna of the k-th block, $k = 1 \ldots n_c$, $l = 1 \ldots n_t$ and $i = 1 \ldots \kappa_{k,l}$, where $\kappa_{k,l}$ is the number of bits transmitted on the l-th antenna of the k-th block. We have $\sum_{k=1}^{n_c} \sum_{l=1}^{n_t} \kappa_{k,l} = w$. Finally, LLR is the sum of $n_t n_c$ independent random variables $\mathrm{LLR}_{k,l} = \sum_{i=1}^{\kappa_{k,l}} \mathrm{LLR}_{k,l,i}$:

$$\mathrm{LLR} = \sum_{k=1}^{n_c} \sum_{l=1}^{n_t} \sum_{i=1}^{\kappa_{k,l}} \mathrm{LLR}_{k,l,i} \tag{2.36}$$

Let $d_{k,l,i}$ denote the distance associated with $\mathrm{LLR}_{k,l,i}$, and define $\gamma_{k,l}^2 = \sum_{i=1}^{\kappa_{k,l}} d_{k,l,i}^2$ the distance associated to $\mathrm{LLR}_{k,l}$. We have

$$\mathrm{LLR}_{k,l} \sim \mathcal{N}\left(\frac{R_{k,l}}{2N_0}, \frac{R_{k,l}}{N_0}\right) \tag{2.37}$$

where $R_{k,l} = \gamma_{k,l}^2 \|H_k(l)\|^2$ and $H_k(l)$ is the l-th row of H_k. For all i, $\mathrm{LLR}_{k,l,i}$ are transmitted over the equivalent $1 \times n_r$ SIMO channel defined by $H_k(l)$, which is chi-square distributed with degree $2n_r$. The $\mathrm{LLR}_{k,l}$ variables are transmited on independent channel states, as for the ergodic channel case, we directly apply (2.33) and obtain the conditional pairwise error probability closed-form expression

$$P_w(X \to X') = P_w(\Delta, \Lambda) = \prod_{k=1}^{n_c} \prod_{l=1}^{n_t} \left(-\frac{2N_0}{\gamma_{k,l}^2}\right)^{n_r} \sum_{n=1}^{n_d} \sum_{i=1}^{n_r \lambda_n} \frac{\alpha_{n,i}}{a(\delta_n)^i} \tag{2.38}$$

where $\delta_n \in \Delta$, and (Δ, Λ) is the pair of sets representing the sequence $\left(\gamma_{1,1}^2, \ldots, \gamma_{n_t,n_c}^2\right)$. The $\alpha_{n,i}$ coefficients are computed thanks to the straightforward application of (2.26).

The asymptotic expression of $P_w(\Delta, \Lambda)$ is

$$P_w(\Delta, \Lambda) \underset{N_0 \to 0}{\sim} \binom{2n_r n_t n_c - 1}{n_r n_t n_c} \prod_{k=1}^{n_c} \prod_{l=1}^{n_t} \left(\frac{2N_0}{\gamma_{k,l}^2}\right)^{n_r} \tag{2.39}$$

The diversity associated with the considered pairs of Hamming weight w is then equal to the exponent $n_t n_c n_r$. The coding gain is given by the geometrical mean of the $\gamma_{k,l}^2$ and is equal to

$$\mathcal{G}_{bf}(\Delta, \Lambda) = \left(\prod_{k=1}^{n_c} \prod_{l=1}^{n_t} \sum_{i=1}^{\kappa_{k,l}} d_{k,l,i}^2\right)^{1/(n_t n_c)} \tag{2.40}$$

We will see in the following how to use this coding gain as a design criterion for the ST-BICM optimization. We now consider an equivalent computation of the coding gain for a linear precoded ST-BICM.

2.2.4 Exact pairwise error probability with linear precoding

When a linear precoder S of size $N_t \times N_t$ is used ($N_t = sn_t$), the detector computes soft outputs on the N_t transmitted symbols and considers the equivalent channel matrix SH_k of size $N_t \times N_r$. Under the ideal interleaving condition, we consider at most a single erroneous bit per block of s time periods in position $1 \leq \ell \leq mN_t$ inside the binary mapping of the transmitted symbol z, leading to symbol $\bar{z}^\ell$. For simplicity reasons, we assume that the error weight w satisfies $w \geq N_t N_c$.

Assume that n_s is a divisor of n_c. Consider the block-diagonal matrix of size $N_t \times N_r$. Assume that H_k contains n_s distinct channel realizations among the s blocks of size $n_t \times n_r$. The channel input-output relation is

$$y_k = z_k S H_k + \eta_k \tag{2.41}$$

where SH_k can be seen in general as a correlated fading channel [94]. All LLR random variables associated with a transmission on the k-th block experience the same channel matrix. Hence, we can apply a factorization of the correlated LLRs as in 2.2.3. Assume that a mono-dimensional mapping is used, the BSKs are transmitted on a single selected input of the matrix SH_k. Let $\mathrm{LLR}_{k,l,i}$ be the i-th LLR among $\kappa_{k,l}$, transmitted on the l-th row of the k-th block channel matrix SH_k. The definition of $\kappa_{k,l}$ gives $\sum_{k=1}^{n_c/n_s} \sum_{l=1}^{N_t} \kappa_{k,l} = w$. Let $d_{k,l,i}$ denote the BSK distance between the two points $z_{k,l,i}$ and $\bar{z}_{k,l,i}^\ell$ associated to $\mathrm{LLR}_{k,l,i}$. Let S_l denote the l-th row of S, we have $\|(z_{k,l,i} - \bar{z}_{k,l,i}^\ell) S H_k\|^2 = d_{k,l,i}^2 \|S_l H_k\|^2$. The $\mathrm{LLR}_{k,l}$ associated with the factorization of l-th row inputs of H_k satisfies

$$\mathrm{LLR}_{k,l} \sim \mathcal{N}\left(\frac{R_{k,l}}{2N_0}, \frac{R_{k,l}}{N_0}\right) \tag{2.42}$$

where $R_{k,l} = \|V_{k,l} H_k\|^2$, $V_{k,l} = \gamma_{k,l} S_l$ and $\gamma_{k,l}^2 = \sum_{i=1}^{\kappa_{k,l}} d_{k,l,i}^2$. The variable $R_{k,l}$ is a generalized chi-square random variable with $2N_r$ correlated centered Gaussian components. The random

variable $\mathrm{LLR}_k = \sum_{l=1}^{N_t} \mathrm{LLR}_{k,l}$ satisfies

$$\mathrm{LLR}_k \sim \mathcal{N}\left(\frac{\sum_{l=1}^{N_t} R_{k,l}}{2N_0}, \frac{\sum_{l=1}^{N_t} R_{k,l}}{N_0}\right) \tag{2.43}$$

We will first consider $n_s = 1$ and extend the result to any value of n_s.

a) The precoding matrix sees one channel realization ($n_s = 1$)

For $n_s = 1$, the quasi-static channel matrix H_k is defined as $H_k = \mathrm{diag}\left(H_k^{[1][1]}, \ldots, H_k^{[1][s]}\right)$. Let the row vector $S_l^{[i]}$ denote the i-th sub-part of size n_t extracted from the l-th row of S. We construct the $s \times n_t$ matrix S'_l whose rows are the s sub-parts $S_l^{[i]}$. Using the same method, we decompose $V_{k,l}$ into the $s \times n_t$ matrix $V'_{k,l} = \gamma_{k,l} S'_l$.

$$S_l = \left(S_l^{[1]}, \ldots, S_l^{[s]}\right) \Rightarrow S'_l = \begin{pmatrix} S_l^{[1]} \\ S_l^{[2]} \\ \vdots \\ S_l^{[s]} \end{pmatrix} \text{ and } V'_{k,l} = \gamma_{k,l} \begin{pmatrix} S_l^{[1]} \\ S_l^{[2]} \\ \vdots \\ S_l^{[s]} \end{pmatrix} \tag{2.44}$$

Define h_i the i-th column of $H_k^{[1][1]}$, the n_r vectors h_i are independent realizations of a $n_t \times 1$ MISO channel. We want to express the characteristic function of the random variable

$$\sum_{l=1}^{N_t} R_{k,l} = \sum_{i=1}^{n_r} \sum_{l=1}^{N_t} h_i^* V'^*_{k,l} V'_{k,l} h_i = \sum_{i=1}^{n_r} h_i^* M_k^* M_k h_i = \mathrm{tr}\left(\sum_{i=1}^{n_r} M_k h_i h_i^* M_k^*\right) \tag{2.45}$$

where M_k is an $n_t \times n_t$ Hermitian square root matrix of

$$\Sigma_k = \sum_{l=1}^{N_t} V'^*_{k,l} V'_{k,l} = U^* \Phi_{\Sigma_n} U \quad \Rightarrow \quad M_k = M_k^* = U^* \sqrt{\Phi_{\Sigma_k}} U \tag{2.46}$$

where $\Phi_{\Sigma_k} = \mathrm{diag}(\vartheta_{k,1}, \ldots, \vartheta_{k,n_t})$, $\vartheta_{k,i}$ is the i-th real eigenvalue of Σ_k and U is a unitary matrix.

The random variable $\sum_{i=1}^{n_r} M_k h_i h_i^* M_k^*$ has a Wishart distribution with n_r degrees of freedom and parameter matrix Σ_k. The characteristic function of the trace of $\sum_{i=1}^{n_r} M_k h_i h_i^* M_k^*$ is given in [69]:

$$E_{H_k}\left[\Psi_{\mathrm{LLR}_k}(j\nu)\right] = E_{H_k}\left[\exp\left(\frac{\nu(j-\nu)}{2} \frac{\mathrm{tr}(\sum_{i=1}^{n_r} M_k h_i h_i^* M_k^*)}{N_0}\right)\right] \tag{2.47}$$

$$= \left(\det(\Sigma_k) \det\left(\Sigma_k^{-1} - \frac{\nu(j-\nu)}{2N_0} I\right)\right)^{-n_r} \tag{2.48}$$

$$= \prod_{i=1}^{n_t} \left(1 - \frac{\nu(j-\nu)}{2N_0} \vartheta_{k,i}\right)^{-n_r} \tag{2.49}$$

where $\vartheta_{k,i}$ is the i-th real eigenvalue of Σ_k.

b) The precoding matrix experiences several channel realizations *($n_s > 1$)*

For $n_s > 1$, we first decompose the rows of S into n_s sub-parts of size N_t/n_s. Let $S_l^{[t]}$ denote the t-th sub-part of the l-th row. Then, each sub-part $S_l^{[t]}$ is decomposed into s sub-parts $S_l^{[t][i]}$ of size n_t and defines the rows of the $s \times n_t$ matrix $S'^{[t]}_l$. The $N_t \times N_t$ precoding matrix S is divided with the following method

$$S = \left[\begin{array}{ccccccccc} \overbrace{S_1^{[1][1]} & \cdots & S_1^{[1][s/n_s]}}^{S_l^{[1]}(1\times N_t/n_s)} & & \overbrace{S_1^{[2][1]} & \cdots & S_1^{[2][s/n_s]}}^{S_l^{[2]}} & \cdots & \overbrace{S_1^{[n_s][1]} & \cdots & S_1^{[n_s][s/n_s]}}^{S_l^{[n_s]}} \\ S_2^{[1][1]} & \cdots & S_2^{[1][s/n_s]} & & S_2^{[2][1]} & \cdots & S_2^{[2][s/n_s]} & & S_2^{[n_s][1]} & \cdots & S_2^{[n_s][s/n_s]} \\ \vdots & & & & \vdots & & & & \vdots & & \\ \underbrace{S_{N_t}^{[1][1]}} & \cdots & \underbrace{S_{N_t}^{[1][s/n_s]}} & & \underbrace{S_{N_t}^{[2][1]}} & \cdots & \underbrace{S_{N_t}^{[2][s/n_s]}} & & \underbrace{S_{N_t}^{[n_s][1]}} & \cdots & \underbrace{S_{N_t}^{[n_s][s/n_s]}} \\ & & N_t/s = n_t \text{ coefficients} & & & & & & & & \end{array}\right]$$

The $s/n_s \times n_t$ matrix $S'^{[t]}_l$ is built as follows:

$$S'^{[t]}_l = \begin{bmatrix} S_l^{[t][1]} \\ S_l^{[t][2]} \\ \vdots \\ S_l^{[t][s/n_s]} \end{bmatrix} \tag{2.50}$$

For different values of t, sub-parts $S_l^{[t][i]}$ multiply independent channel matrices $H_k^{[t][i]}$, which allows us to multiply the characteristic functions associated with the sub-parts. Substituting s with s/n_s in the mathematical development presented in section a) and using the independence of the n_s channel realizations, we directly have

$$E_{H_k}\left[\Psi_{\mathrm{LLR}_k}(j\nu)\right] = \prod_{t=1}^{n_s}\prod_{i=1}^{n_t}\left(1 - \frac{\nu(j-\nu)}{2N_0}\vartheta_{k,i}^{[t]}\right)^{-n_r} \tag{2.51}$$

where $\vartheta_{k,i}^{[t]}$ is the i-th eigenvalue of

$$\Sigma_k^{[t]} = M_k^{[t]*}M_k^{[t]} = \sum_{l=1}^{N_t}\gamma_{k,l}^2 S'^{[t]*}_l S'^{[t]}_l = V'^{*}V' = \sum_{l=1}^{N_t}\gamma_{k,l}^2\sum_{i=1}^{s/n_s} S_l^{[t][i]*}S_l^{[t][i]} \tag{2.52}$$

The set of eigenvalues $\vartheta_{k,i}^{[t]}$ is a function of the precoding matrix S and the BSK distances set reduced to the pair (Δ, Λ). The characteristic functions associated with different indices k can be multiplied thanks to the independence of channel realizations for different k values:

$$\Psi(j\nu) = \prod_{k=1}^{N_c}\prod_{t=1}^{n_s}\prod_{i=1}^{n_t}\left(1 - \frac{\nu(j-\nu)}{2N_0}\vartheta_{k,i}^{[t]}\right)^{-n_r} \tag{2.53}$$

Denote $\Delta = \{\delta_v^2\}$ the set of n_δ non-null eigenvalues extracted from the sequence defined

by the $\vartheta_{k,i}^{[t]}$ values. Each eigenvalue δ_v^2 is repeated λ_v times. Observe that $n_\delta \leq n_c n_t$. Finally, using the partial fraction expansion of $\Psi(j\nu)$ as described in (2.26), the exact pairwise error probability $P_w(\Delta, \Lambda)$ conditioned on $d_H(c, c') = w$ is equal to

$$P_w(\Delta, \Lambda) = \prod_{v=1}^{n_\delta} \left(-\frac{2N_0}{\delta_v^2} \right)^{\lambda_v n_r} \sum_{v=1}^{n_\delta} \sum_{i=1}^{n_r \lambda_v} \frac{\alpha_{v,i}}{a(\delta_\nu)^i} \tag{2.54}$$

The asymptotic expression of $P_w(\Delta, \Lambda)$ is

$$P_w(\Delta, \Lambda) \underset{N_0 \to 0}{\sim} \binom{2n_r N_\delta - 1}{n_r N_\delta} \prod_{v=1}^{n_\delta} \left(\frac{2N_0}{\delta_v^2} \right)^{\lambda_v n_r} \tag{2.55}$$

where $N_\delta = \sum_{v=1}^{n_\delta} \lambda_v$ is the total number of non-null eigenvalues.

The diversity associated with the considered pairs of Hamming weight w is the exponent equal to $\sum_{v=1}^{n_\delta} \lambda_v n_r = N_\delta n_r$. The coding gain is given by

$$\mathcal{G}_{s,n_s}(\Delta, \Lambda) = \left(\prod_{v=1}^{n_\delta} \delta_v^{2\lambda_v} \right)^{1/N_\delta} \tag{2.56}$$

We have derived an exact expression of the pairwise error probabilities of a BICM with linear precoding. The expression is exact for any SNR value, and the asymptotic expression leads to the well known rank and determinant criteria for space-time code optimization over MIMO block fading channels [85][35], where the considered space-time code is the whole BICM structure. As a remark, the asymptotic design criterion is usually derived by first upperbounding the $Q(x)$ function by $\exp(-x^2/2)/2$ and then averaging over the channel realizations. The obtained asymptotic expression has a multiplying coefficient different from $\binom{2n_r N_\delta - 1}{n_r N_\delta}$, which is inexact but provides the same coding gain expression, which proves that the design criterion proposed in [85] are correct.

Moreover, we notice that applying the Tarokh [85] rank and determinant criteria to the precoder alone does not lead to the whole BICM optimization. Quasi-optimal linear precoders will be designed to achieve full diversity and optimal coding gain in Section 3.3. Moreover, we now have the exact pairwise error probability expression which is useful for a tight BER and FER estimation.

2.3 Estimation of the bit and frame error rates

The estimation of the frame error rate or bit error rate for coded systems is not an easy task, even for the basic AWGN channel. Indeed, the objective is to compute the probability that a multi-dimensional additive white Gaussian noise gets out from a non-identified multi-dimensional polygon defining the Voronoi region. Each polygon facet belongs to the mediator hyperplane of two neighboring codewords. We will describe two methods for estimating the BER and FER of ideal BICM over MIMO channels.

All sequences $(d_1, \ldots, d_w)$ corresponding to the same (Δ, Λ) yield the same pairwise error

probability. We have expressed the pairwise error probability between two given codewords c and c' such that $d_H(c,c') = w$ and the transmission of $c - c'$ is characterized by (Δ, Λ). We now have to average this probability over all possible pairs (c, c'). First, let us consider the averaged pairwise error probability P_w conditioned on $d_H(c,c') = w$:

$$P_w = E_{c,c'|w}\left[P_w(c \to c')\right] = E_{c,c'|w}\left[P_w(\Delta, \Lambda)\right] \tag{2.57}$$

Averaging over the pairs (c, c') is equivalent to averaging over (Δ, Λ) thanks to the interleaver. Each pair (Δ, Λ) is representative of $w!/\prod_{i=1}^{n_d} \lambda_i!$ equivalent pairs (Z, Z'), where the w-dimensional Z and Z' vectors are the channel inputs leading to X and X', respectively. As a pair (Z, Z') corresponds to a high number of pairs (c, c'), the complexity of a numerical evaluation is dramatically reduced in practice by performing expectation over Δ and Λ:

$$P_w = E_{\Delta,\Lambda|w}\left[P_w(\Delta, \Lambda)\right] \tag{2.58}$$

2.3.1 Union bound on ergodic channels

The frame error rate at the decoder output FER^{dec} is upper bounded by the classical union bound

$$\mathrm{FER}^{dec} \leq E_c\left[\sum_{c' \in \mathcal{C}, c' \neq c} P(c \to c')\right] \tag{2.59}$$

The input-output weight distribution of the error correcting code $\mathcal{C}$ is

$$A(I,D) = \sum_{w=d_{Hmin}}^{+\infty} \sum_{i}^{+\infty} a_{i,w} I^i D^w \quad \text{and} \quad A(D) = A(1,D) = \sum_{w=d_{Hmin}}^{+\infty} a_w D^w \tag{2.60}$$

where $a_{i,j}$ is the number of codewords with an output Hamming weight w and an input Hamming weight i. We can now express the approximation of the maximum likelihood frame error rate and bit error rate of the ideally interleaved BICM transmitted over a multiple antenna channel:

$$\mathrm{FER}^{dec} \leq \sum_{w=d_{Hmin}}^{+\infty} a_w P(c \to c' | d_H(c,c') = w) = \sum_{w=d_{Hmin}}^{+\infty} a_w P_w \tag{2.61}$$

where P_w is given in 2.58 for ergodic channels, or by the equivalent expressions for block fading channels. Equivalently, we have

$$\mathrm{BER}^{dec} \leq \sum_{j} \sum_{w=d_{Hmin}}^{+\infty} \frac{j}{K_{\mathcal{C}} L_{\mathcal{C}}} a_{j,w} P_w \tag{2.62}$$

where $K_{\mathcal{C}} L_{\mathcal{C}}$ is the number of information bits per codeword.

We can compute the asymptotic expression when the noise level is low. Indeed, the coding gain and diversity are measured for high signal-to-noise ratios, where the performance have a

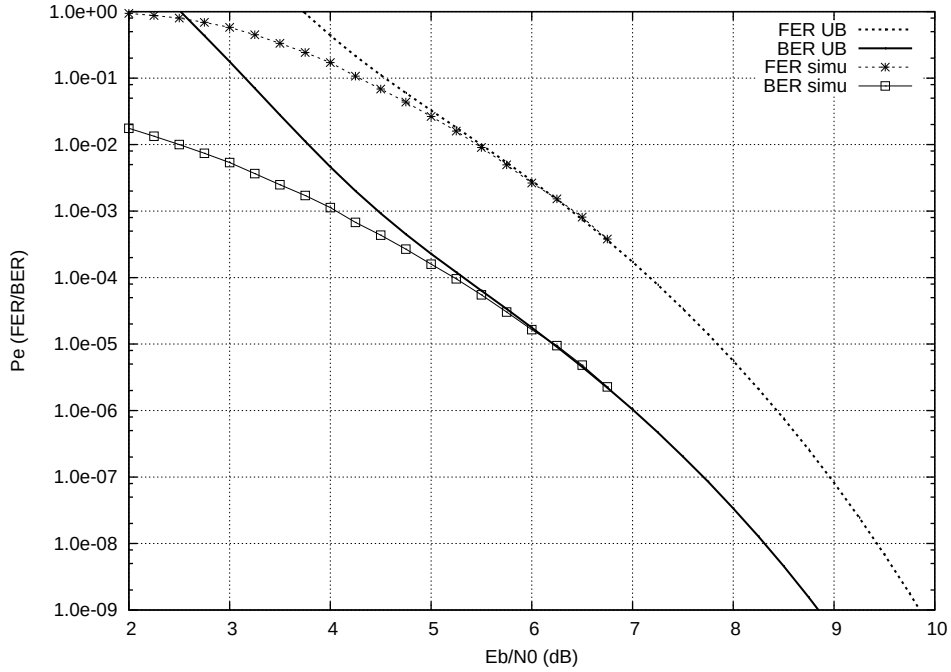

Figure 2.3: 1/2-rate RSC 7,5 convolutional code ($N_{\mathcal{C}}L_{\mathcal{C}} = 1000$) , BPSK over AWGN channel, Union Bound performance (UB) or simulation (simu)

linear asymptote on logarithmic scales. The asymptotic expression of BER^{dec} when $N_0 \to 0$ is

$$\mathrm{BER}^{dec} \underset{N_0 \to 0}{\sim} \sum_{j=1}^{+\infty} \frac{j}{K_{\mathcal{C}} L_{\mathcal{C}}} a_{j,d_{Hmin}} \binom{2n_r d_{Hmin} - 1}{n_r d_{Hmin}} E\left[\prod_{k=1}^{d_{Hmin}} \left(\frac{2N_0}{d_k^2} \right)^{n_r} \right] \tag{2.63}$$

Indeed, the error events with Hamming weight greater than d_{Hmin} have higher diversity and negligible contribution to the performance for high signal-to-noise ratios.

The union bound (UB) for convolutional codes is known to be tight on AWGN channels. Our experimental results showed that the union bound provided by 2.58 and 2.61 is also tight on a MIMO ergodic channel. Indeed, it is well known that the union bound performance is asymptotically (i.e, for a sufficiently high signal-to-noise ratio) a good approximation of convolutional codes performance on AWGN channels with BPSK input. Indeed, there is a dominant term in the sum and other terms are negligible for low noise levels. We can observe the tightness of the union bound for a 4-state convolutional code over AWGN channels with BPSK input on Fig. 2.3.

In our case, the terms corresponding to the error event with a weight equal to d_H observe a diversity equal to $n_r d_H$. At high signal-to-noise ratios, the terms with $d_H > d_{Hmin}$ are negligible. We can observe the tightness of the union bound of a 4-state convolutional code over 2×2 MIMO ergodic channels with 16-QAM input and gray mapping on Fig. 2.4.

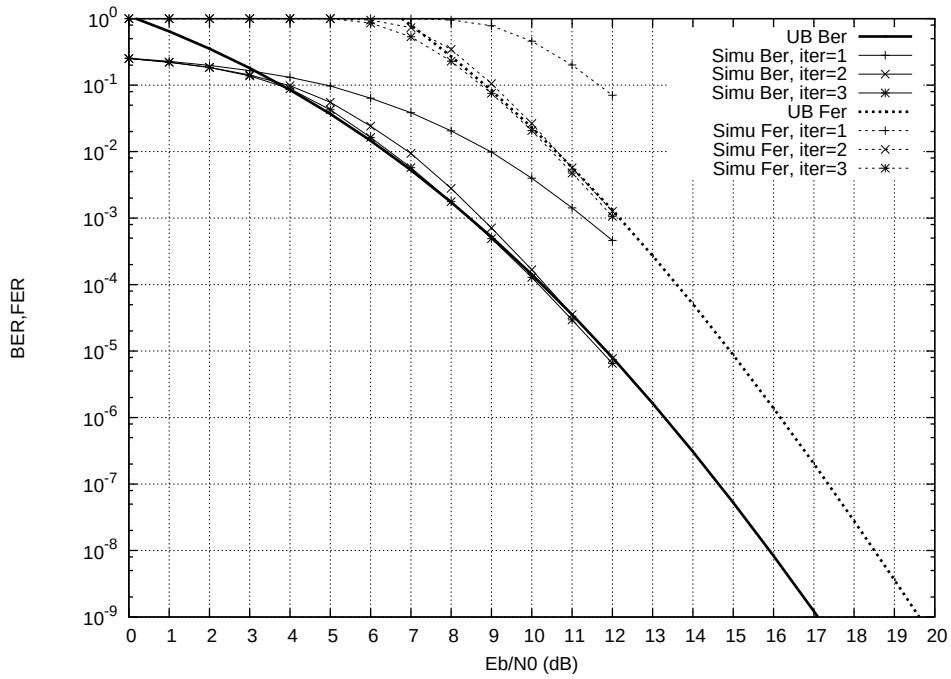

Figure 2.4: 1/2-rate RSC 7,5 ($N_{\mathcal{C}}L_{\mathcal{C}} = 10000$) , 16QAM, Gray mapping, 2×2 MIMO channel, Union Bound performance (UB) or simulation (simu) for BER and FER

2.3.2 Evaluation of the Frame Error Rate on block fading channels

For ergodic channels, the frame error rate is easily computed via a union bound. Indeed, only error events with minimum Hamming distance impact the error rate for a high signal to noise ratio and the observed diversity is equal to $n_r d_{Hmin}$. For block-fading channels, the frame error rate computation is much more tricky since each pairwise error probability is supposed to have the full-diversity order $n_c n_t n_r$. Due to the random nature of each eigenvalue in (2.56), it is difficult to know the impact of each distance configuration on the final FER.

However, one may assume that for a sufficiently high signal to noise ratio, the FER satisfies the following expression :

$$\text{FER} \simeq \sum_{w} \alpha_w E_{(\Delta,\Lambda|w)} \left[P_w(\Delta, \Lambda) \right] \tag{2.64}$$

Where α_w is the weighting coefficient of the impact of pairwise error probabilites with hamming weight w on the global error probability. The interleaver random structure allows for satisfying this equality. Let us define $\mathcal{G}$ the global coding gain. Since each pairwise error probability is supposed to have full diversity, we can write

$$\text{FER} \simeq \binom{2n_r n_t n_c - 1}{n_r n_t n_c} \left(\frac{2N_0}{\mathcal{G}} \right)^{n_r n_t n_c} \tag{2.65}$$

and

$$\mathcal{G}^{-n_r n_t n_c} = \sum_{w} \alpha_w E_{(\Delta,\Lambda|w)} \left[\mathcal{G}(\Delta, \Lambda)^{-n_r n_t n_c} \right] \tag{2.66}$$

where $\mathcal{G}(\Delta, \Lambda)$ is the coding gain associated to one pair of codewords. We can classically remark that optimizing indepently all pairwise error probabilities enhances the global performance, which will be done in the following. Moreover, we observe that the number of receive antennas does not affect the coding gain of a single pairwise error probability. The effect of the receive diversity is shown on the expression of the global coding gain, where a generalized harmonic mean of the gains is processed. As $n_r n_t n_c$ grows, the smallest coding gains have more impact on the final performance. Asymptotically, if $n_r n_t n_c \to +\infty$, only the nearest neighbours in the euclidean code have an influence on the FER, as for AWGN channels.

We will see in section 3.3.1 that the best coding gain is achieved when all eigenvalues $\vartheta_{k,i}^{[t]}$ are equal. In this ideal configuration, the coding gain is shown to be the same as with the same coded modulation transmitted on a $1 \times n_c n_t n_r$ SIMO channel. Simulating this latter case is less complex: the performance curve is semi-analytically computed using a reference curve on an AWGN channel. Alternatively, performance may be obtained by computing the Tangential Sphere Bound for spherical modulations [48]. In the following, *ideal BICM* will refer to the performance of the ideal configuration, which will be drawn on simulation results. This lower bound has the advantage to take the modulation and error correcting code into account and will be useful to evaluate the optimality of both the linear precoder and the channel interleaver.

2.4 Genie concept and performance

2.4.1 Principle

The genie method has been described and intensively used for mapping optimization of a BICM transmitted on a single antenna ergodic channel [24]. The main idea is to consider that for a sufficiently high signal-to-noise ratio, the extrinsic probabilities become very reliable. When processing the detector output during a time period, the genie condition is satisfied if the mN_t a priori probabilities are perfect, i.e $\pi(c_\ell) = c_\ell$. In this case, the extrinsic probability computation of the $\ell - th$ coded bit at the detector output is

$$\xi(c_\ell) = \frac{e^{-\frac{\|y - zSH\|^2}{2N_0}}}{e^{-\frac{\|y - zSH\|^2}{2N_0}} + e^{-\frac{\|y - \bar{z}^\ell SH\|^2}{2N_0}}} \tag{2.67}$$

where z and $\bar{z}^\ell$ have a 0 or a 1 in the ℓ-th position, respectively. We can observe that only the two points z and $\bar{z}^\ell$ are considered, they define a binary shift keying modulation (BSK). The computation of a given extrinsic probability behaves like LLR_k computed on a single time period, and introduced in the ideal BICM ML performance. The BSKs obtained by flipping one bit on the labeling are important to define the BICM geometrical behavior under perfect feedback assumption. This property can be used to design the labeling, this will be discussed in Section 3.1.

However, the genie situation assumed for the whole codeword is very optimistic, as it is equivalent to an error-free scheme, which is impossible. That is why we only consider the genie at the detector and for a single time period decoding. This is a practical design concept, not a physical quantity. However, we will see how this simple design tool is equivalent to the more complex maximum likelihood criterion.

2.4.2 Genie and maximum likelihood analogy

An information bit sequence, coded into a codeword, interleaved and spread over antennas and time periods, leads to a point of $\mathcal{C}_E$ in a space with a number of dimensions equal to the number of receive antennas times $L_{\mathcal{C}} N_{\mathcal{C}}/(mN_t)$, the indices of time periods corresponding to a codeword. With the well-known ML criterion leading to optimum performance in terms of Frame Error rate (FER), we choose the information bit sequence minimizing the distance between the equivalent point and the noisy received point.

If we consider a low noise level, the error probability is quasi-null and very dependent on the distance between the transmitted point and its neighbors. Indeed, the probability that the noise results in a received point far from the transmitted point is very low. In this case, and assuming convolutional encoding, the codeword neighbors of the transmitted sequence are given by simple error paths. Ideally, the few different neighbor bits are separated thanks to the interleaver. If two or more of these bits are grouped in the same time period, the generated interference will degrade the performance. Therefore, the interleaver has to be carefully designed to separate the erroneous bits onto different time periods. If this interleaver condition is satisfied, the distance between the transmitted point and its considered neighbor is equal to the equivalent BSK distances sum. Averaging this remark on all the transmitted sequences and all the simple error paths leads to a construction criterion which is very close to the genie criterion. Indeed, the genie method considers the equivalent BSKs given by considering all the transmitted bits on s time periods.

On one hand, maximizing the distance between two neighboring codewords is not sufficient to optimize performance according to the ML criterion, since only considering two neighbors corresponds to optimizing a ML performance lower bound. Nevertheless, experiments show that performance is mainly lead by neighbors. On the other hand, the genie performance is given by an ideal situation that never exists in practice, so we minimize an inferior bound too. We have shown here that the two optimization criteria given by approximated ML and genie considerations are quite equivalent, provided that the interleaver is well designed. However, the genie performance is easily computable at the detector output. It allows us to consider only s symbol periods instead of considering the whole codeword.

2.4.3 Genie performance closed form expression at the detector output

We will apply 2.33 to compute the genie performance BER^{det} at the output of the detector in the case of ergodic MIMO channels. Since only one time period is considered, the temporal subscripts k are not necessary. The expression of the detector soft value, when the a priori is fed back by a genie, is given in 2.67. The bit error probability BER^{det} is directly related to the decision making on $\xi(c_\ell)$. By conditioning on the channel state H and the transmitted QAM vector z, we can write

$$\mathrm{BER}^{det}_{H,z} = E_\ell \left[P \left(|\xi(c_\ell) - c_\ell| \geq 0.5 \right) \right] \tag{2.68}$$

The symbol $E_\ell[.]$ denotes the mathematical expectation over the position ℓ of the coded bit. Then, using 2.67 and 2.68, we can express BER^{det} as a function of the LLR of a BSK with distance $d = d(z, \bar{z}^\ell)$, averaged over H, z and η:

$$\mathrm{BER}^{det} = E_{H,z,\ell} \left[P_H(z \to \bar{z}^\ell) \right] = E_{z,\ell} \left[\Phi \left(d(z, \bar{z}^\ell) \right) \right] \tag{2.69}$$

where $\Phi\left(d(z,\bar{z}^{\ell}\right) = E_H\left[P_H(z \to \bar{z}^{\ell})\right]$. We notice that the performance under the genie condition at the detector output, or equivalently at the decoder input, is the average probability of the $|\Omega| mn_t$ equivalent BSKs with distance $d(z,\bar{z}^{\ell})$ on an $n_t \times n_r$ MIMO channel. We can directly compute the pairwise error probability from 2.33 choosing $n_d = w = 1$, $d_1 = \delta_1 = d$, $\lambda_1 = 1$. Finally, we just have to identify the coefficients $\alpha_{1,i}$ from

$$\sum_{i=0}^{n_r-1} \frac{\alpha_{1,n_r-i}}{\varepsilon^{n_r-i}} + \mathcal{O}(1) = \sum_{i=0}^{n_r-1} \frac{(-1)^i \binom{n_r+i-1}{i}}{(\beta_{-1}-\beta_1)^{n_r+i}\varepsilon^{n_r-i}} + \mathcal{O}(1) \tag{2.70}$$

using $-\beta_1\beta_{-1} = \frac{2N_0}{d^2}$, we can write the closed form expression of $\Phi(d)$:

$$\Phi(d) = \left(\frac{d^2}{2N_0}\right)^{-n_r} \sum_{k=0}^{n_r-1} \frac{\binom{n_r+k-1}{k}}{(\beta_1-\beta_{-1})^{n_r+k}\beta_1^{n_r-k}} = \sum_{k=0}^{n_r-1} \binom{n_r+k-1}{k} \left(\frac{\beta_1}{\beta_1-\beta_{-1}}\right)^k \left(\frac{\beta_{-1}}{\beta_{-1}-\beta_1}\right)^{n_r} \tag{2.71}$$

$$= \left(\frac{1-\frac{1}{\sqrt{1+8N_0/d^2}}}{2}\right)^{n_r} \sum_{k=0}^{n_r-1} \binom{n_r+k-1}{k} \left(\frac{1+\frac{1}{\sqrt{1+8N_0/d^2}}}{2}\right)^k \tag{2.72}$$

which is the result obtained in [74]-chap.14. Finally, the error probability at the detector output is given by

$$\mathrm{BER}^{det} = \frac{1}{mn_t|\Omega|} \sum_{z\in\Omega} \sum_{l=1}^{mn_t} \Phi\left(d(z,\bar{z}^{\ell})\right) = E_{\{D\}}\left[\Phi(d)\right] \tag{2.73}$$

Conclusions

We have described the BICM transmitter applied to multiple antenna channels and its associated iterative receiver. Then the fundamental ideal interleaving condition is described and exact pairwise error probabilities are computed in both ergodic and block fading channels cases. These exact pairwise error probabilities may be used to compute very tight bounds on the error rates using either a union bound for ergodic channels or a tangential sphere bound for block fading channels. The asymptotic performance expressions give design criteria for the binary labeling, the linear precoder and the error correcting code choice. These optimizations will be discussed in next section. Finally, the genie method and an analogy with the ML performance at the detector output assuming ideal interleaving are described. Section 3 shows that the genie method can be invoked for the labeling and for the linear precoder optimizations.

Chapter 3

Bit-Interleaved Coded Modulation optimizations for MIMO channels

Introduction

In Chapter 2, we have presented the BICM transmitter and iterative receiver structure, and its performance on MIMO channels. We will now optimize each BICM component in order to enhance the Frame Error Rate (FER) or Bit Error Rate (BER).

In Section 3.1, we will focus on the mapping optimization over ergodic MIMO channels (or in the case of a sufficiently high number of independent channel states), providing high coding gains and obtained by increasing Euclidean distances between the global codeword points. We introduce the new idea of multi-dimensional mappings allowing capacity approaching performance with elementary codes.

The case of block fading MIMO channel is much more thorny. We must first maximize the diversity order before thinking of optimizing the coding gain. The BICM components optimization should be done jointly. In Section 3.3, the linear precoding optimization is considered, we present the conditions to be satisfied to achieve the optimal coding gain for a target diversity, and optimize the linear precoder to achieve good performance with an iterative receiver. In section 3.2, we take the linear precoding spreading factor into account in the computation of the Singleton bound on the diversity order, which enables us to find the minimal precoder size that leads to full diversity performance. Finally, in section 3.4, we optimize the interleaver to achieve the potential diversity and coding gains promised by the other elements optimization, under the constraint of ideal interleaving.

The notations required for the reading of this section were presented in Section 2.

3.1 Mapping optimizations

The binary mapping optimization of a signal constellation is an old problem in communication theory. Mappings based on Gray code [2] and Ungerboeck set partitioning [92] are among the

most famous binary labelings for coded and uncoded modulations. Multi-dimensional mapping has been extensively studied in the 80's for coded constellations on bandwidth-limited channels, as in [40] for the transmission of fractional bits, in [93][23][100] for trellis-coded multi-dimensional modulations, and in [41] for lattice constellations. More recently, in a parallel work to ours, a multi-dimensional binary mapping and a construction algorithm have been proposed for QPSK on single antenna fading channels [91]. Also, multi-dimensional mappings for multiple antenna BPSK signaling have been described in [78] using a design criterion which is a special case of our figure of merit (see (3.2) below).

In this section, a figure of merit for the binary mapping is derived from the ideal ML performance on an ergodic multiple antenna channel. A design criterion based on this figure is applied to the signal constellation to find good mappings suited for space-time coding. This ideal ML design criterion coincides with the criterion based on the genie method. Then, it is shown that the mapping figure of merit given by the ML performance is equivalent to the one given by the closed-form expression of the genie performance, related to ideal iterative decoding. The genie method has been previously applied to single antenna fading channels [24][63] and to multiple antenna channels with bi-dimensional mappings [106].

Optimized mappings may be determined either by searching inside a randomly selected list or by applying the binary switching algorithm (BSA) presented in [102][81]. Due to the intractability of the more optimal BSA for large labeling sizes, the first method is used in high complexity systems.

We have presented an approximation of the BICM performance with ideal interleaving and ML decoding. This approximation is a function of the signal-to-noise ratio, the number of transmit antennas and the error-correcting code. Moreover, it mainly depends on the set of distances D given by the binary mapping bit flipping and does not rely on the constellation shape itself. This allows to evaluate the performance of any constellation, even the most unstructured. The performance computation has been processed in the general case of n_t-dimensional distances d_k.

We will first calculate the figure of merit to be optimized for a given n_t-dimensional modulation Ω thanks to its associated distance set D. Then we will apply such an optimization to the classical QAMs and introduce the multi-dimensional mapping concept.

3.1.1 Mapping figure of merit

Let us first extract the asymptotic coding gain from the genie performance at the detector output. The asymptotic expression of BER^{det} when $N_0 \to 0$ is

$$\mathrm{BER}^{det} \sim \binom{2n_r - 1}{n_r} \frac{(2N_0)^{n_r}}{\mathfrak{F}_\Omega^{det}} \tag{3.1}$$

where the figure of merit $\mathfrak{F}_\Omega^{det}$ can be computed via

$$\frac{1}{\mathfrak{F}_\Omega^{det}} = E_{\{D\}}\left[d^{-2n_r}\right] = \frac{1}{mn_t|\Omega|} \sum_{z\in\Omega} \sum_{\ell=1}^{m.n_t} \frac{1}{d(z,\bar{z}^\ell)^{2n_r}} \tag{3.2}$$

The asymptotic expression of BER^{dec} when $N_0 \to 0$ is

$$\mathrm{BER}^{dec}_{N_0 \to 0} = \sum_{j=1}^{+\infty} \frac{j}{k_c L_c} a_{j,d_{Hmin}} \binom{2n_r d_{Hmin} - 1}{n_r d_{Hmin}} E_{\{D\}} \left[\prod_{k=1}^{d_{Hmin}} \left(\frac{d_k^2}{2N_0} \right)^{-n_r} \right] \tag{3.3}$$

Indeed, the error events with Hamming weight greater than d_{Hmin} have higher diversity and negligible contribution to the performance for high signal-to-noise ratios. The distances in the sequence $(d_1, \ldots, d_{d_{Hmin}})$ are independent random variables thanks to the ideal interleaver. The coding gain is a function of the mapping figure of merit $\mathfrak{F}_\Omega^{dec}$

$$\frac{1}{\mathfrak{F}_\Omega^{dec}} = E\left[\prod_{k=1}^{d_{Hmin}} d_k^{-2n_r} \right] = \left(E_{\{D\}} \left[d^{-2n_r} \right] \right)^{d_{Hmin}} \tag{3.4}$$

which leads to $\mathfrak{F}_\Omega^{dec} = \left(\mathfrak{F}_\Omega^{det} \right)^{d_{Hmin}}$. We notice that optimizing the mapping by maximizing the figure of merit derived from the ML decoding criterion is equivalent to maximizing the figure of merit given by the genie method at the detector output. We can compute the asymptotic gain of labeling Ω_2 with respect to labeling Ω_1 as follows:

$$Gain_{dB} \sim \frac{1}{n_r} 10 \log_{10} \left(\frac{\mathfrak{F}_{\Omega_2}^{det}}{\mathfrak{F}_{\Omega_1}^{det}} \right) \tag{3.5}$$

The asymptotic gain only depends on the distance distribution of the equivalent BSKs. We can for example compare two QAM mappings together or a QAM mapping with a PSK mapping.

3.1.2 Multi-dimensional labelings

When we consider classical mono-dimensional complex labelings, the asymptotic gain optimisation is limited by the $m \times n_t$ distances of mono-dimensional complex vectors. Clearly, vectors with more dimensions will lead to higher asymptotic gains. Let us define n_{map} as the number of antennas linked by the labeling.

When performing APP detection, the soft output is computed taking the whole set of transmitted vectors into account. Thus, there is no complexity increase using a multi-dimensional mapping instead of a mono-dimensional mapping. When the spectral efficiency is too high, e.g., 4×4 MIMO with 16-QAM input, the exhaustive detector is intractable, and a near-optimum APP detector such as SISO sphere decoder can be used [107]. When using sub-optimum APP detectors such as SISO-MMSE [32], the multiple antenna channel is considered as n_t interfering $1 \times n_r$ SIMO channels, and an exhaustive APP detector is processed on each sub-channel input. In this case, the multi-dimensional mappings cannot be used. The $n_t \times n_r$ MIMO channel can be viewed as n_{part} sub-channels equivalent to $n_t/n_{part} \times n_r$ MIMO channels. We can use a multi-dimensional mapping with $n_{map} \leq n_{part}$, compute an exhaustive detector on each sub-channel and a sub-optimum low complexity detector to separate the n_{part} sub-channels.

The BICM performance depends on the set of BSK modulations associated with the mapping. For example, the Gray mapping and its associated BSKs are represented on Fig. 3.1-a. The function $\Phi(d^2)$ defined in (2.72) is a decreasing function of d^2, this induces that maximizing the BSK distance improves the constellation mapping. Asymptotically, the mapping figure of merit

	Mean	Variance	Max gain (dB) at random	Max gain (dB) with BSA alg
$n_r = 1$, $n_{map} = 1$	3.15	0.35	7.10	7.23
$n_r = 2$, $n_{map} = 1$	2.40	0.29	7.27	7.42
$n_r = 4$, $n_{map} = 1$	1.43	0.13	7.15	7.36
$n_r = 1$, $n_{map} = 2$	6.75	0.02	7.48	10.68
$n_r = 2$, $n_{map} = 2$	5.65	0.04	6.80	11.12
$n_r = 4$, $n_{map} = 2$	3.59	0.04	5.01	10.98
$n_r = 1$, $n_{map} = 4$	10.97	0.01	10.99	/
$n_r = 2$, $n_{map} = 4$	10.67	0.01	10.71	/
$n_r = 4$, $n_{map} = 4$	8.33	0.02	8.57	/

Table 3.1: Statistics of 16-QAM optimized mappings

is $\mathfrak{F}_{\Omega}^{det}$ defined in (3.2). For example, the genie performance of 16-QAM with Gray labeling and minimal Euclidean distance 2.0 is

$$\mathrm{BER}_{gray}^{det} = \frac{24}{32}\Phi(4) + \frac{8}{32}\Phi(36) \tag{3.6}$$

The genie performance closed-form expression on MIMO $n_t \times n_r$ channels and the asymptotic gain expression (3.5) are very useful when designing binary mappings because of the search procedure low complexity. We choose the mapping at random or using an optimization algorithm such as the Binary Switching Algorithm (BSA) [102][81]. A mapping is optimized for two parameters: n_r and n_{map}. Indeed, for a given labeling, the asymptotic gain is the same for all n_t. We can numerically determine the asymptotic gain probability distribution of a randomly selected binary mapping, taking the Gray mapping as reference. On Fig. 3.2, for a 16-QAM constellation, we see the asymptotic gain distribution when $n_r = 1, 2, 4$ and $n_{map} = 1, 2, 4$. We also listed in Table 3.1 the mean, variance and maximum value of the asymptotic gain found by our search procedure. We randomly selected a large number of 2^m-QAM mappings, the search is not exhaustive. In the case of $n_r = 1$ and $n_{map} = 1$, the best mapping we found exhibits an asymptotic gain of 7.1 dB. When increasing the mapping number of dimensions ($n_{map} > 1$), it is possible to increase the minimum Euclidean distances of the embedded BSKs. This explains why the statistical mean of the asymptotic gain improves for $n_{map} > 1$.

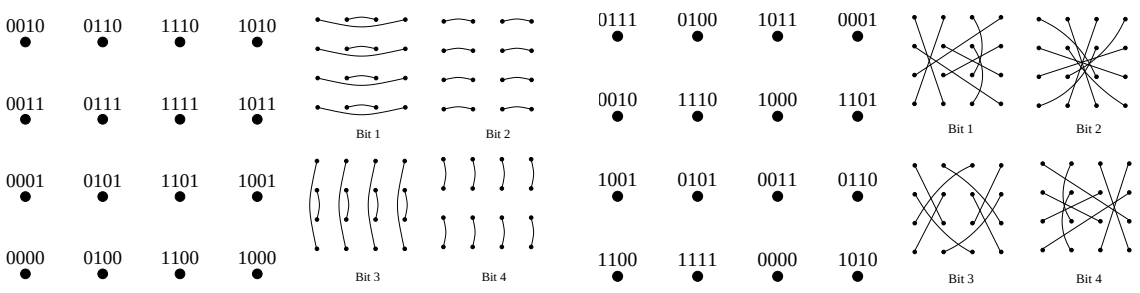

(a) Gray (b) Optimized

Figure 3.1: Mappings of 16-QAM constellation.

	$m=1$	$m=2$	$m=4$	$m=6$
$n_r=1$, $n_{map}=1$	0.00	1.25	7.23	12.62
$n_r=1$, $n_{map}=2$	1.25	5.05	10.68	/
$n_r=1$, $n_{map}=3$	3.55	6.52	/	/
$n_r=1$, $n_{map}=4$	5.05	/	/	/
$n_r=2$, $n_{map}=1$	0.00	1.02	7.42	12.97
$n_r=2$, $n_{map}=2$	1.02	5.02	11.12	/
$n_r=2$, $n_{map}=3$	3.46	6.24	/	/
$n_r=2$, $n_{map}=4$	5.02	/	/	/
$n_r=4$, $n_{map}=1$	0.00	0.69	7.36	12.81
$n_r=4$, $n_{map}=2$	0.69	4.98	10.98	/
$n_r=4$, $n_{map}=3$	3.35	6.16	/	/
$n_r=4$, $n_{map}=4$	4.98	7.26	/	/

Table 3.2: Best found asymptotic gains (in dB) with respect to Gray mapping for 2^m-QAM constellations and n_{map} dimensions

We applied such optimizations to other spectral efficiency values and mapping number of dimensions, the best gains we found with BSA are presented in Table 3.2 for 2^m-QAM constellations. Unfortunately, the BSA algorithm complexity grows strongly with the global spectral efficiency of the system, that is why we are limited to $m.n_{map} < 10$. The number of receive antennas n_r has an impact on the figure of merit. Thus, for a same mapping number of dimensions n_{map}, different values of n_r will lead to different optimized mappings. As an example, when n_r tends to infinity, the minimum distance in D will be dominant in the figure of merit expression, as on an AWGN channel, unlike smaller n_r values.

3.1.3 Increasing the number of dimensions with Space Time precoding

Linear precoding can be used to increase the diversity of systems with a small number of antennas. The symbols of s time periods are grouped together and spread over the transmit antennas and time periods without decreasing the system rate. The linear precoder's matrix S has sn_t rows and columns, where s is called the spreading factor of the linear precoder. A BICM on an ergodic multiple antenna channel exhibits a diversity equal to $d_{Hmin}n_r$. We can increase the observed diversity to $sd_{Hmin}n_r$ using an $sn_t \times sn_t$ complex linear precoder. For example we may use cyclotomic rotations [14][106][109]. If the linear precoder satisfies the norm conditions presented in [106] on an ergodic channel and under a genie condition, maximum precoding gain is obtained and the channel may be seen as a $1 \times sn_r$ SIMO channel. Multi-dimensionnal mappings designed for sn_r receive antennas may be used without any adaptation. The detection is processed over s time periods. We can use at most an sn_t-dimensional mapping. As shown in Section 3.1.5, if $s > 1$, we succeed in enhancing the coding gain via a mapping dimension increase at the cost of detector complexity increase.

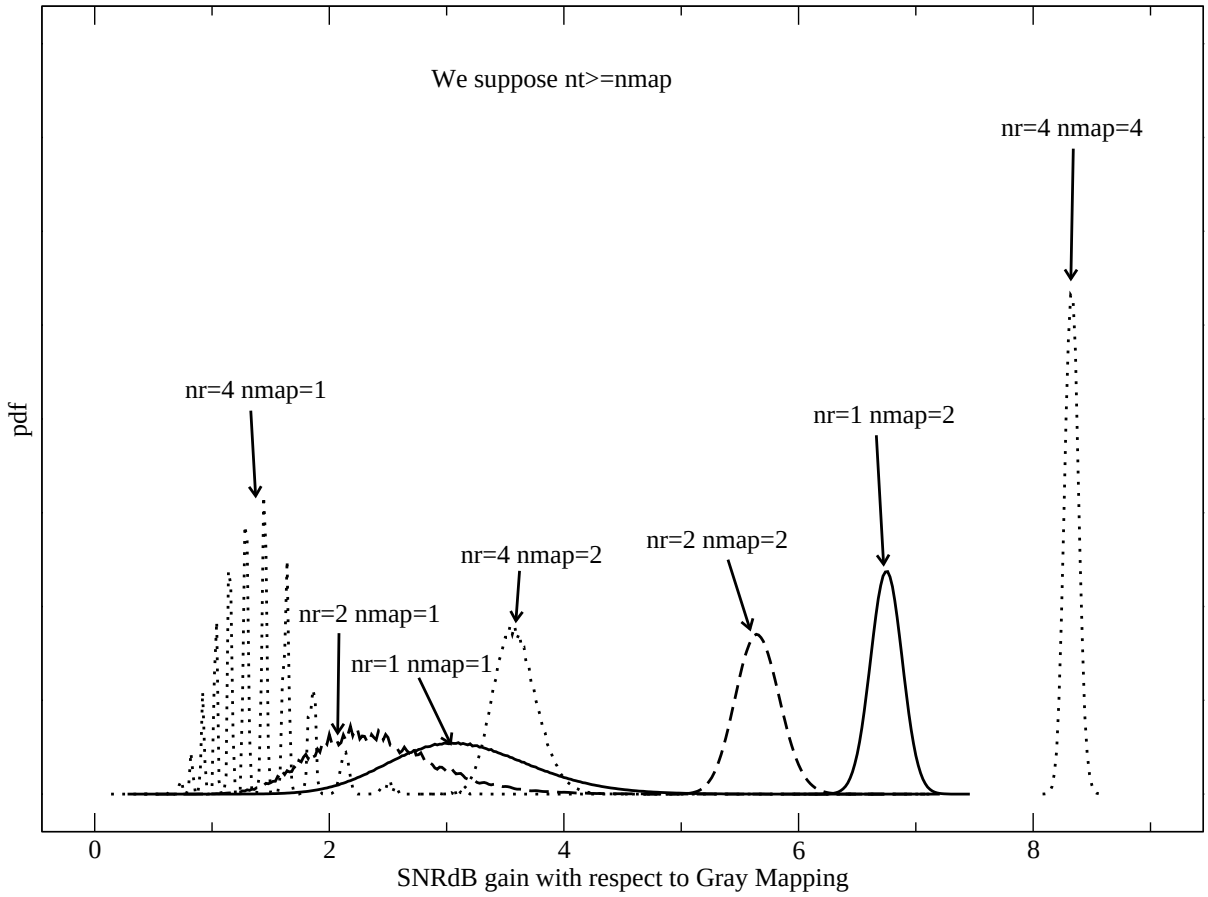

Figure 3.2: Asymptotic gain distribution of random 16-QAM mapping with respect to Gray mapping.

3.1.4 Convergence behavior

We have designed multi-dimensional mappings having large potential gains. Unfortunately, we cannot use such good mappings with a powerful error-correcting code because of convergence problems. Many studies have been made on BICM convergence using exit charts [88] or transfer functions. Most of them conclude that the better the gain at the last iteration, the worst at the first iteration. When considering a joint detection and decoding, the convergence is perfect if the bit error rate at the SISO decoder input in the first iteration is under a given threshold, which corresponds to a SNR value, commonly called waterfall point. The threshold depends on the error-correcting code, and in general, the better the code, the lower the threshold. If the signal to noise ratio is higher than the waterfall point, the system converges to an asymptote after a number of iterations decreasing with the noise level. At very high signal to noise ratio, the mapping gain with respect to Gray mapping is always observed at the output of the error-correcting code. For different mappings, the asymptotes are parallel, their slope are equal to the collected diversity lead by the minimum Hamming distance of the code, the number of receive antennas and the linear precoding factor. If we are interested in a target bit error rate equal to 10^{-5}, we have to find a good compromise between the waterfall and the error floor, as in all iterative processes. In the best case, performance converges to the asymptote exactly at the target error rate. This explains why, when using mappings with high gains,

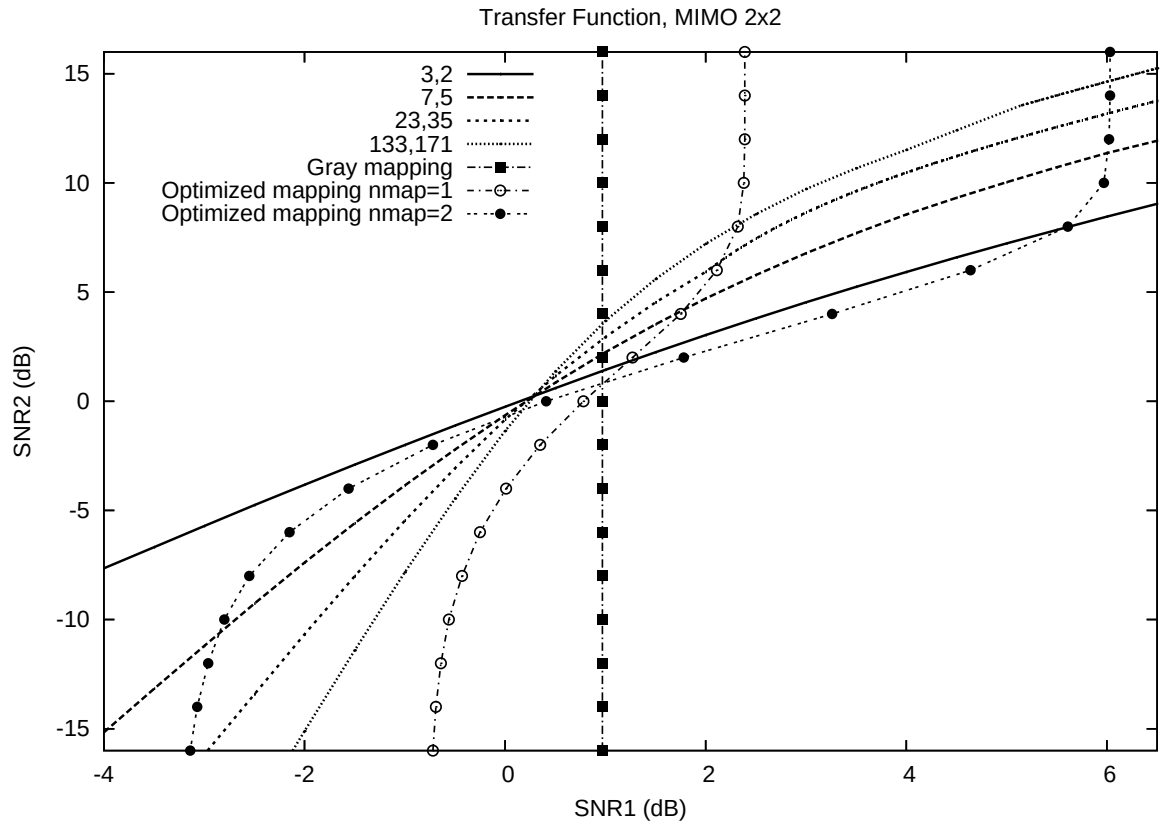

Figure 3.3: Transfer function of RSC codes and QPSK multi-dimensional mappings, $n_t = 2$, $n_r = 2$, $SNR = 4.0$ dB

we have to use "bad" error-correcting codes to ensure a good convergence. We illustrate this point on Fig. 3.3 which represents transfer functions (SNR_{in}^{det},SNR_{out}^{det}) of the detector using a Gaussian approximation with error probability matching [16] and different mappings. The transfer functions (SNR_{in}^{dec},SNR_{out}^{dec}) of different convolutional codes are also drawn. The transfer functions of recursive systematic convolutional codes show us that the better the code, the higher the slopes. The transfer function of the detector of a 2×2 MIMO channel with SNR = 4.0 dB with QPSK input is also represented with different mappings. The higher the asymptotic gain, the higher the right asymptote, but the lower the left asymptote. We deduce the convergence point searching for the fixed point beginning from the bottom left of the graph. For a given signal to noise ratio, when using multi-dimensional mappings with high asymptotic gain, we should use "bad" error-correcting codes in order to achieve a fixed point close to the right asymptotic value of the detector transfer function. This is equivalent to a perfect convergence to the limit obtained by the genie method.

3.1.5 Simulation Results

We present some simulation results illustrating the signal to noise ratio gains produced by multi-dimensional labeling under iterative joint detection and decoding. When considering convolutional codes, an exhaustive APP detector computes the soft values delivered to a single

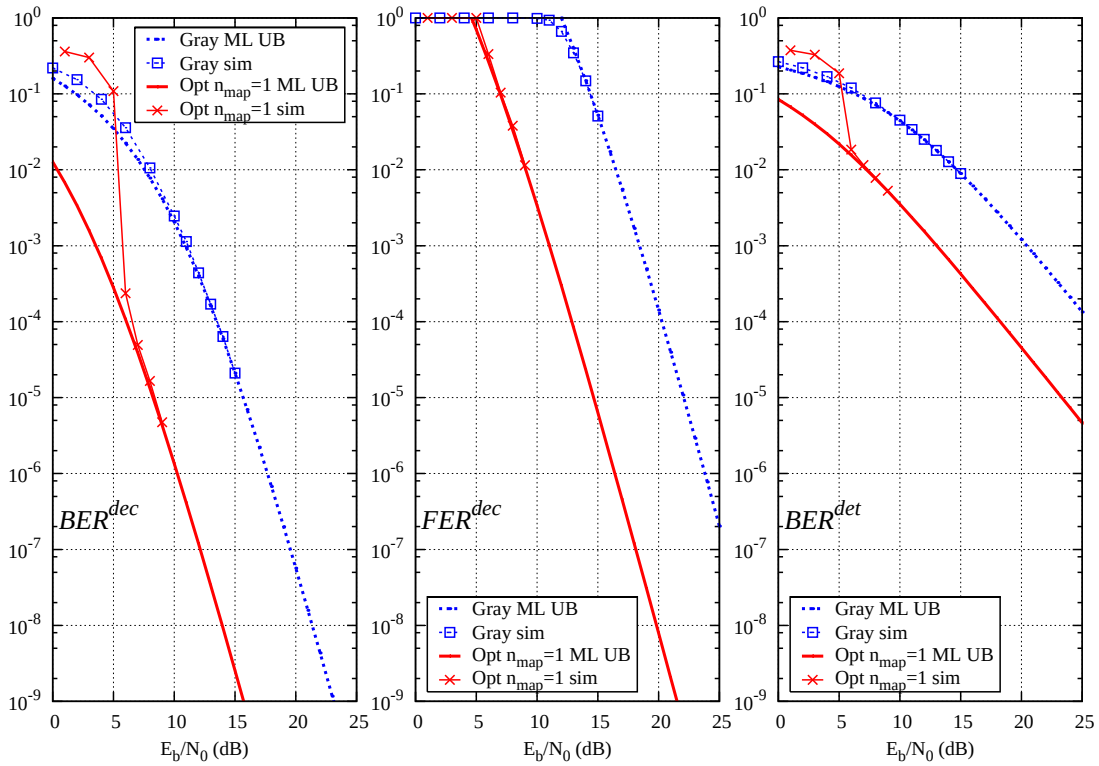

Figure 3.4: Ergodic 2×2 MIMO channel, interleaver size is 10000 bits, 2-state $(3,2)_8$ convolutional code, 16-QAM modulation, 10 decoding iterations. ML upperbound is denoted by "ML UB" and Monte Carlo simulation is denoted by "sim" in the captions.

SISO decoder: one iteration includes one detection and one forward-backward processing on the convolutional code trellis [4]. When a turbo code is used, one iteration at the receiver side includes one detection, one forward-backward processing on the first convolutional constituent code followed by one forward-backward processing on the second constituent code. A more precise study of the scheduling as in [18] is out of the scope of this thesis.

First, Fig. 3.4 illustrates the error rate of a two-state $(3,2)_8$ recursive systematic convolutional code (RSC) on a 2×2 MIMO channel with 16-QAM modulation. All situations presented in Fig. 3.4 correspond to $n_{map} = 1$. Gray mapping is compared to optimized mapping. The latter shows more than 7.4 dB gain with respect to Gray mapping. The three graphs in Fig. 3.4 show how the simulated error rate quickly converges to the ideal ML bound. The left graph depicts the bit error rate at the decoder output, the middle graph depicts the frame error rate at the decoder output and the right graph depicts the bit error rate at the MIMO detector output.

We now consider a target bit error rate equal to 10^{-5}, usually taken as a reference for wireless data transmission. The bounds are not drawn anymore.

A convolutional code cascaded with multi-dimensional mappings is compared to a turbo code in Fig. 3.5. The channel is 2×2 MIMO ergodic with QPSK input. A two-state $(3,2)_8$ non recursive non systematic convolutional code (NRNSC) is combined to mono-dimensional, bi-dimensional and four-dimensional mappings. A parallel turbo code based on an RSC $(7,5)_8$ is cascaded with Gray mapping. Optimized mappings degrade the performance of the turbo code

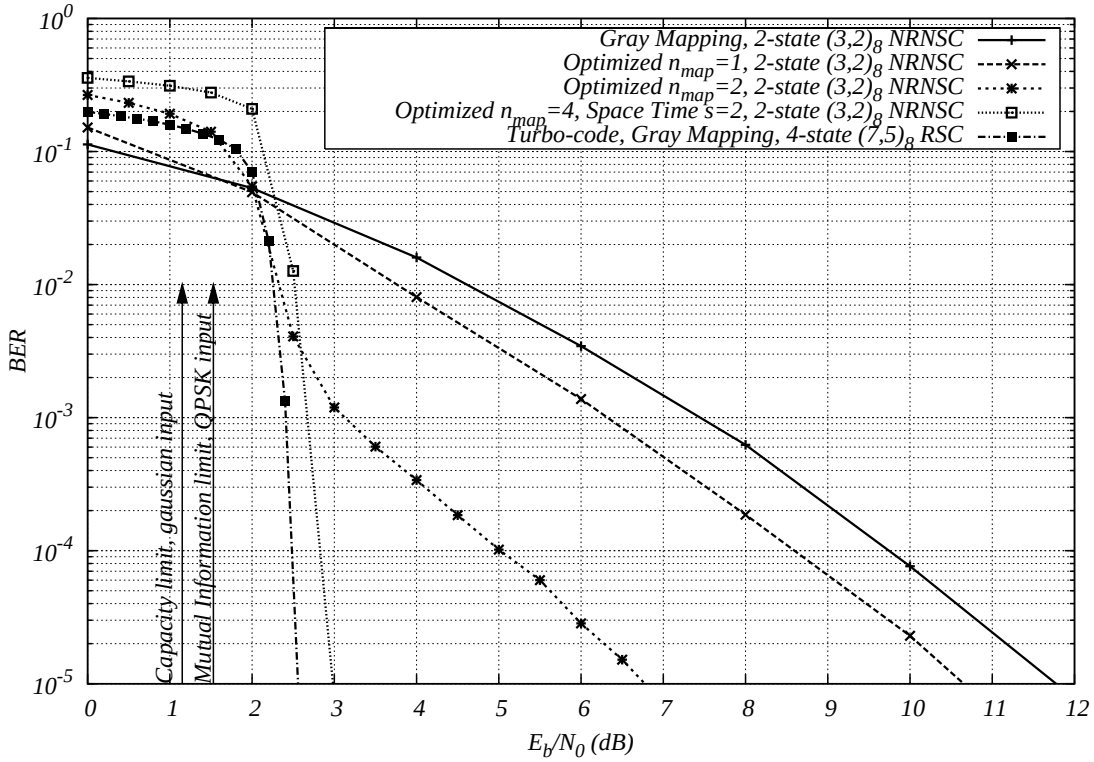

Figure 3.5: Ergodic 2×2 MIMO channel, interleaver size is 9000 bits, rate 1/2 NRNSC and Turbo-codes, QPSK modulation, 20 decoding iterations.

at the first iteration which entails a dramatic signal to noise ratio loss in the waterfall region. Fig. 3.5 shows that a $(3,2)_8$ convolutional code with four-dimensional mapping ($n_{map} = 4 = sn_t = 2 \times 2$) thanks to the linear precoder [106] performs within 0.5 dB from a rate-1/2 Gray mapped turbo code. The price to pay is the increased detection complexity of the time spreaded ($s = 2$) four-dimensional constellation. The optimized mapping with $n_{map} = 2$ and without linear precoding exhibits excellent error rates above 10^{-3}.

On Fig. 3.6, we present some simulation results on a 4×4 ergodic MIMO channel with QPSK input and NRNSC $(3,2)_8$. We used mono-, bi- and four-dimensional optimized mappings. We observe that the 0.69 dB (respectively 4.98 dB) expected gain between Gray and mono-dimensional (respectively bi-dimensional) optimized mappings is achieved. When the four-dimensional mapping simulation converges, the asymptote performs lower than 10^{-5}, this is why we measure slightly less than the 7.26 dB expected gain at this BER value. In the latter configuration, the optimal case when the simulation converges to the asymptote exactly at the target BER 10^{-5} is almost achieved. Finally, the system performs as well as the more complex system including turbo code, without increasing the complexity of the detection process. Indeed, in both cases, 20 iterations between the detector and decoder are necessary to achieve the convergence limit and, in each receiver iteration, the turbo decoding is four times more complex than the 2-state convolutional code decoding.

On Fig. 3.7, we present some simulation results on a 2×2 ergodic MIMO channel with 16-QAM input. When the BER is 10^{-5}, the gain with a mono-dimensional mapping is 7 dB. With a bi-dimensional mapping we achieve 9.1 dB, which is less than the asymptotic 11.12 dB

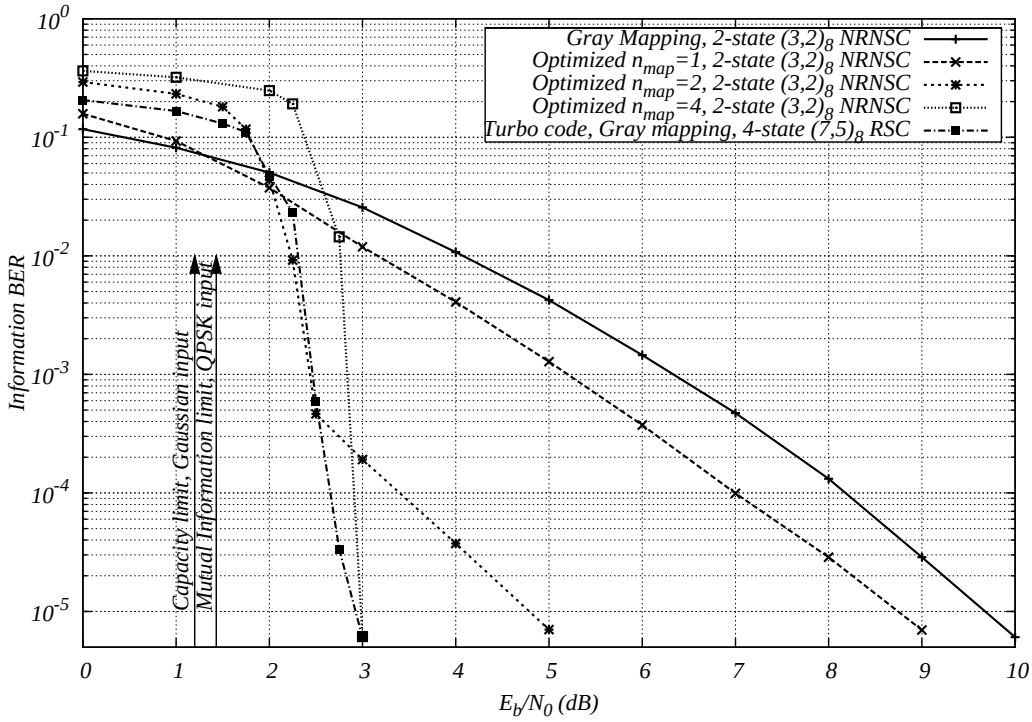

Figure 3.6: Ergodic 4×4 MIMO channel, interleaver size is 8192 bits, rate 1/2 NRNSC and Turbo-codes, QPSK modulation, 20 decoding iterations.

gain because convergence is not reached at 10^{-5}. With high spectral efficiency modulation and a simple NRNSC $(3, 2)_8$, we achieve performance within 0.5 dB from the turbo code performance with RSC $(7, 5)_8$ constituent codes even on the 2×2 ergodic MIMO channel.

The mapping optimization topic has been extensively discussed for BICM on single-antenna channels. In this section, we have presented an extension of this optimization to multi-dimensional mappings. In the case of high spectral efficiency modulations or a large number of transmit antennas, we achieve very high mapping gains and we perform close to turbo-codes with a single convolutional code, without increasing the optimum or near-optimum APP detector's complexity.

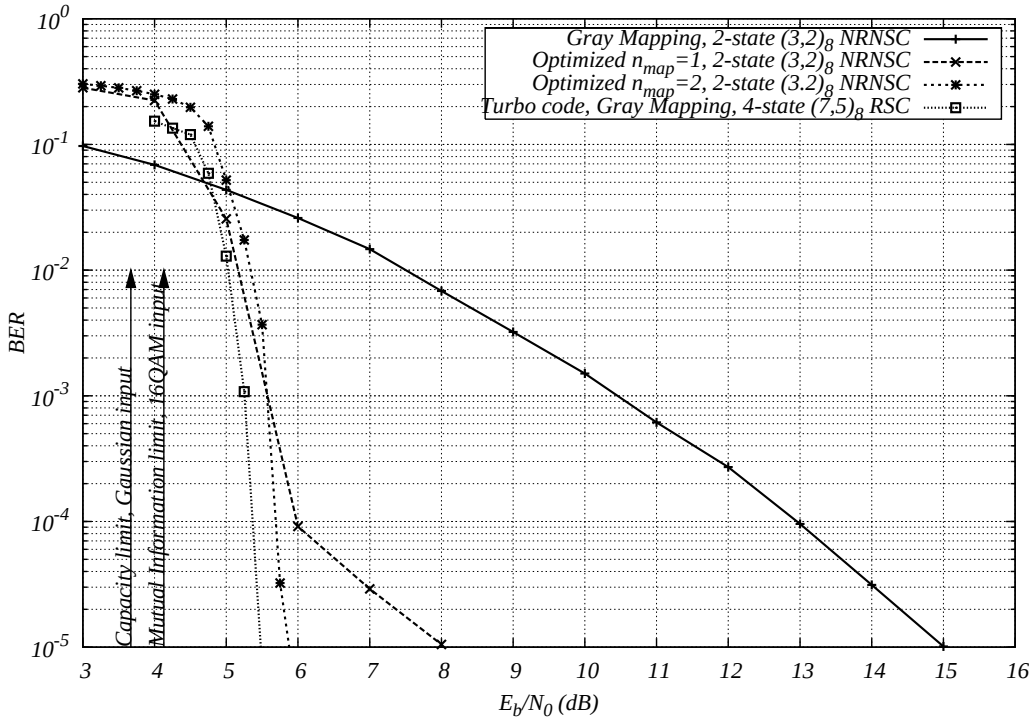

Figure 3.7: Ergodic 2×2 MIMO channel, interleaver size is 8192 bits, rate 1/2 NRNSC and Turbo-codes, 16-QAM modulation, 20 decoding iterations.

3.2 The Singleton bound with linear precoding

Let us now focus on the optimization of BICMs with linear precoding for non-ergodic MIMO channels. The studied ST-BICM is a serial concatenation of a rate R_c binary convolutional code, an interleaver of size $N_{\mathcal{C}}L_{\mathcal{C}}$ bits, and a QAM mapper followed by the precoder as described in Section 2.1.1.

Proposition 1 ensures that any pair of codewords has a full diversity order. In this section, we derive a condition on the existence of a practical interleaver that could achieve the conditions of proposition 1. Let us first make the following hypothesis :

Hypothesis 1 *The detector perfectly converts the $N_t \times N_r$ correlated MIMO N_c-block fading channel SH_k with QAM input into a $1 \times sn_r$ SIMO $n_t n_c/s$-block fading channel with BSK input, assuming that s is a divisor of $n_t n_c$.*

We will present in section 3.3 linear precoders that satisfy hypothesis 1. Under this condition, the detector collects an amount of diversity equal to sn_r. The full diversity $n_t n_c n_r$ is collected by the detector when $s = n_t n_c$, but unfortunately, the APP signal detection has an exponential complexity in s. On the other hand, the BICM channel decoder is also capable of collecting a large amount of diversity, but the latter is still limited by the Singleton bound [54][55][68]. Hence, the lowest complexity solution that reaches full diversity is to draw advantage of the whole channel code diversity and recover the remaining diversity by linear precoding. The best way to choose the spreading factor s is given by the Singleton bound described hereafter.

When S is the identity matrix, the ST-BICM diversity order is upper-bounded by [55]:

$$d \leq n_r \left(\lfloor n_c n_t (1 - R_c) \rfloor + 1 \right) \tag{3.7}$$

The maximal diversity given by the outage limit under a finite size QAM alphabet also achieves the above Singleton bound [44]. With a vanishing coding rate, i.e. $R_c \to 0$, it is possible to attain the overall system diversity order $n_r n_c n_t$ produced by the receive antennas, the transmit antennas and the distinct channel states. Unfortunately, this is unacceptable due to the vanishing transmitted information rate. Precoding is one mean to achieve maximum diversity with a non-vanishing coding rate.

The integer $N_b = n_c n_t / s$ is the best diversity multiplication factor to be collected by $\mathcal{C}$. The length of a $\mathcal{C}$ codeword is $L_{\mathcal{C}} N_{\mathcal{C}}$ binary elements. Let us group $L_{\mathcal{C}} N_{\mathcal{C}} / N_b$ bits into one non-binary symbol creating a non-binary code $\mathcal{C}'$. Now, $\mathcal{C}'$ is a length-N_b code built on an alphabet of size $2^{L_{\mathcal{C}} N_{\mathcal{C}} / N_b}$. The Singleton bound on the minimum Hamming distance of the non-binary $\mathcal{C}'$ becomes $D_H \leq N_b - \lceil N_b R_{\mathcal{C}} \rceil + 1$. Multiplying the previous inequality with the Nakagami law order $s n_r$ yields the maximum achievable diversity order d_{max} after decoding,

$$d_{max} \leq s n_r \left\lfloor \frac{n_c n_t}{s} (1 - R_{\mathcal{C}}) + 1 \right\rfloor \tag{3.8}$$

where d_{max} is an integer. Finally, since d_{max} is upper-bounded by the channel intrinsic diversity and the minimum Hamming distance d_{Hmin} of the binary code, we can write

$$d_{max} \leq \min \left(s n_r \left\lfloor \frac{n_c n_t}{s} (1 - R_{\mathcal{C}}) + 1 \right\rfloor ; n_t n_c n_r ; s n_r d_{Hmin} \right) \tag{3.9}$$

If d_{Hmin} is not a limiting factor (we choose $\mathcal{C}$ accordingly), we can select the value of s that leads to a modified Singleton bound greater than or equal to $n_t n_c n_r$.

Proposition 2 *Considering a BICM with a rate $R_{\mathcal{C}}$ binary error-correcting code on an $n_t \times n_r$ MIMO channel with n_c distinct channel states per codeword, the spreading factor s of a linear precoder must be a divisor of $n_t n_c$ and must satisfy $s \geq R_{\mathcal{C}} n_c n_t$ in order to achieve the full diversity $n_t n_c n_r$ for any pair of codewords. In this case, the ideal interleaving conditions can be achieved with an optimized interleaver.*

The smallest integer s_{opt} satisfying the above proposition minimizes the detector's complexity. If $R_{\mathcal{C}} > 1/2$, then $s_{opt} = n_c n_t$ which involves the highest complexity. If $R_{\mathcal{C}} \leq 1/(n_c n_t)$, linear precoding is not required.

Tables 3.3 and 3.4 show the diversity order derived from the Singleton bound versus s and n_t, for $n_c = 1$ and $n_c = 2$ respectively. The values in bold indicate full diversity configurations. For example, in Table 3.3, for $n_t = 4$, $s = 2$ is a better choice than $s = 4$ since it leads to an identical diversity order with a lower complexity.

3.3 Linear precoder optimizations

We call space-time spreading matrix or linear precoder the particular case of full rate linear space-time block codes. The space-time matrix enhances the diversity by mixing the symbols of

$n_t \diagdown s$	1	2	3	4	5	6	7	8
1	**1**							
2	**2**	**2**						
3	2		**3**					
4	3	**4**		**4**				
5	3				**5**			
6	4	4	**6**			**6**		
7	4						**7**	
8	5	6		**8**				**8**

Table 3.3: Diversity order from modified Singleton bound versus number of transmit antennas n_t and spreading factor s, for $R_{\mathcal{C}} = 1/2$, $n_r = 1$ and $n_c = 1$.

$n_t \diagdown s$	1	2	3	4	5	6	7	8
1	**2**	**2**						
2	3	**4**		**4**				
3	4		**6**			**6**		
4	5	6		**8**				**8**
5	6				**10**			
6	7	8	9			**12**		
7	8						**14**	
8	9	10		12				**16**

Table 3.4: Diversity order from modified Singleton bound versus number of transmit antennas n_t and spreading factor s, for $R_{\mathcal{C}} = 1/2$, $n_r = 1$, $n_c = 2$.

different time periods and antennas.

Many studies have been published on space-time spreading matrices introducing some redundancy, well-known as space-time block codes. On one hand, some of them are decoded by a low-complexity ML decoder, but they sacrifice transmission data rate for the sake of high performance. Among them, the Alamouti scheme [3] is the most famous, but is only optimal for a 2×1 MIMO channel. The other designs allowing low ML decoding complexity are based on an extension of the Alamouti principle (e.g., DSTTD [90]) but also sacrifice the data rate. On the other hand, full rate space-time codes have recently been proposed [7][28][29][30][31][34][70]. However, their optimisation does not take into account their concatenation with an error correcting code. In this section, we describe a near-ideal solution for linear precoding in BICMs under iterative decoding process. Our strategy is to separate the coding step and the geometry properties in order to express some criteria allowing the construction of a space-time spreading matrix for given channel parameters n_t, n_r, n_c. The inclusion of rotations to enhance the BICM performance over single antenna channels has been proposed in [61]. The proposed solution uses this concept for designing a space-time code including a powerfull error correcting code.

When the channel is ergodic, the diversity at the decoder input and output are respectively n_r and $n_r d_{Hmin}$. We have shown in Section 3.1 that some elementary codes (e.g., NRNSC $(3, 2)_8$) could be used to allow a good convergence when using high gain mappings. In this case, the error-floor exhibits low diversity. One solution to enhance the diversity of elementary codes

is the use of linear precoding that allows to recover a diversity order up to $n_r s$ and $n_r s d_{Hmin}$ at the decoder input and output, respectively. The parameter s is called spreading factor.

When the channel is quasi-static or block fading with parameter n_c, the diversity is upper bounded by $n_c n_t n_r$ which may be more limiting than $n_r d_{Hmin}$ (e.g., $n_t = 2$, $n_r = 1$, n_c=1). We introduce a new design criterion of space-time spreading matrices that guarantees a diversity proportional to the spreading factor and a maximal coding gain at the last iteration of an iterative joint detection and decoding.

First, the linear precoder matrix must have a non-null determinant to exhibit full-diversity. Indeed, a non-full rank transformation is equivalent to a reduction of the number of transmit antennas. We suppose that the rows unity norm condition is satisfied but this is not a necessary condition, an unequal power transmission on each dimension could be exploited by a successive interference cancellation receiver. This is not the issue in our case.

In Section 2.2.4, the coding gain of an ideally interleaved BICM with linear precoding is defined by

$$\mathcal{G}_{s,n_s}(\Delta,\Lambda) = \left(\prod_{v=1}^{n_\delta} \delta_v^{2\lambda_v}\right)^{1/N_\delta} \tag{3.10}$$

and $N_\delta = \sum_{v=1}^{n_\delta} \lambda_v$. Remember that the δ_v^2 values are given by the sequence of the non-null eigenvalues $\vartheta_{k,i}^{[t]}$. The value $\vartheta_{k,i}^{[t]}$ denotes the i-th eigenvalue of $M_k^{[t]} M_k^{[t]*}$ where $M_k^{[t]}$ is defined by

$$\forall 1 \le k \le n_c/n_s, \forall 1 \le t \le n_s, \quad \Sigma_k^{[t]} = M_k^{[t]*} M_k^{[t]} = \sum_{l=1}^{N_t} \gamma_{k,l}^2 \sum_{i=1}^{s} S_l^{[t][i]*} S_l^{[t][i]} \tag{3.11}$$

3.3.1 The BICM ideal coding gain

First, remember that the linear precoding converts the $n_t \times n_r$ MIMO n_c-block fading channel into an $N_t \times N_r$ correlated MIMO N_c-block fading channel.

First we look for the best achievable coding gain for the fixed parameters n_t, n_r, n_c, R_c and the appropriate way to choose the error correcting code, the binary mapping, the linear precoder and its parameters s and n_s to achieve the ideal coding gain.

We want to achieve full diversity under ML decoding or iterative joint detection and decoding, this induces that there are $n_c n_t$ non-null eigenvalues $\vartheta_{k,i}^{[t]}$:

$$\mathcal{G}_{s,n_s}(\Delta,\Lambda) = \left(\prod_{k=1}^{N_c} \prod_{t=1}^{n_s} \prod_{i=1}^{n_t} \vartheta_{k,i}^{[t]}\right)^{1/(n_c n_t)} \tag{3.12}$$

Furthermore, we want to maximize the $\mathcal{G}_{s,n_s}(\Delta,\Lambda)$ expression. Assume that the norm of each row S_l is equal to 1, we get

$$\sum_{k=1}^{N_c} \sum_{t=1}^{n_s} \sum_{i=1}^{n_t} \vartheta_{k,i}^{[t]} = \sum_{k=1}^{N_c} \sum_{l=1}^{N_t} \gamma_{k,l}^2 = \sum_{k=1}^{N_c} \sum_{l=1}^{N_t} \sum_{i=1}^{\kappa_{k,l}} d_{k,l,i}^2 \tag{3.13}$$

We use the Lagrange multiplier

$$f = \prod_{k=1}^{N_c}\prod_{t=1}^{n_s}\prod_{i=1}^{n_t} {\vartheta_{k,i}^{[t]}}^{n_r} - \lambda\left(\sum_{k=1}^{N_c}\sum_{t=1}^{n_s}\sum_{i=1}^{n_t}\vartheta_{k,i}^{[t]} - \sum_{k=1}^{N_c}\sum_{l=1}^{N_t}\gamma_{k,l}^2\right) \tag{3.14}$$

The nulling of the derivation of f with respect to $\vartheta_{k',i'}^{[t']}$ leads to

$$\forall k', i', t', \quad \frac{\lambda}{n_r} = \frac{\prod_{k=1}^{N_c}\prod_{t=1}^{n_s}\prod_{i=1}^{n_t}{\vartheta_{k,i}^{[t]}}^{n_r}}{\vartheta_{k',i'}^{[t']}} \Leftrightarrow \vartheta_{k',i'}^{[t']} = \sum_{k=1}^{N_c}\sum_{l=1}^{N_t}\frac{\gamma_{k,l}^2}{n_t n_c} = \sum_{i=1}^{w}\frac{d_i^2}{n_t n_c} \tag{3.15}$$

which induces

$$\mathcal{G}_{ideal}(\Delta,\Lambda) = \sum_{k=1}^{N_c}\sum_{l=1}^{N_t}\frac{\gamma_{k,l}^2}{n_t n_c} = \sum_{i=1}^{w}\frac{d_i^2}{n_t n_c} \tag{3.16}$$

The exact pairwise error probability simplifies to the classical expression of the performance of a BPSK with separation $\sum_{j=1}^{w} d_j^2$ over a diversity channel with order $n_c n_t n_r$.

$$P_{w,ideal}(\Delta,\Lambda) = \left(1-\left(1+\frac{8N_0 n_t n_c}{\sum_{j=1}^{w} d_j^2}\right)^{-1/2}\right)^{n_c n_t n_r} \sum_{k=0}^{n_c n_t n_r - 1} \frac{\binom{n_c n_t n_r + k - 1}{k}}{2^{n_c n_t n_r + k}} \left(1+\left(1+\frac{8N_0 n_t n_c}{\sum_{j=1}^{w} d_j^2}\right)^{-1/2}\right)^{k} \tag{3.17}$$

The ideal coding gain is obtained when all eigenvalues are equal.

With a perfect Shannon code, i.e., gaussian channel inputs, the transmitted vector is close to the surface of a sphere at the channel input, thanks to the sphere hardening phenomenon. After transmission on a fading channel, vectors belong to an ellipsoid. In a ST-BICM, precoded modulation symbols quantify the Shannon sphere and best quantization is obtained by uniformly distribute them on the sphere. Indeed, Bit-Interleaved Coded Modulations are known to be capacity achieving schemes over AWGN channels. This induces that a quasi uniform repartition of the code words on the sphere surface is achieved. At the output of the MIMO channel, the noiseless points are placed, with a high probability, on the surface of the ellipsoid. From equation (3.16), we see that an ideal interleaving leads to an equi repartion of the euclidean distance between two codewords on the $n_t n_c$ channel states. This induces that the euclidean distance varies as a $n_t n_c n_r$ Nakagami distribution. Finally we may conclude that the BICM with ideal precoding and ideal interleaving is an outage capacity achieving scheme. The objective is to be the most as possible near from these two ideal conditions.

The ideal coding gain is a fundamental limit which cannot be outperformed. It is useful to evaluate how optimal the practical design of a BICM is. Our aim is to find the best design, corresponding to eigenvalues which are as much as possible all close together. The more different the eigenvalues are, the lower the product in (3.12) and the coding gain are. From (3.16), we see that the ideal coding gain is the same as with the same coded modulation transmitted on a $1 \times n_c n_t n_r$ SIMO channel, applying the appropriate E_b/N_0 normalization if necessary. This proves that the ideally precoded and interleavd BICM is an orthogonal space time code.

Without linear precoding, the ideal coding gain is only achieved if all $\gamma_{k,l}$ are equal. Remember that each $\gamma_{k,l}$ is a sum of $\kappa_{k,l}$ distances $d_{k,l,i}$. Thanks to the second point of Proposition 1, the $\kappa_{k,l}$ are close to $w/(n_t n_c)$. We conclude that the variance of the $\gamma_{k,l}$ values decreases when w increases. Thus, if the error correcting code is powerful enough with respect to $n_t n_c$ and $|D|$,

it allows for a good averaging of the $d_{k,l,i}$ into the $\gamma_{k,l}$ and quasi-ideal coding gain is observed.

If the error correcting code is not powerful enough to achieve the ideal coding gain, i.e., the $\gamma_{k,l}$ values are very different, we will see in the following that the linear precoder provides an additional coding gain by averaging the $\gamma_{k,l}$ values before transmission. First, we derive the optimal coding gain which can be achieved using an ideal linear precoder for a given binary labeling and error correcting code. The expectation in (3.12) is made over the set of eigenvalues $\vartheta_{k,i}^{[t]}$ which is only dependent on the set of factorized distances $\gamma_{k,l}$. Variables $\gamma_{k,l}$ for different k values correspond to independent channel realizations H_k which are not linked by the linear precoder. Thus, random variables $\prod_{t=1}^{n_s}\prod_{i=1}^{n_t}\vartheta_{k,i}^{[t]\,n_r}$ are independent for distinct values of k. The optimal coding gain with linear precoding is

$$\mathcal{G}_{s,n_s,opt}(\Delta,\Lambda)=\prod_{k=1}^{N_c}\left(\sum_{l=1}^{N_t}\frac{\gamma_{k,l}^2}{n_t n_s}\right)^{1/N_c} \tag{3.18}$$

Equation (3.18) means that an optimal linear precoder is capable of making eigenvalues equal for a same k. However, for different values of k, the $\vartheta_{k,l}^{[t]}$ eigenvalues are different, which induces a coding gain loss.

When the mapping and error correcting code are given and the interleaving is ideal, the choice of linear precoding parameters impacts on optimal coding gain. Let us consider codewords that are equidistant from the transmitted codeword, i.e., a set of distance configurations corresponding to a same value of $\sum_{k,l}\gamma_{k,l}^2$. The variance of $\sum_{l=1}^{N_t}\gamma_{k,l}^2/(n_t n_s)$ over this set decreases when n_s increases, as the number of distances building each $\gamma_{k,l}$ is higher. The lower the variance of eigenvalues, the higher the coding gain. Thus, $\mathcal{G}_{s,n_s,opt}(\Delta,\Lambda)$ is an increasing function of n_s. For a given s, we should choose $n_s=\min(s,n_c)$. The optimal coding gain $\mathcal{G}_{s,\min(s,n_c),opt}(\Delta,\Lambda)$ is an increasing function of s. If $n_s=n_c$ and $s=n_t n_c$, the ideal coding gain is achieved by the optimal precoder. Finally, we can surround the coding gain as follows:

$$\forall s,n_s\quad \mathcal{G}_{ideal}(\Delta,\Lambda)\geq\mathcal{G}_{s,\min(s,n_c),opt}(\Delta,\Lambda)\geq\mathcal{G}_{s,1,opt}(\Delta,\Lambda)\geq\mathcal{G}_{1,1,opt}(\Delta,\Lambda)\geq\mathcal{G}_{bf}(\Delta,\Lambda) \tag{3.19}$$

If, for any pairwise error probability, the error correcting code and the mapping are designed to allow $\mathcal{G}_{bf}(\Delta,\Lambda)\simeq\mathcal{G}_{ideal}(\Delta,\Lambda)$, the linear precoder optimization is useless from a coding gain point-of-view. However, obtaining near-ideal coding gain without precoding requires an optimization of the error correcting code and mapping for any pairwise error probability, which is intractable for non-trivial modulations and codes. Furthermore, the first objective of linear precoding is the diversity control, which has a high influence on the performance even at medium FER ($10^{-2}\sim10^{-3}$), especially for low diversity orders. Therefore, precoding is often useful in the BICM structure.

We saw the impact of the linear precoding for a considered pairwise error probability. We can wonder what is the behaviour of the global performance under linear precoding. As stated in section 2.3.2, if $n_r n_t n_c$ grows, the smallest coding gains have more impact on the final performance. Since the linear precoder provides a more substantial gain for the low hamming weight configurations, the role of the linear precoder will be magnified as the diversity grows. This is particularly true when the number of transmit antennas increases: The increasing diversity gives more and more importance on the nearest neighbours in the euclidean code. These

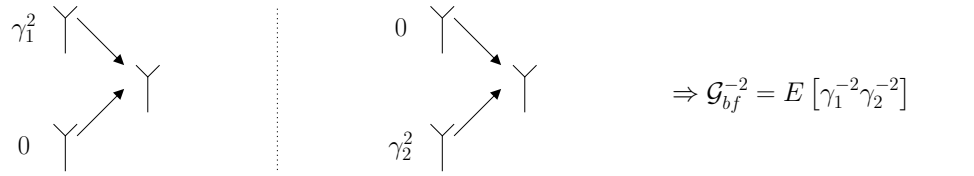

Figure 3.8: Coding gain for unprecoded 2×1 quasi-static MIMO channel

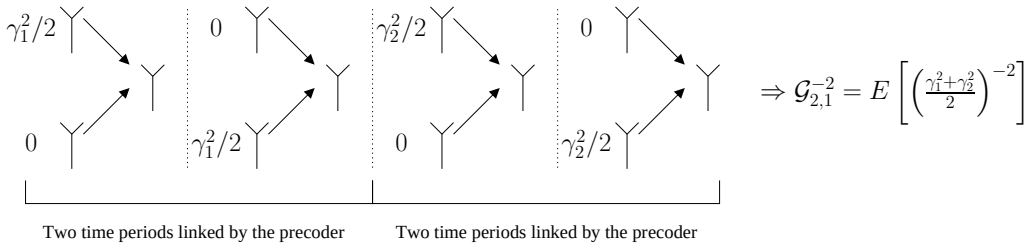

Figure 3.9: Coding gain for precoded 2×1 quasi-static MIMO channel, $s = 2$

neighbours are defined from the error events with the smallest hamming weights. For a given hamming weight, as the number of transmit antenna increases, the variables $\gamma_{k,l}$ decrease and their variance increase. The difference between the coding gain obtained with linear precoding and unprecoded systems finally dramatically increases with n_t.

Example of ideal coding gain with a 2×1 ***quasi-static MIMO channel***
In order to illustrate the role of the linear precoding in the coding gain optimization, we consider a 2×1 quasi-static MIMO channel, a pairwise error probability between two codewords separated by a Hamming distance w bits.

Fig. 3.8 represents the distribution of the two γ_1 and γ_2 values over the two transmit antennas and on two different time periods. This illustrates the factorization of the distances into the γ values. The instantaneous coding gain is equal to $\sqrt{\gamma_1^2\gamma_2^2}$. Suppose that a linear precoder spreads the value γ_1 over two time periods as presented in Fig.3.9 and two transmit antennas dividing the power in two equal parts $\gamma_1^2/2$. The average value $(\gamma_1^2 + \gamma_2^2)/2$ is transmitted on each antenna, the coding gain is optimal and equal to $(\gamma_1^2 + \gamma_2^2)/2$.

For example, consider a BPSK modulation and a pairwise error probability with Hamming weight 3. With optimal linear precoding, the ideal interleaving provides for example $\gamma_1^2 = 2 \times 2^2$ and $\gamma_2^2 = 1 \times 2^2$. With optimal linear precoding, we have a distance $(2 \times 2^2 + 1 \times 2^2)/2$ associated to each antenna. The ratio between the two averaged coding gain is equal to $\sqrt{9/8}$ which predicts a gain of 0.26 dB using linear precoding. If $w = 5$, the coding gain becomes $10\log_{10}(\sqrt{24/25}) \simeq 0.09$ dB. If $w = 11$, the coding gain becomes $10\log_{10}(\sqrt{120/121}) \simeq 0.02$ dB. The higher the Hamming weight involved in the pairwise error probability is, the less the difference between the factorized distances is and the less coding gain is; because the κ_k values are higher.

We can see on Table 3.5 the best gain to be provided by linear precoding for a quasi-satic channel with BPSK input with respect to a full diversity unprecoded scheme. These gains are particularly low because the error correcting code aims at recovering a large amount of coding gain, which shows that a BICM is a very efficient structure. As a remark, if an other modulation

	$w=2$	$w=3$	$w=4$	$w=5$	$w=6$	$w=7$	$w=8$
$n_t=2$	0.00	0.26	0.00	0.09	0.00	0.05	0.00
$n_t=3$	/	0.00	0.25	0.21	0.00	0.08	0.08
$n_t=4$	/	/	0.00	0.22	0.26	0.17	0.00
$n_t=5$	/	/	/	0.00	0.19	0.26	0.24
$n_t=6$	/	/	/	/	0.00	0.17	0.25
$n_t=7$	/	/	/	/	/	0.00	0.15
$n_t=8$	/	/	/	/	/	/	0.00

Table 3.5: Best gain in dB to be provided by linear precoding with respect to an unprecoded system, with ideal interleaving and for a given pair of codeword with hamming distance w and BPSK input.

with Gray mapping is used, the nearest neigbour in the euclidean code has the same distance configuration as the BPSK input case. Moreover, for high diversity orders, the global error rate will be dominated by the neighbours for high SNR and the gain provided by linear precoding will be very close to the ones shown in Table 3.5. However, if the diversity is low, we cannot make the approximation that the error rate is dominated by the errors with the neighbours in the euclidean code. In this case, the gains provided by linear precoding may be much more important. Assume that a 16-QAM modulation with Gray mapping is transmitted on an $n_t = 2$ quasi-static channel. For $w = 5$, there exists a neighbour with distances configuration $(3A, 3A, 3A, A, A)$, and more precisely $\gamma_1^2 = 9A^2 + 9A^2 + 9A^2$ and $\gamma_2^2 = A^2 + A^2$. The gain to be provided by linear precoding is equal to $10\log_{10}(29/2/\sqrt{54}) = 2.95dB$. As already stated, the final coding gain is equal to a weighted sum of all the coding gains, where the weighting coefficients cannot be easily computed in the case of low diversity orders.

Since the linear precoder may be necessary for the diversity order control, we will focus on the creation of linear precoders that maximize the coding gain for a given s.

3.3.2 A class of linear precoders

Under linear precoding, the optimal coding gain is achieved if all $\vartheta_{k,i}^{[t]}$ variables are equal for a same k. Let us first consider the eigenvalues associated to the independent realizations in the spreading matrix, indexed by t. First, two matrices $M_k^{[t_1]}$ and $M_k^{[t_2]}$, as introduced in (2.52), should have the same eigenvalues, which is satisfied if $\forall(t_1,t_2), M_k^{[t_1]} = R^{t_1,t_2*} M_k^{[t_2]} R^{t_1,t_2}$, where R^{t_1,t_2} is a unitary matrix, for example a rotation. Hence, $\forall(t_1,t_2), S'^{[t_1]}_l = S'^{[t_2]}_l R^{t_1,t_2}$. The precoding sub-part $S_l^{[t_1]}$, with spreading factor $s' = s/n_s$, experiences a quasi-static channel. We assume that s' is an integer, divisor of n_t. It is sufficient to design the first sub-part of the precoder matrix rows for a quasi-static channel and rotate it to compute the other sub-parts. Furthermore, any choice of R^{t_1,t_2} leads to the same performance because the eigenvalues remain unchanged. The condition simplifies to $\|S'^{[t_1]}_l\| = \|S'^{[t_2]}_l\|$.

Let us now set the index t and optimize the equivalent precoder over the quasi-static channel $\text{diag}\left(H_k^{[t][1]}, \ldots, H_k^{[t][s']}\right)$. If all the eigenvalues of $M_k^{[t]} M_k^{[t]*}$ are equal, $M_k^{[t]}$ is a weighted unitary

matrix, so is $M_k^{[t]*}$ and

$$M_k^{[t]} M_k^{[t]*} = M_k^{[t]*} M_k^{[t]} = \sum_{l=1}^{N_t} V'^*_{k,l} V'_{k,l} = \sum_{l=1}^{N_t} \gamma_{k,l}^2 S'^{[t]*}_l S'^{[t]}_l \tag{3.20}$$

The $s' \times n_t$ matrix $S'^{[t]}_l$ given by

$$S'^{[t]}_l = \begin{bmatrix} S_l^{[t][1]} \\ S_l^{[t][2]} \\ \vdots \\ S_l^{[t][s']} \end{bmatrix} \tag{3.21}$$

We get

$$\sum_{l=1}^{N_t} \gamma_{k,l}^2 S'^{[t]*}_l S'^{[t]}_l = \sum_{l=1}^{N_t} \gamma_{k,l}^2 \sum_{i=1}^{s'} S_l^{[t][i]*} S_l^{[t][i]} \tag{3.22}$$

Matrix $S_l^{[t][i]*} S_l^{[t][i]}$ has rank one and matrix $\sum_{i=1}^{s'} S_l^{[t][i]*} S_l^{[t][i]}$ has maximal rank s'. It can be shown that it is impossible to get all eigenvalues equal to $\sum_{l=1}^{N_t} \gamma_{k,l}^2 / n_t n_s$ as required to achieve the optimal coding gain. However, in order to insure that $M_k^{[t]} M_k^{[t]*}$ has a rank n_t and that the eigenvalues are as equal as possible, we group ss' values $\gamma_{k,l}$ together and associate them to one of the n_t/s' group of s' eigenvalues: we denote $S_l^{[t][i][j]}$ the j-th sub-part of size s' of $S_l^{[t][i]}$ and $\{l_2, l_1\}$ the index of the $(l_2-1)ss' + l_1$-th row of S, where $l_2 \in [1, n_t/s'], l_1 \in [1, ss']$. Let us assume that $S_{\{l_2,l_1\}}^{[t][i]}$ has only one non-null sub-part in position l_2, i.e.,

$$\forall j \neq l_2 \quad S_{\{l_2,l_1\}}^{[t][i][j]} = [0, \ldots, 0] \tag{3.23}$$

Considering such a structure is equivalent to considering separate precoding on n_t/s' distinct groups of s' transmit antennas. We have

$$\sum_{l=1}^{N_t} \gamma_{k,l}^2 S'^{[t]*}_l S'^{[t]}_l = \sum_{l_2=1}^{n_t/s'} \sum_{l_1=1}^{ss'} \gamma_{k,\{l_2,l_1\}}^2 \sum_{i=1}^{s'} S_{\{l_2,l_1\}}^{[t][i]*} S_{\{l_2,l_1\}}^{[t][i]} \tag{3.24}$$

$$= \sum_{l_2=1}^{n_t/s'} \sum_{l_1=1}^{ss'} \gamma_{k,\{l_2,l_1\}}^2 \mathfrak{D}_{l_2} \left(\sum_{i=1}^{s'} S_{\{l_2,l_1\}}^{[t][i][l_2]*} S_{\{l_2,l_1\}}^{[t][i][l_2]} \right) \tag{3.25}$$

where $\mathfrak{D}_{l_2}(A)$ is a block diagonal matrix with only one non-null block A in position l_2. Now, if we assume that Θ is an $s' \times s'$ scaled unitary matrix, we get $\Theta\Theta^* = \Theta^*\Theta = \sum_{i=1}^{s'} \Theta_i^* \Theta_i = I_{s'}$ where Θ_i is the i-th row of Θ_i. We choose $S_{\{l_2,l_1\}}^{[t][i][l_2]}$ as the i-th row of a $s' \times s'$ unitary matrix. Using $\|S_{\{l_2,l_1\}}^{[t][i][l_2]}\|^2 = 1/s$, we get:

$$\sum_{l=1}^{N_t} \gamma_{k,l}^2 S'^{[t]*}_l S'^{[t]}_l = \sum_{l_2=1}^{n_t/s'} \sum_{l_1=1}^{ss'} \gamma_{k,\{l_2,l_1\}}^2 \mathfrak{D}_{l_2} \left(\frac{1}{s} I_{s'} \right) \tag{3.26}$$

$$= \frac{1}{s} \sum_{l_1=1}^{ss'} \mathrm{diag} \left(\gamma_{k,\{1,l_1\}}^2 I_{s'}, \ldots, \gamma_{k,\{n_t/s',l_1\}}^2 I_{s'} \right) \tag{3.27}$$

which leads to

$$l_2 \leq n_t/s', i \leq s', \quad \vartheta^{[t]}_{k,(l_2-1)ss'+i} = \frac{1}{s}\sum_{l_1=1}^{ss'} \gamma^2_{k,\{l_2,l_1\}} \tag{3.28}$$

The random variables $\gamma^2_{k,\{l_2,l_1\}}$ are independent and identically distributed for different values of l_1 and l_2, the coding gain is

$$\mathcal{G}_{s,n_s}(\Delta,\Lambda) = \prod_{k=1}^{N_c}\prod_{l_2=1}^{n_t/s'}\left(\sum_{l_1=1}^{ss'}\frac{\gamma^2_{k,\{l_2,l_1\}}}{s}\right)^{s'/(N_c n_t)} \tag{3.29}$$

For any value of n_s, the gain expressed in (3.29) is a geometric mean of order $n_t n_c/s$. For a given realization $\{d_1,\ldots,d_w\}$, a given s and for any n_s, $\sum_{k=1}^{N_c}\sum_{l_2=1}^{n_t/s'}\sum_{l_1=1}^{ss'}\gamma^2_{k,\{l_2,l_1\}}$ and thus $\sum_{l_1=1}^{ss'}\gamma^2_{k,\{l_2,l_1\}}$ are constant, ensuring the same coding gain. However, such a precoder does not achieve the optimal coding gain for any value of s'. The summation is made over ss' different values whereas the optimal coding gain in (3.18) necessitates a summation over sn_t values. Only if ss' is high enough, the obtained coding gain is almost optimal. If $s' = n_t$, the complete spatial transmit diversity is collected by the detector and the optimal coding gain is achieved.

Proposition 3 ***Dispersive Nucleo Algebraic (DNA) Precoder*** *Let S be the $N_t \times N_t$ precoding matrix of a BICM over an $n_t \times n_r$ MIMO n_c-block fading channel. Assume that S precodes a channel block diagonal matrix with s blocks and n_s channel realizations. We denote s the spreading factor, $N_t = sn_t$ and $s' = s/n_s$. Let $S_l^{[t]}$ be the t-th sub-part of size N_t/n_s of the l-th row of S. Let $S_l^{[t][i]}$ be the i-th sub-part of size n_t of $S_l^{[t]}$. Let $S_l^{[t][i][j]}$ be the j-th sub-part of size s' of $S_l^{[t][i]}$. The sub-part $S_l^{[t][i][j]}$ is called nucleotide. The linear precoder guarantees full diversity and quasi-optimal coding gain at the decoder output under maximum likelihood decoding of the BICM if it satisfies the two conditions of null nucleotides and orthogonal nucleotides for all $t \in [1,n_s], i \in [1,s'], l_1 \in [1,ss'], l_2 \in [1,n_t/s']$ and $\{l_2,l_1\} = (l_2-1)ss' + l_1$:*

$$\begin{cases} \forall j \neq l_2, j \in [1,n_t/s'], & S^{[t][i][j]}_{\{l_2,l_1\}} = 0_{1\times s'} & \underline{\textit{Null Nucleotide condition}} \\ \forall i' \neq i, i' \in [1,s'], & S^{[t][i][l_2]}_{\{l_2,l_1\}} S^{[t][i'][l_2]*}_{\{l_2,l_1\}} = \frac{1}{s}\mathfrak{d}(i-i') & \underline{\textit{Orthogonal Nucleotide condition}} \end{cases} \tag{3.30}$$

where $\mathfrak{d}(0) = 1$ and $\mathfrak{d}(x \neq 0) = 0$.

Let us take for example $n_t = 4$, $n_s = 1$ and $s = 2$. A DNA matrix would have the following

structure :

$$\mathrm{DNA}(n_t=4,n_s=1,s=2)=\begin{bmatrix} S_{\{1,1\}}^{[1][1][1]} & 0 & S_{\{1,1\}}^{[1][2][1]} & 0 \\ S_{\{1,2\}}^{[1][1][1]} & 0 & S_{\{1,2\}}^{[1][2][1]} & 0 \\ S_{\{1,3\}}^{[1][1][1]} & 0 & S_{\{1,3\}}^{[1][2][1]} & 0 \\ S_{\{1,4\}}^{[1][1][1]} & 0 & S_{\{1,4\}}^{[1][2][1]} & 0 \\ 0 & S_{\{2,1\}}^{[1][1][2]} & 0 & S_{\{2,1\}}^{[1][2][2]} \\ 0 & S_{\{2,2\}}^{[1][1][2]} & 0 & S_{\{2,2\}}^{[1][2][2]} \\ 0 & S_{\{2,3\}}^{[1][1][2]} & 0 & S_{\{2,3\}}^{[1][2][2]} \\ 0 & S_{\{2,4\}}^{[1][1][2]} & 0 & S_{\{2,4\}}^{[1][2][2]} \end{bmatrix} \tag{3.31}$$

Now, let us consider a linear precoder matrix S that satisfies proposition 3. Define $H_k^{\{i\}}$ an $ss' \times N_r$ matrix defined by the extraction of the rows of H_k corresponding to the i-th block of s' transmit antennas. More precisely, we extract every n_t/s'-th block of s' rows of H_k begining with the i-th block

$$\forall i \in [1, n_t/s'], \forall j \in [1, s'], \forall u \in [1, s], v \in [1, N_r], \quad H_k^{\{i\}}(j+us', v) = H_k(j+un_t+is', v) \tag{3.32}$$

Likewise, $S^{\{i\}}$ is the $ss' \times ss'$ matrix obtained from the i-th block of ss' rows of S and every n_t/s'-th block of s' columns beginning with the i-th block. We easily show that

$$SH_k = \begin{bmatrix} S^{\{1\}}H_k^{\{1\}} \\ S^{\{2\}}H_k^{\{2\}} \\ \vdots \\ S^{\{n_t/s'\}}H_k^{\{N_t/s'\}} \end{bmatrix} \tag{3.33}$$

which means that the matrix S independently precodes the n_t/s' blocks of transmit antennas. Thus, the optimization may be split into n_t/s' independent optimizations of linear precoders for $s' \times n_r$ MIMO n_s-block fading channels with linear spreading factor s. As $s = s'n_s$, full space-time spreading of the $s' \times n_r$ block fading channel is performed.

From (2.40) and (3.29), we notice that, at the decoder input and under ideal interleaving condition, the linear precoder at the transmitter end and the detector at the receiver end allow the conversion of the $n_t \times n_r$ MIMO channel with n_c independent blocks into a $1 \times sn_r$ SIMO channel with $n_c n_t/s$ independent blocks with BSK input. The independence of the blocks is provided by the structure of the linear precoding matrix:

1. The null nucleotides dispatch the transmitted symbols on n_t/s' different blocks of s' antennas.
2. The orthogonal nucleotides provide full diversity and a coding gain increasing with the spreading factor.

For instance, if a rate 1/2 BICM is transmitted on a quasi-static 4×2 MIMO channel, linear precoding with $s = 2$ is required to achieve full diversity: a full-rate space-time block code with spreading factor $s = s' = 2$ may independently be applied on 2 separate groups of 2 transmit antennas. Good 2×2 space-time block codes are for instance the TAST [29] and the Golden code [7].

Assume that $n_c = 1$, $n_t = n_r = 2$ and $s = s' = 2$. The Golden code [7] is the best space time code for uncoded 2×2 quasi-static MIMO channels. However, it does not satisfy the equal norm property of orthogonal nucleotides in Proposition 3. Indeed, one row of the Golden linear precoder contains two non-null coefficients of square norm $\alpha_1 = 0.277$ and $\alpha_2 = 0.723$, respectively. Thus 3.29, which assumes equality between the eigenvalues of $M_k^{[t]} M_k^{[t]*}$, does not hold. It can be shown that (let $\gamma_i^2 = \gamma_{1,\{1,i\}}^2$)

$$\mathcal{G}_{Golden}(\Delta,\Lambda) = \sqrt{\left(\alpha_1\left(\gamma_1^2+\gamma_4^2\right)+\alpha_2\left(\gamma_2^2+\gamma_3^2\right)\right)\left(\alpha_1\left(\gamma_2^2+\gamma_3^2\right)+\alpha_2\left(\gamma_1^2+\gamma_4^2\right)\right)} \tag{3.34}$$

As d_{Hmin} increases, $(\gamma_1^2+\gamma_4^2)/(\gamma_2^2+\gamma_3^2)$ tend to 1 for any pairwise error probability and $\mathcal{G}_{Golden}(\Delta,\Lambda) \to \mathcal{G}_{2,1}(\Delta,\Lambda)$. The explain how the error correcting code limits the coding loss due to the non-equal norm of the sub-parts of the Golden code. As a remark, if $\gamma_2^2+\gamma_3^2 = 0$, which exhibits the worst case, the coding loss is $10\log_{10}(\sqrt{\alpha_1\alpha_2/4}) = 0.5dB$.

With DNA precoder and ideal interleaving, hypothesis 1 is satisfied and the modified Singleton bound on the diversity order can apply: the detector perfectly converts the $N_t \times N_r$ correlated MIMO N_c-block fading channel SH_k with QAM input into a $1 \times sn_r$ SIMO $n_t n_c/s$-block fading channel with BSK input, assuming that s is a divisor of $n_t n_c$ All results from the field of error correction coding over block fading channels directly apply without any modification to the new $1 \times sn_r$ SIMO channel with $n_t n_c/s$ independent blocks. The space-time spreading factor s is a parameter that determines which fraction of the space-time diversity will be recovered by the detector and which one by the decoder.

3.3.3 The genie method design criterion for full spreading linear precoders ($s' = n_t$)

A linear precoding design criterion based on the genie performance optimization at the detector output was proposed in [106]. When a genie gives a perfect feedback of the mn_t coded bits in the APP detector computation, the performance is computed by averaging all the pairwise error probabilities obtained when changing only one bit out of mn_t. Denote d the distance of the BSK. Assume that the BSK is transmitted on antenna l, the asymptotic expression of the error probablity with genie is

$$P_{genie}(\Delta,\Lambda) \underset{N_0\to 0}{\sim} \binom{2n_rN_\delta - 1}{n_rN_\delta} \prod_{v=1}^{n_\delta} \left(\frac{\delta_v^2}{2N_0}\right)^{-n_r\lambda_v} \tag{3.35}$$

where $\{\delta_v\}$ is the set of distinct non-null eigenvalues of $d^2 S'^{[t]*}_l S'^{[t]}_l$ for all t, λ_v their frequency and N_δ their number. In the best case, there are s non-null eigenvalues and the coding gain is maximized if they are equal. First, a sufficient condition to have an equality between the eigenvalues of $S'^{[t_1]*}_l S'^{[t_1]}_l$ and $S'^{[t_2]*}_l S'^{[t_2]}_l$ is $\|S'^{[t_1]}_l\|^2 = \|S'^{[t_2]}_l\|^2$. Then, all eigenvalues of $S'^{[t]*}_l S'^{[t]}_l$ are equal if $S'^{[t]}_l$ is a unitary matrix, which leads to the following proposition:

Proposition 4 *A linear precoder achieving a diversity order sn_r with maximum coding gain at the detector output must satisfy the following conditions under perfect iterative APP decoding of the space-time BICM:*

1. *The n_s subparts of the rows in the $sn_t \times sn_t$ precoding matrix have the same Euclidean*

square norm

2. *In each of the n_s subparts, the s subparts (nucleotides) are orthogonal and have the same Euclidean square norm*

If s' would not be equal to n_t, this proposition would not be optimal in terms of maximum likelihood performance. However, this is a first step to satisfy proposition 3. As $s' = n_t$, propositions 3 and 4 are equal, so we can use the separation of the optimization of an $N_t \times N_t$ linear precoder with spreading factor s into n_t/s' optimizations of full spreading $s's \times s's$ linear precoders. The optimization of S is now decomposed into two steps

1. Apply the genie method to design a full spreading $s's \times s's$ linear precoder for $s' \times n_r$ MIMO channel with n_s blocks, satisfying proposition 4
2. Place the non-null sub-parts in S as described in proposition 3.

3.3.4 Modified cyclotomic DNA rotations: Full spreading optimal linear precoder

It was shown that if a full spreading is processed by the linear precoder, i.e., if $s = n_t n_s$, proposition 4 is sufficient to achieve optimality and has the great advantage to be more intuitive.

We can see the block fading MIMO channel is an ergodic MIMO channel in which the different realizations are those of a quasi-static MIMO channel. Let us define A as a block diagonal matrix, the block of which have size $n_t^2 \times n_t^2$. Any linear combination of the lines of the $N_t \times N_t$ matrix A satisfies proposition 4, this implies that for all $N_t \times N_t$ matrices M, the matrix $S = MA$ satisfies proposition 4 too. The other condition to satisfy proposition 3 is the norm equality between the considered parts of a same row.

We have shown that any full spreading matrix that satisfies proposition 3 achieves the same genie performance at the detector output. In practice, the genie limit and the ML performance when using iterative joint detection and decoding are never reached. However, the performance can be close to both limits if the convergence quality is good. The system convergence is very dependent on the first iteration performance at the detector output which has the same behavior as the lattice decoding ML performance. Thus, our goal is to construct S both satisfying proposition 4 and achieving good uncoded ML performance. In general, rotations give good lattices performance.

Denote $A_{l,v}^{[t][i]}$ the v-th coefficient of $A_l^{[t][i]}$, the l-th row of A. Let us focus on the particular case in which all non null N_t/n_s-lengthed parts of the rows of A are equal, i.e.,

$$\forall (l,l') \in [1,N_t], \forall (t,t') \in [1,n_s], i \in [1,n_t], \quad A_{l,v}^{[t][i]} = A_{l',v}^{[t'][i]} \tag{3.36}$$

A can be decomposed into two matrices Δ and U ($A = U\Delta$), where Δ is a diagonal matrix and U is a block diagonal matrix where each block is an $n_t \times n_t$ matrix filled with ones. In this particular case, the diagonal elements are $\Delta_v^{[i][j]}$ satisfying

$$\forall i, v, \quad \Delta_v^{[i]} = A_{1,v}^{[1][i]} \tag{3.37}$$

i.e., the coefficients of the n_t^2-lengthed parts of the first row of A are put on the diagonal of the matrix and repeated n_s times. Matrix A has of course non-full rank. We now apply the matrix M to obtain a space-time spreading matrix $S = MU\Delta$, being a rotation. Thus, S has to satisfy $SS^* = MU\Delta\Delta^*(MU)^* = I$. For example, if Δ and MU are rotations, the equality is satisfied. Based on this method, we will now explicitly describe the space-time spreading matrix construction using cyclotomic rotations.

Choosing Δ as a rotation implies that the norms of its diagonal elements are equal to 1. The diagonal of Δ is built from the n_s-fold repetition of one block with size n_t^2 satisfying proposition 4. This block may be constructed as the concatenation of the lines of an $n_t \times n_t$ rotation matrix. Furthermore, this rotation must have all elements with unit norm, in order that Δ has diagonal element norms equal to 1. Cyclotomic rotations satisfy this property.

An $n \times n$ cyclotomic rotation Θ is defined by [13][14]

$$\Theta_{i,\ell} = \exp\left(2j\pi(i-1)\left(\frac{1}{\Phi^{-1}(2n)} + \frac{\ell-1}{n}\right)\right) \tag{3.38}$$

where $\Phi(.)$ is the Euler's function. The non-null diagonal coefficients Δ are defined by:

$$\Delta_v^{[i]} = \exp\left(2j\pi(i-1)\left[\frac{1}{\Phi^{-1}(2n_t)} + \frac{v-1}{n_t}\right]\right) \tag{3.39}$$

The matrix $S = MU\Delta$ satisfies the conditions of orthogonality for any choice of matrix M. Since S has to be a rotation, the choice of M is restricted to matrices satisfying $BB^* = MUU^*M^* = I$. Taking B as a rotation matrix, $B\Delta$ must satisfy proposition 4, i.e.,

$$\forall(l,t), i \neq i', \sum_{v=1}^{n_t} B_{l,v}^{[t][i]} B_{l,v}^{[t][i']*} \exp\left(2j\pi(i-i')\left[\frac{1}{\Phi^{-1}(2n_t)} + \frac{v-1}{n_t}\right]\right) = 0 \tag{3.40}$$

which is satisfied if

$$\forall(l,t), i \neq i', v \neq v', \quad B_{l,v}^{[t][i]} B_{l,v}^{[t][i']*} = B_{l,v'}^{[t][i]} B_{l,v'}^{[t][i']*} \tag{3.41}$$

The property (3.41) is satisfied by cyclotomic rotations. Indeed, if B is an $N_t \times N_t$ cyclotomic rotation, the coefficients of which are

$$B_{l,v}^{[t][i]} = \exp\left(2j\pi(l-1)\left[\frac{1}{\Phi^{-1}(2N_t)} + \frac{(t-1)n_t^2 + (i-1)n_t + v - 1}{N_t}\right]\right) \tag{3.42}$$

we have

$$B_{l,v}^{[t][i]} B_{l,v}^{[t][i']*} = \exp\left(2j\pi(l-1)\left[\frac{1}{\Phi^{-1}(2N_t)} + \frac{(i-i')n_t}{N_t}\right]\right) \tag{3.43}$$

which is independent of v.

Finally, we obtain a modified cyclotomic rotation given by $S = B\Delta$, the coefficients of S being equal to

$$S_{l,v+(i-1)n_t+(t-1)n_t^2} = \frac{1}{n_t}\exp\left(2j\pi\left[(l-1)\left(\frac{1}{\Phi^{-1}(2N_t)}+\frac{(t-1)n_t^2+(i-1)n_t+v-1}{N_t}\right)+(i-1)\left(\frac{1}{\Phi^{-1}(2n_t)}+\frac{v-1}{n_t}\right)\right]\right) \quad (3.44)$$

$\frac{1}{\sqrt{N_t}}$ is a normalisation term. Let $\mathcal{S}(n_t, n_r, n_s)$ be the modified cyclotomic rotation designed for $n_t \times n_r$ MIMO block fading channel, assuming that the precoder sees n_s channel realizations.

In order to confirm the choice of the modified cyclotomic space-time matrix, we will describe another construction. We have already said that cyclotomic rotations are good candidates for spreading matrices because of their norm properties, their easy construction and their performance as lattices in the ML sense. Let Θ be an $N_t \times N_t$ cyclotomic rotation, it does not satisfy the property 3. We apply multiplicative correction terms $e^{2j\pi\alpha_{l,v}^{[t][i]}}$ to Θ coefficients so that Θ satisfies proposition 3.

$$\Theta_{l,v}^{[t][i]} = \frac{1}{\sqrt{N_t}}\exp\left(2j\pi\left[(l-1)\left(\frac{1}{\Phi^{-1}(2N_t)}+\frac{v-1+(i-1)n_t+(t-1)n_t^2}{N_t}\right)+\alpha_{l,v}^{[t][i]}\right]\right) \quad (3.45)$$

First, Θ has to be a rotation

$$\begin{aligned}&\forall l,l', \textstyle\sum_{t,i,v}\Theta_{l,v}^{[t][i]}\Theta_{l',v}^{[t][i]*} = \mathfrak{d}(l,l')\\ &\Leftrightarrow \textstyle\sum_{t,i,v}\frac{1}{n_t}\exp\left(2j\pi\left[(l-l')\left(\frac{1}{\Phi^{-1}(2N_t)}+\frac{v-1+(i-1)n_t+(t-1)n_t^2}{N_t}\right)+\alpha_{l,v}^{[t][i]}-\alpha_{l',v}^{[t][i]}\right]\right) = \mathfrak{d}(l,l')\end{aligned} \quad (3.46)$$

which is satisfied if $\forall(l,l'), \alpha_{l,v}^{[t][i]} = \alpha_{l',v}^{[t][i]}$. Since each coefficient is a complex exponential, the norm properties are satisfied, the last property to be satisfied is the orthogonality between the subparts which leads to

$$\exp\left(2j\pi(l-1)\frac{i-i'}{n_t}\right)\sum_{v=1}^{n_t}\frac{1}{n_t}\exp\left(2j\pi(\alpha_{l,v}^{[t][i]}-\alpha_{l,v}^{[t][i']})\right) = \mathfrak{d}(i,i') \quad (3.47)$$

The equality is satisfied if $\exp(2j\pi\alpha_{l,v}^{[t][i]})$ is chosen like the phase coefficient (i,v) of an $n_t \times n_t$ cyclotomic rotation, i.e.,

$$\alpha_{l,v}^{[t][i]} = (i-1)\left(\frac{1}{\Phi^{-1}(2n_t)}+\frac{v-1}{n_t}\right) \quad (3.48)$$

We directly obtain the same modified cyclotomic matrix $\mathcal{S}(n_t, n_r, n_s)$, which gives full diversity and optimal coding gain at the detector and decoder output under ideal interleaving assumption.

3.3.5 Non-full spreading quasi-optimal linear precoder: DNA cyclotomics

Proposition 3 gives the design criterion for optimal full and non-full spreading quasi-optimal linear precoders. We first choose an quasi-optimal linear precoder designed for a full interleaving of an $s' \times n_r$ MIMO block-fading channel with n_s channel states in each precoded matrix. For example, let us choose $\mathcal{S}(s', n_r, n_s)$ defined in 3.44. Then place n_t/s' times each subpart of $\mathcal{S}(s', n_r, n_s)$ in the precoding matrix in order to satisfy 3.44. This leads to the quasi-optimal linear precoder for any parameters n_t, n_s and s. Let $\mathcal{P}(n_t, n_s, s)$ denote such an quasi-optimal

linear precoder ($s' = s/n_s$ and $N'_t = s's$), its coefficients are equal to

$$\begin{array}{l}\forall l_2 \in [1, n_t/s'], \forall l_1 \in [1, ss'], \forall t \in [1, n_s], \forall i \in [1, s'], \forall v \in [1, s'], \\ S_{(l_2-1)s's+l_1, v+(l_2-1)n_t/s'+(i-1)n_t+(t-1)s'n_t} = \\ \frac{1}{\sqrt{N'_t}} \exp\left(2j\pi\left[(l_1-1)\left(\frac{1}{\Phi^{-1}(2N'_t)} + \frac{v-1+(i-1)s'+(t-1)s'^2}{N'_t}\right) + (i-1)\left(\frac{1}{\Phi^{-1}(2s')} + \frac{v-1}{s'}\right)\right]\right) \\ \text{and 0 elsewhere.}\end{array} \quad (3.49)$$

3.3.6 Performance of the quasi-optimal precoder with iterative receiver

We have presented quasi-optimal linear precoders providing good coding gain and full diversity ML performance under ideal interleaving. However, the ML decoder of the global Euclidean code does not exist and we process iterative joint detection and decoding. Proposition 3 is satisfied by an infinity of matrices, all providing the same ML performance. Let us consider the performance behaviour after the first iteration. As no a priori information is available at the detector, errors before decoding are numerous and not necessarily transmitted on different precoding time periods. Let us consider one precoding time period and assume that we observe two erroneous bits. If the bits are transmitted on the same modulation symbol, the Euclidean distance d_k changes but this does not affect the linear precoder optimization. However, if the two bits are placed onto two different rows of S, the average performance might be modified and interference inside a block and between blocks should be considered. An optimization of the precoder following the Tarokh criterion should be done, under the conditions presented in proposition 3. Simulation results show that the modified cyclotomic rotation has good uncoded ML performance, close to algebraic full rate space-time block codes. Thus we expect good performance at the first iteration of a joint detection and decoding process, which is desirable to reduce the number of iterations needed to achieve the near ML performance and to provide good performance with non-iterative receivers. The optimization of the first iteration is not addressed in this thesis, but first answers can be found in [112].

3.4 Interleaver optimizations

The maximum diversity to be gathered is limited by the channel properties, the linear precoding spreading factor, the minimum Hamming distance of the binary code and the Singleton bound of the global code. Assume that the linear precoder spreading factor s is chosen thanks to the modified Singleton bound. Thus, there exists an interleaver that allows ML performance with full diversity. We present a new BICM interleaver design which satisfies proposition 1 and leads to the concept of full diversity BICM since the system exhibits a predetermined diversity whatever the parameters of the considered block fading channel.

3.4.1 The BICM diversity with convolutional codes

On fading channels, the diversity of a coded modulation can be defined by the number of independent channel states affecting a codeword. More precisely, the diversity is the exponent associated with the signal-to-noise ratio in the bit error rate expression.

We usually consider convolutional codes when designing BICM, because of their flexibility. A transition in the trellis of a convolutional code is defined by a state, $K_{\mathcal{C}}$ information bits at the code input and $N_{\mathcal{C}}$ coded bits at the code output. The code rate is $R_{\mathcal{C}} = K_{\mathcal{C}}/N_{\mathcal{C}}$. A path in the trellis is equivalent to a codeword. The length of the path in the trellis is $L_{\mathcal{C}}$ branches, i.e., a codeword has length $L_{\mathcal{C}}N_{\mathcal{C}}$ coded bits. The protection of the information bits comes from the code trellis structure since only predetermined transitions are allowed. However, some errors occur when the noise makes at least one other path more reliable (in the Euclidean distance sense) than the transmitted path. On binary symmetric channels, the most probable error path, called minimum error path, has the smallest number of different coded bits from the transmitted path. The number of bit errors in this case is equal to d_{Hmin}, the so-called minimum distance of the code (in the Hamming sense). We will call "neighbor path" a path in the trellis that differs from the transmitted codeword exactly by d_{Hmin} bits. On fading channels, a neighbor is a codeword minimizing the Euclidean distance. This is not always equivalent to minimize the Hamming distance, but equivalence can be assumed to be an average behavior.

The maximum achievable diversity d_{max} is upper-bounded by the number of independent laws generated by the channel $n_t n_r n_c$, the minimal Hamming distance of the binary code, and the Singleton bound of the global code:

$$d_{max} \leq \min\left(sn_r\left\lfloor\left\lfloor\frac{n_c n_t}{s}\right\rfloor(1-R_{\mathcal{C}})+1\right\rfloor; n_t n_c n_r; sn_r d_{Hmin}\right) \tag{3.50}$$

3.4.2 Interleaver design criteria

A simple way to theoretically estimate the bit error rate is to use the union bound. This upper bound is the sum of the pairwise error probabilities, it is dominated by the minimum error paths. In order to be able to efficiently design the system, we make the optimistic assumption that improving the dominant term of the sum will improve the global sum and that the gain obtained on the union bound will also be obtained for the exact bit error rate.

Let us consider a neighbor in the trellis. It is defined by a block of $l_{\mathcal{C}}N_{\mathcal{C}}$ coded bits, d_{Hmin} of which are erroneous ($l_{\mathcal{C}}$ is the code constraint length). We can say that a good protection is given by the channel if these coded bits see a maximum number of independent channel states. This is the fundamental concept of diversity exploitation. The minimum Hamming distance of the code is chosen to be non-limiting. The Singleton bound is a limiting factor: it can be increased by judiciously choosing the linear precoding. Without this space-time spreading, the interleaver should be designed to achieve the Singleton bound diversity order.

Considering a general $n_t \times n_r$ MIMO block fading channel with n_c blocks, we collect a minimum diversity equal to n_r at the detector output, and, since the decoder cannot degrade performance, the reception diversity n_r is always obtained at the decoder output. The challenge is to collect the transmission diversity given by the n_t transmit antennas and the n_c channel states.

In order to achieve the full diversity, the erroneous bits of an error event should be equally distributed over all the transmit antennas and channel time realizations. Moreover, the interference of these bits in the time periods should be limited to first enhance the diversity and then the coding gain.This will be explained in the following.

Let us consider an error event with w erroneous bits. Assume that the maximum diversity

order is d_{max}. If $w \geq d_{max}$, we can expect to achieve full diversity if at least d_{max} bits over w see the d_{max} independent fading random variables. In a time period k where more than one erroneous bits are transmitted, the transmitted and interfering points are called $x_k = z_k H_k$ and $x'_k = z'_k H_k$. When computing ML decoding or APP detection, we are interested by the equivalent BSK defined by the two points x_k and x'_k. It was shown that the vector $\frac{z_k - z'_k}{d(z_k, z'_k)} H_k$ has n_r independent circular symmetric Gaussian variables components. We can conclude that even if the erroneous bits are transmitted on different antennas, the generated diversity is n_r. However, if the erroneous bits are transmitted on different time periods and see different fading random variables, a higher diversity is achieved.

For a given diversity, the coding gain is given by the distance between the transmitted codeword X and the considered erroneous codeword X'. If all the w erroneous bits are transmitted over j different time periods, the number of non-null components of $X - X'$ is $n_r j$. On average, the distance is maximized if $j = w$. An optimal coding gain is obtained if the Gaussian variables components of a multi-dimensional vector have same variance. We can approach such a property by uniformly placing the erroneous bits over all the random variables.

Moreover, if no interference is observed between the erroneous bits in the time periods, the situation is very similar to the genie condition. In the case of a sufficient number of independent laws, we can use optimized mappings that exhibit a large amount of coding gain under perfect convergence of the iterative processing. In such mappings, the bits are not equally protected, the interleaver must then distribute the bit positions over all the available fadings. Such remarks lead to the fundamental design criterion of the interleaver:

Proposition 5 *In order to take the advantage of the available diversity and coding gain given by the concatenation of a BICM and a block fading MIMO channel, the interleaver should uniformly place consecutive bits on all the channel time realizations, transmit antennas, bit positions of the mapping and prohibit the interference of these consecutive bits in the time periods.*

We will now build, step by step, an interleaver that satisfies such conditions. First, we will build an interleaver that enables to achieve maximum diversity on an $n_t \times n_r$ quasi-static MIMO channel with BPSK input. Then, we will extend it to the case of higher spectral efficiency modulations and to block fading channels with n_c channel states.

3.4.3 Interleaver design for quasi-static MIMO channels with BPSK input

On quasi-static channels, only one channel realization is experienced by a codeword. Let us consider an error event in the code trellis where d_H coded bits differ from the transmitted codeword. All error events are supposed to have a non-null probability, the interleaver should be designed for any of them. Let us ensure that $L_I N_{\mathcal{C}}$ successive coded bits, $L_I N_{\mathcal{C}}$ being the length of an error path with L_I branches, are transmitted by all the n_t transmit antennas in the same proportion. The maximum transmit diversity is upper bounded by n_t, d_{Hmin} and the Singleton bound.

The Singleton bound cannot be improved with a designed interleaver. However, we will design it in the aim of achieving the $n_t n_r$ diversity, keeping in mind that the maximal achievable diversity is upper-bounded by the Singleton bound.

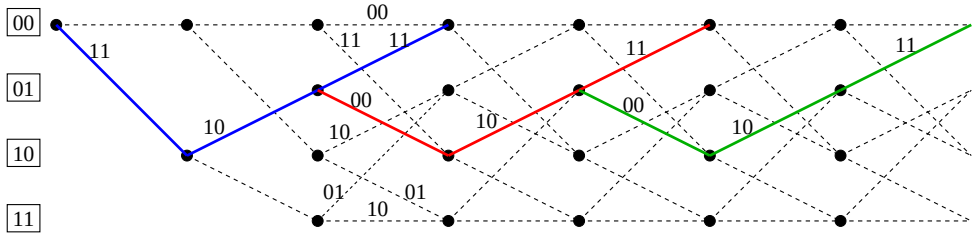

Figure 3.10: NRNSC 7,5 trellis

Another condition to optimize the performance is the non-interference of the erroneous bits in the time periods. In the maximum-likelihood sense, two interfering erroneous bits can either degrade the diversity or coding gain. When considering the iterative processing, a time period corresponds to a channel node in the graph. Ideally, the considered bit probabilities should be independent, practically, coming from branches far away from each other in the trellis. These conditions lead to a design criterion for quasi-static channels, well known in the space-time coding theory as the "rank criterion" and applied here to the BICM interleaver.

We want to design an interleaver ensuring that consecutive bits are mapped on different symbol times over all the transmit antennas. To achieve this property, we demultiplex the $L_{\mathcal{C}}N_{\mathcal{C}}$ coded bits into n_t vectors of length $L_{\mathcal{C}}N_{\mathcal{C}}/n_t$. Each of the n_t sub-frames will be transmitted on a predetermined transmit antenna. However, the demultiplexing step is not simply processed selecting every n_t bits. Indeed, we can observe on Fig.3.10 the trellis of the half-rate, four states NRNSC $7,5$ code. In bold lines, we drew the error event leading to minimum weight ($d_{Hmin} = 5$) and error events maximizing the number of branches with a constant weight (e.g., 6 and 7). Such error events are good candidates to frequently occur at high signal-to-noise ratios, and we remark that the error positions (represented by a "1") are not equally distributed on the positions modulo n_t. As an example, if we consider $n_t = 2$ and an error event "$\underline{1}1\underline{1}0\underline{0}0\underline{1}0\underline{0}0\underline{1}0\underline{1}1$", 5 errors over 7 would be transmitted on the first antenna with a classical demultiplexing scheme. In order to equally distribute the erroneous bits on the n_t antennas, for all convolutional code parameters, we apply the demultiplexing:

$$0 \leq i < n_t, 0 \leq j < L_{\mathcal{C}}N_{\mathcal{C}}/n_t, V_i(j) = V\left((i+j)\text{mod } n_t + jn_t\right) \tag{3.51}$$

where V is the codeword to be demultiplexed, V_i is the i-th demultiplexed frame, and .mod . the modulo operator. This ensures the uniform distribution of the erroneous bits over the n_t transmit antennas all along the transmitted frame. Once the n_t frames are extracted, each frame is interleaved separately and transmitted over an antenna.

We now have to limit the erroneous bits interference in the time periods. First, we can assume that only simple error events occur. If each of the n_t frames is interleaved by a different interleaver, we cannot control the interferences because of the randomness of each interleaver. On the contrary, if the same interleaver is used, the n_t consecutive bits are in the same positions of the interleaved frames, we can limit the interference by sliding each frame by one bit position and transmit all the frames serially on their associated antenna. This ensures that bits in the same position in the interleaved frames will not be transmitted in the same time period, but does not guarantee that the considered $L_I N_{\mathcal{C}}$ successive bits are transmitted over different time periods.

To satisfy this strong condition, we use a particular S-Random interleaver which guarantees

that any L_I successive bits in the interleaved frames are not transmitted during the same block of n_t time periods. If we consider that bit position i is placed at position $\Pi_s(i)$ by the interleaver Π_s, we should have

$$0 \leq j < L_{\mathcal{C}} N_{\mathcal{C}}/n_t - L_I, 0 \leq i < L_I, \quad \left\lfloor \frac{\Pi_s(j)}{n_t} \right\rfloor \neq \left\lfloor \frac{\Pi_s(j+i)}{n_t} \right\rfloor \tag{3.52}$$

We find such an interleaver by choosing it at random until the conditions are satisfied. Each of the n_t frames V_i are interleaved to V_i':

$$0 \leq i < n_t, 0 \leq j < L_{\mathcal{C}} N_{\mathcal{C}}/n_t, \quad V_i'\left(\Pi_s(j)\right) = V_i\left(j\right) \tag{3.53}$$

Then, the bits of the interleaved frame V_i' will be placed in another sub-frame V_i'', before the serial transmission on i-th antenna, with the following method: Blocks of n_t bits of V_i' are transmitted in the corresponding block of n_t time periods, with a time slide equal to i and a modulo n_t to stay in the block of n_t time periods (cyclic shift of i positions in a block of size n_t).

$$0 \leq i < n_t, 0 \leq j_1 < L_{\mathcal{C}} N_{\mathcal{C}}/n_t^2, 0 \leq j_2 < n_t, \quad V_i''\left((i+j_2) \text{mod } n_t + j_1 n_t\right) = V_i'\left(j_2 + j_1 n_t\right) \tag{3.54}$$

3.4.4 Basic interleaver construction

In the following, we consider a basic interleaver $\mathcal{I}_{N_I,S_I,L_I}$ designed for N_I channel inputs, a frame size S_I and a separation L_I. It should satisfy the conditions presented above for diversity and coding gain optimizations. It will be used again in the following, this explains the introduction of the general notation $\mathcal{I}_{N_I,S_I,L_I}$. However, in the previous subnewsection, we considered the $\mathcal{I}_{n_t,L_{\mathcal{C}}N_{\mathcal{C}},L_I}$ interleaver.

In Fig. 3.11, we present the basic interleaver with $N_I = 4$ channel inputs, the bits of the codeword are colored in 4 different colors, each one corresponding to a specific channel input. This illustrates the way the codeword is demultiplexed into N_I vectors V_i, $i = 1, \ldots, N_I$, of length S_I/N_I, as presented before. Step 1 corresponds to this demultiplexing. Each vector V_i of size S_I/N_I is then interleaved by the S-random interleaver in step 2 into a vector V_i'. In step 3, we build the $N_I \times S_I/N_I$ matrix as the concatenation of S_I matrices of size $N_I \times N_I$. The first row of an $N_I \times N_I$ matrix contains the N_I first values of the vector V_0' for channel input 1. The second row contains the first N_I values of the vector V_1' for channel input 2, shifted by 1 position modulo N_I. Rows 3 and 4 are built from vectors V_2' and V_3' similarly. All S_I/N_I^2 matrices of size $N_I \times N_I$ are constructed the same way using the following bits of the N_I vectors V_i'.

In this last step, we see the space-time distribution for the $N_I = 4$ first bits of each interleaved frame, each channel input is represented by a row. We can notice that the cyclic diagonal thread on the space-time domain in each block is very similar to the threaded algebraic space-time codes.

Finally, the $N_I \times S_I/N_I$ matrix is transmitted on the channel with a space-time repartition on transmit antennas and time periods given by the rows and columns, respectively.

In a block of N_I bits transmitted on one of the N_I channel inputs, the bits are separated by more than L_I bits in the demultiplexed frame, which correspond to a bit separation equal to $N_I(L_I - 1) + L_I \text{mod } N_I$ in the codeword. The cyclic diagonal repartition of the bits in one block

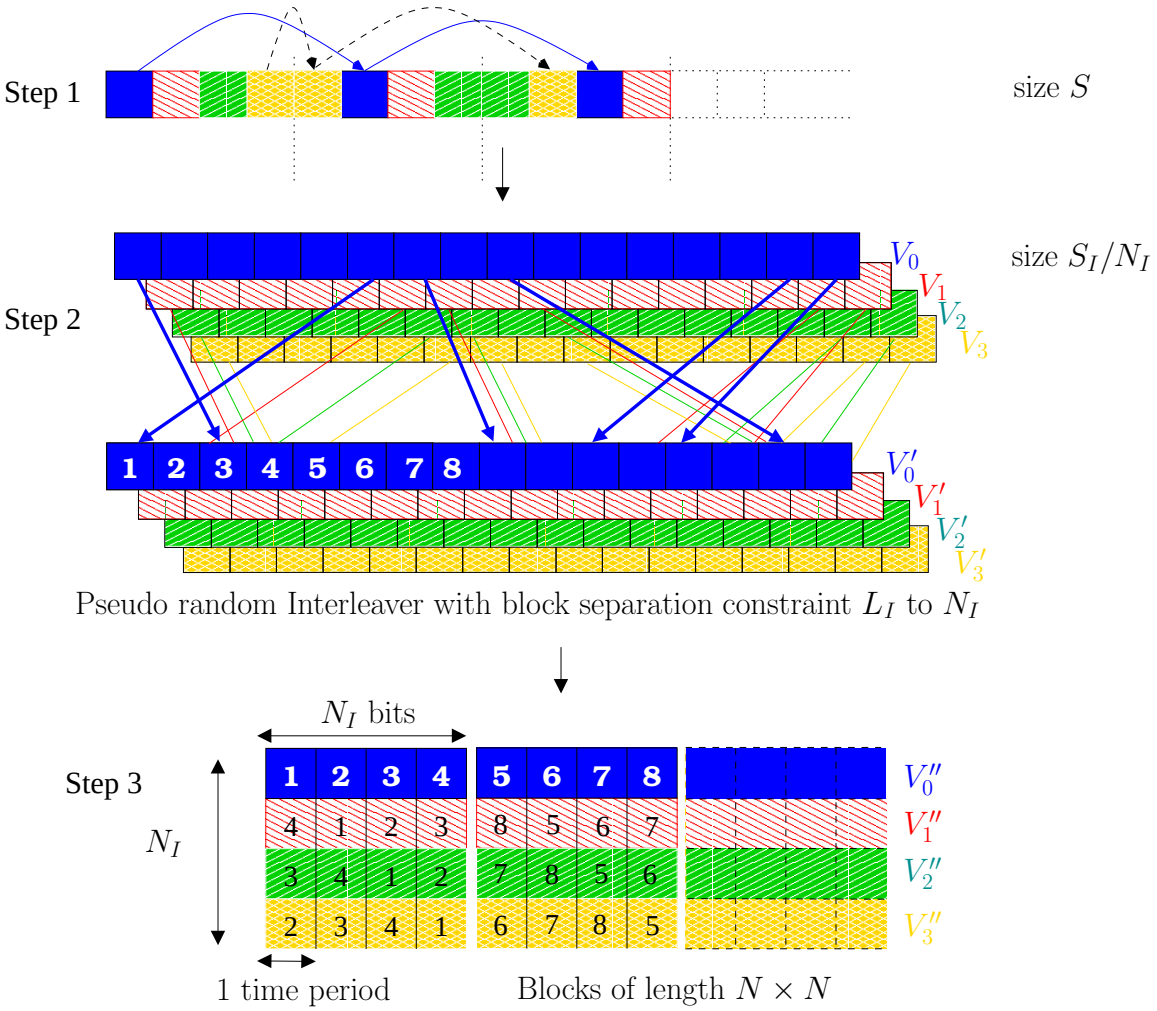

Figure 3.11: Basic interleaver design for N_I inputs, a frame size S_I and a separation L_I

of N_I time periods guarantees that the bits contained in one symbol period, i.e., in 1 column of the final matrix, were originally separated by $N_I(L_I-2)+L_I \bmod N_I+1$ bit positions before interleaving. Moreover it guarantees that $N_I(L_I-2)+L_I \bmod N_I+1$ consecutive bits before interleaving are equally distributed on all transmit antennas and mapped on different symbol periods. Practically, the parameter L_I of the S-random-like interleaver should be maximized in order to take the long error events into account.

3.4.5 Interleaver design for quasi-static MIMO channels with M-ary input

We have presented an interleaver for MIMO quasi static channels and BPSK modulation. This interleaver tries to exploit the maximum diversity and to limit the interference of erroneous bits in the time period. The extension of such interleavers is straightforward for higher spectral efficiency modulations if we only consider the diversity criterion. However, it has been shown that labeling optimisation allows high coding gain under iterative decoding on ergodic channels. In some cases, there is a sufficient transmit diversity order in the channel to exploit the mapping gain, but the less the diversity order is the more the interleaver has to be optimized.

When the genie condition is satisfied, only one bit is changed in a time period, so the labeling can be optimized to maximize the average distance of the equivalent BSKs. In order to take advantage of the coding gain given by the optimized labeling, we have to design the interleaver such that a genie-like situation occurs.

Erroneous bits in an error path should be dispatched on different time periods and equally transmitted over all the transmit antennas and bit positions. Moreover, the transmitted bits should not interfere in the time periods. These conditions are satisfied by the $\mathcal{I}_{mn_t,L_CN_C,L_I}$ interleaver.

It is clear that the diversity is more important than the coding gain. If an error event has a Hamming weight $w < mn_t$, all the sub-frames mn_t cannot carry an erroneous bit. The n_t first rows of the last interleaver matrix should be transmitted on the n_t transmit antennas and on the first mapping bit, for example. Then the second block of n_t rows will be transmitted on the second mapping bit, and so on.

3.4.6 Application to linear precoding

When a linear precoder is used to recover a part of the transmit diversity, the new channel matrix SH has $sn_t \times sn_t$ rows and columns. If at most one erroneous bit is observed on each time period, optimal linear precoders have been optimized in 3.3. We have shown that the precoded channel output is divided into independent blocks, we modify the order of the rows as follows ($s'=s/n_s$ and $N'_t=s's$)

$$\begin{array}{l}\forall l_2 \in [1, n_t/s'], \forall l_1 \in [1, ss'], \forall t \in [1, n_s], \forall i \in [1, s'], \forall v \in [1, s'], \\ S_{(l_1-1)n_t/s'+l_2, v+(l_2-1)n_t/s'+(i-1)n_t+(t-1)s'n_t} = \\ \frac{1}{\sqrt{N'_t}} \exp\left(2j\pi\left[(l_1-1)\left(\frac{1}{\Phi^{-1}(2N'_t)}+\frac{v-1+(i-1)s'+(t-1)s'^2}{N'_t}\right)+(i-1)\left(\frac{1}{\Phi^{-1}(2s')}+\frac{v-1}{s'}\right)\right]\right) \\ \text{and 0 elsewhere.}\end{array} \quad (3.55)$$

Now, the n_t/s' consecutive rows of S lead to independent row vectors $S_l H_k$ that look like a true multiple antenna channel. In this case, the interleaver $\mathcal{I}_{smn_t, L_{\mathcal{C}} N_{\mathcal{C}}, L_I}$ is designed for diversity and gain exploitation. As presented in the previous subsection, the sn_t first rows of the last interleaver matrix will be transmitted on the first mapping bit, and so on.

3.4.7 Interleaver design for block fading MIMO channels

For block fading channels, n_c different channel realizations occur during the codeword. Note that $n_c = 1$ corresponds to the quasi-static context and $n_c = L_{\mathcal{C}} N_{\mathcal{C}}/n_t$ to the ergodic context. We directly apply the two design criteria described above to generalize the conditions that should be satisfied by the BICM interleaver: In order to take advantage of the transmission and time diversity given by the transmit antennas and the n_c different realizations of a block fading MIMO channel, the interleaver of a BICM should place consecutive bits on different time periods and equally distribute them among all transmit antennas and all n_c channel realizations. The n_c channel states are grouped together into blocks of length $L_{\mathcal{C}} N_{\mathcal{C}}/(n_c n_t)$ time periods. We will extract n_c sub-frames from the codeword , each sub-frame will be transmitted on one of the n_c blocks, and only see one channel state. We can interleave each sub frame with the interleaver optimized for MIMO quasi-static channel to exploit the n_t transmit antenna diversity. The demultiplexing of the n_c frames is done in the same manner as for the transmit antenna separation for the same reasons.

$$0 \leq i_{n_c} < n_c, 0 \leq j < L_{\mathcal{C}} N_{\mathcal{C}}/(n_c n_t), V_i^{n_c}(j) = V\left((i_{n_c} + j) \bmod n_c + j n_c\right) \tag{3.56}$$

This demultiplexing/interleaving is sufficient to exploit the time diversity. Indeed, there is no interference between the symbols applied to the different channel states in opposition to symbols transmitted on different antennas, bits positions and time periods.

3.4.8 Interleaver design: algorithm

We will present the algorithm for an easy implementation of the interleaver designed for a $2^m - QAM$, precoded by an $sn_t \times sn_t$ matrix, and transmitted on an $n_t \times n_r$ MIMO block fading channel with n_c blocks. A codeword contains $L_{\mathcal{C}} N_{\mathcal{C}}$ coded bits, each sub-frame is $L_{\mathcal{C}} N_{\mathcal{C}}/(smn_c n_t)$ bits long. Let us first consider the pseudo S-Random interleaver for each of the $smn_t n_c$ sub-frames. It should guarantee that any L_I successive bits in the interleaved sub-frame are not transmitted during the same block of smn_t time periods. If we consider that bit position i is placed at position $\Pi_s(i)$ by the interleaver Π_s, we should have

$$0 \leq j < L_{\mathcal{C}} N_{\mathcal{C}}/(smn_t) - L_I, 0 \leq i < L_I, \quad \left\lfloor \frac{\Pi_s(j)}{smn_t} \right\rfloor \neq \left\lfloor \frac{\Pi_s(j+i)}{smn_t} \right\rfloor \tag{3.57}$$

We can find such an interleaver by choosing it at random until the conditions are satisfied. Let V_{in}, a vector of $L_{\mathcal{C}} N_{\mathcal{C}}$ coded bits, be the input of the interleaver, and V_{out} the output vector to be given to the mapper.

Algorithm 1: Optimized interleaver for precoded $N_t \times N_r$ MIMO channel with n_c blocks, 2^m-QAM

input : A codeword V_{in} of size $L_{\mathcal{C}} N_{\mathcal{C}}$ coded bits.

output: A frame V_{out} of size $L_{\mathcal{C}} N_{\mathcal{C}}$ bits, ready for serial to parallel and mapping conversion for transmission on the n_t transmit antenna.

init : $L_1 \leftarrow L_{\mathcal{C}} N_{\mathcal{C}}/n_c$, $L_2 \leftarrow L_1/(mN_t)$

```
for k = 0 to n_c − 1 do
    for i = 0 to mN_t − 1 do
        for j = 0 to L_2 − 1 do V_2(j) ← V_in((j + (in_c + k)) mod mN_t n_c + jmN_t n_c)
        for j = 0 to L_2 − 1 do V_3(Π_s(j)) ← V_2(j)
        for j = 0 to L_2/(mN_t) − 1 do
            for v = 0 to mN_t − 1 do
                V_4((v + i) mod mN_t + jmN_t) ← V_3(v + jmN_t)
        for j = 0 to L_2 − 1 do V_5(i + jmN_t) ← V_4(j)
    for i = 0 to L_1/(mN_t) − 1 do
        for j = 0 to N_t − 1 do
            for u = 0 to m − 1 do
                V_out(u + jm + imN_t + kL_1) ← V_5(j + uN_t + imN_t)
```

3.4.9 Application to turbo-codes

The BICM precoder and interleaver have been designed to provide full-diversity and optimal coding gain for any pairwise error probability. However, the final error rate is given by the probability to get out from the Voronoi region. The facets of this decision region belong to the median hyperplanes of the BSKs considered in the pairwise error probabilities. When using convolutional codes, the number of neighbors increases with the frame length whereas the minimal Hamming distance d_{Hmin} remains constant. The minimal Euclidean distance in $\mathcal{C}_E$ depends on d_{Hmin}, we can deduce that the frame error rate will increase with the frame length. The idea is to find a code whose Euclidean distance increases with the frame length. If the performance gain provided by the Euclidean distance increase is greater than the performance attenuation provided by the number of neighbors increase, the frame error rate will decrease with the frame length. It has been shown in [44][17] that turbo-like codes can achieve such a proposition over block fading channels. We use the coding scheme presented in Fig. 3.12. Information bits are encoded by an RSC1 encoder. The information bits are interleaved by the turbo-code interleaver Π_t, encoded by an RSC2 encoder. The coded bits of RSC2 are then de-interaleaved by Π_t^{-1}. This last step is not processed in classical parallel turbo-code schemes, but it allows us to perfectly control the position of the information bits and associated coded bits. Indeed, the presented optimized channel interleaver is designed using the simple observation that the error events are localized. Then a 1/2 puncturing is computed on each coded bit stream, followed by

a multiplexing. Let $b(i)$ denote the i-th information bit, $c_1(i)$ denote the i-th coded bit at the output of $RSC1$ and $c_2(i)$ the i-th coded bit at the output of RSC2. The final coded stream has the following form

$$b(0)\ c_1(0)\ b(1)\ c_2(1)\ b(2)\ c_1(2)\ b(3)\ c_2(3)\ b(4)\ c_1(4)\ b(5)\ c_2(5)\ \cdots \tag{3.58}$$

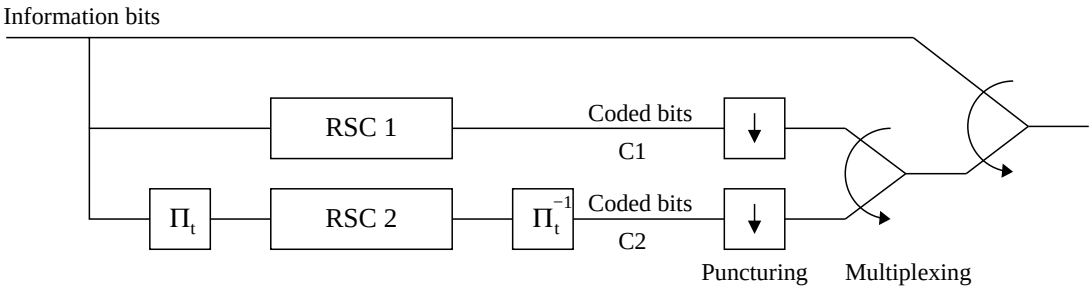

Figure 3.12: Parallel turbo-code encoder

The error events occur locally at different positions in the frame. This induces that the optimized interleaver is directly applicable.

3.5 Simulation results

In this section, we evaluate the performance of actual iterative joint detection and decoding of the ST-BICM. The APP detector is performed by exhaustive marginalization. The set of 2^{mN_t} noiseless received precoded symbols zSH is computed once per channel block realization since the channel matrix SH is constant during the block. This results in a complexity reduction for the marginalization, which now requires around $L_{\mathcal{C}}N_{\mathcal{C}}/(msn_t)2^{mN_t}$ operations per iteration if $s \ll L_{\mathcal{C}}N_{\mathcal{C}}$. Reduced complexity quasi-optimal or sub-optimal MIMO detectors could also be used, e.g., a SISO list sphere decoder [49][75][6][107], a SISO-MMSE detector [89] or a detector using sequential Monte Carlo method [33].

Let us consider a 2×1 quasi-static ($n_c = 1$) MIMO channel and QPSK modulation. We use $(7,5)_8$ NRNSC or $(3,2)_8$ NRNSC codes with rate 1/2 and a blocklength of 1024 coded bits. From the Singleton bound we know that full diversity can be achieved without linear precoding. We compare on Fig. 3.13 the performance obtained with a classical PR interleaver and the performance obtained with the optimized interleaver described in section 3.4. Full diversity order is only achieved with the optimized interleaver, for which the performance slope is equal to the one of the outage probability. The optimized interleaver provides performance improvement without any increase of complexity neither at the transmitter nor at the receiver. In most cases, the PR interleaver only provides a diversity n_r, i.e., it does not allow any transmit diversity order recovery. The $(7,5)_8$ NRNSC code achieves a higher coding gain than the $(3,2)_8$ NRNSC code. It achieves performance within only 2.5dB from the outage capacity with Gaussian input and within 1.5dB from the outage capacity with QPSK input. The performance lower bound corresponding to ideally precoded BICM is also drawn. It is obtained from the performance of the same coded modulation transmitted on a $1 \times n_c n_t n_r$ SIMO channel, as explained in section 3.3.1. There is a 1dB gap between ideal and actual performance with the $(3,2)_8$ NRNSC code and a 0.75dB gap with the more powerful $(7,5)_8$ NRNSC code. This confirms the analytical

result of section 3.3.1 obtained for ML performance: the higher the Hamming weight is, the closer to the ideal performance the actual iterative receiver can perform. However, a better code does not always provide better frame error rate. Indeed, we saw that, when $w \geq n_t n_c$, the full diversity of the considered pairwise error probability can be achieved with an ideal interleaver. The remaining $w - n_t n_c$ BSK distances are uniformly distributed among all the channel states. A better error correcting code with greater Hamming weights w' does not enhance the diversity but the coding gain per pairwise error probability. However, the degradation induced by the increased number of neighbors may be higher than the improvement brought by increased coding gains. How to handle this trade-off is left for further study.

In Fig. 3.14, we show the performance of a rate-1/2 $(7,5)_8$ NRNSC code over a 2×2 MIMO block fading channel with $n_c = 2$ and QPSK input. The frame length is 256 coded bits. With a PR interleaver, a diversity order $n_r = 2$ is achieved, as transmit diversity is not collected. Even with the optimized interleaver, full diversity is not obtained at the last iteration. Indeed, the Singleton bound is equal to 6 without linear precoding. Two different linear precoders, the Golden code and the DNA code, both with $s = 2$, are used to achieve the full diversity order 8. The Golden code does not satisfy the equal norm condition, which induces a slight loss in coding gain. However, this loss is fully compensated by the averaging of the $d_{k,l,i}$ into the $\gamma_{k,l}$ provided by the error correcting code as explained in 3.3.1. The slope difference between diversity orders 6 and 8 is not significant. However, linear precoding provides an additional coding gain which allows to perform within 2dB from the outage capacity with Gaussian input using a four-state convolutional code and a small frame length. For a higher frame length, the performance with convolutional codes is degraded. Therefore, we will also investigate performance with turbo-codes.

In Fig. 3.15, we compare two strategies for achieving full diversity with BICM: linear precoding and constellation expansion. Constellation expansion consists in increasing m while decreasing the coding rate, in order to achieve the full diversity without precoding and with the same spectral efficiency. A MIMO 2×2 channel with $n_c = 2$ is considered. The frame length is 1024 coded bits. Using QPSK modulation and rate-1/2 coding, full diversity is not achieved. Using a precoded QPSK with $s = 2$ and a 16-state rate-1/2 $(23,35)_8$ NRNSC code having minimal Hamming distance 7, we get the same spectral efficiency, 2 bits per channel use, and the Singleton bound is equal to 8, the full diversity order. We compare this full-diversity scheme using linear precoding with a scheme using constellation expansion from QPSK to 16-QAM with a 64-state rate-1/4 NRCSC code having generator polynomials $(135,135,147,163)_8$ and minimal Hamming distance 20. With the latter scheme, we get the same spectral efficiency and the Singleton bound is also equal to 8. The linear precoder provides a greater diversity order at the first iteration. At the last iteration, both schemes have same diversity and the precoded scheme slightly outperforms the scheme with constellation expansion. Since the detector complexity is around $L_{\mathcal{C}} N_{\mathcal{C}} / (msn_t) 2^{mN_t}$ operations per iteration if $s \ll L_{\mathcal{C}} N_{\mathcal{C}}$, the detection of the precoded system is as complex as the detection of the one with constellation expansion. However, channel decoding of the 64-state $(135,135,147,163)_8$ NRNSC code is more complex than the decoding of the 16-state $(23,35)_8$ NRNSC code. Thus, to get a same performance, it is less complex to use linear precoding than to use constellation expansion. When choosing a 64-state NRNSC $(133,171)_8$ code with rate 1/2 and minimal Hamming distance 10, the coding gain is increased by almost 1 dB.

In order to increase the frame length without degrading performance, we now consider turbo-codes. Fig. 3.16 illustrates the performance of a $(7,5)_8$ RSC turbo-code over a 1×1 channel with

$n_c = 4$, QPSK input and either a PR or an optimized interleaver. Two different frame lengths (256 and 2048 coded bits) are tested. With the PR interleaver and without precoding, the full diversity order 4 is not achieved. If the optimized interleaver is used, the full diversity order is not achieved, but the smaller slope is not visible down to a FER equal to 10^{-3}. A similar behavior is obtained with PR interleaver and precoding $s = 2$. Finally, the DNA precoded modulation with optimized interleaver achieves full diversity performance within less than 2dB from the outage capacity with Gaussian input.

Fig. 3.17 illustrates the performance of a $(7, 5)_8$ RSC turbo-code over a 2×2 quasi-static channel with QPSK input and either a PR or an optimized interleaver. Two different frame lengths (256 and 2048 coded bits) are tested. With the PR interleaver, the full diversity order 4 is not achieved, and the performance degrades when the frame length increases, as with convolutional codes. With the optimized interleaver, the full diversity order is achieved and the frame error rate decreases when the frame length increases. The system using DNA precoding ($s = 2$), optimized interleaver and a turbo code finally performs within 1dB from the outage capacity with Gaussian input.

Fig. 3.18 represents the performance of a $(7, 5)_8$ RSC turbo-code over a 4×1 quasi-static channel with BPSK input and either a PR or an optimized interleaver. Two different frame lengths (256 and 2048 coded bits) are tested. Without linear precoder and using a PR interleaver, the full diversity gain is not achieved. Asymptotically, the observed diversity is $n_r = 1$, but for low SNRs the performance is close to the performance obtained with the optimized interleaver. Indeed, the turbo-code generates a large amount of errors for low SNRs and the probability of satisfying the ideal interleaving condition with a PR interleaver is high. However, when the number of errors is low at high SNRs, it is crucial to place the few erroneous bits over all the channel states. This behaviour is stressed with increased frame length. To achieve maximum diversity, according to the Singleton bound, a precoding with at least $s = 2$ is needed. This is confirmed by the simulation results and again the error rate decreases when the frame length increases. With the 4×1 MIMO channel, a large amount of interference exists between the transmit antennas. Nevertheless, performance is within 2.5 dB from the outage probability with Gaussian input. Performance will be even closer to the outage probability with a higher number of receive antennas or channel realizations.

On Fig. 3.19, performance of NRNSC codes and parallel turbo-codes with RSC constituent codes are drawn versus frame size for a given signal-to-noise ratio equal to 15 dB over a 2×1 quasi-static MIMO channel. Performance of the Alamouti scheme [3] having same spectral efficiency without channel coding is also drawn as a reference. The frame error rate increases with the frame size when using Alamouti scheme or NRNSC codes whereas it remains constant when using turbo codes. This strong property is in part explained by the interleaving gain of the turbo-code but it needs further research to be clearly expressed.

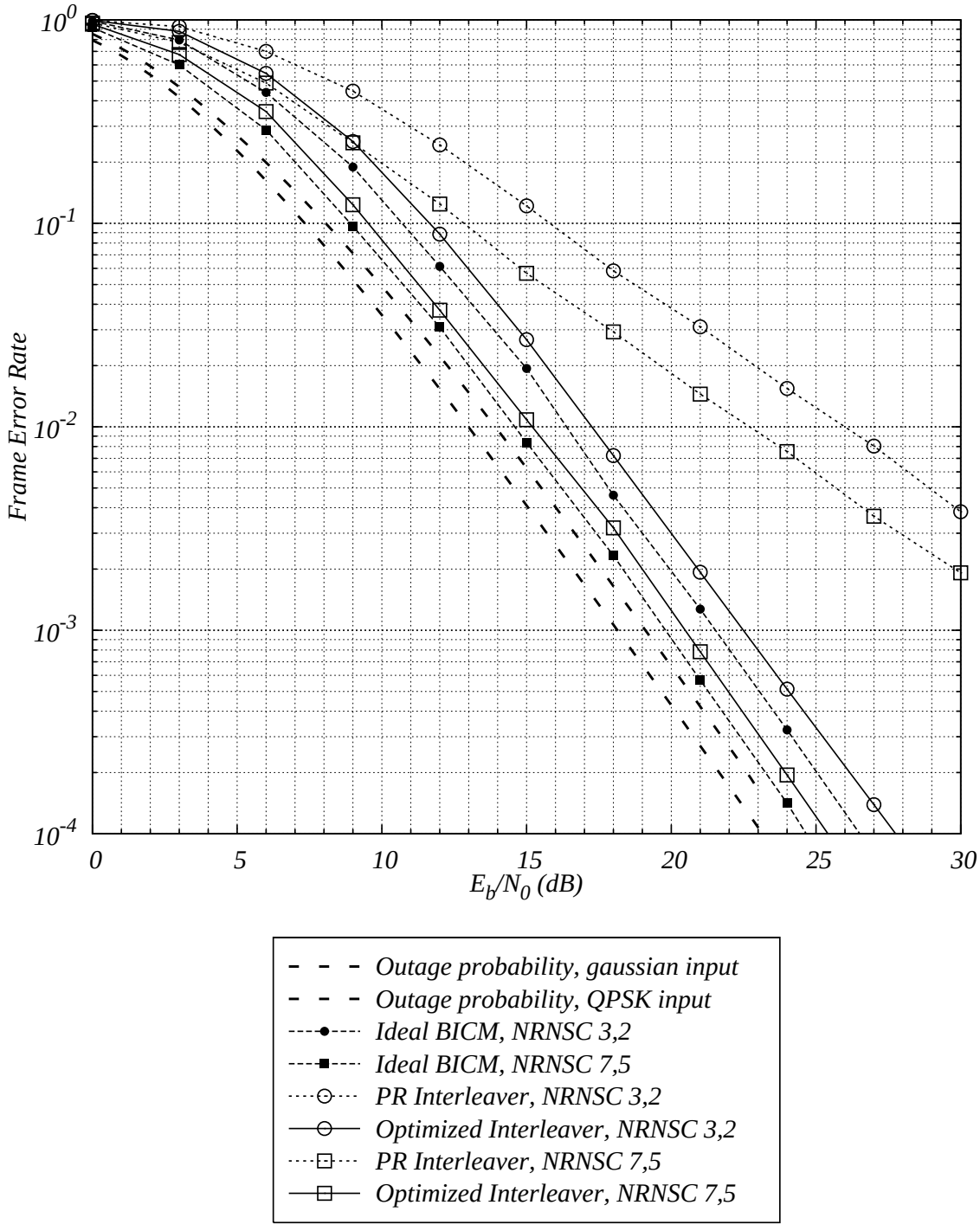

Figure 3.13: Optimized interleaver with rate-1/2 NRNSC codes - QPSK modulation, 2×1 MIMO channel, $n_c = 1$, 10 iterations, $L_c N_c = 1024$.

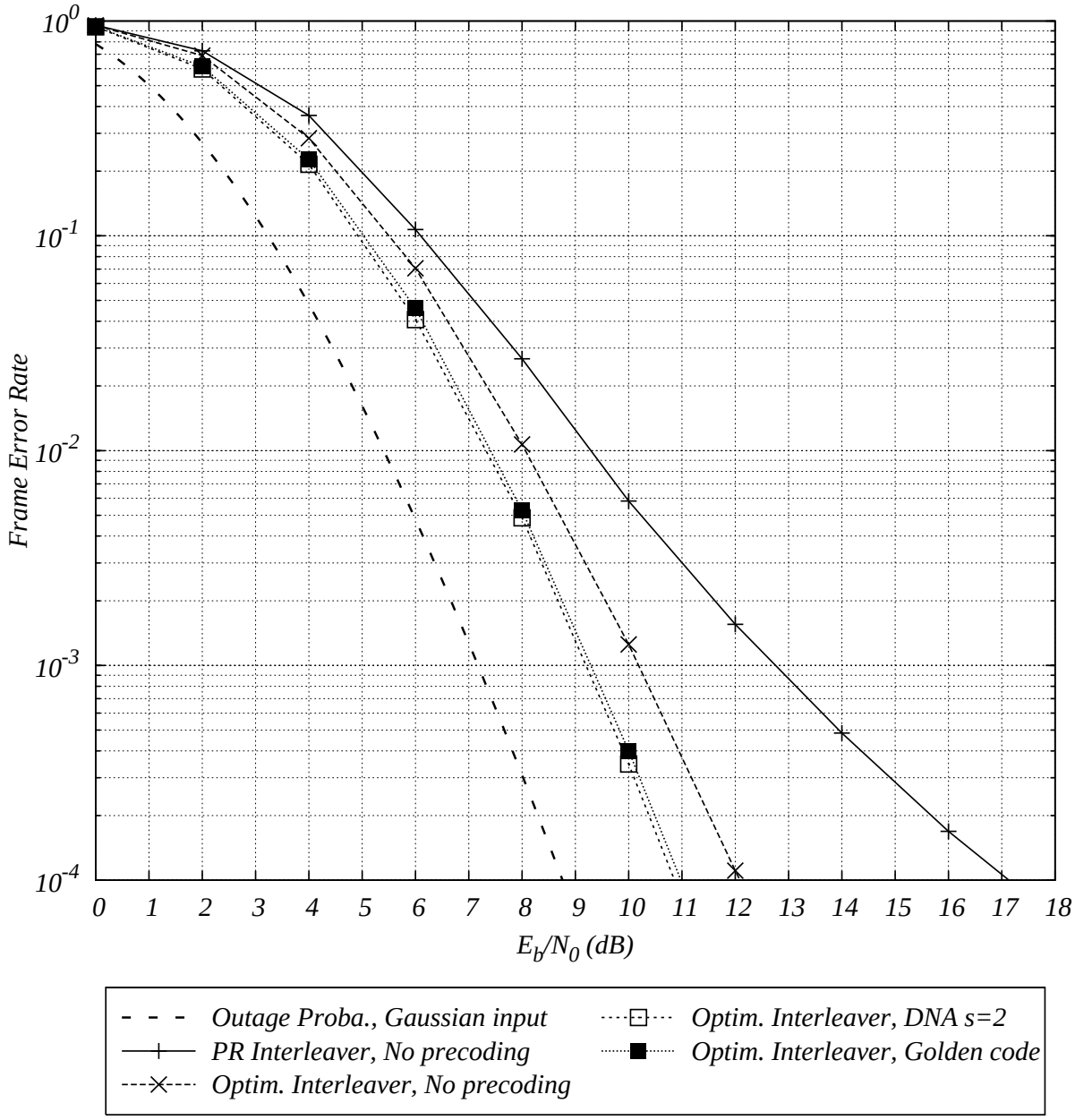

Figure 3.14: Optimized interleaver with rate-1/2 $(7,5)_8$ NRNSC code and linear precoders - QPSK, 2×2 MIMO channel, $n_c = 2$, 5 iterations, $L_c N_c = 256$ - No linear precoder, DNA cyclotomic precoder $(s = 2, n_s = 1)$, Golden code $(s = 2, n_s = 1)$.

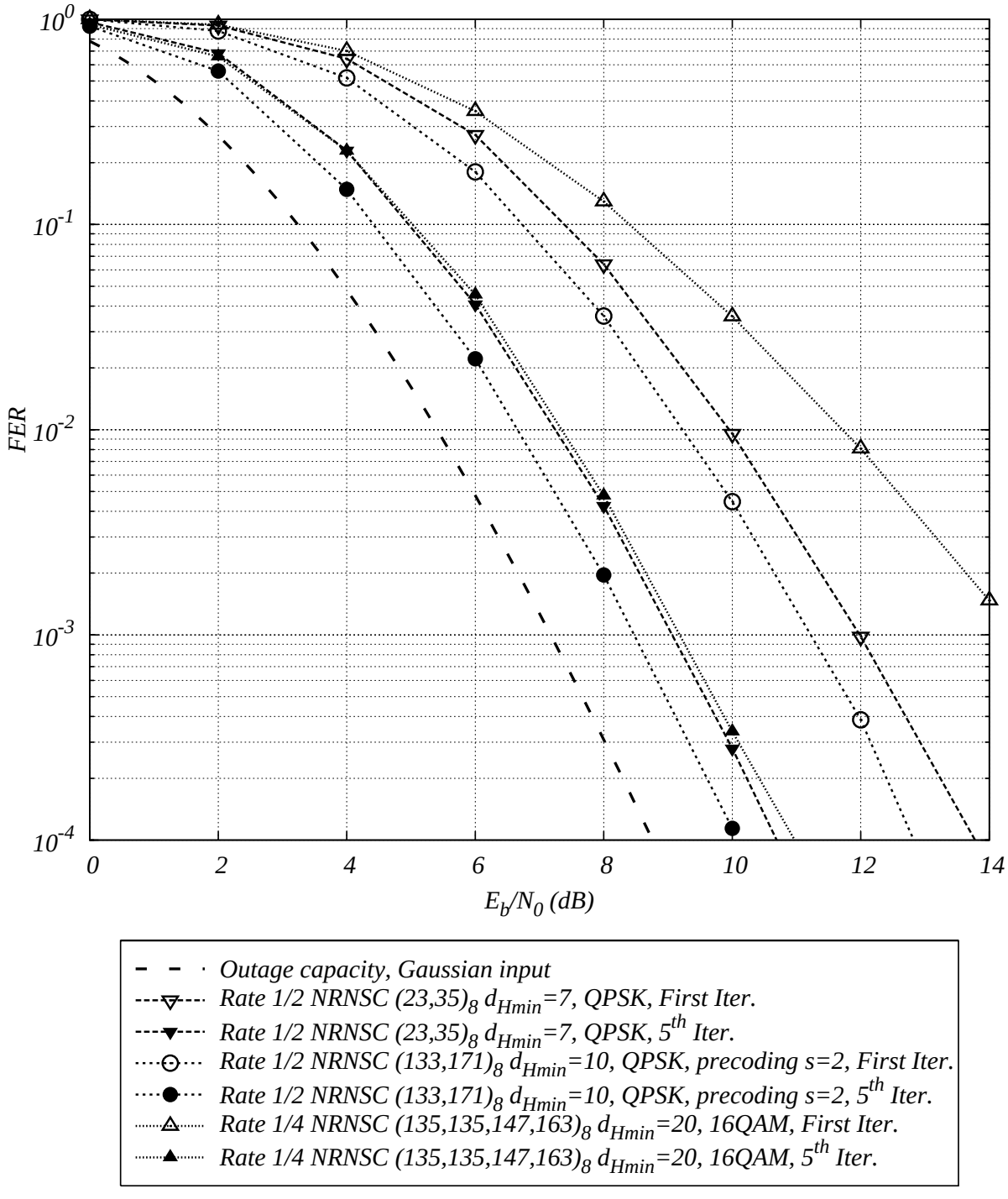

Figure 3.15: Constellation expansion versus linear precoding - 2×2 MIMO channel, $n_c = 2$, $L_c N_c = 1024$, optimized interleaver.

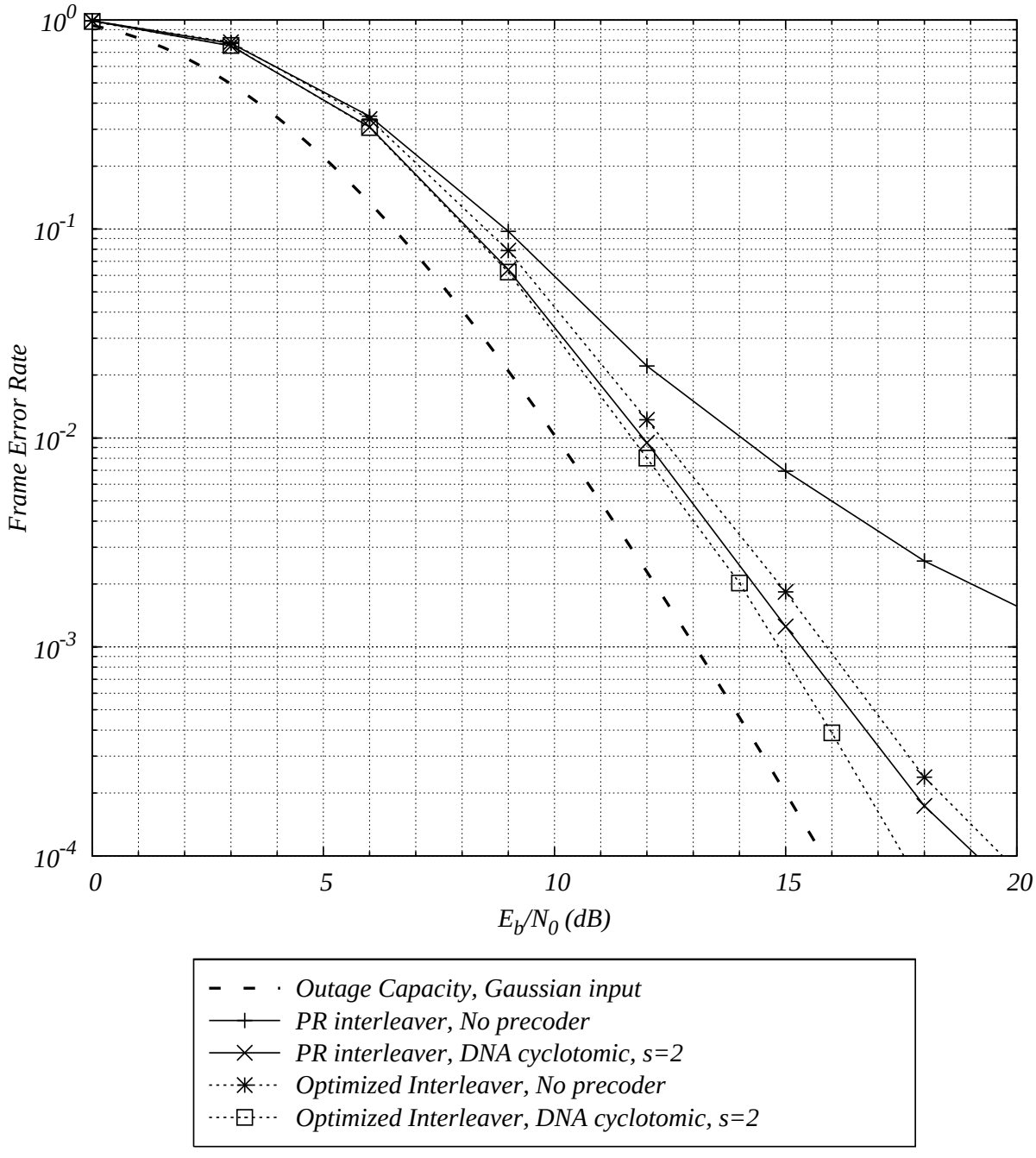

Figure 3.16: Optimized interleaver with rate-1/2 RSC $(7,5)_8$ turbo-code and DNA cyclotomic precoder - QPSK, 1×1 MIMO channel, $n_c = 4$, 15 iterations, $L_c N_c = 2048$ - Parity check bits of the second constituent are multiplexed via the inverse turbo interleaver.

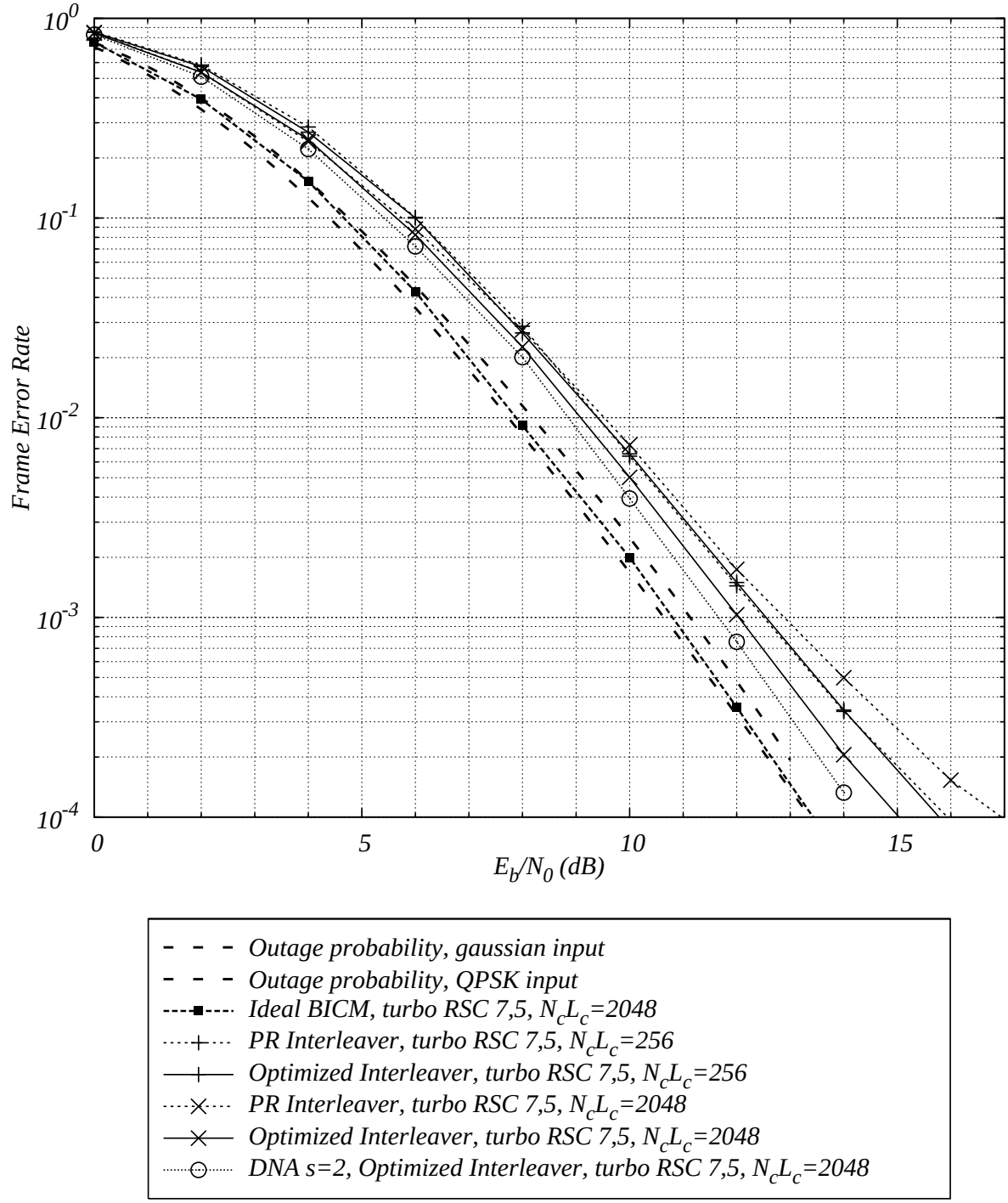

Figure 3.17: Impact of frame size with a rate-1/2 RSC $(7,5)_8$ turbo-code - QPSK, 2×2 MIMO channel, $n_c = 1$, 15 iterations - Parity check bits of the second constituent are multiplexed via the inverse turbo interleaver.

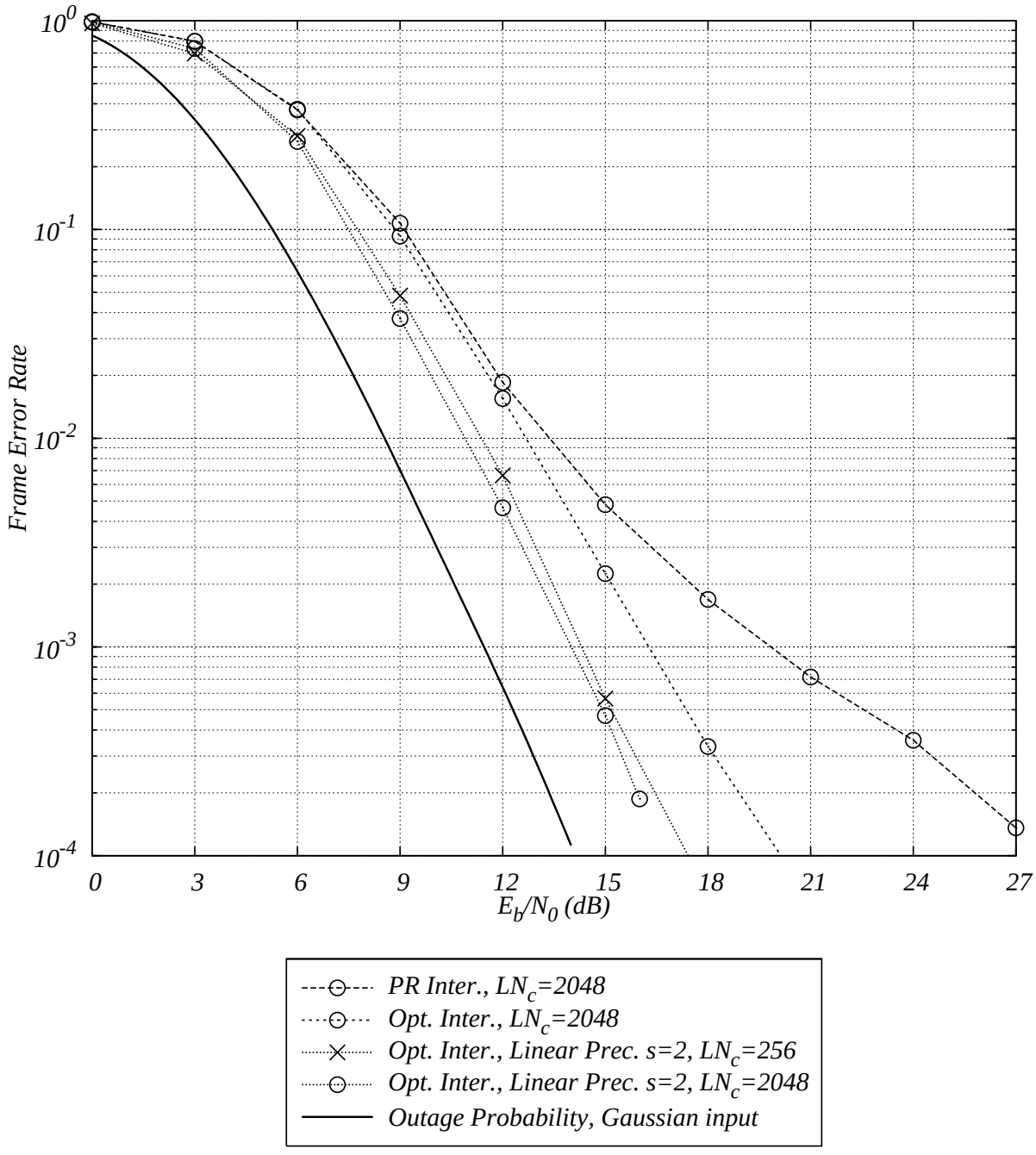

Figure 3.18: Impact of frame length with a rate-1/2 RSC $(7,5)_8$ turbo-code - BPSK, 4×1 MIMO channel, $n_c = 1$, 15 iterations - Parity check bits of the second constituent are multiplexed via the inverse turbo interleaver.

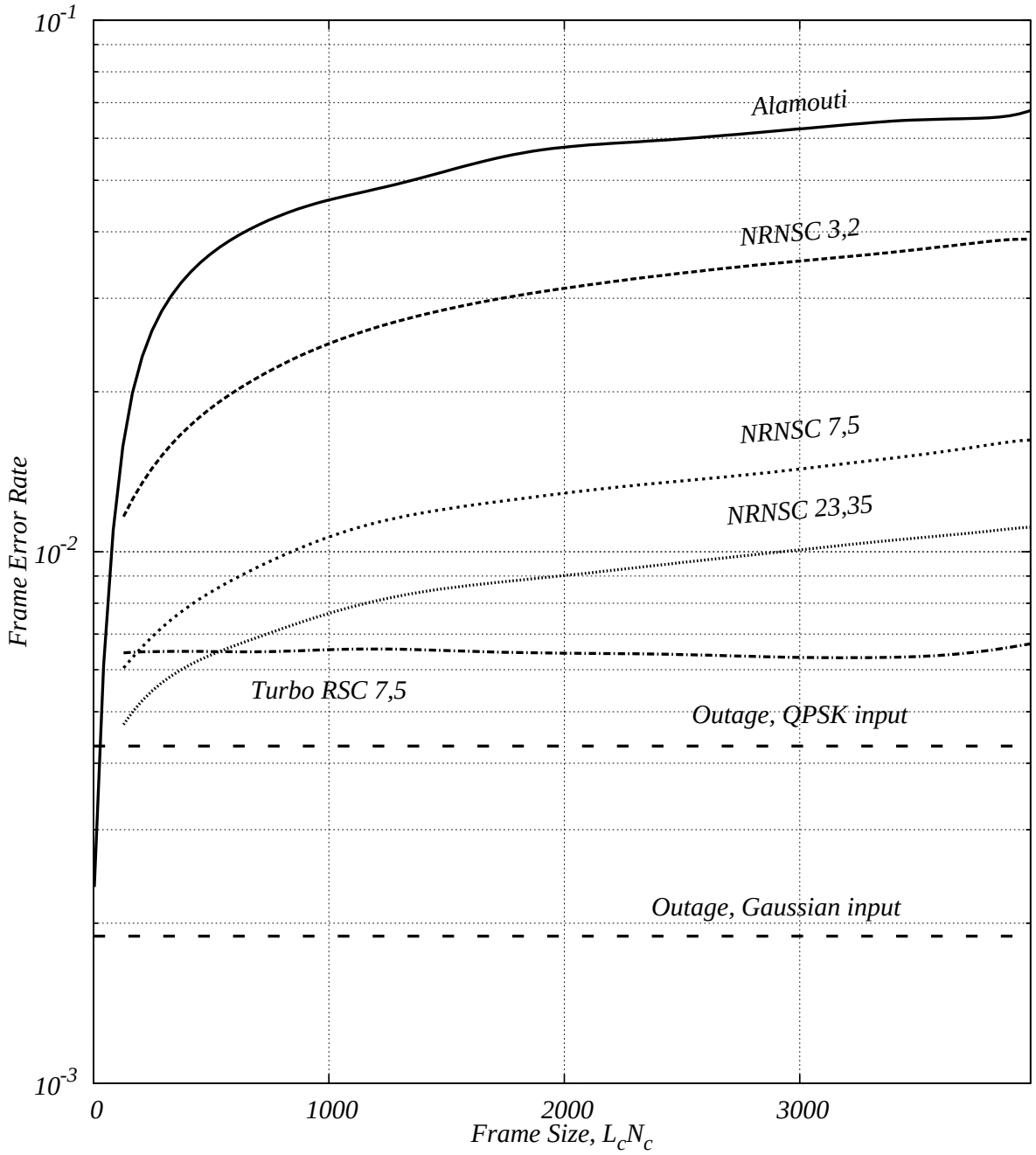

Figure 3.19: Frame error rate versus the frame size L_cN_c - BPSK, 2×1 MIMO channel, $n_c = 1$, SNR = 15 dB - Alamouti STBC, NRNSC codes, parallel turbo codes - Parity check bits of the second constituent are multiplexed via the inverse turbo interleaver.

Conclusions

We have presented bit-interleaved coded modulation optimizations for multiple antenna channels. We achieve near capacity on ergodic channels thanks to turbo-codes or optimized interleavers. It is shown that the design for ergodic channels is much easier than for block fading channels. In this last case, the full diversity is the first objective to be achieved by the receiver. The Singleton bound gives the maximum diversity the decoder can recover and the minimum spreading factor that guarantees full diversity. Next the coding gain has to be optimized using a well chosen binary code, an optimized interleaver and an optimized linear precoder. Finally we have presented a modification of the turbo-codes in order to achieve near outage performance. The error rate decreases with an increasing frame length.

Chapter 4

BICM receivers for MIMO channels

Introduction

In order to improve the data transmission rate over fading channels, most of new transmission systems use a set of multiple antennas at the transmitter and receiver side. However, the receiver has to be sophisticated enough to recover the large amount of data received with a large amount of interference. Iterative techniques, such as iterative joint detection and decoding, seem to be a judicious choice for high performance receivers with tractable complexity. This requires soft-input soft-output detectors and decoders. However, when using high spectral efficiency QAM modulations with multiple transmit antennas, the classical exhaustive soft list detector becomes intractable. Recently, a sub-optimum soft list detector has been proposed in [49], but some weaknesses are still existing to achieve near optimum soft detection performance. We will present some modifications to the list construction and complexity reduction in the case of block fading channels.

In Section 4.1, some basics on lattices are presented, the multiple antenna (MIMO) channel lattice model is expressed. Some simple lattice theory tools are also introduced, they will be helpful to describe and optimize the maximum likelihood Sphere Decoder presented in Section 4.2. In Section 4.3, we present the soft-input soft-output (SISO) spherical list detector and its application to MIMO channels joint detection and decoding. In Section 4.4, the SISO-MMSE described in [32] is modified for MIMO channels with some complexity reductions. Complexity and performance comparison between the presented SISO detectors is discussed in section 4.5 to conclude this chapter.

4.1 Basics on lattices

4.1.1 MIMO channel equivalent lattice

Lattice theory and coding theory are applied to efficiently encode and decode information in a digital transmission system with multiple antennas. For some information theoretical reasons (see [87]) it is assumed that $n_t = n_r$ throughout this section.

Lattice theory [26] is a powerful mathematical tool to geometrically represent the modulation and channel concatenation. It helps us to better understand its behavior, in order to design a good modulator and its corresponding demodulator. Since multi-dimensional QAM constellations are subsets of $\mathbb{Z}^n$, we can write $z \in \mathbb{Z}^{2n_t}$. Let n_Λ denote the dimension of the real Euclidean space,

$$n_\Lambda = 2 \times n_t = 2 \times n_r \tag{4.1}$$

The equality $x = zH$ is now extended to the real space $\mathbb{R}^{n_\Lambda}$ to get

$$x = zM_\Lambda, x \in \mathbb{R}^{n_\Lambda}, z \in \mathbb{Z}^{n_\Lambda} \tag{4.2}$$

Therefore, the MIMO channel output $y = x + \nu$ is obtained by perturbing a lattice point z with additive white noise ν. A lattice Λ is a discrete subgroup of $\mathbb{R}^{n_\Lambda}$, i.e. it is a $\mathbb{Z}$-module of rank n_Λ. In (4.2), the lattice Λ is generated by the $n_\Lambda \times n_\Lambda$ real matrix M_Λ, which is derived from the channel matrix H by the following simple expression

$$M_\Lambda = \begin{pmatrix} \Re h_{11} & \Im h_{11} & \dots & \dots & \Re h_{1n_r} & \Im h_{1n_r} \\ -\Im h_{11} & \Re h_{11} & \dots & \dots & -\Im h_{1n_r} & \Re h_{1n_r} \\ \dots & \dots & \Re h_{ij} & \Im h_{ij} & \dots & \dots \\ \dots & \dots & -\Im h_{ij} & \Re h_{ij} & \dots & \dots \\ \Re h_{n_t1} & \Im h_{n_t1} & \dots & \dots & \Re h_{n_tn_r} & \Im h_{n_tn_r} \\ -\Im h_{n_t1} & \Re h_{n_t1} & \dots & \dots & -\Im h_{n_tn_r} & \Re h_{n_tn_r} \end{pmatrix} \tag{4.3}$$

When z is restricted to a finite QAM integer constellation, x belongs to a finite lattice constellation denoted by Ω. For example, if $n_t = n_r = 8$ antennas and $m = 4$ (16-QAM), the constellation Ω at the MIMO channel output has $2^{mn_t} = 2^{32} (\simeq 4)$ billion points. Each point in Ω has a binary label of 32 bits. Before combining an error-correcting code with a digital modulation for use on a MIMO channel, we first analyze the main parameters of the lattice Λ associated with multiple antenna channels. Such a geometrical analysis is complementary to the one made by information theory concerning Shannon capacity of MIMO channels.

4.1.2 Important lattice parameters

The matrix M_Λ is called a *lattice generator matrix* of the lattice $\Lambda(M_\Lambda)$. Let P_Λ be the set of points that satisfy

$$P_\Lambda = \{x \in \mathbb{R}^n / x = \alpha M_\Lambda, \quad \alpha \in [0 \dots 1]^n\} \tag{4.4}$$

P_Λ is called the fundamental parallelotope of Λ (see Fig. 4.1).

The first lattice parameter to be considered is the *fundamental volume* $\mathrm{vol}(\Lambda)$, which represents the volume of the fundamental parallelotope defined by

$$\mathrm{vol}(\Lambda) = |det(M_\Lambda)| = \sqrt{det(G)} \tag{4.5}$$

where the Gram matrix G defining the quadratic form $Q(z)$ associated with the lattice is related to M_Λ by

$$G = M_\Lambda M_\Lambda^t, ||x||^2 = zGz^t = Q(z) = \sum_{ij} g_{ij} z_i z_j \tag{4.6}$$

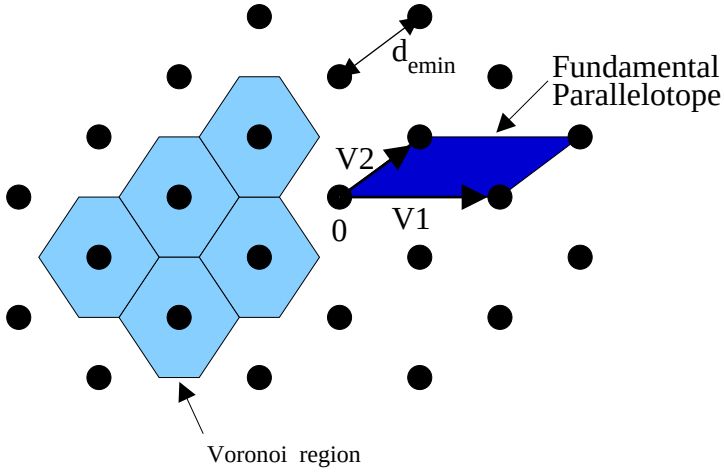

Figure 4.1: Lattice parameters.

The second lattice parameter is the *minimum Euclidean distance* $d_{Emin}(\Lambda)$ defined by

$$d_{Emin}(\Lambda) = \min_{p1,p2} ||p_1 - p_2|| \quad p_1, p_2 \in \Lambda, p1 \neq p2 \tag{4.7}$$

The problem of computing $d_{Emin}(\Lambda)$ is hard (it is NP-complete). Thus, we suggest three different methods to get an estimation of the minimum Euclidean distance in Λ:

1. The rows of M_Λ are a $\mathbb{Z}$-basis for Λ. Read the n_Λ Euclidean norms in the *lattice basis* and keep the minimum. This yields an upper bound on $d_{Emin}(\Lambda)$. In practice, we equivalently search for the minimum element of the Gram matrix diagonal.
2. Reduce the basis M_Λ by finding another lattice basis with shorter vectors. We suggest here to use the efficient LLL reduction algorithm [62], or the more complex Korkine-Zolotarev algorithm ([58]). This yields a tight upper bound on $d_{Emin}(\Lambda)$. If a Minkovsky reduction can be processed, we find the exact value of $d_{Emin}(\Lambda)$.
3. Find the exact minimum distance by enumerating lattice points inside a sphere centered on the origin, then take the minimal norm of a non-zero point. We suggest the application of *Short vectors* algorithm [72] to determine the exact value of $d_{Emin}(\Lambda)$.

Of course, the three methods above are listed in increasing order of complexity. As shown later in this study, the estimation of $d_{Emin}(\Lambda)$ helps to accelerate the Sphere Decoder algorithm [98] used to find the maximum likelihood (ML) lattice point. Given the lattice minimum distance and its fundamental volume, it is possible to derive the normalized squared minimum distance, called *fundamental gain*, given by

$$\gamma(\Lambda) = \frac{d^2_{Emin}(\Lambda)}{\text{vol}(\Lambda)^{2/n_\Lambda}} \tag{4.8}$$

Usually, the fundamental gain is expressed in decibels, $\gamma_{dB} = 10log_{10}(\gamma)$. A lattice sphere packing is non-dense if $\gamma_{dB} < 0$, i.e. the lattice is less dense than the cubic integer lattice $\mathbb{Z}^{n_\Lambda}$. When $\gamma_{dB} > 0$, the dense lattice is associated with a *good* MIMO channel that may perform better than an AWGN single antenna channel. Such a performance comparison should also take into account the kissing number of Λ [26] which is completely random and difficult to estimate in a multiple antenna channel context.

Number of antennas	$d^2_{Emin}(exact)$ mean/variance	$d^2_{Emin}(LLL)$ mean/variance	$d^2_{Emin}(Gram)$ mean/variance	$\gamma(dB)$ mean/variance	$\gamma(dB) < 0$ Percentage
2	0.979/0.542	0.979/0.543	1.250/0.687	-1.10/2.04	78.1
4	1.607/0.576	1.608/0.579	2.182/0.803	-0.65/1.42	66.9
8	3.867/1.004	3.875/1.019	4.488/1.272	+0.76/0.75	17.1
16	9.719/2.231	9.734/2.274	9.770/2.309	+1.98/0.59	1.15

Table 4.1: Main lattice parameters of the MIMO channel (first table).

Number of antennas	$d^2_{Emin}(exact < LLL)$ Percentage	$d^2_{Emin}(LLL < Gram)$ Percentage	$d^2_{Emin}(exact < Gram)$ Percentage
2	0.19	40.02	40.07
4	0.92	61.60	61.86
8	3.18	53.82	54.67
16	2.36	4.79	5.64

Table 4.2: Main lattice parameters of the MIMO channel (second table).

Nevertheless, the three above-mentioned main parameters are sufficient to understand the geometrical behavior of Λ. Tables 4.1 and 4.2 show the main parameters of a MIMO lattice and some statistics related to these parameters.

As expected, the lattice minimum distance increases with the number of antennas. Indeed, the channel diversity order is proportional to the number of antennas. The percentage of dense lattices is surprisingly high, especially for 8 and 16 antennas. This predicts a performance extremely close to the Gaussian channel when $n_t = n_r$ is large. If the channel matrix H is known at the transmitter, it is possible to take a waterfilling approach where the information instantaneous rate is proportional to $\gamma(\Lambda)$. Two important results may be deduced from Table 4.2:

1. The LLL reduction algorithm is extremely efficient in finding the minimum distance of a MIMO lattice. The failure percentage varies from 0.19% to 3.18% only
2. The simplest method (method 1 based on the diagonal of the Gram matrix) seems also to be quite efficient for a large number of antennas, (only 5.64% failure with 16 antennas)

Finally, Fig. 4.2, 4.3 and 4.4 give more details on the distribution of $d_{Emin}(\Lambda)$ and $\gamma(\Lambda)$ versus the number of antennas. Note that in Fig. 4.4, in the case of 16 antennas, γ is limited to -1dB for non-dense lattices and upper bounded by 4dB for dense lattices. For comparison, we recall that $n_t = n_r = 16$ antennas correspond to a lattice in $\mathbb{R}^{32}$ for which some known structured dense lattices have a fundamental gain equal to 6dB.

4.1.3 Lattice generator matrix QR decompositions

A matrix decomposition is a transformation of a given matrix into a canonical form. For example, we cite LU, Singular Value, eigenvalue, and Schur decompositions. In this chapter, we are interested in QR decompositions of M_Λ:

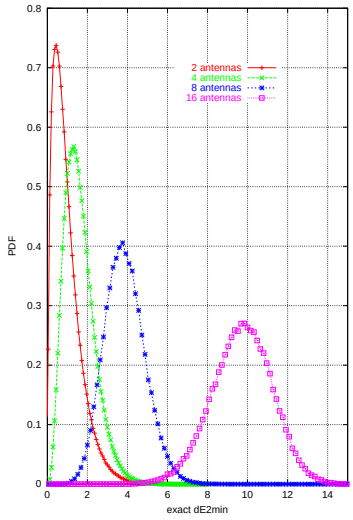

Figure 4.2: Distribution of the exact minimum squared distance d^2_{Emin}.

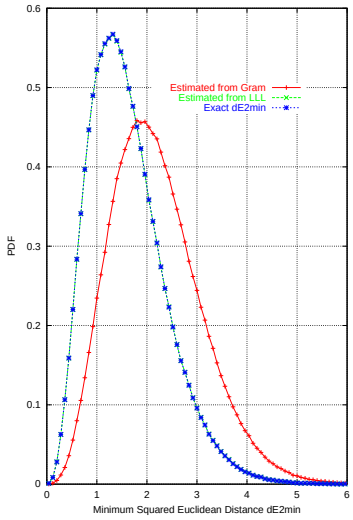

Figure 4.3: Comparison of different estimations of d^2_{Emin} for 4 antennas.

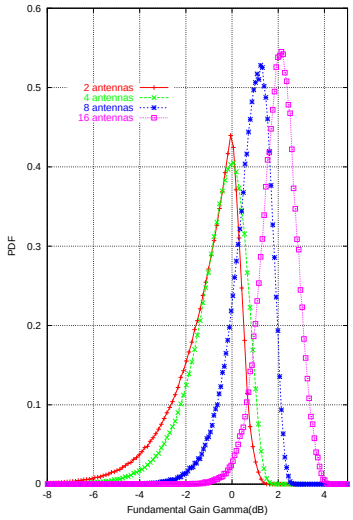

Figure 4.4: Distribution of the fundamental gain $\gamma(dB)$ in the MIMO channel.

Let M_Λ be a square matrix, there exists a lower triangular matrix Δ and a rotation matrix Q ($QQ^t = I$) such that $M_\Lambda = \Delta Q$.

Let us rotate the first basis vector of $\Lambda(M_\Lambda)$ to fit the first Euclidean basis vector. The applied rotation is called Q_{n_Λ}, and we define the rotated matrix $\Delta_1 = M_\Lambda Q_{n_\Lambda}$. The first row of Δ_1 has only one non-null coefficient on the first position. We extract a $n_\Lambda - 1 \times n_\Lambda - 1$ matrix from the last $n_\Lambda - 1$ rows and columns of Δ_1 and apply a rotation $Q_{n_\Lambda - 1}$ that aligns the first basis vector to the first $n_\Lambda - 1$ dimensional space. This operation repeated $n_\Lambda - 1$ times leads to a lower triangular matrix, via $n_\Lambda - 1$ rotations. The global transformation is a rotation Q:

$$\Delta = M_\Lambda Q = M_\Lambda Q_{n_\Lambda} \mathrm{diag}(I_{1,1}, Q_{n_\Lambda - 1}) \dots \mathrm{diag}(I_{k,k}, Q_{n_\Lambda - k}) \dots \mathrm{diag}(I_{n_\Lambda, n_\Lambda}) \tag{4.9}$$

where $\mathrm{diag}(I_{k,k}, Q_{n_\Lambda - k})$ is a block diagonal matrix with two blocks: a $k \times k$ identity matrix and a $n_\Lambda - k$-dimensional rotation.

In order to efficiently process the QR decomposition, we use the simple observation that a rotation is a Householder reflexion $R = I - 2m_\perp^t m_\perp$, where $m_\perp$ is the normal vector of the reflexion hyperplane. We see a geometrical representation of a 2-dimensional Householder reflexion in Fig. 4.5. The vector $m_\perp$ that transforms a given vector x into $[\|x\|, 0, \dots, 0]$ by reflexion is

$$m_\perp = \frac{1}{\sqrt{\|x\|(\|x\| + |x_1|)}} [x_1 + \mathrm{sgn}(x_1)\|x\|, x_2, \dots, x_n] \tag{4.10}$$

We apply the Householder reflexions to compute the transformation of the M_Λ and I matrices, respectively leading to Δ and Q. The complexity in flops (floating point operations, i.e., any addition, multiplication, division, square root of a floating point variable) is $5n_\Lambda^3/3 + 2n_\Lambda^2 + 16n_\Lambda/3$.

Another method to compute Δ is to apply a Cholesky decomposition of the Gram matrix $G = M_\Lambda M_\Lambda^t = \Delta Q Q^t \Delta^t = \Delta\Delta^t$: the main idea of the Cholesky decomposition is to observe

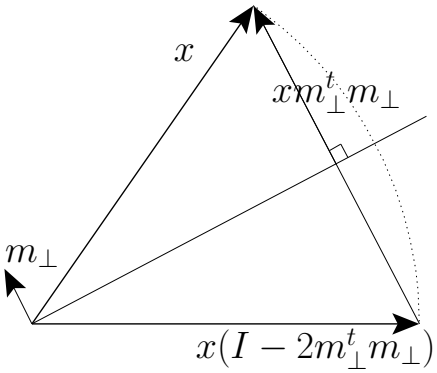

Figure 4.5: Householder reflexion of x with respect to an hyperplane defined by the normal vector $m_\perp$.

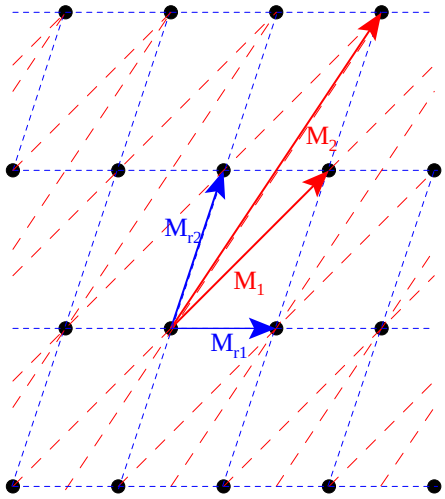

Figure 4.6: Basis reduction example.

that

$$\forall 0 < i \leq n_\Lambda, \qquad \Delta_{i,i}^2 = G_{ii} - \sum_{j=1}^{i-1} \Delta_{i,j}^2 \tag{4.11}$$

$$\forall i < k \leq n_\Lambda, \quad \Delta_{k,i}\Delta_{i,i} = G_{ik} - \sum_{j=1}^{i-1} \Delta_{k,j}\Delta_{i,j} \tag{4.12}$$

which is sufficient to compute Δ. This method exactly leads to the same matrix as QR decomposition. The algorithm complexity is $5n_\Lambda^3/6 - 3n_\Lambda^2/2 + 2n_\Lambda/3$ flops. However, the Gram matrix computation ($n_\Lambda(n_\Lambda+1)(2n_\Lambda-1)/2$ flops) has to be added if Cholesky is used for M_Λ triangular decomposition. The algorithm does not allow an easy computation of the rotation matrix Q. Some algorithms do not require Q but a matrix Θ such that:

$$\forall 1 \leq i \leq n, \qquad \Theta_{i,i} = \Delta_{i,i}^2 \tag{4.13}$$

$$\forall 1 \leq i < j \leq n, \qquad \Theta_{i,j} = \frac{\Delta_{j,i}}{\Delta_{i,i}} \tag{4.14}$$

which is easily provided by the Cholesky decomposition.

4.1.4 Lattice reductions

The MIMO channel leads to a random lattice structure. The basis of the lattice, given by M_Λ is not always the best in terms of orthogonality and vectors' shortness. The procedure of finding a better lattice basis is called reduction. This work was initiated by Gauss who proposed some algorithms for dimensions two and three, but the main three algorithms were proposed by

1. H. Minkovsky
2. Ch. Hermite, enhanced by A. Korkine and G. Zolotareff (KZ reduction, [58])
3. A. K. Lenstra, H. W. Lenstra, Jr. and L. Lovàsz (LLL reduction, [62])

No efficient algorithms are known to find the shortest non-zero basis of an arbitrary lattice. However, the LLL algorithm, proposed in 1982, computes an approximation of the smallest basis in polynomial time.

Since the basis reduction is a basis change, the lattice remains the same after reduction and the reduction matrix is unitary V:

$$M_r = VM_\Lambda, \quad \Lambda(M_\Lambda) = \Lambda(M_r) \tag{4.15}$$

Fig. 4.6 presents an example of basis reduction, the basis $(M_{r,1}, M_{r,2})$ is the reduced version of (M_1, M_2). We will briefly present some basic knowledge on lattice reduction that will help us to accelerate the decoding of MIMO channels.

First, let us recall the Gram-Schmidt Orthogonalization computation. Let $(v_1, \ldots, v_n)$ be a basis of $\mathbb{R}^n$, an orthogonal basis $(u_1, \ldots, u_n)$ is obtained by the recurrence:

$$\forall i = 1 \ldots n, \quad v_i = u_i - \sum_{j=1}^{i-1} \frac{u_i v_j^t}{\|v_j\|^2} v_j = u_i - \sum_{j=1}^{i-1} \mu_{i,j} v_j \tag{4.16}$$

i.e., recursively substracting the non-orthogonal components of the basis vectors. The Gram-Schmidt Ortoghonalization is not a basis reduction since the resultant basis does not generate the same lattice, the $\mu_{i,j}$ coefficients are not integers. Now, we present the definition of basis reduceness:

A lattice Λ basis $(u_1, \ldots, u_n)$ is reduced if $\forall 1 \leq i < j \leq n, \quad \|\mu_{i,j}\| \leq \frac{1}{2}$

The Gram-Schmidt orthogonalization is directly applied into basis reduction:

1. Compute the Gram-Schmidt orthogonalization basis $(u_1, \ldots, u_n)$ of $(v_1, \ldots, v_n)$
2. Compute the algorithm:

   for $i = 1..n\{$ for $j = i - 1..1\{$ $u_i \leftarrow u_i - \lfloor \mu_{i,j} \rceil u_j$; for $k = 1..j\{$ $\mu_{i,k} \leftarrow \mu_{i,k} - \lfloor \mu_{i,j} \rceil \mu_{j,k}\}\}\}$

The algorithm complexity is $\frac{1}{3}n^3 + n^2 - \frac{4}{3}n$ flops, but the provided basis is not particularly orthogonal, no vector exchanges have been processed. However, we will see that this reduction will be very useful for lattice constellation decoding because of the triangular property of the reduction basis change matrix.

An efficient algorithm to compute reduced basis is the LLL reduction [62] which statisfies a sub-optimal reduction criterion:
A lattice Λ with basis $(u_1, \ldots, u_n)$ and Gram-Schmidt orthogonal basis $(v_1, \ldots, v_n)$, is said to be LLL-reduced if and only if:

$$\begin{aligned} &\forall 1 \leq j < i \leq n, && |\mu_{i,j}| \leq \tfrac{1}{2} \\ &\forall 1 \leq i \leq n-1, && |v_i|^2 \leq \tfrac{4}{3} \left| u_{i+1} - \textstyle\sum_{j=1}^{i-1} \mu_{i+1,j} v_j \right|^2 \end{aligned}$$

This is a looser property than the one used by the more efficient but more complex algorithm KZ [58].

4.2 Sphere decoding

The sphere decoder is an algorithm providing ML performance on lattice channels. For example, we can cite rotated rayleigh channels [14], CDMA or MC-CDMA [19] [20][21][25][36][101]. As described, the MIMO channel can also be seen as a lattice, the sphere decoder is well suited for ML decoding of the received point.

A lattice point $x \in \Lambda(H)$ represents the signal received after a transmission over a MIMO channel (or any lattice channel). Here, $\Lambda(H) = \Lambda(M_\Lambda)$ refers to the real lattice of rank n_Λ generated by M_Λ, or equivalently by H. A maximum likelihood lattice decoder applied to the received point $y = x + \nu$ determines the nearest lattice point to y, i.e., it minimizes $\|y - x\|^2$. The point that minimizes the distance is called the closest point. In our case, x is perturbed by an n-dimensional centered additive white Gaussian noise of variance N_0, the likelihood is $p(y/x) = e^{-\|y-x\|^2/2N_0}/\sqrt{2\pi N_0}$; maximizing the likelihood is equivalent to minimizing the Euclidean distance, the maximum likelihood point is the closest lattice constellation point.

The so-called closest point problem is not straightforward, except for orthogonal lattices. Indeed, in this trivial case, the lattice Voronoi region is parallelepipedic and the ML point is found by simple independent quantization on each dimension. When the lattice matrix is non-diagonal, the Voronoi region is a complex polygon we cannot use for decoding. The only way to perform ML decoding is then to compare the distance $\|y - x\|^2$ between the received vector and a set of points including the ML point. If the transmitted set of points cardinality is small enough, we apply an exhaustive computation of all the distances $\|y - x\|^2$. However, for high spectral efficiency systems, or for lattices (infinite number of points), the exhaustive decoding is intractable. If we use a 2^m-QAM transmitted on n_t transmit antennas, the constellation cardinality is $2^{2n_t m}$, which leads to a comparison of $2^{16} = 65536$ distances for 16-QAM over 4 transmit antennas.

The Sphere Decoder is a very efficient algorithm to find the closest point in a lattice [97][98]. The main idea of this algorithm is to enumerate all the lattice points x belonging to a sphere $\mathcal{S}(y, R_\mathcal{S})$ of radius $R_\mathcal{S}$ centered on y, and to compute the distances $\|y-x\|^2$. If no point is found, the radius of the sphere has to be enlarged. Each time a point is found, the radius of the sphere is reduced to the distance of this new point, which limits the number of enumerated points but still ensures the closest point criterion.

4.2.1 The Sphere Decoder based on Pohst point enumeration strategy

The Sphere Decoder based on Pohst strategy [72] was applied by Viterbo and Boutros (VB) [98] to digital communications. The key idea is to enumerate lattice points inside an ellipsoid in the integer space corresponding to a spherical search region in the real space. This technique is derived from the *short vectors* algorithm, initially thought up for the first lattice shells' point enumeration. The point enumeration in $\mathbb{Z}^{n_\Lambda}$ is straightforward, processed by coordinate increment. The enumeration of the lattice points belonging to the sphere $\mathcal{S}(y, R_\mathcal{S})$ is equivalent to the enumeration of the $\mathbb{Z}^{n_\Lambda}$ points belonging to an ellipsoid $\mathcal{E}(\omega, R_\mathcal{S}, M_\Lambda^{-1})$ centered on $\omega = yM_\Lambda^{-1}$. This is illustrated in Fig. 4.7. The $\mathbb{Z}^n$ points belonging to the ellipsoid satisfy the equation

$$z \in \mathcal{E}(\omega, R_\mathcal{S}, M_\Lambda^{-1}) \cap \mathbb{Z}^{n_\Lambda} \Leftrightarrow \|(\omega - z)M_\Lambda\|^2 = \|\delta M_\Lambda\|^2 \leq R_\mathcal{S}^2 \tag{4.17}$$

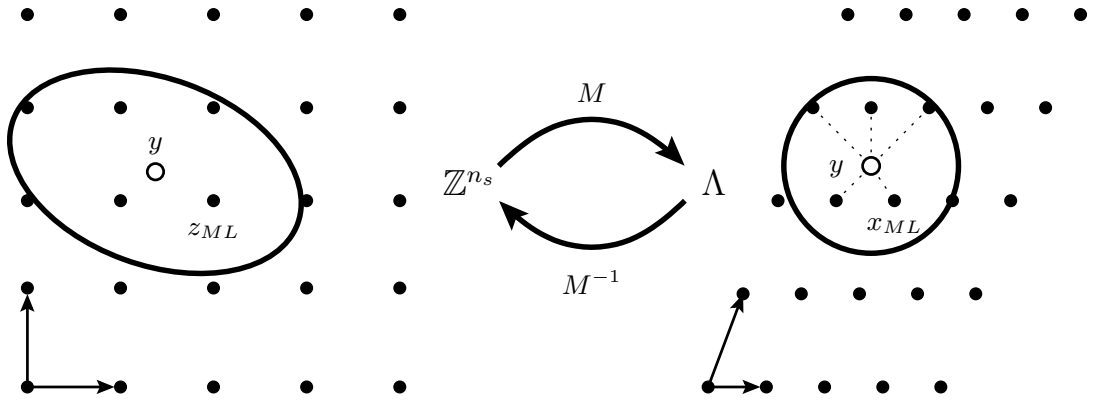

Figure 4.7: Equivalence between a search of Λ points in a sphere and $\mathbb{Z}^{n_\Lambda}$ point in an ellipsoid.

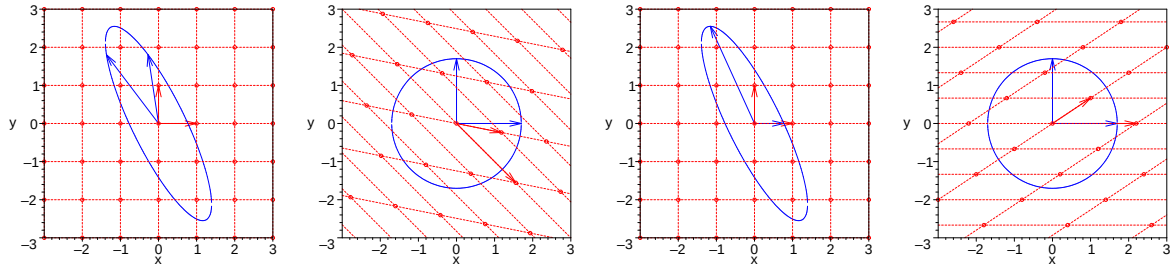

(a) Ellipsoid in $\mathbb{Z}^{n_\Lambda}$ and sphere in $\Lambda(M_\Lambda)$ without QR decomposition.

(b) Ellipsoid in $\mathbb{Z}^{n_\Lambda}$ and sphere in $\Lambda(\Delta_1)$ with QR decomposition.

Figure 4.8: Effect of the lattice generator matrix decomposition into a lower triangular form on the ellipsoid bounds computation.

where δ is the difference vector between the tested point z and the Zero-Forcing point ω. Unfortunately, in the general case, M_Λ has non-zero off-diagonal coefficients and all the δ components are linked together, so this does not allow a simple enumeration without solving an $n_\Lambda \times n_\Lambda$ equation system.

Let us rotate the first basis vector of $\Lambda(M_\Lambda)$ to fit the first Euclidean basis vector, which is equivalent to make one ellipsoid axis collinear to the first basis vector of $\mathbb{Z}^{n_\Lambda}$ as presented in Fig.4.8. The applied rotation is called Q_1, and we define $\Delta_1 = M_\Lambda Q_1$ the new generator matrix of $\Lambda(\Delta_1)$. In this case, z_1 only occurs in the first coordinate x_1 of $x \in \Lambda(\Delta_1)$, with a scaling factor $\Delta_{1,1}$. The ellipsoid bounds are directly linked to the sphere bound along this dimension. If we fix the value of z_1, the projection of the ellipsoid on the corresponding $\mathbb{Z}^{n_\Lambda - 1}$ space is always an ellipsoid, we turn one basis vector to one of the ellipsoid's axis thanks to the rotation Q_2 leading to $\Delta_2 = \Delta_1 Q_2$, and so on until the last dimension, which does not need to be rotated. Finally, the lattice has been rotated $n_\Lambda - 1$ times, the global transformation is a rotation Q and transforms M_Λ into a lower diagonal matrix Δ via $n_\Lambda - 1$ successive rotations:

$$\Delta = M_\Lambda Q = M_\Lambda Q_1 Q_2 \dots Q_{n_\Lambda - 1} \tag{4.18}$$

We saw that if we rotate M_Λ to Δ, a lower triangular matrix, the ellipsoid bounds are computed recursively. We apply a QR decomposition of M_Λ to compute Δ.

Let us now describe the maximum likelihood Sphere Decoder based on Pohst strategy. As-

sume a set of transmitted points z belonging to a lattice constellation $[z_{min}, z_{max}]^{n_\Lambda}$. Such constellation is an homothetie of a 2^m-QAM constellation of an $n_\Lambda/2 \times n_\Lambda/2$ MIMO channel, and enables easier manipulation (the symbol energy is divided by 4 with respect to the classical QAM constellation). Using $QQ^t = I$, the considered square Euclidean distance for ML decoding is

$$\|\delta M_\Lambda\|^2 = \|\delta\Delta\|^2 = \delta\Delta\Delta^t\delta^t = \delta G\delta^t \leq R_{\mathcal{S}}^2 \tag{4.19}$$

Using the lower triangular property of Δ, and defining $\Theta_{i,i} = \Delta_{i,i}^2$ and $\Theta_{i,j} = \Delta_{j,i}/\Delta_{i,i}$, we have that

$$\|\delta\Delta\|^2 = \sum_{i=1}^{n_\Lambda}\left(\sum_{j=i}^{n_\Lambda}\delta_j\Delta_{j,i}\right)^2 = \sum_{i=1}^{n_\Lambda}\Theta_{i,i}\left(\delta_i + \sum_{j=i+1}^{n_\Lambda}\delta_j\Theta_{i,j}\right)^2 \tag{4.20}$$

We want to enumerate all the points belonging to the translated integer lattice $\delta \in (\mathbb{Z}^{n_\Lambda} + \omega)$, this is done by first computing the bounds of δ_{n_Λ}

$$-\sqrt{\frac{R_{\mathcal{S}}^2}{\Theta_{n_\Lambda,n_\Lambda}}} \leq \delta_{n_\Lambda} \leq \sqrt{\frac{R_{\mathcal{S}}^2}{\Theta_{n_\Lambda,n_\Lambda}}} \tag{4.21}$$

and recursively deducing the other bounds, assuming $\{\delta_{k+1}, \ldots, \delta_{n_\Lambda}\}$ known,

$$-\sqrt{\frac{R_{\mathcal{S}}^2 - \sum_{i=k+1}^{n_\Lambda}\Theta_{i,i}\left(\delta_i + \sum_{j=i+1}^{n_\Lambda}\delta_j\Theta_{i,j}\right)^2}{\Theta_{k,k}}} \tag{4.22}$$

$$\leq \delta_k + \sum_{i=k+1}^{n_\Lambda}\Theta_{k,i}\delta_i \leq \sqrt{\frac{R_{\mathcal{S}}^2 - \sum_{i=k+1}^{n_\Lambda}\Theta_{i,i}\left(\delta_i + \sum_{j=i+1}^{n_\Lambda}\delta_j\Theta_{i,j}\right)^2}{\Theta_{k,k}}} \tag{4.23}$$

Substituting $\delta_k = \omega_k - z_k$ and using $z_k \in [0, z_{max}]$, we obtain

$$Max\left(0, \left\lceil \omega_k - \sqrt{\frac{R_{\mathcal{S}}^2 - \sum_{i=k+1}^{n_\Lambda}\Theta_{i,i}\left(\delta_i + \sum_{j=i+1}^{n_\Lambda}\delta_j\Theta_{i,j}\right)^2}{\Theta_{k,k}}} \right\rceil\right) \tag{4.24}$$

$$\leq z_k - \sum_{i=k+1}^{n_\Lambda}\Theta_{k,i}\delta_i \leq \tag{4.25}$$

$$Min\left(z_{max}, \left\lfloor \omega_k + \sqrt{\frac{R_{\mathcal{S}}^2 - \sum_{i=k+1}^{n_\Lambda}\Theta_{i,i}\left(\delta_i + \sum_{j=i+1}^{n_\Lambda}\delta_j\Theta_{i,j}\right)^2}{\Theta_{k,k}}} \right\rfloor\right) \tag{4.26}$$

Originally, the Sphere Decoder performs on a lattice without constellation bound restrictions. However, introducing equations 4.24, 4.25, and 4.26 is a straightforward but necessary trick that strongly reduces the complexity, or, in other words, not activating it would strongly increase the complexity.

If different PAM sizes are used on each antenna, for example for spectral efficiency tuning or adaptive modulations, the constellation is rectangular parallelepipedic, the constellation bounds $[z_{min,i}, z_{max,i}]$ vary for each dimension i.

Notice that the algorithm only requires M_Λ^{-1}, Δ and the Θ matrix. This shows us that a Cholesky decomposition is more pertinent than QR decomposition (see subsection 4.1.3).

The computed bounds are updated recursively thanks to the equations [98]

$$S_k = S_k(\delta_{k+1}, \ldots, \delta_{n_\Lambda}) = \omega_k + \sum_{i=k+1}^{n_\Lambda} \Theta_{k,i}\delta_i \tag{4.27}$$

$$T_{k-1} = T_{k-1}(\delta_k, \ldots, \delta_{n_\Lambda}) = R_{\mathcal{S}}^2 - \sum_{i=k}^{n_\Lambda} \Theta_{i,i} \left(\delta_i + \sum_{j=i+1}^{n_\Lambda} \Theta_{i,j}\delta_j \right)^2 \tag{4.28}$$

$$= T_k - \Theta_{kk}(S_k - z_k)^2 \tag{4.29}$$

and finally, each time a vector z is found, the distance between y and $x = zM_\Lambda$ is

$$\hat{d}^2 = R_{\mathcal{S}}^2 - T_0 \tag{4.30}$$

Since we are interested in the point minimizing $\hat{d}$, the radius $R_{\mathcal{S}}^2$ is reduced to $\hat{d}$ each time a point is found. This strongly reduces the complexity and keeps the optimality. When no points are found, the last found point is the ML point.

4.2.2 The Sphere Decoder based on Schnorr-Euchner point enumeration strategy

The Sphere Decoder based on Schnorr-Euchner strategy [80] was first introduced in digital communications by Agrell, Eriksson,Vardy and Zeger (AEVZ) in [1]. The key idea is to view the lattice as laminated hyperplanes and then start the search for the closest point in the nearest hyperplane. A radius is specified in order to limit the explored region to a sphere. If no radius reduction is applied during the search, all the points belonging to the sphere would be enumerated, as for the Pohst strategy, which justifies the name of Sphere Decoder too.

a) Laminated hyperplanes structure of the lattice

Using the QR decomposition $\Delta = M_\Lambda Q$, we get

$$\breve{y} = yQ = zM_\Lambda Q + \eta Q = z\Delta + \breve{\eta} \tag{4.31}$$

where $\breve{y}$ and $\breve{\eta}$ are the rotated version of y and η, respectively. The matrix Δ can be decomposed into

$$\Delta = \left[\begin{array}{c|c} \Delta^{[n_\Lambda-1]} & \begin{matrix} 0 \\ \vdots \\ 0 \end{matrix} \\ \hline \Delta_{n_\Lambda} & \end{array}\right] = \left[\begin{array}{c|c} \Delta^{[n_\Lambda-1]} & \begin{matrix} 0 \\ \vdots \\ 0 \end{matrix} \\ \hline \Delta_{n_\Lambda}^{[n_\Lambda-1]} & \Delta_{n_\Lambda,n_\Lambda} \end{array}\right] \tag{4.32}$$

where $\Delta^{[n_\Lambda-1]}$ is an $n_\Lambda - 1 \times n_\Lambda - 1$ matrix obtained by extracting the first $n_\Lambda - 1$ rows and columns of $\Delta = \Delta^{[n_\Lambda]}$, and $\Delta_{n_\Lambda}^{[n_\Lambda-1]}$ contains the first $n_\Lambda - 1$ components of the row Δ_{n_Λ}. Any

lattice point can be written as the sum of a $\Lambda(\Delta^{[n_\Lambda-1]})$ point and a translation vector $z_{n_\Lambda}\Delta_{n_\Lambda}$:

$$\Lambda(\Delta^{[n_\Lambda]}) = \Lambda(\Delta^{[n_\Lambda-1]}) + \mathbb{Z}\Delta_{n_\Lambda} \tag{4.33}$$

The lattice is decomposed into an infinite set of parallel sub-lattices, obtained by translating an initial lattice by an integer multiple of the vector Δ_{n_Λ}. The lattice $\Lambda_0^{[n_\Lambda-1]} = \Lambda(\Delta^{[n_\Lambda-1]})$ is taken as the reference, we can use the notation $\Lambda_i^{[n_\Lambda-1]} = \Lambda_0^{[n_\Lambda-1]} + i\Delta_{n_\Lambda}$ to describe the parallel hyperplanes set. The translation vector Δ_{n_Λ} can be decomposed into $\Delta_{n_\Lambda,\|} = \left[\Delta_{n_\Lambda}^{[n_\Lambda-1]}, 0\right]$ and $\Delta_{n_\Lambda,\perp} = [0,\ldots,0,\Delta_{n_\Lambda,n_\Lambda}]$, the collinear and orthogonal components to the hyperplane $\Lambda_0^{[n_\Lambda-1]}$, respectively. The distance between the parallel hyperplanes $d\left(\Lambda_i^{[n_\Lambda-1]}, \Lambda_{i+1}^{[n_\Lambda-1]}\right)$ is $|\Delta_{n_\Lambda,n_\Lambda}|$. Each lattice $\Lambda_i^{[n_\Lambda-1]}$ has a triangular generator matrix and can be decomposed into a set of parallel lattices with a translation vector $\Delta_{n_\Lambda-1}^{[n_\Lambda-1]}$, and so on.

b) Closest point computation

The received point $\breve{y}$ is located between two hyperplanes $\Lambda_{v_{n_\Lambda}}^{[n_\Lambda-1]}$ and $\Lambda_{v_{n_\Lambda}\pm1}^{[n_\Lambda-1]}$. Let us consider that $\Lambda_{v_{n_\Lambda}}^{[n_\Lambda-1]}$ is the closest hyperplane. The indice v_{n_Λ} is found by the normalized projection of $\breve{y}$ on $\Delta_{n_\Lambda,\perp}$:

$$v_{n_\Lambda} = \left\lfloor \frac{\breve{y}\Delta_{n_\Lambda,\perp}^t}{\|\Delta_{n_\Lambda,\perp}\|^2} \right\rceil = \left\lfloor \frac{\breve{y}_{n_\Lambda}}{\Delta_{n_\Lambda,n_\Lambda}} \right\rceil \tag{4.34}$$

where $\lfloor . \rceil$ is the nearest integer rounding function. Let $\varrho = \mathrm{sgn}\left(v_{n_\Lambda} - \frac{\breve{y}_{n_\Lambda}}{\Delta_{n_\Lambda,n_\Lambda}}\right)$ be the direction of the nearest hyperplane, we can sort the set of hyperplanes by increasing order of distances to y:

$$\left\{\Lambda_{v_{n_\Lambda}}^{[n_\Lambda-1]}, \Lambda_{v_{n_\Lambda}-\varrho}^{[n_\Lambda-1]}, \Lambda_{v_{n_\Lambda}+\varrho}^{[n_\Lambda-1]}, \Lambda_{v_{n_\Lambda}-2\varrho}^{[n_\Lambda-1]}, \Lambda_{v_{n_\Lambda}+2\varrho}^{[n_\Lambda-1]}, \ldots\right\} \tag{4.35}$$

The projection of y on any hyperplane associated with $\Lambda_{z_{n_\Lambda}}^{[n_\Lambda-1]}$ where $z_{n_\Lambda} = v_{n_\Lambda} + k$, $k \in \mathbb{Z}$, is $\breve{y}^{[n_\Lambda-1]}$. However, the lattice is translated from the origin with a vector $v_{n_\Lambda}\Delta_{n_\Lambda,\|}$, in order to consider a noisy point in a centered lattice, we apply the translation to $\breve{y}^{[n_\Lambda-1]}$ and obtain the new noisy point:

$$\breve{y}_{\Lambda_{z_{n_\Lambda}}^{[n_\Lambda-1]}} = \breve{y}^{[n_\Lambda-1]} - z_{n_\Lambda}\Delta_{n_\Lambda}^{[n_\Lambda-1]} \tag{4.36}$$

The Euclidean distance between the received point $\breve{y}$ and the hyperplane associated with $\Lambda_{z_{n_\Lambda}}^{[n_\Lambda-1]}$ is

$$d\left(\Lambda_{z_{n_\Lambda}}^{[n_\Lambda-1]}, \breve{y}\right)^2 = [\breve{y}_{n_\Lambda} - z_{n_\Lambda}\Delta_{n_\Lambda,n_\Lambda}]^2 \tag{4.37}$$

Fig. 4.9 illustrates the laminated hyperplanes structure and notations.

The hyperplanes are sorted in decreasing order of likelihood, it seems natural to begin a closest point search in the first sub-lattice $\Lambda_{v_{n_\Lambda}}^{[n_\Lambda-1]}$. It is important to insist on the fact that there is no guarantee that the ML point belongs to the nearest sub-lattice $\Lambda_{v_{n_\Lambda}}^{[n_\Lambda-1]}$, we indeed have no knowledge of the $n_\Lambda - 1$ other dimensions at this step of the algorithm. After projecting $\breve{y}$ on the nearest hyperplane $\Lambda_{v_{n_\Lambda}}^{[n_\Lambda-1]}$ (with translation), we repeat the same processing recursively by sorting the sub-lattices $\Lambda_{v_{n_\Lambda},j}^{[n_\Lambda-2]}$, projecting the new received point, and so on, until the last

dimension, where the closest point search over $\Lambda^{[1]}_{v_{n_\Lambda},\dots,v_{2},j}$ is made by a simple quantization.

The first point found by the algorithm is called the Babai point, which is a sub-optimal detection point, yet more reliable than Zero-Forcing. This can be seen as a decision feedback equalization on the laminated hyperplane structure: once a decision is taken on one symbol, a part of its interference contribution is subtracted by orthogonal projection. Fig. 4.10 shows a simple example where the ZF point, Babai point and ML point are all different. It can easily be shown that the Babai point always leads to smaller distances than ZF which is obtained after non-orthogonal projections parallel to the lattice basis. For any received point, the ZF point always equals the Babai point if and only if the lattice is orthogonal, and in this case ZF is ML. This remark is illustrated in Fig. 4.10 via the ZF, Babai and ML decision regions limits. Moreover, the Babai point depends on the order in which the dimensions are treated. There exists an optimal order that minimizes the Euclidean distance, but this depends on the region $\breve{y}$ belongs to, and this will be treated later. As an example, in Fig. 4.10-(c), we see the Babai point obtained by first considering dimension 1, but we can notice in Fig. 4.10-(d) that the Babai point obtained by first considering dimension 2 is the ML point.

Once the Babai point is found, we can reduce the radius search to the distance $d(\breve{y}, x_{Babai})$, and continue the enumeration considering the next most likely hyperplane of previous dimension, and so on recursively until no more point belongs to the sphere.

We now have to express the recursive processing of the sphere bounds and point enumeration. Let us define ν_k a noisy point in the hyperplane of $\Lambda^{[k]}_{z_{n_\Lambda}=0,\dots,z_{k+1}=0}$. The point ρ_k is the ZF point of ν_k, obtained by the relation $\nu_k \nabla^{[k]} = \rho_k$, where $\nabla^{[k]} = (\Delta^{[k]})^{-1}$ is lower triangular. The vector $\frac{d_k}{|\Delta_{k,k}|}\Delta_k^{\perp}$, projects the point ν_k on the hyperplane $\Lambda^{[k-1]}_{z_{n_\Lambda}=0,\dots,z_{k+1}=0,z_k}$, leading to $\nu_k^{[k-1]}$. We can compute

$$d_k = \nu_{k,k} - z_k \Delta_{k,k} = \frac{\rho_{k,k} - z_k}{\nabla_{k,k}} \tag{4.38}$$

The distance $\|d_k\|^2$ is the component for the k-th step of the distance between the lattice point found and the received point y. Then $\nu_k^{[k-1]}$ is translated by $z_k\Delta_k^{[k-1]}$ to consider the equivalent problem in $\Lambda^{[k-1]}_{z_{n_\Lambda}=0,\dots,z_k=0}$. The new noisy point is

$$\nu_{k-1} = \nu_k^{[k-1]} - z_k \Delta_k^{[k-1]} \tag{4.39}$$

We can compute ρ_{k-1}:

$$\rho_{k-1} = \nu_{k-1}\nabla^{[k-1]} = \rho_k^{[k-1]} - \nu_{k,k}\nabla_k^{[k-1]} - z_k\Delta_k^{[k-1]}\nabla^{[k-1]} \tag{4.40}$$

and noticing that $\Delta_k^{[k-1]}\nabla^{[k-1]} + \Delta_{k,k}\nabla_k^{[k-1]} = I_k^{[k-1]} = [0,\dots,0]$, we have that

$$\rho_{k-1} = \rho_k^{[k-1]} - d_k \nabla_k^{[k-1]} \tag{4.41}$$

It is important to see that the variables ρ_k, ν_k, d_k depend on the choice of coordinates $z_{n_\Lambda},\dots,z_k$. The authors in [1] use equations (4.41) and (4.38) to process the recursive enumeration while computing the distance, but we will see in the sequel why (4.39) is useful to make a parallel with the Pohst strategy. An implementation version is avalaible on Alg .2 and a commented version is available on next paragraph.

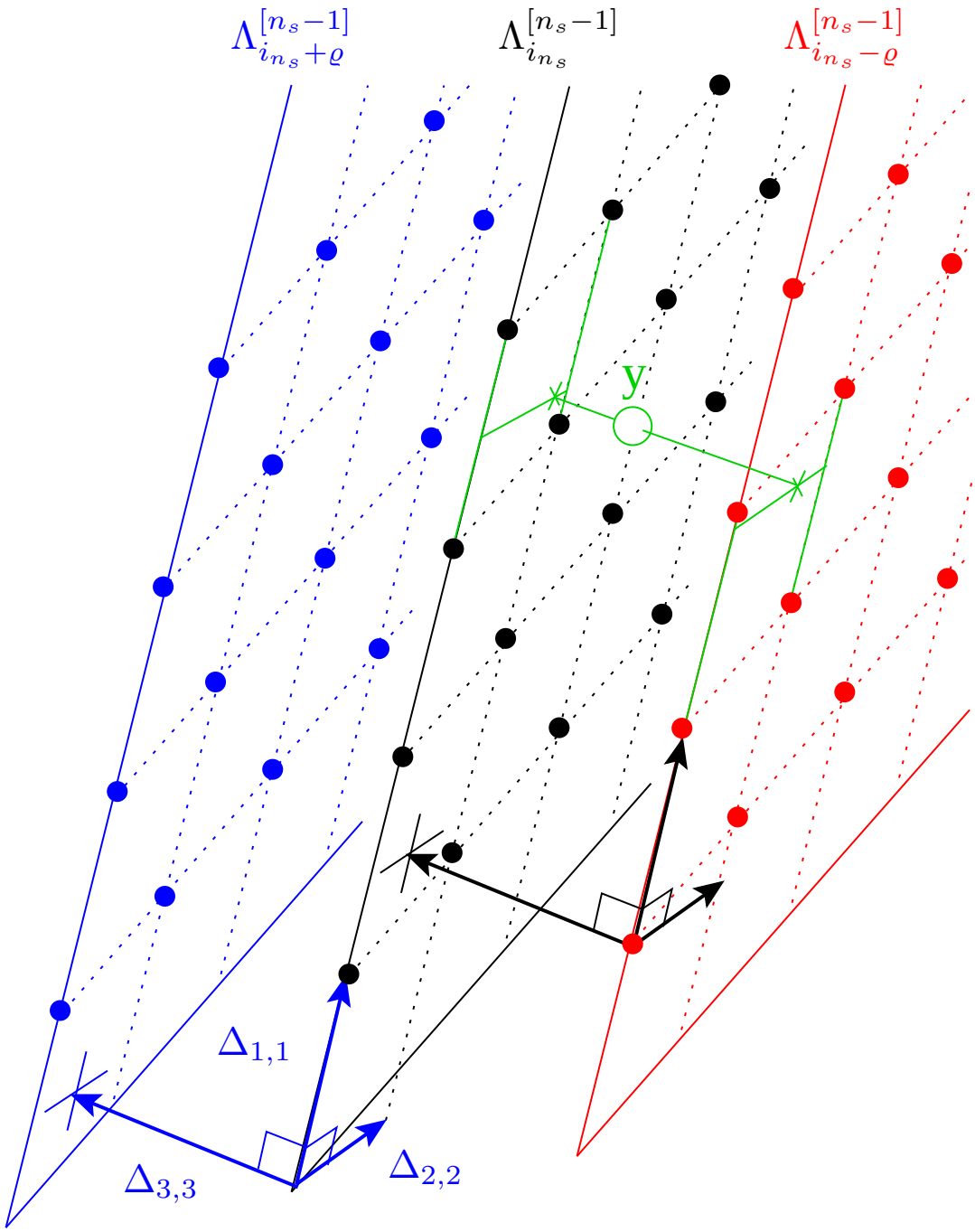

Figure 4.9: Laminated hyperplanes structure of the lattice.

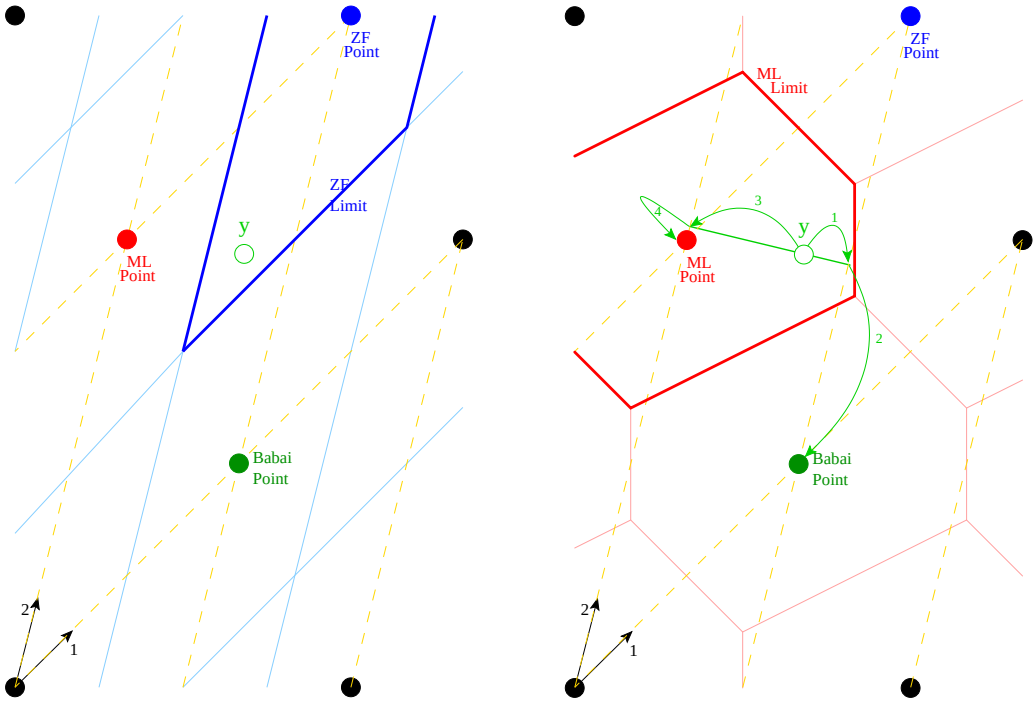

(a) ZF decoding

(b) ML decoding

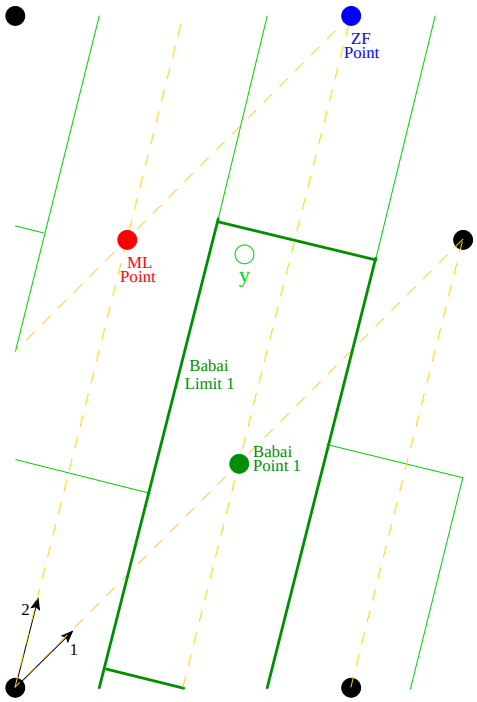

(c) Babai decoding : dimension 1 first

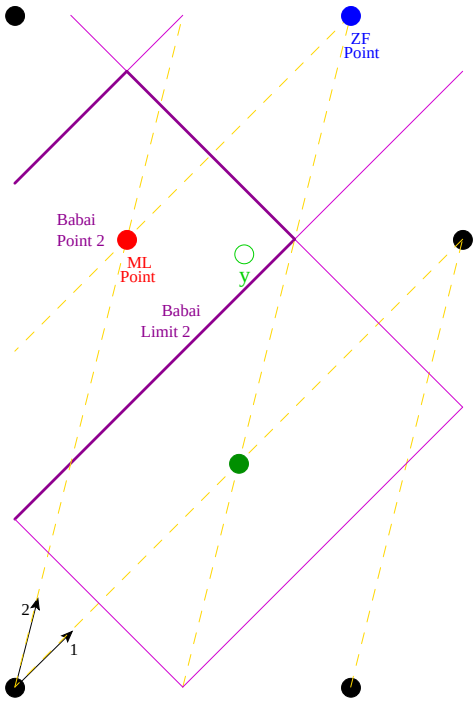

(d) Babai decoding : dimension 2 first

Figure 4.10: Schnorr-Euchner point enumeration, 2-dimensional example.

Algorithm 2: Schnorr-Euchner strategy + boundaries of the constellation processing.

input : A received point y, the generator matrix $M_\Lambda(n_\Lambda \times n_\Lambda)$ of the lattice, the radius R of the sphere, and the bounds z_{min} and z_{max} of the constellation.
output : The ML point $\hat{z}$ belonging to the constellation and the squared Euclidean distance *bestdist* between y and $\hat{z}M_\Lambda$

Pre-processing
QR decomposition $M_\Lambda = \Delta Q$ where Δ is lower-triangular and $QQ^t = I$
$\nabla \leftarrow \Delta^{-1}$
$\breve{y} = yQ^t$
Initialization
$bestdist \leftarrow R^2$, $k \leftarrow n_\Lambda$
$dist_k \leftarrow 0$
$e_k \leftarrow \breve{y}\nabla$
$z_k \leftarrow [e_{kk}]$, $z_k \leftarrow max(z_k, z_{min})$, $z_k \leftarrow min(z_k, z_{max})$
$\rho \leftarrow (e_{kk} - z_k)/(\nabla_{kk})$
$step_k \leftarrow \mathrm{sgn}(\rho)$
Label 1
$newdist \leftarrow dist_k + \rho^2$
if $newdist < bestdist$ *and* $k \neq 1$ **then Goto** Label 2
else Goto Label 3
Label 2
for $i = 1$ *to* $k-1$ **do** $e_{k-1,i} \leftarrow e_{k,i} - \rho\nabla_{ki}$
$k \leftarrow k - 1$
$dist_k \leftarrow newdist$
$z_k \leftarrow [e_{kk}]$, $z_k \leftarrow max(z_k, z_{min})$, $z_k \leftarrow min(z_k, z_{max})$
$\rho = (e_{kk} - z_k)/(\nabla_{kk})$
$step_k \leftarrow \mathrm{sgn}(\rho)$
Goto Label 1
Label 3
if $newdist < bestdist$ **then**
    $\hat{z} \leftarrow z$
    $bestdist \leftarrow newdist$
else if $k = n_\Lambda$ **then** return $\hat{z}$ and terminate
else $k \leftarrow k + 1$
$z_k \leftarrow z_k + step_k$
if $z_k < z_{min}$ *or* $z_k > z_{max}$ **then**
    $step_k \leftarrow -step_k - \mathrm{sgn}(step_k)$
    $z_k \leftarrow z_k + step_k$
    if $z_k < z_{min}$ *or* $z_k > z_{max}$ **then Goto** Label 3
$\rho \leftarrow (e_{kk} - z_k)/\nabla_{kk}$
$step_k \leftarrow -step_k - \mathrm{sgn}(step_k)$
Goto Label 1

The SE algorithm for multiple antenna channels with extended explanations:

Input. A received point y, the generator matrix $M_\Lambda(n_\Lambda \times n_\Lambda)$ of the lattice, the radius R of the sphere, and the bounds z_{min} and z_{max} of the constellation. You can set the radius R to $+\infty$ or to an optimized value.

Output. The ML point $\hat{z}$ belonging to the constellation and its squared Euclidean distance *bestdist* to y.

Step 1. **Pre-processing**: Compute the QR decomposition $M_\Lambda = \Delta Q$, where Δ is lower-triangular and $QQ^t = I$. Compute the inverse $\nabla = \Delta^{-1}$ and $\breve{y} = yQ^t$.

Step 2. **Initialization - Dimension n_Λ:** Set $bestdist \leftarrow R^2$, $k \leftarrow n_\Lambda$, $dist_k \leftarrow 0$ (The algorithm starts with dimension n_Λ, the cumulative distance $dist_{n_\Lambda}$ between the received point and the hyperplane with dimension $n_\Lambda + 1$ (not existing) is 0). Set $e_k \leftarrow \breve{y}\nabla$ (Vector e_k contains the n_Λ real coordinates of the received point $\breve{y}$ in the vector space with dimension n_Λ). Set $z_k \leftarrow [e_{kk}]$ (The closest hyperplane with fixed coordinate z_{n_Λ} is chosen by taking the closest integer value of $e_{n_\Lambda n_\Lambda}$). Set $z_k \leftarrow max(z_k, z_{min})$, $z_k \leftarrow min(z_k, z_{max})$ (If the hyperplane does not belong to the constellation, the closest hyperplane belonging to the constellation is chosen). Compute $\rho = (e_{kk} - z_k)/(\nabla_{kk})$ (This is the coordinate distance between the received point and the chosen hyperplane of dimension $n_\Lambda - 1$, $-1 \leq \rho \leq 1$). Set $step_k \leftarrow \mathrm{sgn}(\rho)$ (This is the increment for the next z_{n_Λ} value, to test the second closest hyperplane, which is located "on the other side" of the received point).

Step 3. **Distance computation:** Compute $newdist \leftarrow dist_k + \rho^2$ (The distance between the current hyperplane and the received point is computed by the Pythagore algorithm, since projections are orthogonal. The squared new distance $newdist$ is obtained by summing the squared distance $dist_k$ between the hyperplane of dimension $k+1$ and the received point and the distance ρ between the projection on the hyperplane of dimension $k+1$ and its projection on the hyperplane of dimension k. **If** $newdist < bestdist$ and $k \neq 1$

go to Step 4 (the hyperplane is valid, it may contain points with an associated distance smaller than $bestdist$ and no point has been reached yet ($k \neq 1$)).

else

go to Step 5 (either a valid point has been found ($k = 1$) or the hyperplane with dimension k is too far from the received point, i.e., the distance between all the points it contains and the received point is higher than $bestdist$).

endif.

Step 4. **Processing of a lower dimension:** Compute for $i = 1, ..., k-1$ $e_{k-1,i} \leftarrow e_{k,i} - \rho\nabla_{ki}$ (The coordinates of the projected point on the hyperplane of dimension $k-1$ in the lattice contained in this hyperplane are computed). Decrement k (We now consider the projection on an hyperplane with one dimension less). Set $dist_k \leftarrow newdist$ (The cumulative distance $dist_k$ between the received point and the hyperplane with dimension $k+1$ is $newdist$). Set $z_k \leftarrow [e_{kk}]$ (The closest hyperplane with fixed coordinates $z_{n_\Lambda}, z_{n_\Lambda - 1}, \ldots, z_k$ is chosen by taking z_k equal to the closest integer value of e_{kk}). Set $z_k \leftarrow max(z_k, z_{min})$, $z_k \leftarrow min(z_k, z_{max})$ (If the hyperplane does not belong to the constellation, the closest hyperplane belonging to the constellation is chosen). Compute $\rho = (e_{kk} - z_k)/(\nabla_{kk})$ (This is the coordinate distance between the projected point on the hyperplane with dimension k and the chosen hyperplane of dimension $k-1$, $-1 \leq \rho \leq 1$). Set $step_k \leftarrow \text{sgn}(\rho)$ (This is the increment for the next z_k value, to test the second closest hyperplane, which is located "on the other side" of the point projected on the hyperplane with dimension k). **Go to Step 3**.

Step 5. **Termination of a branch:**

If $newdist < bestdist$

set $\hat{z} \leftarrow z$, $bestdist \leftarrow newdist$ (A valid point has been found ($k = 1$) with an associated distance smaller than $bestdist$. Thus, the point is stored and $bestdist$ is updated. Since the next closest hyperplane with dimension $k - 1 = 0$ (point) is obviously located at a higher distance than $bestdist$, it is not necessary to change z_1).

else if $k = n_\Lambda$

return $\hat{z}$ and **terminate** (The closest hyperplane with dimension $n_\Lambda - 1$ is located at a higher distance than $bestdist$, the algorithm is finished).

endif. Increment k (The closest hyperplane with dimension $k-1$ for fixed values $z_{n_\Lambda}, \ldots, z_k$ is located at a higher distance than $bestdist$ or we have found the best value z_1 ($k = 1$) for fixed values $z_{n_\Lambda}, \ldots, z_2$, i.e., it is not necessary to change z_k. The fixed value for dimension $k+1$, z_{k+1} has to be changed). Compute $z_k \leftarrow z_k + step_k$ (The fixed coordinate in dimension k is changed to test the next closest hyperplane). **If** $z_k < z_{min}$ or $z_k > z_{max}$

set $step_k \leftarrow -step_k - \text{sgn}(step_k)$ (The next closest hyperplane is outside the constellation, the next closest hyperplane at the "opposite side" will be test). Set $z_k \leftarrow z_k + step_k$ (The z_k value is updated in order to test the next closest hyperplane at the "opposite side"). **If** $z_k < z_{min}$ or $z_k > z_{max}$

go to Step 5 (The next closest hyperplane at the opposite side is also outside the constellation. It is not necessary to further change z_k. The fixed value for dimension $k+1$, z_{k+1} has to be changed).

endif.

endif. Compute $\rho \leftarrow (e_{kk} - z_k)/\nabla_{kk}$ (This is the coordinate distance between the projected point on the hyperplane with dimension k and the chosen hyperplane of dimension $k-1$, $-1 \leq \rho \leq 1$). Set $step_k \leftarrow -step_k - \text{sgn}(step_k)$ (Step is prepared to test the next closest hyperplane at the "opposite side" later on). **Go to Step 3**.

4.2.3 Strategies differences and similarities

The two strategies presented in 4.2.1 and 4.2.2 are often presented as different and the comparison often tips the scales in favor of Schnorr-Euchner enumeration strategy. In this subsection, we will make a comparison between these two algorithms based on the tree exploration.

The two Sphere Decoders can be seen as a tree search using the intrinsic tree structure of the lattice. If the search is performed over all the points belonging to the intersection of a $(2^m - \text{QAM})^{n_t}$ constellation and the lattice, the tree has a depth n_Λ and $2^{m/2}$ states by stage. The chosen metric is the Euclidean distance between the projected received point and the chosen hyperplane. We can see the tree of a 4-PAM over a 3×3 random lattice in Fig 4.11, the abscissa represents the cumulative distances of the enumerated points, the ordinate represents the explored dimension. The square distances of all the constellation points can be read at the branches end, on the abscissa. The ML point corresponds to the path achieving the smallest

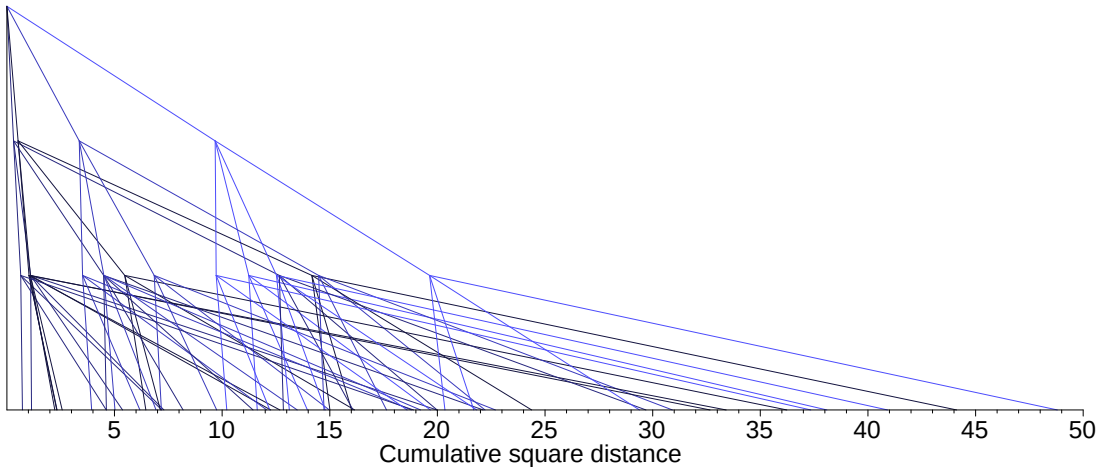

Figure 4.11: Lattice constellation tree representation, cumulative distances through exploration of dimensions.

value on the abscissa.

When the noise places the received point close to the median limit between two hyperplanes, the two corresponding branches are merged. This effect is emphasized by strong fading and interference, and results in the crossing of branches, which slows down the research process.

The sphere radius corresponds to an abscissa limit for the branches, which is shifted left for each new computed point. It cuts some branches adaptatively with the found points. We will later use such a representation to justify some complexity reductions.

The two presented Sphere Decoders (Pohst and Schnorr-Euchner) iniatially do not seem to have the same point enumeration strategy, neither the same tree. Indeed, Pohst strategy enumerates the points in $\mathbb{Z}^{n_\Lambda}$ while Schnorr-Euchner strategy uses the lattice laminated hyperplane structure for the direct enumeration in Λ. The branches end of both trees are the same since the same lattice points are enumerated. Let us compare the two tree constructions in order to see the differences between the two strategies.

	Pohst	Schnorr-Euchner
Tree depth	n_Λ	
States at stage k	The set of coordinates $\{z_{n_\Lambda}, \ldots, z_k\}$	
Number of outgoing branches by states	$2^{m/2}$	
Branch Metric	$\Theta_{kk}(S_k - z_k)^2$	$\left(\frac{\rho_{k,k} - z_k}{\nabla_{k,k}}\right)^2$

The branch metric of Pohst strategy is equal to

$$\Theta_{kk}(S_k - z_k)^2 = \Theta_{kk}\left[\omega_k + \sum_{i=k+1}^{n_\Lambda} \Theta_{k,i}(\omega_i - z_i) - z_k\right]^2 = \left[y_k - \sum_{i=k}^{n_\Lambda} \Delta_{ik} z_i\right]^2 \tag{4.42}$$

Furthermore, the branch metric of Schnorr-Euchner strategy can be modified using (4.38),

(4.39) and $\nu_{n_\Lambda} = y$, we have that

$$\left(\frac{\rho_{k,k} - z_k}{\nabla_{k,k}}\right)^2 = (\nu_{k,k} - z_k\Delta_{k,k})^2 = \left[y_k - \sum_{i=k}^{n_\Lambda} \Delta_{ik} z_i\right]^2 \tag{4.43}$$

We can conclude that both algorithms compute the ML point by browsing the same tree. The difference between the two algorithms sums up in the order the $2^{m/2}$ branches are selected from a given state, and the equations used for computing the metrics.

Once the tree structure is defined, we can use a global tree decoding method such as branch-and-bound algorithm. This has been proposed for example in [65] with the memorization of the whole tree structure, which is not necessary. This tree browsing technique is strictly equivalent to the Schnorr-Euchner decoding, and is optimal when considering the total number of selected branches. Indeed, the sub trees are scanned by decreasing order of likelihood. We can see the Schnorr-Euchner algorithm as a branch-and-bound algorithm on the intrinsic tree structure of the lattice.

Initially, the Pohst method was designed to enumerate the lattice points belonging to a sphere. Any enumeration strategy would lead to the same list. When the algorithm was applied in [98], the radius reduction has been added but the enumeration strategy kept unchanged. Clearly, an ordering of branches in each dimension would accelerate the decoding, the optimal choice is the sorting by decreasing order of likelihood. In the dimension k, the integer components to enumerate belong to the interval

$$\left[-\sqrt{\frac{R_{\mathcal{S}}^2 - \sum_{i=k+1}^{n_\Lambda} \Theta_{i,i}\left(\delta_i + \sum_{j=i+1}^{n_\Lambda} \delta_j \Theta_{i,j}\right)^2}{\Theta_{k,k}}}, \sqrt{\frac{R_{\mathcal{S}}^2 - \sum_{i=k+1}^{n_\Lambda} \Theta_{i,i}\left(\delta_i + \sum_{j=i+1}^{n_\Lambda} \delta_j \Theta_{i,j}\right)^2}{\Theta_{k,k}}}\right] \tag{4.44}$$

The Sphere Decoder in [98] enumerates the points of this dimension from the lower to the upper bound, but an optimal enumeration would begin from the center (most likely value) and alternate around this value as for the hyperplanes selection in Schnorr-Euchner. With this new enumeration, the two Sphere Decoders perform exactly the same search in the tree and they only differ on the recursive equations complexity. We will now compare the complexity associated with each branch and to the pre-processing computations.

Pohst enumeration complexity analysis

The pre-processing for Pohst enumeration strategy has complexity equal to $n_\Lambda^2(5n_\Lambda - 1)/2$, including:

1. the channel matrix M_Λ inversion: $2n_\Lambda^3/3 + n_\Lambda^2/2 - n_\Lambda/6$ flops
2. the Gram G matrix calculation (using the symmetry): $n_\Lambda(n_\Lambda + 1)(2n_\Lambda - 1)/2 = n_\Lambda^3 + n_\Lambda^2/2 - n_\Lambda/2$ flops
3. the Δ and Θ matrices computation via Cholesky decomposition: $5n_\Lambda^3/6 - 3n_\Lambda^2/2 + 2n_\Lambda/3$

The initialization for Pohst enumeration strategy includes the ZF point computation which requires $2n_\Lambda^2$ flops. The computation of a tree branch metric in the dimension k requires $2(n_\Lambda - k) + 10$ flops.

Schnorr-Euchner complexity analysis
The pre-processing for Schnorr-Euchner enumeration strategy requires $7n_\Lambda^3/3 + 3n_\Lambda^2/2 + 31n_\Lambda/6$ flops:

1. the Δ and Θ matrices computation via QR decomposition: $5n_\Lambda^3/3 + 2n_\Lambda^2 + 16n_\Lambda/3$
2. the channel matrix Δ inversion (triangular): $2n_\Lambda^3/3 - n_\Lambda^2/2 - n_\Lambda/6$ flops

The initialization for Schnorr-Euchner enumeration strategy requires $2n_\Lambda^2 - 2n_\Lambda + 3$ flops. The computation of a tree branch metric in the dimension k requires $3k - 1$ flops.

Complexity comparison
First, we can notice that the complexity of the initialization phase of the Pohst and Schnorr-Euchner strategies are quite equivalent.

The branch complexity varies with $n_\Lambda - k$ for the modified Pohst strategy, and with k for Schnorr-Euchner. However, the algorithm computes more branches in the dimension with lower indices, which justifies why Schnorr-Euchner is often less complex than Pohst strategies, applied to sphere decoding. The optimal choice would be to compute the Pohst recursive equations for the higher dimension indices $k > n_\Lambda/2$ and the Schnorr-Euchner recursive equations for the lower dimension indices $k \leq n_\Lambda/2$. However, the Schnorr-Euchner initializations, necessary at each new shift between the two strategies, are as complex as the complexity reduction given by the use of the Pohst recursive equations for the higher dimension indices $k > n_\Lambda/2$.

In the end, the Schnorr-Euchner strategy seems to be a judicious choice for decoding a lattice constellation. Based on this conclusion, we will now always consider this strategy for ML sphere decoding until the end of the thesis report. The algorithm will be called for simplicity SD-SE (Sphere Decoder with Schnorr-Euchner strategy).

In Fig. 4.12, we can observe the Point Error Rate, i.e., the probability that the n_Λ-dimensionnal decoded point is not the transmitted point for QPSK and 16-QAM transmissions over MIMO channels. Even with 16 antennas, i.e. 32 real dimensions, the accelerated Sphere Decoder finds the ML point with a reasonable complexity.

4.2.4 Complexity reductions

The complexity of the Sphere Decoder depends on many parameters. As a non-exhaustive list, we cite:

- the sphere point enumeration strategy (Pohst or Schnorr-Euchner)
- the choice of the sphere radius, and possibly its reduction through iterations
- the constellation bounds processing
- the lattice basis modification via reduction
- the dimensions exploration order, where the objective is to separate as much as possible tree branches

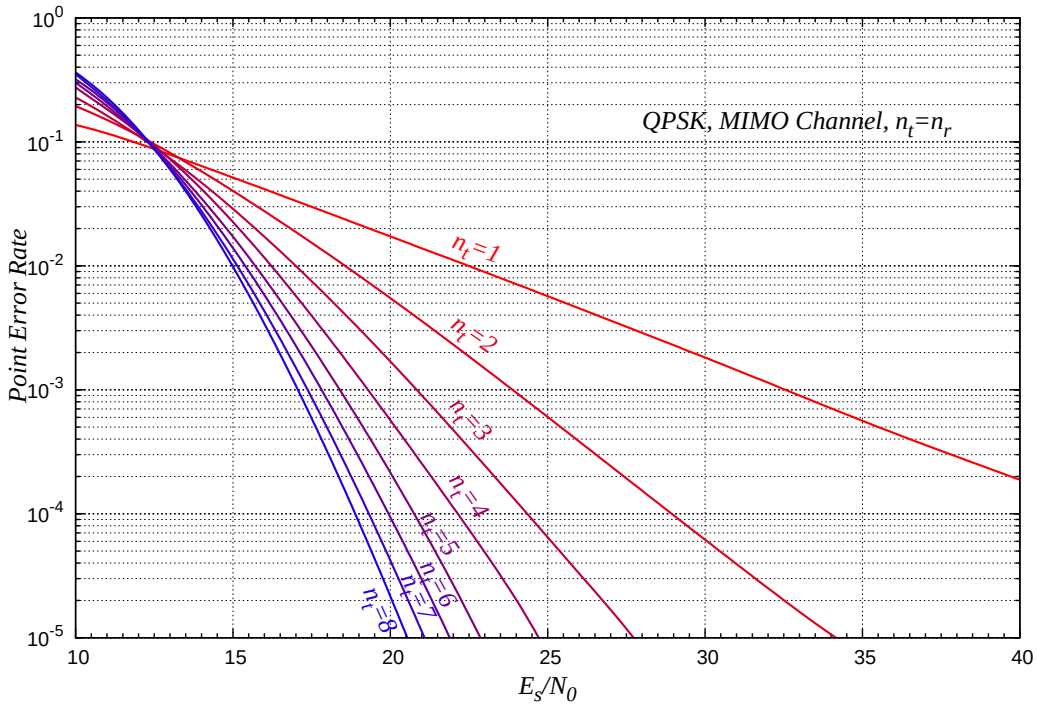

Figure 4.12: Point error rate of a QPSK on a MIMO channel.

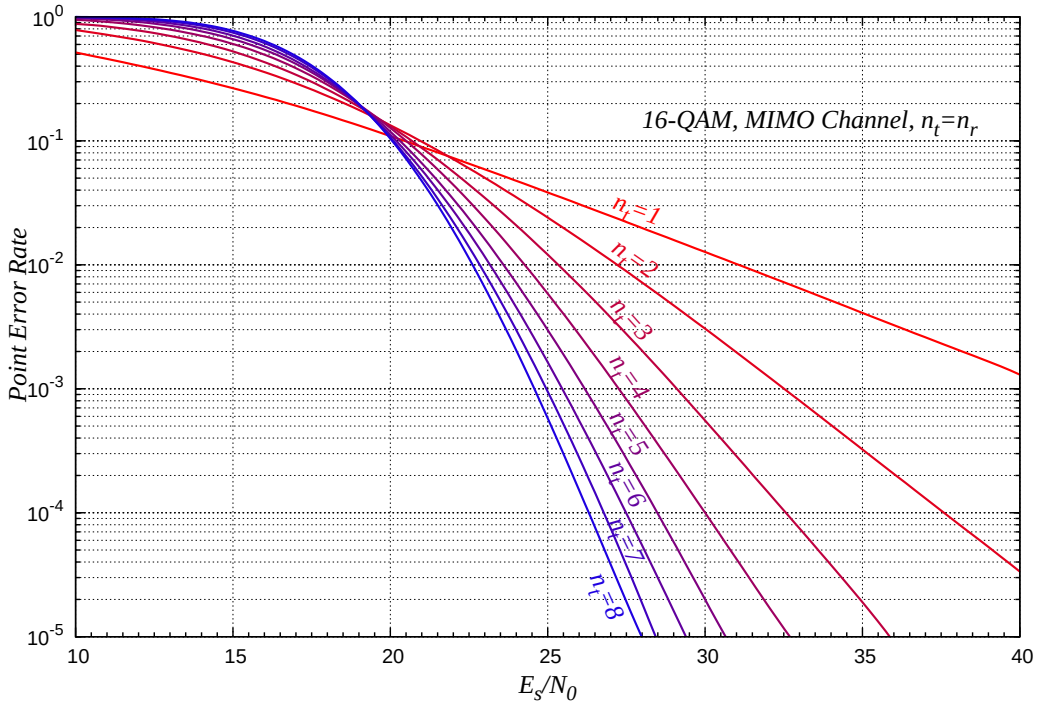

Figure 4.13: Point error rate of a 16-QAM on a MIMO channel.

a) Initial Sphere radius choice

The optimal radius choice would be $\tilde{R}_S^2 = \|y - x_{ML}\|^2$ since only the ML point would belong to the sphere. However, such a choice is impossible without any pre-computation. We can first notice that $y - x_{ML} = x - x_{ML} + \eta$ which leads to some conclusions:

- If $x = x_{ML}$, which is about achieved only when the signal-to-noise ratio is high (low error rate), we have that $|y - x_{ML}\|^2 = \|\eta\|^2$ only depends on the n_Λ-dimensional real Gaussian noise square norm, which is a random variable with chi-square distribution:

$$p_\eta(r > 0) = \frac{1}{(2N_0)^{n_\Lambda/2}(\frac{n_\Lambda}{2} - 1)!} r^{n_\Lambda/2-1} e^{-r/2N_0} \tag{4.45}$$

  The probability that the noise square norm is greater than $R_\mathcal{S}^2$ is equal to

$$F(R_\mathcal{S}^2) = \int_0^{R_\mathcal{S}^2} p_\eta(x)dx = 1 - e^{-R_\mathcal{S}^2/2N_0} \sum_{k=0}^{n_\Lambda/2-1} \frac{1}{k!} \left(\frac{R_\mathcal{S}^2}{2N_0}\right)^k \tag{4.46}$$

  which gives the probability $p_{R_\mathcal{S}^2}(x \notin \mathcal{S})$ that the transmitted point x does not belong to the search sphere. We can inverse this function to find the sphere radius that leads to a given $p_{R_\mathcal{S}^2}(x \notin \mathcal{S})$. As an example, we could choose a set of radii $R_{\mathcal{S},1} < R_{\mathcal{S},2} < R_{\mathcal{S},3} < R_{\mathcal{S},4}$ such that $p_{R^2_{\mathcal{S},1}}(x \notin \mathcal{S}) = 0.1$, $p_{R^2_{\mathcal{S},2}}(x \notin \mathcal{S}) = 0.01$, $p_{R^2_{\mathcal{S},3}}(x \notin \mathcal{S}) = 10^{-4}$, $p_{R^2_{\mathcal{S},4}}(x \notin \mathcal{S}) = 10^{-9}$. If no point is found with the first radius, the processing is repeated with the second radius, and so on until one point is found. It is very difficult to find the optimal choice of probability set that minimizes the average complexity because the complexity of fixed radius decoding is not known.
- If the received point belongs to the constellation volume, i.e., if the Zero-Forcing point belongs to $[0, z_{max}]^{n_\Lambda}$, the maximal distance to a constellation point is $d_{Emin}/2$. The search radius may e limited to this value. This is particularly useful at reasonable signal-to-noise ratio, when the point belongs to the constellation and the radius given by the noise statistics is too large. Indeed, the lower the signal-to-noise ratio, the lower the probability to be within the constellation limits. We can compute the lattice minimal distance d_{Emin} using a Sphere Decoder on the lattice, with the received point at the origin. Unfortunately, this is as complex as the sphere decoding itself. If the channel is quasi-static or block fading with few blocks, it could be economical to process such a computation for each new channel block. If the channel is ergodic, we can use some upper bounds on the lattice minimum Euclidean distance, for example the minimum Gram matrix diagonal element as suggested in section 4.1.2.
- Noticing that $\forall x \in \Omega_\Lambda, \|y - x_{ML}\|^2 < \|y - x\|^2$, we can choose a radius performing a simple detection $\hat{x}$ such as ZF, MMSE or DFE, and compute the radius $R^2_{S,\hat{x}} = \|y - \hat{x}\|^2$. This last technique has the great advantage to take into account the instantaneous noise amplitude and received point position, whereas the other techniques do not make benefit from any knowledge of y.

Finally, we can take advantage of each technique to find the best radius that limits the complexity.

In Fig. 4.14, we can observe the complexity of SD-SE with an infinite initial radius over a 4×4 MIMO channel and different modulation sizes. The complexity decreases exponentially

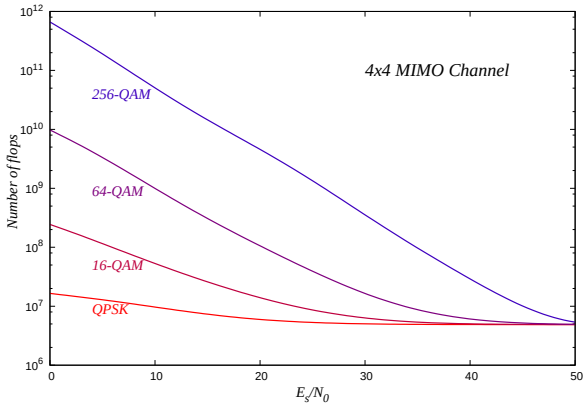

Figure 4.14: Complexity of SE-SD in flops, on a 4×4 MIMO channel.

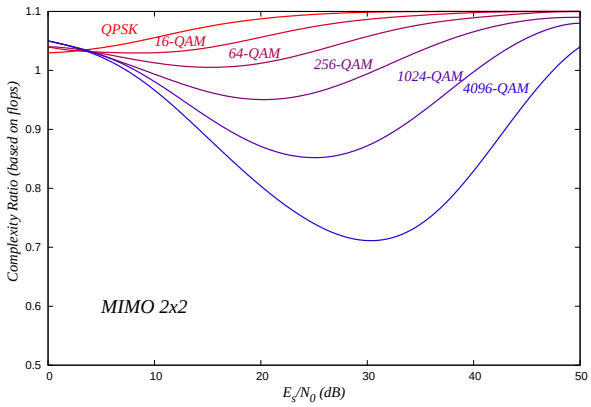

Figure 4.15: Complexity reduction factor of SE-SD with a radius pre-computation. 2×2 MIMO channel.

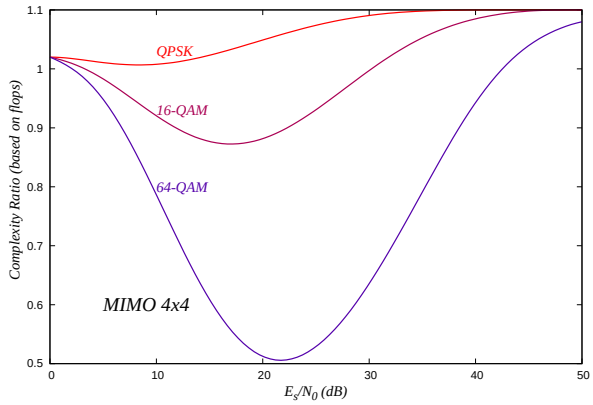

Figure 4.16: Complexity reduction factor of SE-SD with a radius pre-computation. 4×4 MIMO channel.

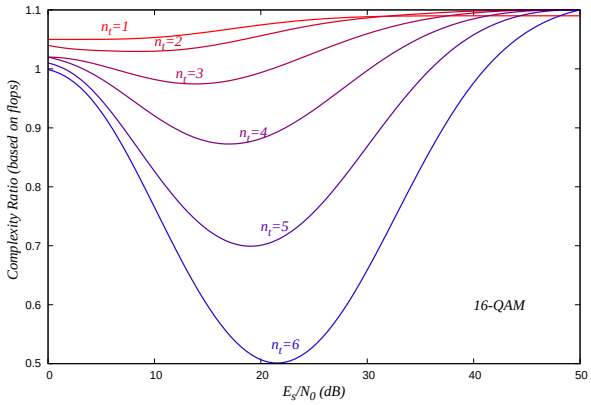

Figure 4.17: Complexity reduction factor of SE-SD with a radius pre-computation. 16-QAM.

with the noise level. For high signal-to-noise ratios, the complexity converges to a constant value given by the complexity to decode one point. The complexity increases with the spectral efficiency. In Fig. 4.15, Fig. 4.16 and Fig. 4.17, we can observe the complexity ratio between an SD-SE with a radius pre-computation and an SD-SE with an infinite initial radius. We can notice that for the practical signal-to-noise range, a complexity reduction is achieved using the well-designed initial radius taking into account the noise variance and the minimum distance evaluation when the point is inside the constellation. This reduction factor increases with the number of dimensions and spectral efficiency.

As a conclusion, we can notice that the complexity attenuation is never huge. Taking into account the constellation boundaries in the search algorithm provides a substantial complexity reductions.

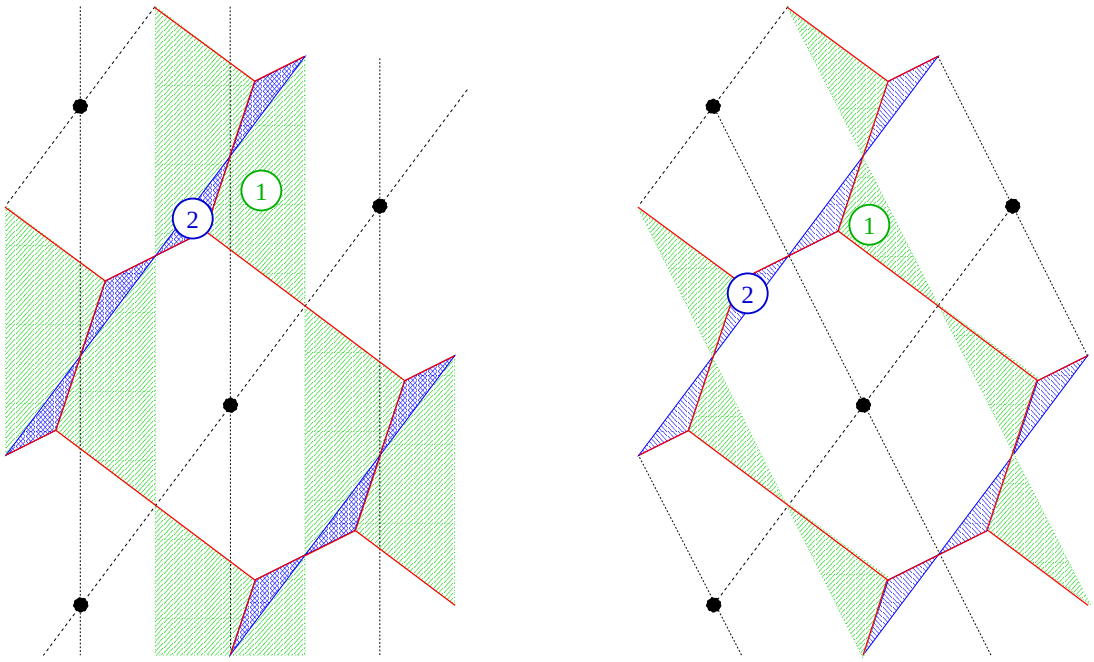

Figure 4.18: Babai wrong decision region without (left) and with (right) lattice reduction.

b) Lattice basis modifications

We will present two lattice basis modifications that can lead to complexity reduction: lattice reduction and basis vector re-ordering. As presented in section 4.1.4, lattice reductions can be used to change the random channel basis into a more orthogonal and shorter one. We already have seen that if the lattice basis is orthogonal, the ZF , Babai and ML points are the same. We can deduce that the more orthogonal the basis is, the simpler the decoding is. In this case, each decision in the tree is more reliable and this involves that lattice basis reduction reduces sphere decoding complexity. Studies supported by computer simulations showed that Schnorr-Euchner Decoder is two to four times faster than Pohst Sphere Decoder in finding the nearest point in a completely random lattice perturbed by uniformly distributed noise [1]. The factor 4 in speed ratio is measured after applying basis reduction like LLL (Lenstra-Lenstra-Lovasz [62]) or KZ (Korkine-Zolotareff [58]).

In Fig. 4.18, we observe the Voronoi regions and the Babai decision regions with and without reduction. When the received point belongs to one of the two cross hatched regions, the Babai point is not ML. The two regions (1) and (2) are given by the dimension decoding order. Notice that without any reduction, the order leading to region (2) will provide faster decoding since the Babai point is more reliable. With a reduction, we first notice that the regions (1) and (2) are disjoint, which indicates that for each received point, the lattice reduction associated with a point-specific dimension ordering enables the Babai point to always be ML. However, this optimal ordering consideration is at least as complex as the ML decoding itself. Nevertheless, it shows that the reduction always enhances the Babai decoding and accelerates the Sphere Decoder.

In Fig. 4.19, we observe the complexity gain obtained by an LLL reduction when decoding an $n_t \times n_t$ MIMO channel equivalent lattice with a Schnorr-Euchner Sphere Decoder. At high signal-

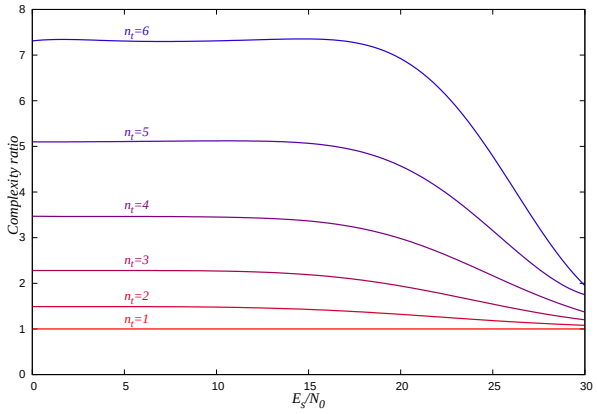

Figure 4.19: Sphere Decoding of $n_t \times n_t$ MIMO channel lattice with Schnorr-Euchner strategy. Number of flops gain when using LLL reduction.

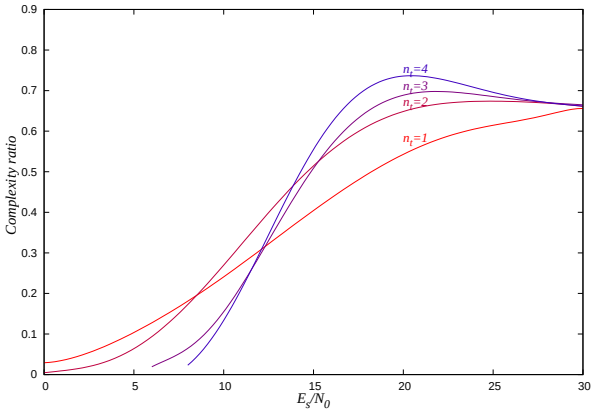

Figure 4.20: Sphere Decoding of $n_t \times n_t$ MIMO channel 16-QAM constellation with Schnorr-Euchner strategy (Number of flops). LLL reduction without constellation bounds computation versus constellation bounds computation without reduction.

to-noise ratio, the Babai point is often the ML point and the reduction is less useful. However, at low signal-to-noise ratio, we can observe the gain factors obtained thanks to reduction and increasing with the number of dimensions.

However, such a complexity reduction is difficult to obtain for QAM modulations on MIMO channels, and that for different reasons:

- If the channel is ergodic, the reduction has to be computed at each new channel realization, in this case the complexity gain might be inferior to the complexity of the reduction. The first conclusion is that lattice reductions have to be used for block fading MIMO channels, and computed only at each new channel realization.

- The bounds of the constellation cannot be computed anymore, indeed, the channel reduction transforms the cubic constellation into a parallelepipedic constellation where each bound depends on all the dimensions at the same time. The complexity reduction given by the restriction to the cubic constellation bound is higher than the one given by the reduction, this can be seen in Fig. 4.20.

The constellation boundaries can be computed after a reduction if and only if the basis change matrix V is triangular, where $M_r = VM_\Lambda$ is the reduced basis from M_Λ. Indeed, the transmitted point $x \in \Lambda$ is associated with $z \in \mathbb{Z}^{n_\Lambda}$ and $z' \in \mathbb{Z}^{n_\Lambda}$ considering the generator matrices M_Λ or M', equivalently. Using the relation $z = z'V$ between z and z', we can see that if V is lower triangular, the decisions on z can be computed, dimension by dimension and recursively. Unfortunately, some simulation results have shown that the complexity reduction obtained with the *bad* reduction is inferior to the recursive bounds processing complexity addition.

4.3 Soft-output list decoding of a lattice constellation

Usually, to compute the soft-output of the mn_t coded bits transmitted on each time period , an exhaustive marginalization which takes into account all the 2^{mn_t} possible transmitted symbols has to be processed. However, for complexity issues in the case of high spectral efficiency, this marginalization is limited to some well chosen points in a spherical list. However, the list has to be well chosen to keep near-optimal performance while strongly reducing the complexity of the APP detector.

4.3.1 Limitation of the likelihood in exhausive APP detector

For systems whose equivalent lattice dimension is too important, the exhaustive marginalization becomes too complex. For the example of 16-QAM modulations, a 2×2 MIMO channel requires a marginalization of 2^{16} points by channel use, and an 8×8 MIMO channel requires a marginalization of 2^{64} points by channel use. We propose to limit the marginalization to the points belonging to a list $\mathfrak{L}$. The approximated soft value becomes

$$\xi(c_j) = \frac{\sum_{z' \in \Omega(c_j=1) \cap \mathfrak{L}} \left[\left(e^{-\frac{\|y - z' M_\Lambda\|^2}{2\sigma^2}} \right) \prod_{r \neq j} \pi(c_r) \right]}{\sum_{z \in \Omega \cap \mathfrak{L}} \left[\left(e^{-\frac{\|y - z M_\Lambda\|^2}{2\sigma^2}} \right) \prod_{r \neq j} \pi(c_r) \right]} \tag{4.47}$$

We observe that the soft outputs depend on both the geometrical configuration when considering the likelihoods and the a priori probability configuration given by a decoder. In the case of an exhaustive list ($\mathfrak{L}$ contains the 2^{mn_t} points), some of the likelihoods in the expression (4.47) are negligible. Let us suppose that all the points whose likelihood is not negligible belong to a list $\mathfrak{L}$:

$$\forall z' \notin \mathfrak{L}, \quad \forall z \in \mathfrak{L}, \quad \frac{1}{2\pi\sigma^2} e^{-\frac{\|y - z' M_\Lambda\|^2}{2\sigma^2}} \ll \frac{1}{2\pi\sigma^2} e^{-\frac{\|y - z M_\Lambda\|^2}{2\sigma^2}} \tag{4.48}$$

The geometrical limit that separates these likelihoods is a sphere centered on the received point that justifies the construction of a non-exhaustive list with the points of a sphere. The choice of the sphere radius determines the performance and the complexity of the corresponding soft-input soft-output detector and is the main difficulty of the solution presented by the authors. Indeed, the random nature of the channels implies a non-stability in the list size. Another difficulty appears in the case of bursted channels, the list directly depends on the received point y, which requires the reconstruction of the list for each new received point, i.e., at each symbol time. Indeed, even if the channel is constant, the noise varies continuously and so does y.

4.3.2 A shifted spherical list

In the case of an ergodic channel, once the ML point is found, we choose to center the list on the ML point instead of centering it on the received point. Clearly, the marginalization (4.47) does not give the same results since the points in the list are different. We make the approximation that the output of the marginalization is quasi-equal to the output when the sphere is centered on the received point. Indeed, to compute efficient soft values, the radius of the sphere must be

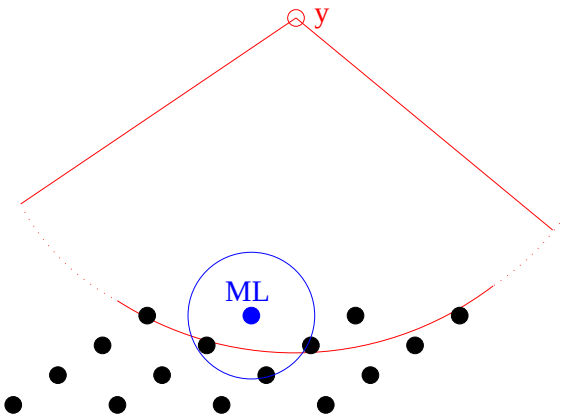

Figure 4.21: Comparison between the sphere centered on the ML point and the sphere centered on the received point y.

relatively high, and the points that will differ in the list are close to the surface of the sphere, so they have the smallest likelihoods. In Fig. 4.21, we clearly see the advantages of the ML center when compared to the received point center. Indeed, when the received point is outside the constellation, which has a high probability when considering a large number of dimensions, the sphere centered on the received point enumerates a large number of lattice points to find a small number of constellation points. When the sphere is centered on the ML point, the number of listed points is reduced and the high likelihood points are taken into consideration.

Since a classical SD finds the closest point to a noisy received point in a lattice, some changes have to be made to the SD algorithm to extend it to a soft-output sphere detector: the radius of the sphere is not reduced during the search like presented before, every point found in the intersection of the sphere and the constellation is stored, together with its distance to the received point. A double Pohst recursion is used to enumerate the points. Indeed, the first classical recursion is needed to check all lattice points at a squared distance less than the radius of the sphere centered on the ML point. We added a parallel second recursion to compute the distances between the enumerated points and the received point y (see step 1 and variables with an upperscript d in the description of the algorithm 2) with a reduced complexity.

Instead of centering the sphere on the ML point, we evaluate it with classical sub-optimal methods to reduce the complexity of the system. As a non-exhaustive list, we cite some known methods that can be implemented as an alternative to the Sphere Decoder:

- Zero Forcing (ZF) with or without a hard decision
- Minimum Mean Square Equalizer (MMSE) with or without a hard decision
- Interference Cancelation with or without ordering (MMSE or ZF)
- Babai point in the constellation

Until the end of this document, we will only discuss the case when the sphere is centered on the ML point, the above simplifications can be applied in most cases.

Algorithm 3: Spherical list enumeration.

input : A received point y, a point of the lattice x, the generator matrix $M_\Lambda(n_\Lambda \times n_\Lambda)$ of the lattice, the radius r of the sphere, and the bounds z_{min} and z_{max} of the constellation.

output : A list $\mathfrak{L}$ of points of the lattice that belong to the sphere, a list of the distance between y and each point of the list.

Pre-processing
$M_I \leftarrow M_\Lambda^{-1}$
$G \leftarrow M_\Lambda M_\Lambda^T$
Cholesky's reduction $\{R, \Theta\} = Cholesky(G)$. Θ is upper-triangular.
$u \leftarrow xM_I$,$\rho \leftarrow yM_I$
Initialization
$d^2 \leftarrow r^2$, $T_{n_\Lambda} \leftarrow r^2$, $T^d_{n_\Lambda} \leftarrow r^2$, $i \leftarrow n_\Lambda$
for $j = 1$ **to** n_Λ **do**
  $S_j \leftarrow u_j$, $S^d_j \leftarrow \rho_j$
Step 1
$L_i \leftarrow min\left(\left\lfloor \sqrt{T_i/\Theta_{ii}} + S_i \right\rfloor, z_{max}\right)$
$z_i \leftarrow max\left(\left\lceil -\sqrt{T_i/\Theta_{ii}} + S_i \right\rceil, z_{min}\right) - 1$
Step 2
$z_i \leftarrow z_i + 1$
if $z_i \leq L_i$ **then**
  if $i > 1$ **then**
    $\xi_i \leftarrow u_i - z_i$
    $\xi^d_i \leftarrow \rho_i - z_i$
    $T_{i-1} \leftarrow T_i - \Theta_{ii}(S_i - z_i)^2$
    $T^d_{i-1} \leftarrow T^d_i - \Theta_{ii}(S^d_i - z_i)^2$
    $S_{i-1} \leftarrow u_{i-1} + \sum_{j=i+1}^{n_\Lambda} \Theta_{i-1,j}\xi_j$
    $S^d_{i-1} \leftarrow \rho_{i-1} + \sum_{j=i+1}^{n_\Lambda} \Theta_{i-1,j}\xi^d_j$
    $i \leftarrow i - 1$
    Goto Step 1
  else
    $\hat{d}^2 \leftarrow r^2 - T^d_i + \Theta_{11}(S^d_1 - z_1)^2$
    store z and $\hat{d}$ in $\mathfrak{L}$
    Goto Step 2
else if $i = n_\Lambda$ **then** Teminate
else
  $i \leftarrow i + 1$
  Goto Step 2

4.3.3 Choice of the radius

The choice of the sphere radius R for this list Sphere Decoder is as important as the choice of the radius for the conventional SD. Having too many points in the sphere heavily slows down the detection while not having enough points degrades significantly the performance. In this section, some properties of lattices are exploited to determine a sphere radius that guarantees a stability in the number of points in the list. Let us assume we want to find N_p points to create a list centered on the origin. We make the approximation that the volume of a sphere containing N_p points is equal to the volume of N_p fundamental parallelotopes. Hence, the radius R of a sphere that contains N_p points is well approximated by

$$R = \left(\frac{N_p \times \mathrm{vol}(\Lambda)}{V_n}\right)^{\frac{1}{n}} \tag{4.49}$$

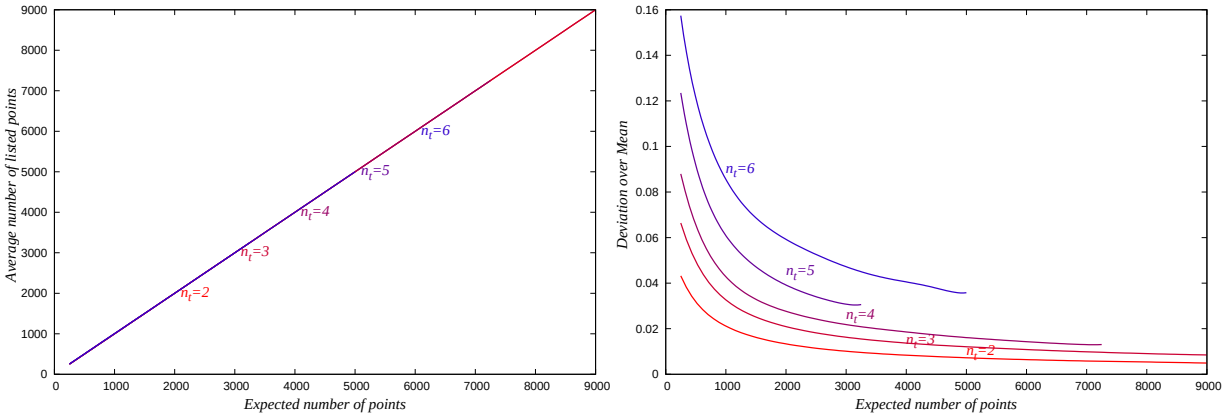

(a) Mean, lattice.

(b) Deviation over mean, lattice

Figure 4.22: Mean and Deviation of the number of points in the list for a MIMO lattice decoding. The list sphere radius is derived from the fundamental volume.

where $vol\,(\Lambda)$ is the fundamental volume of the lattice and V_n is the volume of a unitary sphere in dimension n:

$$V_n = \frac{\pi^{n/2}}{\Gamma(n/2+1)} = \begin{cases} \frac{\pi^{n/2}}{(n/2)!} & n \text{ even} \\ \frac{2^n \pi^{(n-1)/2}((n-1)/2)!}{n!} & n \text{ odd} \end{cases} \tag{4.50}$$

This method of choosing the radius is quite stable in a lattice when N_p is high. We can see the average number of points obtained in a lattice with this method in Fig. 4.22-(a). The average number of listed points is equal to the expected number of points N_p for any value of n_t. In Fig. 4.22-(b), we can see the deviation over the mean of the number of listed points, and we notice that for high values of N_p, the list becomes more and more stable, as expected.
When considering a constellation, the intersection between the sphere and the constellation significantly disminishes the number of selected points. Depending on the position of the ML point in the constellation, the number of enumerated points varies. Fig. 4.24 shows a situation where 13 points are enumerated in the lattice and only 7 points in the constellation. In Fig. 4.23-(a)(b), we can see the mean and deviation of the number of listed points in the intersection of the spherical list and a 16-QAM modulation. First, we can notice that the average number of points is significantly lower than the expected number of points, and this depends on the number of transmit antennas. Indeed, the number of listed points saturates to 2^{mn_t}.

In order to have more stability in the number of listed points and to avoid small and large lists, we can adjust the sphere radius taking into account the number of hyperplanes n_{hyp} the ML point belongs to. The number of expected points N_p is multiplied by $\alpha[n_{hyp}]$, an expansion factor of the list size which depends on n_{hyp}. Indeed, the more the number of hyperplanes the ML point belongs to, the less we have points in the list. For example, the choice $\alpha[i] = 1 + \frac{i}{n_\Lambda}$ gives good results. We can see respectively in Fig. 4.25-(a) and Fig. 4.25-(b) the average number of points in the list, with and without the expansion factor $\alpha[i]$. We can observe that the expansion factor succeeds in correcting the average number of points for any parameter n_{hyp}. The average number of points is lower than N_p, this has to be taken into consideration when n_p is chosen.

We will now try to reduce the number of points deviation, using the observation that the number of listed points is also influenced by the lattice geometry. The more dense the lattice

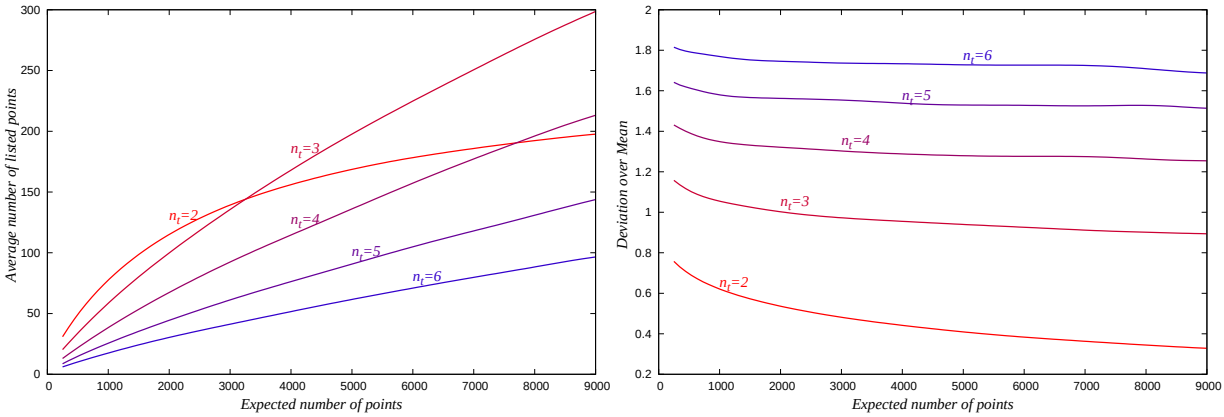

(a) Mean, 16-QAM constellation (b) Deviation over mean, 16-QAM constellation

Figure 4.23: Mean and Deviation of the number of points in the list for a MIMO constellation. The list sphere radius is derived from the fundamental volume.

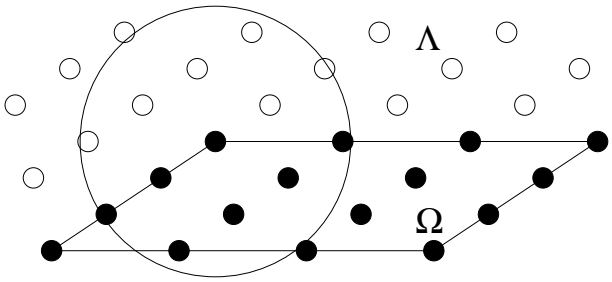

Figure 4.24: The loss of points in the list in the case of constellations.

is, the more stable the list becomes, and we have less side effects. To take into account this property, we can use the fundamental volume $\gamma(\Lambda)$ and add a pre-correction of the expected number of points to the list radius. The problem of finding d^2_{Emin} is NP complex, that is why we approximate it by the minimum of the diagonal of the Gram matrix. We will call $g^2_{min}(\Lambda)$ this quantity and γ_G the approximation of the fundamental gain of Λ:

$$\gamma_G(\Lambda) = \frac{g^2_{min}(\Lambda)}{|det(M_\Lambda)|^{2/n_\Lambda}} \tag{4.51}$$

We then use a simple criterion for an additional expansion μ of the number of points:

$$\begin{cases} \gamma_G(\Lambda)dB > \gamma_1 \Rightarrow \mu_\gamma = \mu_1 \\ \gamma_G(\Lambda)dB > \gamma_2 \Rightarrow \mu_\gamma = \mu_2 \end{cases} \tag{4.52}$$

E.g., we take $\gamma_1 = 3dB, \gamma_2 = 6dB, \mu_1 = 4, \mu_2 = 16$. Finally, the new radius is given by

$$R = \left(\frac{\alpha[n_{hyp}] \times \mu_\gamma \times N_p \times det\,(G)}{V_n} \right)^{\frac{1}{n}} \tag{4.53}$$

If the number of points in the list is too small, we can reenumerate the points in a larger sphere, for example by multiplying the radius by 1.5.

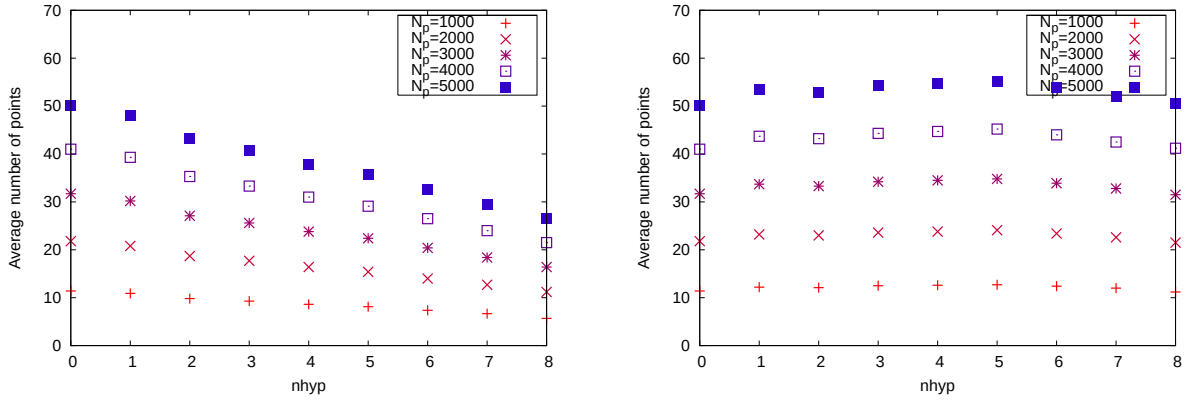

(a) No expansion factor (b) Expansion factor $\alpha[i]$

Figure 4.25: Average number of listed points with or without the expansion factor $\alpha[i]$.

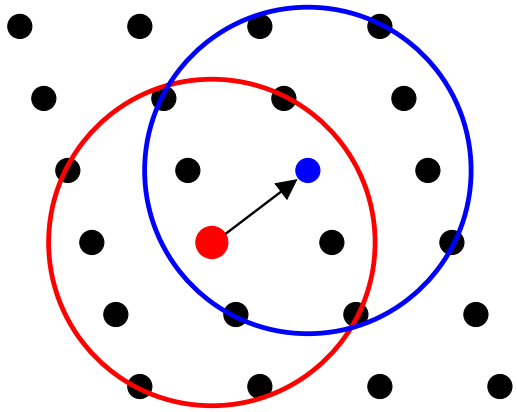

Figure 4.26: Translation invariance of the lattice.

4.3.4 Complexity reduction for block fading channels

Let us define N_{block} the number of symbols in a code word. In the case of an ergodic channel, we have to store N_{block} lists to compute the observations on all coded bits before giving them to the observation input of the SISO decoder. In the case of a block fading channel, the channel remains unchanged during the block. Thanks to the lattice structure, we can find the points in the sphere centered on the origin of the lattice and translate them to find the points in the sphere centered on x_{ML}. This invokes the translation invariance of the lattice (cf Fig. 4.26).

In the list centered on the origin, we store $n_{\mathfrak{L}}$ points zH belonging to the lattice. For each channel use, the noise changes, so does the ML point and the distances to the received point have to be reprocessed. An efficient implementation is to store the list as a dynamic tree, based on the tree structure of the lattice. In this case, a recursive computation of the distances to the received, the constellation bounds and binary labelling point strongly reduces the overall complexity.

A less performant version only takes into account the distance to the ML point, so the distances are processed once at the beginning of each block. We can also enumerate a larger list and sort it with the distance to the origin. This can be seen as a list of concentric spheres. If

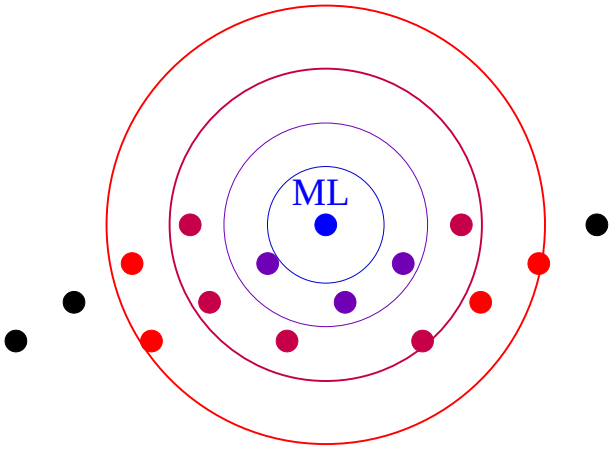

Figure 4.27: A concentric list of spheres.

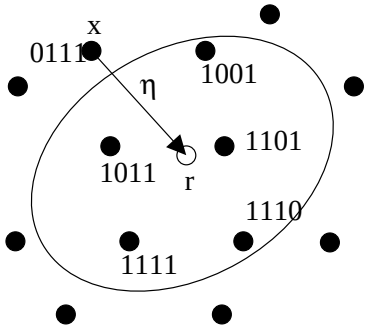

Figure 4.28: Situation leading to inconsistency.

the first sphere leads to a list which is too small, we consider the second sphere and so on (see Fig. 4.27).

4.3.5 Applications to iterative detection and decoding of BICM

In this section, we illustrate the application of the new soft detector to BICM on MIMO. The symbols z_i belong to an M-QAM constellation. The binary information elements are encoded using a rate R_c convolutional code. The coded bits $\{c_\ell\}$ are randomly interleaved and fed to a QAM mapper ($M = 2^m$) that generates z. The spectral efficiency of the system is $R_c \times m \times n_t$ bits per channel use, or equivalently $R_c \times m \times n_t$ bits/sec/Hz.

When there is only one symbol representing one bit in the list, the observation is either 1 or 0. In that case, there is no point in the constellation with the other symbol, which can cause computation inconsistency when marginalizing. For example, in Fig. 4.28, if we consider that the a priori of the first bit is equal to 0.0, the SISO decoder fails because there is no point corresponding to a first bit equal to 0 in the list. Without loss of generality, we will consider this case until the end of this section.

A first solution to solve the inconsistency problem is to replace the APP of the considered

bit by the minimum among the contributions in the list, (4.47) becomes

$$\tilde{\xi}(c_j) = \left[1 + \frac{\min_{z' \in \Omega(c_j=1) \cap \mathfrak{L}} \left(\left(e^{-\frac{\|y - z' M_\Lambda\|^2}{2\sigma^2}} \right) \prod_{r \neq j} \pi(c_r) \right)}{\sum_{z' \in \Omega(c_j=1) \cap \mathfrak{L}} \left[\left(e^{-\frac{\|y - z' M_\Lambda\|^2}{2\sigma^2}} \right) \prod_{r \neq j} \pi(c_r) \right]} \right]^{-1} \tag{4.54}$$

Another solution is to consider the worst case when the nearest point that does not belong to the list lies on the surface of the sphere. We consider the sphere radius to compute its likelihood. The corresponding a priori probability π_v of this virtual point can be chosen using different ways:

- By an average case when all a priori probabilities are equal to 0.5:

$$\pi_v = 0.5^{m.n_t - 1} \tag{4.55}$$

- By the worst case when the point is of higher a priori probability:

$$\pi_v = \prod_{r \neq j} \max \{\pi(c_r), 1 - \pi(c_r)\} \tag{4.56}$$

With this method, (4.47) becomes

$$\tilde{\xi}(c_j) = \left[1 + \frac{\pi_v . e^{-\frac{R^2}{2\sigma^2}}}{\sum_{z' \in \Omega(c_j=1) \cap \mathfrak{L}} \left[\left(e^{-\frac{\|y - z' M_\Lambda\|^2}{2\sigma^2}} \right) \prod_{r \neq j} \pi(c_r) \right]} \right]^{-1} \tag{4.57}$$

Another efficient way to reduce insconsistency computation problems is to apply a ceiling on the soft values exchanged between the blocks. A first ceil with parameter ϵ_c is applied to soft values given by the soft decoder to the detector, i.e., a priori probabilities for the detector:

$$\forall j, \quad \begin{cases} \pi(c_j) < \epsilon_c \Rightarrow \pi(c_j) \leftarrow \epsilon_c \\ \pi(c_j) > 1 - \epsilon_c \Rightarrow \pi(c_j) \leftarrow 1 - \epsilon_c \end{cases} \tag{4.58}$$

The same method can be applied at the output of the detector with parameter ϵ_l, but it is preferable to apply the ceiling during the computation of the a priori probabilities product.

$$\begin{gathered} \text{Initialization } \alpha_j \leftarrow 1 - \epsilon_l \\ \text{for } r = 0 \text{ to } m \times n_t \text{ and } r \neq j,\ \alpha_j \leftarrow \alpha_j \times \pi(c_r), \alpha_j \leftarrow \max \{\alpha_j, \epsilon_l\} \end{gathered}$$

Indeed, we can see that the perfect case when $\alpha_j = 1$ is solved by initializing α_j to $1 - \epsilon_l$. During the computation, if the current product becomes inferior to ϵ_l, a ceiling is done, which limits the calculation distortion. At the end of the computation, α_j gives an estimate of the product of the a priori probabilities in the computation (4.57). The parameters ϵ_l and ϵ_c can be chosen equal to 10^{-5} for example.

4.4 Soft-input soft-output MMSE

In the previous section, we have presented an a posteriori probability detector for multiple antenna channels. It has the high advantage of providing good performance but has an NP complexity. We will now present a sub-optimal soft-input soft-ouput detector based on the minimum mean square error (MMSE) criterion. Such a SISO-MMSE equalizer has been presented in [32] in the case of single antenna dispersive channel. We describe the direct application to MIMO channels and present supplementary complexity reductions.

4.4.1 SISO-MMSE processing

Let us assume that a mono-dimensional complex mapping Ω^1 is used to independently convert m bits into a constellation symbol on each transmit antenna. This independence allows to see the $n_t \times n_r$ channel as n_t interfering $1 \times n_r$ channels. If the feedback from the SISO decoder is sufficiently reliable, we can assume that the interference is perfectly removed and the extrinsic probability of a coded bit computed by an exhaustive marginalization over Ω^1. We clearly see the complexity reduction at a cost of performance degradation for low signal-to-noise ratios. The basic SISO-MMSE is fully presented in Appendix B. However, we will recall the main equations for the soft output processing.

Assume that the constellation has zero mean, i.e, $E_{z_i \in \Omega^1}(z_i) = 0$. The constellation variance is equal to the symbol energy $E_s = E_{z_i \in \Omega^1}(z_i^2)$. Note $\mathfrak{e}_i = [0, \ldots, 0, 1, 0, \ldots, 0]$ the null vector with a 1 in position i. The SISO-MMSE is computed from the following steps

1. $\forall 0 \leq i < n_t$, compute the vectors $\bar{z} = [\bar{z}_0, \ldots, \bar{z}_{n_t-1}]$ and $\sigma_z^2 = \left[\sigma_{z,0}^2, \ldots, \sigma_{z,n_t-1}^2\right]$

$$\pi(z_i) = \prod_{j=m.i}^{m.i+m-1} \pi(c_j) \tag{4.59}$$

$$\bar{z}_i = \sum_{z_i} z_i \pi(z_i) \tag{4.60}$$

$$\sigma_{z,i}^2 = \sum_{z_i} |z_i|^2 \pi(z_i) - |\bar{z}_i|^2 \tag{4.61}$$

2. $\forall 0 \leq i < n_t$, compute

$$\Gamma_i = \text{diag}\left[\sigma_{z,0}^2, \ldots, \sigma_{z,i-1}^2, E_s, \sigma_{z,i+1}^2, \ldots, \sigma_{z,n_t-1}^2\right] \tag{4.62}$$

$$\tilde{z}_i = E_s \left[y - (\bar{z} - \mathfrak{e}_i \bar{z} i) H\right] \left[H^* \Gamma_i H + N_0 I\right]^{-1} (\mathfrak{e}_i H)^* \tag{4.63}$$

$$\mu_i = E_s \left(\mathfrak{e}_i H\right) \left[H^* \Gamma_i H + N_0 I\right]^{-1} (\mathfrak{e}_i H)^* \tag{4.64}$$

$$p(\tilde{z}_i | z_i) = \exp\left[-\frac{|\tilde{z}_i - \mu_i z_i|^2}{\mu_i (1 - \mu_i) E_s}\right] / (\mu_i (1 - \mu_i) E_s \pi) \tag{4.65}$$

3. $\forall 0 \leq i < n_t$, $\forall 0 \leq j < m$ compute

$$\xi(c_{j+im}) = \frac{\sum_{z_i \in \Omega(c_j = 1)} p(\tilde{z}_i | z_i) \prod_{l \neq j} \pi(c_l)}{\sum_{z_i \in \Omega} p(\tilde{z}_i | z_i) \prod_{l \neq j} \pi(c_l)} \tag{4.66}$$

4.4.2 Complexity reductions of matrix inversions

Without any complexity reduction, the SISO MMSE requires the computation of n_t matrix inversions (size $n_r \times n_r$) for each iteration and time period. We will first show how to compute only one matrix inversion per iteration and time period and present some ideas to limit the number of matrix inversions in the whole iterative process.

a) Application of the Sherman-Morrison Formula

To compute $\tilde{z}_i, \forall 0 \leq i < n_t$, the SISO-MMSE requires the computation of the $n_r \times n_r$ matrix inversion:

$$A^{-1} = [H^* \Gamma_i H + N_0 I]^{-1} \tag{4.67}$$

where

$$\Gamma_i = \text{diag}\left[\sigma^2_{z,0}, \ldots, \sigma^2_{z,i-1}, E_s, \sigma^2_{z,i+1}, \ldots, \sigma^2_{z,n_t-1}\right] \tag{4.68}$$

varies at each iteration (the $\sigma^2_{z,i}$ variables are computed from the a priori probabilities given by the error correcting code SISO decoder) and for each antenna. Notice that

$$A^{-1} = \left[H^* \left(\Gamma + (E_s - \sigma^2_{z,i})\mathfrak{E}_i\right) H + N_0 I\right]^{-1} \tag{4.69}$$

where $\Gamma = \text{diag}\left[\sigma^2_{z,j}\right]$ and $\mathfrak{E}_i$ is a matrix having only one non-zero coefficient equal to 1 and coordinates (i,i). With the property $\mathfrak{E}_i^* \mathfrak{E}_i = \mathfrak{E}_i$, we deduce that

$$H^* \mathfrak{E}_i H = (\mathfrak{E}_i H)^* \mathfrak{E}_i H = h_i^* h_i \tag{4.70}$$

where h_i is the i-th row of H. If we define $B = [H^* \Gamma H + N_0 I]$, we get

$$A^{-1} = \left[B + (E_s - \sigma^2_{z,i}) h_i^* h_i\right]^{-1} \tag{4.71}$$

by applying the Sherman-Morrison formula, and using the Hermitian symmetry $v^* = B^{-1} h_i^* = (h_i B^{-1})^*$, we obtain

$$A^{-1} = B^{-1} - \frac{(E_s - \sigma^2_{z,i})}{1 + (E_s - \sigma^2_{z,i}) h_i v^*} v^* v \tag{4.72}$$

As a conclusion, and at each iteration, we only have to compute the $n_r \times n_r$ matrix inversion B^{-1}, and for each antenna, we have to compute one "*matrix by vector*" multiplication and two "*vector by vector*" multiplications. Finally, we have

$$\tilde{z}_i = \frac{E_s \left[y - (\bar{z} - \mathfrak{e}_i \bar{z} i) H\right] \left[H^* \Gamma H + N_0 I\right]^{-1} h_i^*}{1 + (E_s - \sigma^2_{z,i}) \left(E_s + N_0 \left(H H^*\right)^{-1}_{ii}\right)} \tag{4.73}$$

b) Matrix series expansion applied to the matrix inversion

The $n_r \times n_r$ matrix inversion B^{-1} has to be done at each new iteration. We will use in some adapted situations a series expansion of this matrix to evaluate the inversion. At the n-th iteration, we have to compute

$$B^{-1} = [H^* \Gamma H + N_0 I]^{-1} \tag{4.74}$$

Direct method, series expansion on Γ

After some iterations, Γ is supposed to be quasi null in the case of converging high SNR systems. We will use this property of Γ to evaluate the inversion B^{-1}. We have

$$B^{-1} = \frac{1}{N_0}\left[\Theta + I\right]^{-1} \tag{4.75}$$

with $\Theta = \frac{1}{N_0}H^*\Gamma H$. We can compute B^{-1} thanks to the power series expansion under some convergence conditions. Let us define the spectral radius $r(\Theta) = \max_i |\lambda_i|$ the maximum of the modulus of the eigenvalues λ_i of Θ. The convergence condition of the series expansion is $r(\Theta) < 1$. The computation of the eigenvalues is too complex, so we will use a straightforward application of the Gershgorin Theorem that gives a loose upper bound on $r(\Theta)$:

$$r(\Theta) < \max_i \left(\sum_j |\Theta_{ij}| \right) \tag{4.76}$$

If the convergence criteria is verified, the series expansion is given by

$$\max_i \left(\sum_j |\Theta_{ij}| \right) < 1 \Rightarrow B^{-1} = \frac{1}{N_0} \sum_{i=0}^{\infty} (-\Theta)^i \tag{4.77}$$

In conclusion, we can limit the order of the series expansion to L, which leads to

$$\max_i \left(\frac{1}{N_0} \sum_j \Gamma_{jj} \left| (H^*H)_{ij} \right| \right) < 1 \Rightarrow \quad B^{-1} \simeq \frac{1}{N_0} \sum_{i=0}^{L} \left(\frac{-1}{N_0} H^*\Gamma H \right)^i \tag{4.78}$$

The series expansion can be expressed by the less complexity consuming recurrent relation

$$B^{-1} \simeq \frac{1}{N_0} H^* \left(I - \frac{1}{N_0}\Gamma H H^* \left(I - \frac{1}{N_0}\Gamma H H^* \left(I - \ldots \right) \right) \right) H^{-H} \tag{4.79}$$

Hence, HH^* can be pre-computed each time the channel changes, and Γ is diagonal, which simplifies the processing of ΓHH^*. The number of matrix multiplications, which are predominant in terms of complexity, is $L + 2$, this method is useful if $L + 2 < 2n_r$

Series expansion on the difference $\Gamma_{n+1} - \Gamma_n$

Even at low SNR, the system converges to a state when the difference $\Upsilon_{n+1} = \Gamma_{n+1} - \Gamma_n$ is quasi null. We can apply the power series expansion in this case, indeed at the n-th iteration, we have an estimation of B_n^{-1}. We want to evaluate B_{n+1}^{-1} from the new feedback correction Υ_{n+1}. We can write

$$M_{n+1} = HB_{n+1}^{-1}H^* = M_n \left[I + \Upsilon_{n+1} M_n \right]^{-1} \tag{4.80}$$

We can directly apply the results seen above:

$$\max_i \left(\sum_j \Upsilon_{n+1,jj} \left| M_{n,ij} \right| \right) < 1 \Rightarrow M_{n+1} \simeq M_n \left(I - \Upsilon_{n+1} M_n \left(I - \Upsilon_{n+1} M_n \left(I - \ldots \right) \right) \right) \tag{4.81}$$

This recurrent evaluation of B^{-1} can be computed by these different points

- Iteration 0: compute or evaluate B_0^{-1} and $M_0 = HB_0^{-1}H^*$
- Iteration $n+1$: if the convergence condition is satisfied, compute $\Upsilon_{n+1}M_n$ and M_{n+1} thanks to Eq. (4.81), and compute $B_{n+1}^{-1} = H^{-1}M_{n+1}H^{-H}$

4.4.3 Application to Space-Time precoders

In order to improve the diversity order of the system, we introduce a new class of precoders based on a modification of cyclotomic rotations. The precoder spreads the symbols in space and time with a factor s thanks to a $s.n_t \times s.n_r$ matrix S. The new extended $s.n_t \times s.n_r$ channel matrix H is block diagonal, each block on the diagonal is a $n_t \times n_r$ matrix H_t corresponding to the MIMO channel matrix during symbol period t. Our precoder is a rotation, so $SS^* = I$ and $S^*S = I$. At the first iteration, all the variances $\sigma_{z,i}^2$ are equal, this induces that $\Gamma = \sigma_{z,0}^2 I$ Without any considerations on S, we should compute the inversion of $B^{-1} = [H^*S^*\Gamma SH + N_0 I]^{-1}$ which is $s.n_r \times s.n_r$. Since $S^*S = I$, we have

$$\begin{aligned} B^{-1} &= [H^*\Gamma H + N_0 I_{s.n_r}]^{-1} \\ &= \text{diag}\left\{ \left[\sigma_{z,0}^2 H_1^* H_1 + N_0 I_{n_r}\right]^{-1}, \ldots, \left[\sigma_{z,0}^2 H_s^* H_s + N_0 I_{n_r}\right]^{-1} \right\} \end{aligned} \tag{4.82}$$

We compute s inversions of $(n_t \times n_r)$ matrices for s symbol periods (as if there was no precoder) instead of 1 inversion of $(n_t.s \times n_r.s)$ matrix. Then at high signal-to-noise ratio we can compute the matrices series expansions methods.

4.5 Performance and complexity comparison

In this section, we will compare the performance and complexity of the three iterative receivers presented in the previous sections. We consider a 4×4 ergodic MIMO channel with 16-QAM input. The objective of the near APP detector design is to achieve performance not far from the capacity limit.

Let us consider a rate 1/2 parallel turbo-code [9] whose constituent codes are two $(1, 5/7)$ recursive systematic convolutional codes. The rate 1/2 constituents are punctured in order to increase the concatenation rate from 1/3 to 1/2. Figure 4.29 shows the achievable information rate for 4×4 multiple antenna channel with 16-QAM input alphabet. The mutual information value of 8.0 bits per channel use yields a minimum achievable signal-to-noise ratio equal to 4.0dB. The capacity limit with a Gaussian input at 8.0 bits per channel use is 3.7 dB. Figure 4.29 illustrates an application of the soft output Sphere Decoder to the evaluation of MIMO channel information rate under the constraint of a finite QAM constellation input. Two scenarios are presented: 1- A target list size $N_p = 1000$. The effective list size was distributed between $N_e(min) = 256$ and $N_e(max) = 2300$ with an average equal to 1000. 2- A target list size $N_p = 60000$. The effective list size was distributed between $N_e(min) = 4000$ and $N_e(max) = 26000$ with an average equal to 10000. It is clear that mutual information evaluation is useful at high coding rates ($R_c \geq 1/2$) where its value diverges from the Gaussian input capacity. A reduced size list is sufficient in this region.

In Fig. 4.30, we observe the turbo-code performance over the 4×4 MIMO channel. We compare a shifted list sphere decoder and a list sphere decoder centered on y both performing at 1.3 dB from the mutual information limit. The complexity ratio is 3.7 in favor of the shifted list sphere decoder. In this case, the effective number of listed points histograms are presented in Fig. 4.31. We can see that the shifted list sphere decoder succeeds in limiting the small and large lists whereas the list sphere decoder centered on y often generates very small list and with a non-null probability large lists. When the list sphere decoder centered on y has the same complexity as the shifted list sphere decoder, a loss of 0.5 dB gain is experienced.

In Fig. 4.32, we can observe the behavior of the shifted list sphere decoder with the number of expected points N_p and the interleaver size. First, we observe that the higher the interleaver size, the steeper the waterfall region. Then we observe that arround 1 dB gain is observe between $N_p = 400$ and $N_p = 2500$ and only 0.1 dB gain more is obtained choosing $N_p = 30000$ which induces that the APP detector is near-optimum. The system performs at 1.2 dB from the mutual information limit,which is the best performance known for 16-QAM over a 4×4 MIMO channel. Moreover, we show that the SISO-MMSE performs at 1.25 dB from the best List APP detection. However, the complexity is not comparable between the two detectors. In Fig. 4.33, we can see the performance of the SISO-MMSE detector over a quasi-static MIMO channel and observe that it is far from being optimal. The more the number of channel states, the more the SISO-MMSE will be optimal.

Conclusions

In this section, we have fully described the lattice model of the MIMO channel and the maximum likelihood sphere decoder. We have shown that the Schnorr-Euchner strategy is optimal for a given lattice constellation. Then we introduced a new soft-input soft-output detector for MIMO channels. A spherical list is constructed arround the ML point processed with the sphere decoder, and a marginalization is computed over the list points. The sphere radius is computed to enumerate a target number of points N_p. Such a list construction limits the number of small and large list, which stabilizes the effective number of listed points and reduces the complexity or enhances the performance.

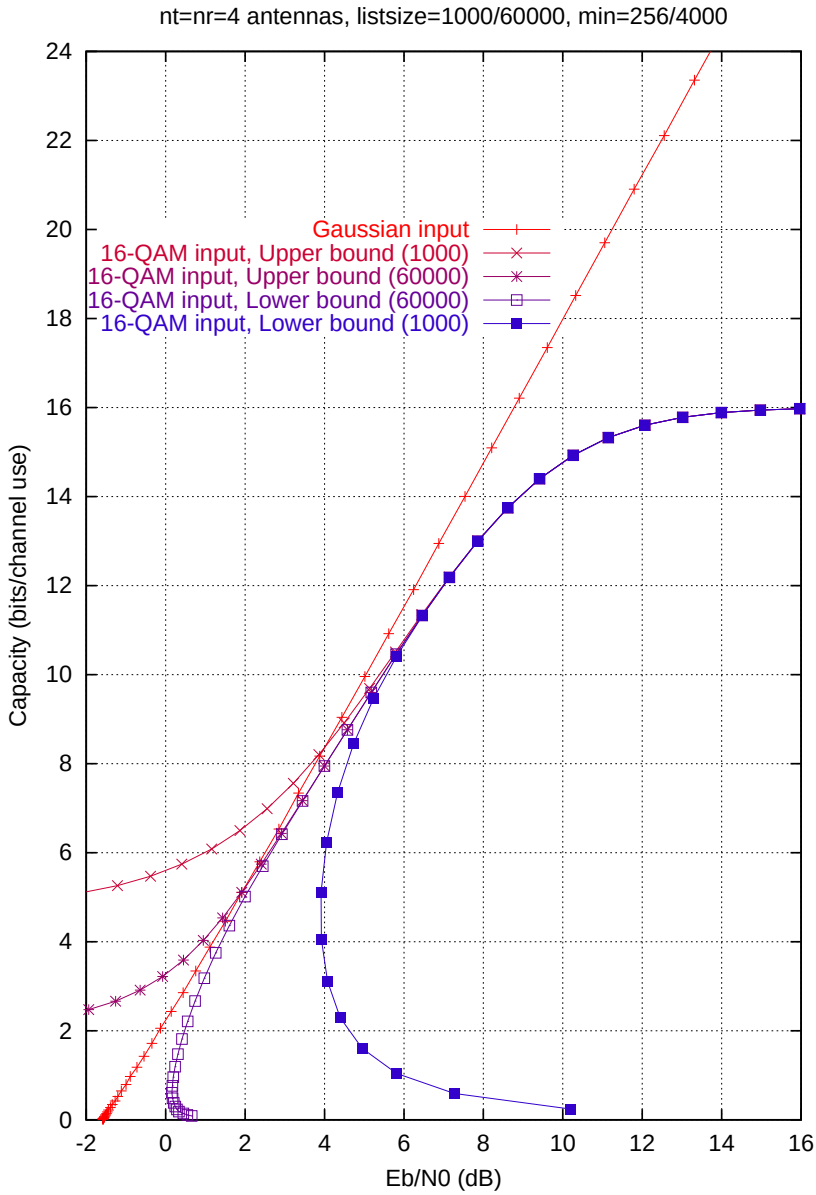

Figure 4.29: Achievable rate on a 4×4 ergodic MIMO with 16-QAM input, $N_p = 1000/60000$, $N_e(min) = 256/4000$.

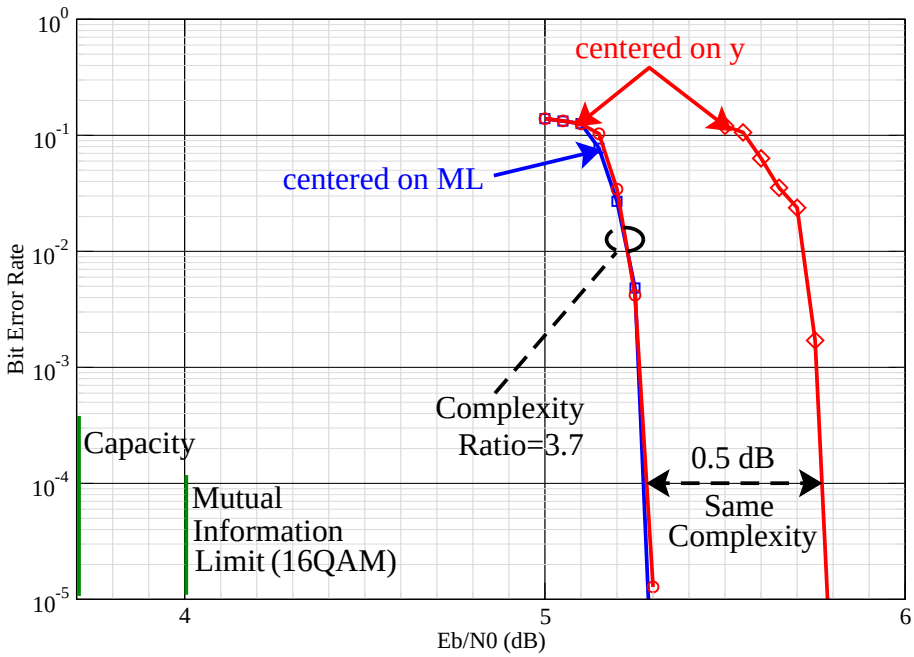

Figure 4.30: Performance of a $(1, 5/7)_8$ parallel turbo-code over an ergodic 4×4 MIMO channel with 16-QAM input. Comparison between the shifted list sphere decoder and the list sphere decoder centered on the received point. Performance comparison for equal performance - Performance comparison for equal complexity.

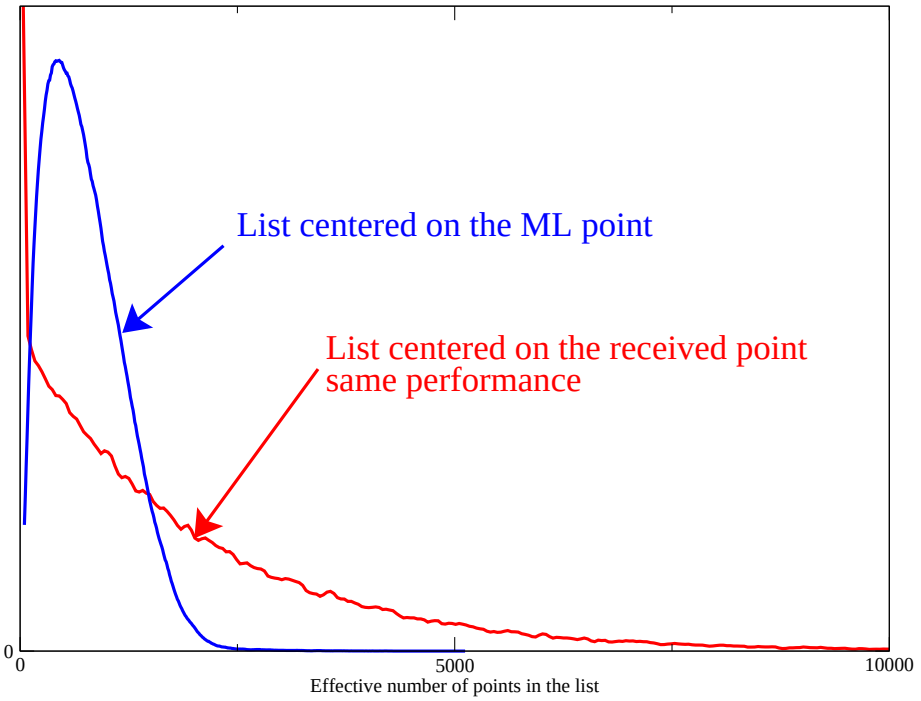

Figure 4.31: Histograms of the number of points in the list of the shifted list sphere decoder and the list sphere decoder centered on the received point.$(1, 5/7)_8$ parallel turbo-code over an ergodic 4×4 MIMO channel with 16-QAM input. SNR=5.3dB, BER=10^{-5}.

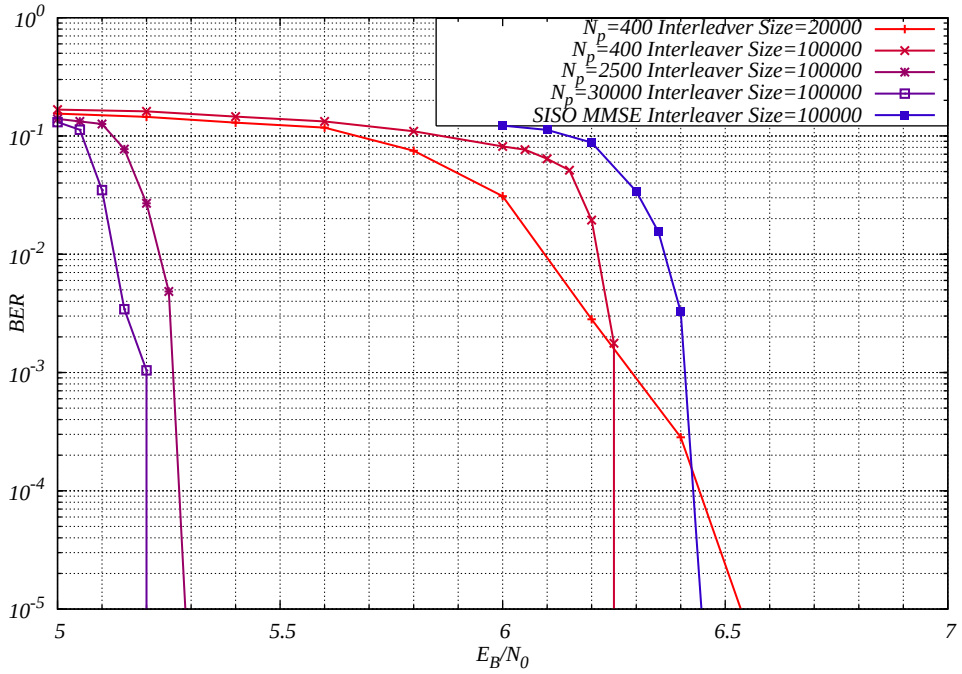

Figure 4.32: Performance of a $(1, 5/7)_8$ parallel turbo-code over an ergodic 4×4 MIMO channel with 16-QAM input. The frame size is 20000 or 100000 coded bits. Performance of the shifted list sphere decoder for different parameters N_p. Performance of the SISO-MMSE.

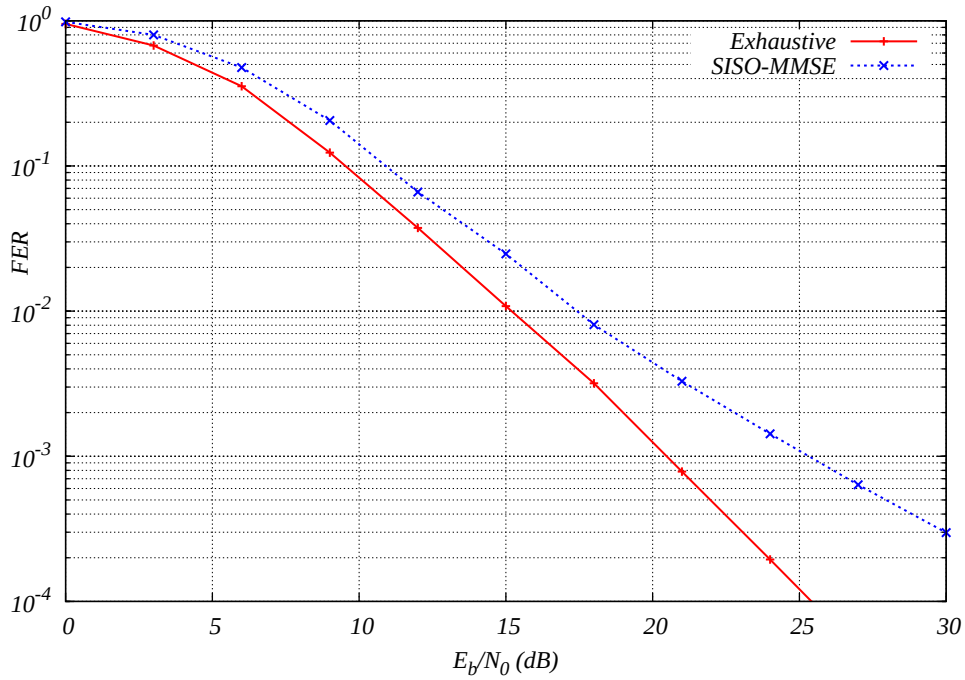

Figure 4.33: Performance of a $(7, 5)_8$ NRNSC over a quasi-static 2×1 MIMO channel with QPSK input. The frame size is 1024 coded bits. Performance of the SISO-MMSE detector and exhaustive detector.

Conclusions and perspectives

We presented near capacity and near outage performance over multiple antenna channels thanks to optimized bit-interleaved coded modulations. The design conclusions sum up in the following points, original material found in this thesis report is underlined and indicated by a star.

- If the channel is ergodic, the amount of available time diversity is much more greater than the minimum Hamming distance of the code. In this case the objective is not to achieve full diversity but to maximize the coding gain. We presented two methods to achieve near capacity performance for a target bit error rate:
  - Use a turbo-code to protect the binary data and process iterative joint detection and decoding with a near optimum or exhaustive APP detector. A gray mapping provides the best performance with such a good code.
  - Use an optimized multi-dimensional mapping* with large potential gain. A simple error correcting code is necessary to allow a good convergence and achieve near turbo-codes performance.
- It the channel is block fading and the amount of available diversity low, the system should be designed to guarantee the full diversity order. This is achieved with the three following steps :
  - The detector converts the MIMO block fading channel into a simple block fading channel. The error correcting code is capable of collecting an amount of diversity limited by the Singleton bound applied to the equivalent block fading channel. When a linear precoder is used, compute the minimum time spreading* factor that guarantees full diversity distributing the diversity exploitation between the detector and the decoder.
  - Design a linear precoder* that provides a diversity proportional to the spreading factor times the number of receive antennas.
  - Choose an error correcting code whose Hamming distance is greater than the maximum transmit diversity order. Design a channel interleaver* taking the error correcting code structure into account in the aim of satisfying the ideal interleaver condition. Note that the ideal interleaver existence is given by the choice of the spreading factor with the Singleton bound.

  Once the full diversity order is guaranteed, the coding gain is maximized if the linear precoder satisfies the DNA condition under ideal interleaving. Optimize the channel interleaver to approach the ideal channel interleaving condition. In general, the frame error rate increases with the frame size. However, concatenated error correcting codes such as turbo-codes allow to observe a frame error rate decreasing with the frame size, and achieve near outage capacity performance.

We have expressed exact pairwise error probabilities* for ergodic, block fading, and precoded MIMO channels. The asymptotic expressions of the performance give the design criteria for the binary labeling, the linear precoder and the choice of the error correcting code. Moreover, the pairwise error probabilities can be used to tightly evaluate the error rates of the ideally interleaved BICM using either a union bound or a tangential sphere bound.

The bit-interleaved coded modulation is designed in the case of a maximum likelihood decoding on the global Euclidean code. However, such a decoder is intractable and an iterative joint detection and decoding is processed to achieve near-ML performance. The detector complexity evolves exponentially with the spectral efficiency. We proposed a new list sphere decoder* that achieves near optimal APP detection and allows a strong complexity reduction on both ergodic and block-fading channels.

The future work should include:

- Optimize the binary mappings for block fading channels. The derived pairwise error probability over a MIMO block fading channel provides the design criterion.
- Minimize the error rate at the first iteration in the goal of accelerating the iterative processing and giving good performance if no computational resources are available at the receiver for iterative processing. Indeed, the linear precoders satisfying the DNA condition guarantee optimal coding gain and full diversity under ideal interleaving condition and ML decoding or converging iterative joint detection and decoding. However, if the optimized interleaver cannot achieve the ideal condition, more than one erroneous bit can be transmitted in a time period. Since the DNA condition does not fix all the system freedom degrees, the precoder can be designed to minimize the error rate when different rows of the linear precoder matrix are interfering at the same time. Furthermore, at the first iteration of the decoding process, the detector has no feedback from the decoder and all the rows of the linear precoder matrix are interfering.
- Find the condition to be satisfied by an error correcting code to allow an error rate decreasing with the frame length, and the expression of this decreasing function. The behavior of the error rate with the frame length can be deduced from the error rate expressions.
- Other concatenated codes than turbo-codes can be used to achieve the outage probability. One objective is to design LDPC-like codes for MIMO block fading channels.

Such a bit-interleaved coded modulation achieves near capacity performance at the price of a large complexity. A sub-optimal soft-input soft-output minimum mean square error can be used instead of the list APP detector. If the channel is ergodic, we observe right shifting of the waterfall region and if the channel is block fading, we observe a coding gain loss. Since the bit-interleaved coded modulation optimized in this thesis report are designed for ML decoding, any sub-optimal system being asymptotically near-ML should have full diversity and optimal coding gain too. Some supplementary research will be made to consider low-complexity scheme for practical system applications. Finally, the space-time bit-interleaved coded modulation can be applied to OFDM and multi-user techniques such as MC-CDMA for the next generations of mobile phones and Internet wireless technologies.

Appendix A

Influence of the frame length on the Frame Error Rate over quasi-static channels

A.1 Uncoded case

Assume that a frame is subdivided into N coded blocks, transmitted by an orthogonal design. Let m define the diversity order recovered by an uncoded scheme, for example an orthogonal design. For a given channel realization, the probability of error of each independent code is a function $f(\beta, y)$ where β denotes the coding gain multiplied by the signal to noise ratio, and y is a chi-square random variable. Remember that

$$y = \sum_{i=1}^{n} y_i^2 \quad y_i \sim \mathcal{N}(0, \sigma^2) \tag{A.1}$$

and

$$p(y) = \frac{y^{n/2-1} e^{-y/2\sigma^2}}{\sigma^n 2^{n/2} \Gamma(n/2)} \tag{A.2}$$

Since we are considering MIMO block fading channels, assume that $\sigma^2 = 1/2$, n even and $m = n/2$,

$$p(y) = \frac{y^{m-1}}{(m-1)!} e^{-y} \tag{A.3}$$

and

$$\int_0^x p(y)dy = 1 - e^{-x} \sum_{k=0}^{m-1} \frac{x^k}{k!} \tag{A.4}$$

Let I_N denote the frame error rate as a function of N:

$$I_N = \int_0^{+\infty} \left[1 - (1 - f(\beta, y))^N\right] p(y)dy \tag{A.5}$$

First consider $\forall x \in [0,1], g(x) = 1-(1-x)^N$. The concavity of $g(x)$ allows to define the following upper and lower bound ($x_0 \in [0,1]$), represented in Fig. A.1 :

$$J\left(x_0, g(x_0)\right) \leq 1-(1-x)^N \leq J\left(1/N, 1\right) \tag{A.6}$$

where $J(a,b) = \min\left(b, \frac{b}{a}x\right)$.

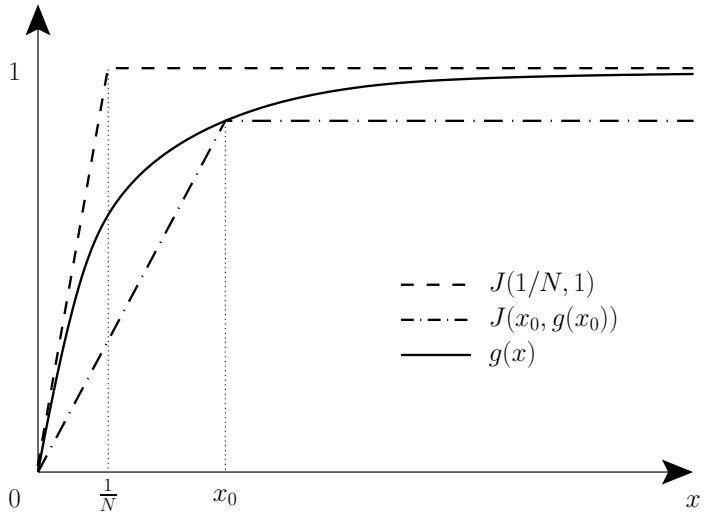

Figure A.1: Upper and lower bound of $g(x)$.

Let x_0 be a function of N such that $x_0 \sim 1/N$ and $g(x_0) \sim 1$ (We can choose for example $x_0 = N^{1/\sqrt{ln(N)}-1}$). In this case

$$\begin{cases} J\left(x_0, g(x_0)\right) \underset{N\to+\infty}{\sim} J\left(1/N, 1\right) \\ 1-(1-x)^N \underset{N\to+\infty}{\sim} J\left(1/N, 1\right) \end{cases} \tag{A.7}$$

Finally, $f\left(\beta, y\right)$ is a decreasing bijection from $y \in [0, +\infty]$ to $[0,1]$, we get

$$I_N \underset{N\to+\infty}{\sim} \int_0^{\alpha} p(y)dy + \int_{\alpha}^{+\infty} N f\left(\beta, y\right) p(y)dy \tag{A.8}$$

where α is defined as

$$f\left(\beta, \alpha\right) = 1/N \tag{A.9}$$

Let us now assume that

$$f\left(\beta, y\right) \underset{\beta\to+\infty}{\sim} Ae^{-y\beta/2} \Rightarrow \alpha \underset{\beta\to+\infty}{\sim} \frac{2}{\beta}\log\left(\frac{NA}{2}\right) \tag{A.10}$$

where A is the number of neighbours having an influence on the errror rate over an AWGN channel. Moreover, we choose β such that $\lim_{N\to+\infty,\beta\to+\infty}\alpha = 0$. The first term of the sum satisfies

$$\int_0^{\alpha} p(y)dy = e^{-\alpha}\sum_{k=m}^{+\infty}\frac{\alpha^k}{k!} \underset{\alpha\to 0}{\sim} \frac{\alpha^m}{m!} \underset{\beta\to+\infty,N\to+\infty}{\sim} \frac{\left(\frac{2}{\beta}\log\left(\frac{NA}{2}\right)\right)^m}{m!} \tag{A.11}$$

and the second term satisfies

$$\int_{\alpha}^{+\infty} N f(\beta, y)\, p(y) dy \underset{\beta \to +\infty}{\sim} \int_{\alpha}^{+\infty} N \frac{y^{m-1} e^{-y\beta/2}}{2(m-1)!}) dy \tag{A.12}$$

$$\underset{\beta \to +\infty}{\sim} \frac{N e^{-\alpha\beta/2}}{2(\beta/2)^m} \sum_{k=0}^{m-1} \frac{(\alpha\beta/2)^k}{k!} \underset{\beta \to +\infty}{\sim} \frac{1}{2A(\beta/2)^m} \tag{A.13}$$

Finally, the frame error rate of an uncoded system degrades while increasing N, the behaviour of the degradation is $\log(N)^m$.

A.2 Coded case

Let us consider a coded modulation, assume that the code is geometrically uniform and that $\sum_{i=0}^{L-1} a_i(N)$ is the number of points defining the shape of the decision Voronoi region of each codeword on an AWGN channel. Denote $d_i(N)$ the increasing euclidean distances associated to the coeffcient $a_i(N)$ ($d_0(N)$ is the minimal distance of the euclidean code). The frame error rate over a quasi-static channel with intrinsic diversity order m is upper bounded by

$$FER \leq \int_{y=0}^{+\infty} \min\left(1, \sum_{i=0}^{L-1} \frac{a_i(N)}{2} e^{-d_i(N) y\beta/2}\right) p(y) dy \tag{A.14}$$

$$\leq \int_{y=0}^{\alpha} p(y) dy + \left(\sum_{i=0}^{L-1} a_i(N)\right) \frac{1}{2} \int_{y=\alpha}^{+\infty} e^{-d_0(N) y\beta/2} p(y) dy \tag{A.15}$$

where $\alpha = \frac{2}{\beta d_0(N)} \log\left(\sum_{i=0}^{L-1} \frac{a_i(N)}{2}\right)$. We finally have an upper bound on the FER that behaves like $\log\left(\sum_{i=0}^{L-1} a_i(N)\right)^m / d_0(N)$.

The difficulty is now to determine the number of neighbours that have an influence on the shape of the Voronoi region and the behaviour of the coefficients $\sum_{i=0}^{L-1} a_i(N)$ with N. If a convolutional code is used, $d_0(N)$ is constant and $a_i(N)$ is linear in N and the behaviour of the FER degradation is $\log(N)^m$. It is difficult to know the real behaviour of $a_i(N)$ when turbo-codes are used. However, simulation results have shown that the FER seems to be asymptotically constant with N. In wireless mobile networks, the number of coded bits to be transmitted is around 10000. Even with a high spectral efficiency (e.g 8 bpcu), N is large enough to dramatically degrade the performance on quasi-static channels (see fig 3.19 page 86). This result is directly transposable to block-fading channels, using m as the diversity collected by the coded modulation scheme.

Appendix B

Soft-input soft-output MMSE Detector

In this Annex, we remind the SISO-MMSE construction presented for single antenna frequency selective channels in [32] and adapted to MIMO channels. Such a soft-input soft-ouput detector is sub-optimal when compared to the APP exhaustive detector, specially for low signal-to-noise ratios. However, it has the great advantage to provide near-optimum performance for a sufficiently high signal-to-noise ratio and with a strong complexity reduction for ergodic channels. The principle of such a detector is to view the $n_t \times n_r$ channel as n_t interfering $1 \times n_r$ MIMO sub-channels. It uses the information given at each iteration by the decoder to cancel the interference of the sub-channels.

First we compute the a priori probability associated with the modulation symbols from the a priori on the coded bits given back by the SISO decoder. Then, we are able to estimate the constellation symbols thanks to the a priori probabilities on the symbols. Finally, we convert the estimated symbols into extrinsic probabilities to be given to the SISO decoder input as a priori probabilities.

The classical SISO detector computes extrinsic probabilities $\{\xi(c_j)\}$ taking into account the a priori probabilities $\{\pi(c_j)\}$ with $j \neq i$. In an iterative processing between two blocks, the probability at the output of a block in iteration n should not be given back in the input of iteration $n+1$, since this would introduce dependence between the random variables.

A priori probabilities of the constellation symbols

First of all, we have to compute the a priori probabilities $\pi(z_i)$ of the modulation symbols Ω from the a priori probabilities $\pi(c_j)$ of the coded bits. Assuming independence between the interleaved coded bits:

$$\pi(z_i) = \prod_{j=m.i}^{m.i+m-1} \pi(c_j) \tag{B.1}$$

Where m is the modulation spectral efficiency. We define the a priori-based mean $\bar{z}_i$ of the

symbol z_i by

$$\bar{z}_i \triangleq E\{z_i\} = \sum_{z_i} z_i \pi(z_i) \tag{B.2}$$

The a priori-based variance $\sigma^2_{z,i}$ of the symbol z_i is defined by

$$\sigma^2_{z,i} \triangleq E\left\{|z_i|^2\right\} - |\bar{z}_i|^2 = \sum_{z_i} |z_i|^2 \pi(z_i) - |\bar{z}_i|^2 \tag{B.3}$$

Symbol estimation

A MMSE detector for the symbol z_i on the i-th antenna is a linear filter w_i that provides

$$\tilde{z}_i = E\{z_i\} + [y - E\{y\}]\, w_i^* \tag{B.4}$$

by minimizing the mean square error $E\left[|z_i - \tilde{z}_i|^2\right]$, we find

$$w_i = \mathrm{cov}\{y, z_i\}\, \mathrm{cov}\{y, y\}^{-1} \tag{B.5}$$

The covariance function $\mathrm{cov}\{x, y\}$ is defined by

$$\mathrm{cov}\{x, y\} \triangleq E\{[x - E\{x\}]^* [y - E\{y\}]\} \tag{B.6}$$

The a priori information of the considered symbol z_i should not be used for the estimate $\tilde{z}_i$. We define

$$\bar{\mathfrak{z}}_i \triangleq [\bar{z}_0, \ldots, \bar{z}_{i-1}, 0, \bar{z}_{i+1}, \ldots, \bar{z}_{n_t-1}] \tag{B.7}$$

We have

$$\mathrm{cov}\{y, y\} = H^* \Gamma_i H + N_0 I \tag{B.8}$$

where

$$\Gamma_i = \mathrm{cov}\{z, z\} = \left[\sigma^2_{z,0}, \ldots, \sigma^2_{z,i-1}, E_s, \sigma^2_{z,i+1}, \ldots, \sigma^2_{z,n_t-1}\right] \tag{B.9}$$

Indeed, the independence between the coded bits leads to the independence between the symbols and $\mathrm{cov}\{z_i, z_j\} = 0$ for $i \neq j$. The two quantities N_0 and E_s are the variances of the additive noise and transmitted signal, respectively. We have

$$\mathrm{cov}\{y, z_i\} = \mathrm{cov}\{z, \mathfrak{z}_i\} H = E\{z_i^* | z - \bar{z}_i|\}\, H = E_s \mathfrak{e}_i H \tag{B.10}$$

where $\mathfrak{e}_i$ is a vector with a unique non-null term equal to 1 in position i.

Using (B.4), (B.5), (B.8), (B.10) and noticing that $E\{z_i\} = 0$ and $E\{y\} = \bar{\mathfrak{z}}_i H$, we can write the expression of the symbol estimate $\tilde{z}_i$ as

$$\tilde{z}_i = E_s\, [y - \bar{\mathfrak{z}}_i H]\, [H^* \Gamma_i H + N_0 I]^{-1}\, (\mathfrak{e}_i H)^* \tag{B.11}$$

It is important to notice that the matrix inversion has to be computed for each symbol detection (n_t times), each iteration and time period, even for block fading channels. If no a priori is available (first iteration), the soft detector is equivalent to a classical MMSE detector.

Soft-output on the bits

We make the assumption that the estimated symbol $\tilde{z}_i$ is transmitted on an equivalent AWGN

channel, i.e, there is no interference anymore from the $n_t - 1$ other transmit antennas. This situation occurs when the feed back from the decoder is sufficiently reliable to effectively cancel the interference.

$$\tilde{z}_i = \mu_i z_i + \eta'_i \tag{B.12}$$

The two parameters of the equivalent AWGN channel $\tilde{z}_i \sim \mathcal{N}_{\mathbb{C}}(\mu_i z_i, \sigma^2_{\eta'_i})$ have to be estimated for each new symbol detection.

$$E\{z_i^*, \tilde{z}_i\} = \mu_i E_s = E\left\{z_i^* | z - \bar{\mathfrak{z}}_i|\right\} H w_i^* = E_s \mathfrak{e}_i H w_i^* \tag{B.13}$$

which leads to

$$\mu_i = \mathfrak{e}_i H w_i^* = E_s \left(\mathfrak{e}_i H\right) \left[H^* \Gamma_i H + N_0 I\right]^{-1} \left(\mathfrak{e}_i H\right)^* \tag{B.14}$$

The variance $\sigma^2_{\eta'_i}$ is given by

$$\sigma^2_{\eta'_i} = E\{|\eta_i|^2\} = w_i \left[H^* \Gamma_i H + N_0 I\right]^{-1} w_i^* - \mu_i^2 E_s = \mu_i (1 - \mu_i) E_s \tag{B.15}$$

Thanks to the AWGN channel assumption and the Bayes rule, we can write

$$P(z_i|y) \approx P(z_i|\tilde{z}_i) = \frac{p(\tilde{z}_i|z_i)\pi(z_i)}{p(\tilde{z}_i)} \tag{B.16}$$

The extrinsic probability can be deduced:

$$\xi(z_i) \propto \frac{P(z_i|y)}{\pi(z_i)} \propto p(\tilde{z}_i|z_i) \tag{B.17}$$

Using the complex AWGN equivalent channel hypothesis, we can write

$$p(\tilde{z}_i|z_i) = \frac{1}{\sigma^2_{\eta'_i}\pi} \exp\left[-\frac{|\tilde{z}_i - \mu_i z_i|^2}{\sigma^2_{\eta'_i}}\right] \tag{B.18}$$

Assume a mono-dimensional complex mapping Ω^1 is used independently on each transmit antenna. The extrinsic probabilities on the coded bits $\xi(c_{j+im})$ can be expressed by the expression

$$\xi(c_{j+im}) = \sum_{z_i \in \Omega(c_j)} p(\tilde{z}_i|z_i) \prod_{l=i.m,\, l\neq j}^{l=i.m+m-1} \pi(c_l) \tag{B.19}$$

where $\Omega^1(c_j)$ represents the set of mono-dimensional complex constellation symbols with their j-th bit equal to c_j $(0 \leq j \leq m-1)$. In order to solve the proportionality issue, we compute the normalization of the soft-output:

$$\xi(c_{j+im}) = \frac{\sum_{z_i \in \Omega^1(c_j=1)} p(\tilde{z}_i|z_i) \prod_{l\neq j} \pi(c_l)}{\sum_{z_i \in \Omega^1} p(\tilde{z}_i|z_i) \prod_{l\neq j} \pi(c_l)} \tag{B.20}$$

Appendix C

Partial fraction expansion

We want to decompose a function having the following form:

$$f(x) = \frac{1}{\prod_{k=1}^{n}(x+a_k)^{n_k}}$$

into partial fractions. We assume that $\forall(i \neq j), a_i \neq a_j$. Applying the Bezout's theorem, we can say that there exists polynomials $A_k(x)$ with $deg(A_k(x)) < n_k$ such that

$$f(x) = \frac{1}{\prod_{k=1}^{n}(x+a_k)^{n_k}} = \sum_{k=1}^{n} \frac{A_k(x)}{(x+a_k)^{n_k}}$$

Moreover, the Taylor's theorem shows that $\frac{A_k(x)}{(x+a_k)^{n_k}} = \sum_{i=1}^{n_k} \frac{\alpha_{k,i}}{(x+a_k)^i}$, in this case, we can decompose $f(x)$ into

$$f(x) = \frac{1}{\prod_{k=1}^{n}(x+a_k)^{n_k}} = \sum_{k=1}^{n}\sum_{i=1}^{n_k} \frac{\alpha_{k,i}}{(x+a_k)^i}$$

We can compute the $\alpha_{j,i}$ coefficients via a series expansion with $x = \varepsilon - a_j$.

$$\begin{aligned}
\frac{1}{\prod_{k=1}^{n}(x+a_k)^{n_k}} &= \frac{1}{\varepsilon^{n_j}\prod_{k=1,k\neq j}^{n}(a_k-a_j)^{n_k}} \prod_{k=1,k\neq j}^{n} \frac{1}{(1+\frac{\varepsilon}{a_k-a_j})^{n_k}} \\
&= \frac{1}{\varepsilon^{n_j}\prod_{k=1,k\neq j}^{n}(a_k-a_j)^{n_k}} \left[\prod_{k=1,k\neq j}^{n}\sum_{i=0}^{n_j-1} \frac{(-1)^i\binom{n_k+i-1}{i}\varepsilon^i}{(a_k-a_j)^i} + \mathcal{O}(\varepsilon^{n_j})\right] \\
&= \sum_{i=0}^{n_j-1} \frac{\gamma_{j,i}}{\varepsilon^{n_j-i}} + \mathcal{O}(1) = \sum_{i=0}^{n_j-1} \frac{\alpha_{j,n_j-i}}{\varepsilon^{n_j-i}} + \mathcal{O}(1)
\end{aligned}$$

In this case, $\alpha_{j,n_j-i} = \gamma_{j,i}$, where the $\gamma_{j,k}$ coefficients are obtained by identifying the degree $k < n_j$ coefficients of the series expansion

$$\sum_{i=0}^{n_j-1} \alpha_{j,n_j-i}X^i + \mathcal{O}(X^{n_j}) = \prod_{k=1,k\neq j}^{n}\sum_{i=0}^{n_j-1} \frac{(-1)^i\binom{n_k+i-1}{i}}{(a_k-a_j)^{n_k+i}}X^i + \mathcal{O}(X^{n_j})$$

Appendix D

Applications of the spherical list to MIMO channel mutual information computation

D.1 MIMO Mutual information computation

The capacity C of a channel and its mutual information $I(z;y)$ between its input z and output y are two essential quantities that are necessary to be computed when designing quasi-optimal performance systems. Indeed, for a given coding Rate R_c, they give lower bounds on the signal to noise ratio E_b/N_0 that allow error-free transmissions. The capacity C of a MIMO channel has been established in ([87]), g is a complex gaussian entries vector:

$$C = E_H \left\{ \log_2 \left(\det \left(I + \frac{H.R_{gg}.H^H}{N_0} \right) \right) \right\} \tag{D.1}$$

Let us consider a constellation point z and the output vector of the MIMO channel H, denoted $y = zH + \eta$, where η is the additive white gaussian noise vector. The mutual information between the input and output of the channel is

$$I(z;y) = m.n_t - \frac{1}{2^{m.n_t}} \sum_z \int_y p(y/z) \log_2 \left(\frac{\sum_{z'} p(y/z')}{p(y/z)} \right) dy \tag{D.2}$$

This quantity can be computed by a Monte-Carlo simulation:

$$I(z;y) = m.n_t - E_{z,H,\eta} \left\{ log_2 \left(\frac{\sum_{x'} p(y/z')}{p(y/z)} \right) \right\} \tag{D.3}$$

We have the choice to make the expectation over z, H and η separately or jointly. The best results will be given by a separated expectation but will need longer time. We will take into account some symetries of the channel that enables to limit the complexity of the first expectation

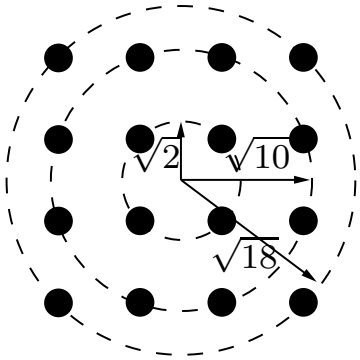

Figure D.1: Modulos of a 16QAM constellation

process. Let us define:

$$f(z,H) = -\int_y \sum_z p(y/z)p(z)\log_2\left(\frac{\sum_{z'} p(y/z')p(z')}{p(y/z)}\right)dy \tag{D.4}$$

The average mutual information (we suppose a non-stationnary channel) is given by

$$I(Z;Y) = E_{H,z,\eta}\left(I_H(Z=z;Y=y)\right) = \int_H p(H)\sum_z f(z,H)dH \tag{D.5}$$

The evaluation of this mutual information with a separated expectation Monte-Carlo method is prohibitive when we consider more than 2 antennas in emission and reception and a 16-QAM modulation (this expectation needs $2^{m.n_t} \times N_H \times N_\eta$ random samples where N_H is the number of samples for the channel and N_η is the number of samples for the noise). We can use a property of the channel to simplify the evaluation of this mean. Indeed, the phase of each entry of a MIMO channel is uniformly distributed. We consider two points z and z' of equal norm:

$$z' = \{z'_0 = z_0 e^{j\phi_0}, \dots z'_{n_t} = z_{n_t} e^{j\phi_{n_t}}\} = \phi z \tag{D.6}$$

Where the matrix ϕ is diagonal defined by

$$\phi = \mathrm{diag}\{e^{j\phi_i}\} \tag{D.7}$$

The phase of each entries of the matrix H is uniformly distributed, so $p(H(\rho,\phi)) = p(H(\rho))$:

$$\int_H p(H)f(z,H)dH = \int_\rho\int_\phi p(H(\rho))f(z,H(\rho,\phi))d\phi d\rho \tag{D.8}$$

$$f(z',H(\rho,\phi)) = f(z,H(\rho,\phi')) \tag{D.9}$$

$$\Rightarrow \int_H p(H)f(z,H)dH = \int_H p(H)f(z',H)dH \tag{D.10}$$

We can replace all the points that have the same module configuration by a single "virtual point", for example on Fig. D.1 we can see that only 3 "virtual points" have to be taken into account in the sum over z for a 16-QAM input. The point with modulo $\sqrt{2}$ has a weight equal to 4, the point with modulo $\sqrt{10}$ has a weight equal to 8 and the point with modulo $\sqrt{18}$ has a

weight equal to 4. We consider the weights $N_p(z)$ to be the number of points that have the same module configuration than z. For example, when we consider 2 antennas in emission with a 16-QAM constellation, we only have to consider 3^2 points instead of 16^2. Let Ω be the set of points that are sufficient to calculate the mutual information, $\Omega \in \Lambda$, where Λ is the constellation. The mutual information is now given by

$$I(Z;Y) = \log_2 2^{m.n_t} - \frac{1}{2^{m.n_t}} \int_H \int_y \sum_{z \in \Omega} N_p(z) p(y/z) log_2 \left(\frac{\sum_{z'} p(y/z')}{p(y/z)} \right) dy dH \tag{D.11}$$

We can estimate this mutual information with a Monte-Carlo simulation, with N_n realizations of the noise, N_H realizations of the channel.

$$\widetilde{I}(Z;Y) = m.n_t - \frac{1}{2^{m.n_t} N_n N_H} \sum_{H}^{N_H} \sum_{z \in \Omega} N_p(z) \sum_{b}^{N_n} log_2 \left(\frac{\sum_{z' \in \Omega} e^{-\|y - z'H\|^2 / 2N_0}}{e^{-\|y - zH\|^2 / 2N_0}} \right) \tag{D.12}$$

Nonetheless, the numerator of the logarithm is computed by an exhaustive marginalization of the $2^{m.n_t}$ symbols z' of the constellation Ω, which limits simulations to $m.n_t \leq 8$ (for example 16-QAM on MIMO 4x4 is unfeasible).

D.2 Bounds with a spherical list

The complexity of the marginalization can be reduced by computing the marginalization over points chosen in a subset of the constellation. For example, one may choose the spherical list $\mathfrak{L}$ of radius R centered on the received point described before. Each point z' that does not belong to the sphere has a likelihood upper bounded by the likelihood $p(y/z_s)$ of a point z_s lying at the surface of the sphere:

$$p(y/z_s) = \frac{exp\left(-R^2/2N_0\right)}{\sqrt{2\pi N_0}} \tag{D.13}$$

There are $(|\Omega| - |\mathfrak{L}|)$ points that do not belong to the list $\mathfrak{L}$, where $|\Omega|$ and $|\mathfrak{L}|$ are equal to the cardinals of Ω and $\mathfrak{L}$, respectively. We can express upper and lower bounds to the numerator of the logarithm in (D.2):

$$\sum_{z \in \mathfrak{L}} p(y/z) \leq \sum_{z \in \Omega} p(y/z) \leq \sum_{z \in \mathfrak{L}} p(y/z) + (|\Omega| - |\mathfrak{L}|) . p(y/z_s) \tag{D.14}$$

This leads to upper and lower bounds to $I(z;y)$:

$$\begin{cases} I(z;y) \geq m.n_t - E_{z,H,\eta} \left\{ log_2 \left(\frac{\sum_{z' \in \mathfrak{L}} p(y/z') + (|\Omega| - |\mathfrak{L}|).p(y/z_s)}{p(y/z)} \right) \right\} \\ I(z;y) \leq m.n_t - E_{z,H,\eta} \left\{ log_2 \left(\frac{\sum_{z' \in \mathfrak{L}} p(y/z')}{p(y/z)} \right) \right\} \end{cases} \tag{D.15}$$

We have already seen in the list detector section that the number of point belonging to the list centered on the received point y is not as controllable as the one belonging to the list centered on the ML point. Indeed, the radius of the sphere can be corrected before the enumeration step depending on the position of the ML point in the constellation. Nevertheless, we do not have again a lower bound on the mutual information $I(z;y)$ when considering the substitution of the likelihoods of the missing points by the likelihood $p(y/z_s)$. For example, in Fig. D.2, we can

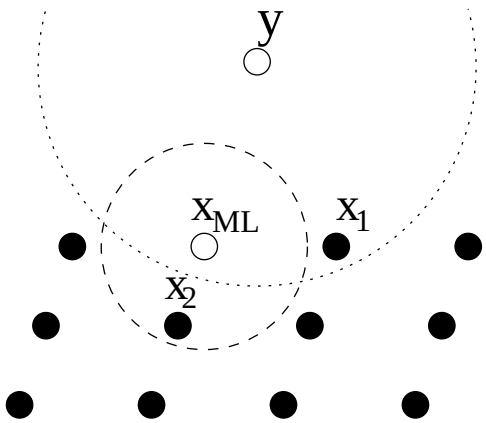

Figure D.2: Lists centered on received and ML points

see that the x_2 point's likelihood is lower than the x_1 point's one, the likelihood of the missing points cannot be upper bounded. As a remark, the upper bound provided by the list centered on the ML point is still avalaible.

D.3 Computer simulations and numerical results

Figure D.3 shows the achievable information rate for 4×4 multiple antenna channel with 16-QAM input alphabet. The mutual information value of 8.0 bits per channel use yields a minimum achievable signal-to-noise ratio equal to 4.0dB. The capacity limit with a Gaussian input at 8.0 bits per channel use is 3.7 dB. Figure D.3 illustrates two scenarios: 1- A target list size $N_p = 1000$. The effective list size was distributed between $N_e(min) = 256$ and $N_e(max) = 2300$ with an average equal to 1000. 2- A target list size $N_p = 60000$! The effective list size was distributed between $N_e(min) = 4000$ and $N_e(max) = 26000$ with an average equal to 10000. It is clear that mutual information evaluation is useful at high coding rates ($R_c \geq 1/2$) where its value diverges from the gaussian input capacity. A reduced size list is sufficient in this region. Similarly, Figure D.4 shows the achievable information rate for 8×8 multiple antenna channel with 16-QAM input.

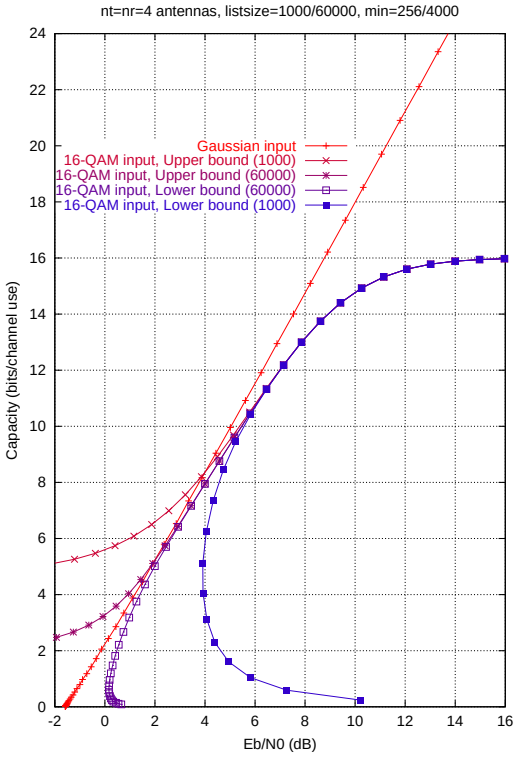

Figure D.3: Mutual information evaluation for 4×4 MIMO with 16-QAM

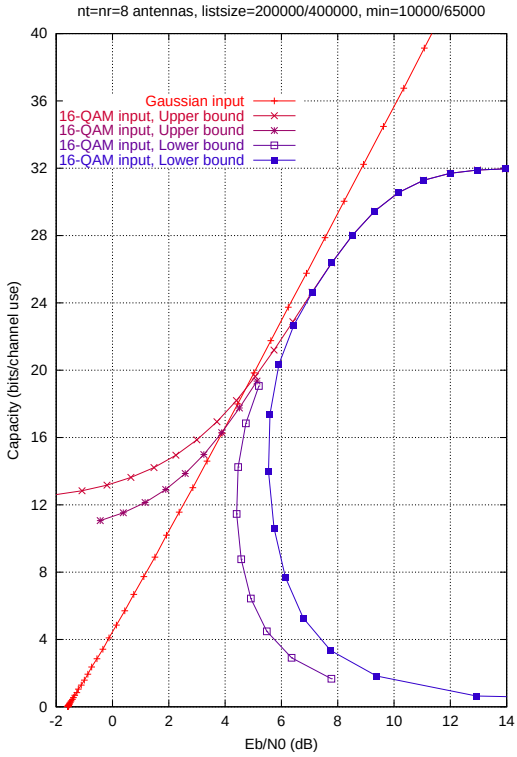

Figure D.4: Mutual information evaluation for 8×8 MIMO with 16-QAM

Bibliography

[1] E. Agrell, T. Eriksson, A. Vardy and K. Zeger, "Closest point search in lattices," *IEEE Transactions on Information Theory*, pp. 2201-2214, August 2002.

[2] E. Agrell, J. Lassing, E.G. Ström, and T. Ottosson, "On the optimality of the binary reflected Gray code," to appear in *IEEE Transactions on Information Theory*, 2004.

[3] S.M. Alamouti, "A simple transmit diversity technique for wireless communications," *IEEE Journal on Selected Areas in Communications*, vol. 16, pp. 1451-1458, October 1998.

[4] L.R. Bahl, J. Cocke, F. Jelinek and J. Raviv, "Optimal decoding of linear codes for minimizing symbol error rate," *IEEE Transactions on Information Theory*, vol. 20, pp. 284-287, March 1974.

[5] G. Battail, "Théorie de l'Information," *Editions Masson, Collection Pédagogique de Télécommunications*, 1997.

[6] S. Baro, J. Hagenauer, and M. Witzke, "Iterative detection of MIMO transmission using a list-sequential (LISS) detector," in *Proc. ICC'03*, Anchorage, pp. 2653-2657, May 2003.

[7] J.-C. Belfiore, G. Rekaya and E. Viterbo, "The Golden Code: A 2x2 Full-Rate Space-Time Code with Non-Vanishing Determinants," *submitted to IEEE Trans. on Information Theory.*

[8] S. Benedetto, G. Montorsi, D. Divsalar and F. Pollara, "Serial concatenation of interleaved codes: Performance analysis, design and iterative decoding," *TDA Progress Report 42-126*, JPL, August 1995.

[9] C. Berrou, A. Glavieux and P. Thitimajshima, "Near Shannon limit error-correcting coding and decoding: turbo-codes," *Proceedings of ICC'93*, Genève, pp. 1064-1070, Mai 1993.

[10] C. Berrou and A. Glavieux, "Near optimum error correcting coding and decoding: Turbo-codes," *IEEE Transactions on Communications*, vol. 44, pp. 1261-1271, October 1996.

[11] C. Berrou, "The ten-year-old turbo codes are entering into service," *IEEE Comm. Mag.*, vol. 41, no. 8, pp. 110-116, August 2003.

[12] E. Biglieri, D. Divsalar, P.J. McLane and M.K. Simon, "Introduction to trellis coded modulation with applications," New York, Macmillan, 1991.

[13] J. Boutros, "Lattice codes for Rayleigh fading channels," *Thèse de Doctorat, ENST*, Paris, June 1996.

[14] J. Boutros and E. Viterbo, "Signal space diversity: a power- and bandwidth-efficient diversity technique for the Rayleigh fading channel," *IEEE Transactions on Information Theory*, vol. 44, pp. 1453-1467, July 1998.

[15] J. Boutros, F. Boixadera and C. Lamy, "Bit-interleaved coded modulations for multiple-input multiple-output channels," *Proc. of the IEEE 6th International Symposium on Spread Spectrum Techniques & Applications*, New Jersey, September 2000.

[16] J.J. Boutros, "Iterative APP decoding of linear transforms", *Proc. of the ISITA'00*, Hawai, November 2000.

[17] J. Boutros, E. Calvanese Strinati and A. Guillén i Fàbregas, "Turbo code design in the block fading channel," *in Proc. 42nd Annual Allerton Conference on Communication, Control and Computing, Allerton,* IL, September-October 2004.

[18] F. Brännström, L. K. Rasmussen and A. Grant, "Optimal scheduling for iterative decoding", *Proc. of IEEE ISIT'03*, Yokohama, Japan, July 2003.

[19] L. Brunel, "Optimum multiuser detection for MC-CDMA systems using sphere decoding," *PIMRC'01*, San Diego, California, October 2001.

[20] L. Brunel, "Optimum and sub-optimum multiuser detection based on sphere decoding for Multi-Carrier Code Division Multiple Access systems," *ICC'02*, New York, April 2002.

[21] L. Brunel and J. Boutros, "Lattice decoding for joint detection in direct sequence CDMA systems," *IEEE Transactions on Information Theory*, vol. 49, no. 4, pp. 1030-1037, April 2003.

[22] G. Caire, G. Taricco and E. Biglieri, "Bit-interleaved coded modulation," *IEEE Transactions on Information Theory*, vol. 44, no. 3, pp. 927-946, May 1998.

[23] A. R. Calderbank and N. J. A. Sloane, "New trellis codes based on lattice and cosets," *IEEE Trans. on Information Theory*, vol. 33, no. 2, pp. 177-195, March 1987.

[24] A. Chindapol and J.A. Ritcey, "Design, analysis, and performance evaluation for BICM-ID with square QAM constellations in Rayleigh fading channels," *IEEE Journal on Selected Areas in Communications*, vol. 19, no. 5, pp. 944-957, May 2001.

[25] A. Chouly, A. Brajal and S. Jourdan: "Orthogonal multicarrier techniques applied to direct sequence spread spectrum CDMA systems," *Proc. of GLOBECOM'93*, pp. 1723-1728, November 1993.

[26] J. H. Conway and N. J. Sloane, "Sphere packings, lattices and groups," 3rd edition, 1998, Springer-Verlag, New York.

[27] T.M. Cover, J.A. Thomas, "Elements of Information Theory," John Wiley & Sons, 1991.

[28] M. O. Damen, K. Abed-Meraim, and J.-C. Belfiore, "Diagonal algebraic space-time block codes," *IEEE Trans. on Information Theory*, vol. 48, pp. 628-636, March 2002.

[29] M. O. Damen, H. El Gamal and N. C. Beaulieu, "Linear threaded algebraic space-time constellation", *IEEE Trans. on Information Theory, special issue on space-time coding*, vol. 49, pp. 2372-2388, October 2003.

[30] M. O. Damen, H. El Gamal and N. C. Beaulieu, "Systematic construction of full diversity algebraic constellations," *IEEE Trans. on Information Theory*, vol. 49, pp. 3344-3349, December 2003.

[31] P. Dayal and M. K. Varanasi, "An Optimal Two Transmit Antenna Space-Time Code," *submitted, IEEE Trans. Inform. Th.,* July 2003.

[32] A. Dejonghe and L. Vanderdope, "Turbo-equalization for multilevel modulation: an efficient low-complexity scheme," *Proc. of the IEEE ICC 2002*, vol. 25, no. 1, pp. 1863-1867, April 2002.

[33] B. Dong, X. Wang and A. Doucet, "A New Class of Soft MIMO Demodulation Algorithms," *IEEE Trans. Signal Processing,* vol. 51, no. 11, pp. 2752-2763, Nov. 2003.

[34] H. El Gamal and M. O. Damen, "Universal space-time coding," *IEEE Trans. on Information Theory*, vol. 49, pp. 1097-1119, May 2003.

[35] H. El Gamal and A. R. Hammons Jr, "On the design of algebraic space-time codes for MIMO block fading channels," *IEEE Transactions on Information Theory*, vol. 49, no. 1, January 2003.

[36] K. Fazel and L. Papke, "On the performance of convolutionally-coded CDMA/OFDM for mobile communication system," *Proc. of PIMRC'93*, pp. 468-472, September 1993.

[37] G. J. Foschini, Jr. and M. J. Gans, "On limits of wireless communication in a fading environment when using multiple antennas," *Wireless Personal Communications*, vol. 6, no. 3, pp. 311-335, March 1998.

[38] G. D. Forney, "The Viterbi Algorithm," *Proceedings of the IEEE,* vol. 61, no.. 3, pp.. 268-278, March 1973.

[39] G.D. Forney, "Concatenated Codes," *Cambridge, MIT press,* 1966.

[40] G. D. Forney, R.G. Gallager, G. R. Lang, F. M. Longstaff, and S. U. Qureshi, "Efficient modulation for band-limited channels," *IEEE Journal on Selected Areas in Communications*, vol. 34, pp. 632-647, Sept. 1984.

[41] G. D. Forney, "Coset codes I: introduction and geometrical classification," *IEEE Trans. on Information Theory*, vol. 34, pp. 1123-1151, Sept. 1988.

[42] R.G. Gallager, "Low-density parity-check codes," *Cambridge, MIT press,* 1963.

[43] R.G. Gallager, "Information Theory and Reliable Communication, Wiley," New York, 1968.

[44] A. Guillén i Fàbregas and G. Caire, "Turbo-like Codes are Good in the Block-Fading Channel," *in Proc. 2004 International Symposium on Information Theory and Applications (ISITA),* Parma, Italy, October 2004.

[45] A. Guillén i Fàbregas, "Concatenated Codes for Block-Fading Channels," *PhD thesis report*, Ecole Polytechnique Fédérale de Lausanne (EPFL), Lausanne, Switzerland, 2004.

[46] Hagenauer, J. Hoeher, "A Viterbi algorithm with soft-decision outputs and its application", *IEEE GLOBECOM '89.*, vol. 3, pp. 1680-1686, November 1989.

[47] H. Herzberg and G. Poltyrev, "Techniques of Bounding of the Decoding Error for Block Coded Modulation Structures," *IEEE Transactions on Information Theory*, vol. 40, pp. 903-911, May 1994.

[48] H. Herzberg and G. Poltyrev, "The Error Probability of M-ary PSK Block Coded Modulation Schemes," *IEEE Transactions on Communications*, vol. 44, pp. 427-433, April 1996.

[49] B. M. Hochwald and S. ten Brink, "Achieving near-capacity on a multiple-antenna channel," *IEEE Trans. Inform. Theory,* vol. 51, no. 3, pp. 389-399, March 2003.

[50] Y. Huang and J.A. Ritcey, "Tight BER bounds for iteratively decoded bit-interleaved space-time coded modulation," *IEEE Comm. Letters*, vol. 8, no. 3, pp. 153-155, March 2004.

[51] H. Imai and S. Hirakawa, "A new multilevel coding method using error-correcting codes," *IEEE Transactions on Information Theory*, vol. 23, pp. 371-377, May 1977.

[52] "Special issue on codes on graphs and iterative algorithms," *IEEE Transactions on Information Theory*, vol. 47, no. 2, February 2001.

[53] H. Jafarkhani, "A quasi-orthogonal space-time block code," *IEEE Transactions on Communications*, vol. 49, pp. 1-4, January 2001.

[54] R. Knopp, P. Humblet, "Maximizing diversity on block fading channels," *IEEE International Conference on Communications*, vol. 2, pp. 647-651, Montreal, June 1997.

[55] R. Knopp, P. Humblet, "On coding for block fading channels," *IEEE Transactions on Information Theory*, vol. 46, no. 1, pp. 189-205, January 2000.

[56] R. Koetter and A. Vardy, "Algebraic soft-decision decoding of Reed-Solomon codes", *IEEE International Symposium on Information Theory*, Sorrento, Italy, June 2000.

[57] R. Koetter, A.C. Singer and M. Tuchler, "Turbo equalization," *IEEE Signal Processings Mag.*, vol. 21, no. 1, pp. 67-80, January 2004.

[58] A.N. Korkin and E.I. Zolotarev. "Sur les formes quadratiques," *Math. Ann.*, vol. 6, pp. 366-389, 1873.

[59] F. Kschischang, B. Frey and H. A. Loeliger, "Factor graphs and the sum-product algorithm," *IEEE Transactions on Information Theory*, vol. 47, no. 2, February 2001.

[60] F.R. Kschischang, "Codes defined on graphs," *IEEE Comm. Mag.*, vol. 41, no. 8, pp. 118-125, August 2003.

[61] C. Lamy, "Communications à grande efficacité spectrale sur le canal à évanouissement," *Thèse de Doctorat, ENST*, Paris, avril 2000.

[62] A. Lenstra, H. Lenstra Jr. and L. Lovasz. "Factoring polynomials with rational coefficients," *Mathematische Annalen*, vol. 215, pp. 515-534, 1982.

[63] X. Li and J.A. Ritcey, "Bit-interleaved coded modulation with iterative decoding," *IEEE Communications Letters*, vol. 1, no. 6, November 1997.

[64] H.-A. Loeliger, "Some remarks on factor graphs," *Proc. 3rd International Symposium on Turbo Codes and Related Topics,* Brest, France, pp. 111-115, September 2003.

[65] Luo, J., Pattipati, K., Willett, P. and Brunel, L., "Branch-and-bound-based fast optimal algorithm for multiuser detection in synchronous CDMA," *IEEE International Conference on Communications,* vol. 5, pp. 3336-3340, 11-15 May 2003.

[66] D.J.C. MacKay and R.M. Neal, "Near Shannon limit performance of low density parity check codes," *Electronics Letters,* vol. 33, no. 6, pp. 457-458, March 1997.

[67] D.J.C. MacKay, "Good error-correcting codes based on very sparse matrices," *IEEE Transactions on Information Theory*, vol. 45, no. 2 , March 1999. Page(s): 399 -431

[68] E. Malkamaki and H. Leib, "Coded diversity on block-fading channel," *IEEE Transactions on Information Theory*, vol. 45, pp. 771-781, March 1999.

[69] D. Maiwald and D. Kraus, "Calculation of the moments of complex Wishart and complex inverse Wishart distributed matrices," *IEE Proc. Radar, Sonar Navig.*, vol. 147, no.4, August 2000.

[70] F. Oggier, G. Rekaya, J.-C. Belfiore, and E. Viterbo, "Perfect Space Time Block Codes," *submitted to IEEE Trans. on Information Theory.*

[71] J. N. Pierce and S. Stein, "Multiple diversity with nonindependent fading," *Proc. IRE*, vol. 48, pp. 89-104, January 1960.

[72] M. Pohst, "On the computation of lattice vectors of minimal length, successive minima and reduced bases with applications," *ACM SIGSAM Bull.*, vol. 66, pp. 181-191, 1994.

[73] G. Poltyrev, "Bounds on Decoding Error Probability of Binary Linear Codes via Their Spectra," *IEEE Transactions on Information Theory*, vol. 40, pp. 1261-1271, October 1996.

[74] J.G. Proakis, "Digital Communications," 3rd edition, McGraw-Hill, New York, 1995.

[75] A. B. Reid, A. J. Grant, and A. P. Kind, "Low-complexity list-detection for high-rate multiple-antenna channels," in *Proc. IEEE Int. Symp. Inform. Theory,* Yokohama, Japan, p. 273, 2003.

[76] T.J. Richardson and R.L. Urbanke, "The capacity of low-density parity-check codes under message-passing decoding," *IEEE Transactions on Information Theory*, vol. 47, no. 2, February 2001.

[77] T. Richardson and R. Urbanke, "The renaissance of Gallager's low-density parity-check codes," *IEEE Comm. Mag.*, vol. 41, no. 8, pp. 126-131, August 2003.

[78] F. Simoens, H. Wymeersch, and M. Moeneclaey, "Spatial mapping for MIMO systems", *Proc. of IEEE ITW'04*, San Antonio, Oct. 2004.

[79] C.E. Shannon, "A Mathematical Theory of Communication," Bell Systems Technical Journal, vol. 27, July and October 1948.

[80] C.P. Schnorr and M. Euchner, "Lattice basis reduction: improved practical algorithms and solving subset sum problems," *Mathematical Programming*, vol.66, pp. 181-191, 1994.

[81] F. Schreckenbach, N. Gortz, J. Hagenauer and G. Bauch, "Optimized symbol mappings for bit-interleaved coded modulation with iterative decoding," *Proc. of the IEEE GLOBECOM 2003*, San Francisco, December 2003.

[82] A. Stefanov and T.M. Duman, "Turbo-coded modulation for systems with transmit and receive antenna diversity over block fading channels: system model, decoding approaches, and practical considerations," *IEEE Journal on Sel. Areas in Comm.*, vol. 19, pp. 958-968, May 2001.

[83] M. Sudan, "Decoding of Reed-Solomon Codes beyond the Error-Correction Bound," *Journal of Complexity*, vol. 13, no. 1, pp. 180-193,1997.

[84] R.M. Tanner, "A recursive approach to low complexity codes," *IEEE Transactions on Information Theory*, vol. 27, September 1981.

[85] V. Tarokh, N. Seshadri and A. R. Calderbank, "Space-time codes for high data rate wireless communication: Performance criterion and code construction," *IEEE Transactions on Information Theory*, vol. 44, no. 2, pp. 744-765, March 1998.

[86] V. Tarokh, H. Jafarkhani and A.R. Calderbank, "Space-time block codes from orthogonal designs," *IEEE Transactions Information Theory*, vol. 45, July 1999.

[87] E. Telatar, "Capacity of multi-antenna gaussian channels," *Technical report, AT&T Bell Laboratories*, 1999.

[88] S. Ten Brink, "Convergence of iterative decoding," *Electronics Letters*, vol. 35, no. 10, pp. 806-808 ,May 1999.

[89] M. Tüchler, A. Singer and R. Koetter, "Minimum mean squared error equalization using a-priori information," *IEEE Trans. on Signal Processing,* vol. 50, pp. 673-683, Mar. 2002.

[90] Texas Instruments, "Improved Double-STTD schemes using asymmetric modulation and antenna shuffling," *3GPP RAN1 contribution,* May 21-25, 2001 Busan, Korea.

[91] N. H. Tran and H. H. Nguyen, "Improving the performance of QPSK BICM-ID by mapping on the hypercube," *Proc. of IEEE VTC Fall'04*, Los Angeles, Sept. 2004.

[92] G. Ungerboeck, "Channel coding with multilevel/phase signals," *IEEE Transactions on Information Theory*, vol. 28, pp. 55-67, January 1982.

[93] G. Ungerboeck, "Trellis-coded modulation with redundant signal sets, Part II," *IEEE Communications Magazine*, vol. 25, no. 2, February 1987.

[94] V. V. Veeravalli, "On Performance Analysis for Signaling on Correlated Fading Channels," *IEEE Transactions on Communications*, vol. 49, no. 11, pp. 1879-85, November 2001.

[95] A. J. Viterbi, "Error Bounds for Convolutional Codes and an Asymptotically Optimum Decoding Algorithm," *IEEE Transactions on Information Theory,* vol. IT, pp. 260-269, 1967.

[96] A.J. Viterbi and J.K. Omura, "Principles of Digital Communication and Coding," McGraw-Hill, New York, 1979.

[97] E. Viterbo and E. Biglieri, "A universal lattice decoder," *Proceedings of 14ème Colloque GRETSI*, Juan-les-Pins, pp. 611-614, September 1993.

[98] E. Viterbo and J. Boutros, "A universal lattice code decoder for fading channels," *IEEE Transactions on Information Theory*, pp. 1639-1642, July 1999.

[99] U. Wachsmann, R.F.H. Fischer and J.B. Huber, "Multilevel codes: theoretical concepts and practical design rules " *IEEE Transactions Inform. Theory*, vol. 45, pp. 1361-1391, July 1999.

[100] L.F. Wei, "Trellis-coded modulation with multidimensional constellations," *IEEE Trans. on Information Theory*, vol. 33, no. 4, pp. 483-501, July 1987.

[101] N. Yee, J.P. Linnartz and G. Fettweis: "Multicarrier CDMA in indoor wireless radio networks," *Proc. of PIMRC'93*, Yokohama, pp. 109-113, September 1993.

[102] K. Zeger and A. Gersho, "Pseudo-Gray Coding," *IEEE Transactions on communications*, vol. 38, pp. 2147-2158, December 1990.

[103] E. Zehavi, "8-PSK trellis codes for a Rayleigh channel," *IEEE Transactions on Communications*, vol. 40, pp. 873-884, May 1992.

[104] L. Zheng and D. Tse, "Diversity and multiplexing: A fundamental tradeoff in multiple antenna channels," *IEEE Transactions on Information Theory,* vol. 49, pp. 1073–1096, May 2003.

Publications

[105] J. Boutros , N Gresset, L. Brunel and M. Fossorier, "Soft Ouptput detection for multiple antennas: accelerated sphere decoding and shifted list enumeration," *Proc. of GRETSI 2003, Paris.*

[106] J. Boutros, N. Gresset, L. Brunel, "Turbo coding and decoding for multiple antenna channels," *International Symposium on Turbo Codes*, Brest, Sept. 2003. Available at *http://www.enst.fr/∼gresset* and *http://www.enst.fr/∼boutros/coding.*

[107] J. Boutros , N Gresset, L. Brunel and M. Fossorier, "Soft-input soft-output lattice sphere decoder for linear channels," *Proc. of the IEEE GLOBECOM'03*, San Francisco, December 2003.

[108] N. Gresset, J. Boutros and L. Brunel, "Linear precoding under iterative processing for multiple antenna channels," *Proc. of IEEE ISCCSP 2004, Hammamet.*

[109] N. Gresset, J. Boutros and L. Brunel, "Optimal linear precoding for BICM over MIMO channels," *Proc. of the IEEE ISIT'04*, Chicago, June 2004.

[110] N. Gresset, J. Boutros and L. Brunel, "Multi-dimensional mappings for iteratively decoded BICM on multiple antenna channel," *IEEE Transactions on Information Theory,* vol. 51, no. 9, September 2005.

[111] N. Gresset, J. Boutros and L. Brunel, "Space-Time coding with Bit-Interleaved Coded Modulations," *In preparation for IEEE Transactions on Information Theory.*

[112] G. Kraidy, N. Gresset, and J. Boutros, "Information theoretical versus algebraic constructions of linear unitary precoders for non-ergodic multiple antenna channels," *Canadian Workshop on Information Theory*, Montréal, Canada, June 2005.

Filed Patents

- List Sphere Decoding of Symbols Transmitted in a Telecommunication System.
- Method for transmitting data in a MIMO telecommunication system offering a high diversity as perceived by a receiver end.
- Method for transmitting optimally interleaved data in a MIMO telecommunication system.
- Method allowing an enhanced iterative interpretation of received symbols.
- Method for interpreting transmitted symbols allowing an iterative adaptation of a basic list of symbols.
- Method for interpreting transmitted symbols involving a list sphere radius tuning step.
- Method for transmitting uniformly distributed data in MIMO telecommunication system.